

# *Development of Biosensors for Medical Applications*

**Dissertation zur Erlangung des Doktorgrades der  
Naturwissenschaften (Dr. rer. nat.)**

der Fakultät Chemie und Pharmazie  
der Universität Regensburg  
Deutschland



vorgelegt von

**Meike Bauer geb. Hermann**

aus Regensburg

im Jahr 2022



*“Nothing in life is to be feared; it is only to be understood.  
Now is the time to understand more, so that we may fear less.”*

- Marie Curie -



Die vorgelegte Dissertation entstand in der Zeit von Dezember 2018 bis März 2022 am Institut für Analytische Chemie, Chemo- und Biosensorik der Universität Regensburg.

Die Arbeit wurde angeleitet von Prof. Dr. Antje J. Bäumner.

Promotionsgesuch eingereicht am: 31. Mai 2022

Kolloquium am: 22. Juli 2022

### **Prüfungsausschuss**

Vorsitzender: Prof. Dr. Oliver Tepner

Erstgutachterin: Prof. Dr. Antje J. Bäumner

Zweitgutachter: Prof. Dr. Axel Dürkop

Drittprüfer: Prof. Dr. Rainer Müller



# Acknowledgement

---

First, I like to express my great gratitude for **Prof. Dr. Antje J. Bäumner**. She gave me the opportunity to work on a comprehensive, challenging, sometimes frustrating, and anything but boring Ph.D. project. I like to honor her trust in my abilities and the continuous support during all the time, especially the from time-to-time necessary pep talks.

Furthermore, I like to thank **Prof. Dr. Axel Dürkop** for his on-site support, helpful suggestions and the always opened door.

Thanks to **Prof. Dr. Oliver Tepner** and **Prof. Dr. Rainer Müller** for being the chairman of the colloquium and the third auditor.

I like to thank all former and current members of the **workgroup** and my **lovely lab mates** for their support and the cozy atmosphere particularly during the numerous after work activities (before and some kind of after the pandemic).

Especially I like to honor **Barbara Grotz** and **John Galligan** for their excellent work and our motivating Monday Morning Meetings. Another big “thank you” goes to **Simone Rink**, **Franziska Beck** and **Christian Griesche** for the enlightening research discussions and the numerous pizza parties and BBQs (always in compliance with current Corona laws).

Thank you, **Vanessa Tomanek**, for your nice graphical abstract drawings and your help together with **Joachim Rewitzer** for doing the ICP-OES measurements.

In alphabetical order I like to thank all my supervised bachelor and ERASMUS students as well as the interns: **Alexander Erhard**, **Blaž Kozjan**, **Florian Blaser**, **Iga Malicka**, **Julia Ciechocińska**, **Laura Deml**, **Maxi Födlmeier** and **Rahel Grünberger**. You did great work!

I like to acknowledge the perpetual support of my amazing husband **Markus “Lieblingsbau”**, my wonderful parents **Erwin** and **Helga**, and **my whole family** and **friends**.

Thanks to **Sibylle**, **Max** and **Steffen** for being the best neighborhood, going together through thick and thin.

Thanks to **Merlin**, the best home office co-worker ever. He works hard(ly) all the time.

♥♥♥ DANKE ♥♥♥

... and, **dear honored reader**, thank you for reading my thesis ...



# Declaration of Collaboration

---

Most of the theoretical and experimental work presented in this thesis was conducted solely by the author. However, parts of the results were gained in collaboration with other researchers, which are stated in this section in accordance with §8 Abs. 1 Satz 2 Punkt 7 of the “Ordnung zum Erwerb des akademischen Grades eines Doktors der Naturwissenschaften (Dr. rer. nat.) an der Universität Regensburg vom 18. Juni 2009“.

## **Relevance and Structure of the Thesis (Chapter 1)**

The literature search and writing of the chapter was solely done by the author.

## **A Critical Review: Polymer and Hydrogel Deposition Techniques Used for Preparation of Optical and Electrochemical Bioanalytical Sensors (Chapter 2)**

The literature search and writing of the manuscript was solely done by the author. Vanessa Tomanek created the graphical abstract. Antje J. Baeumner and Axel Duerkop revised most parts of the manuscript. AJB will be corresponding author.

## **Electrochemical Multi-Analyte Point-of-Care Perspiration Sensors Using On Chip Three-Dimensional Graphene Electrodes (Chapter 3)**

Most of the experimental work was solely done by the author. Data plots, other images and text passages which are already published within the scope of the author’s Master’s Thesis (in whole or in part) are marked with an asterisk [\*] after the respective sentence or paragraph or in the respective caption. The Master’s thesis is entitled “Development of Wearable, Electrochemical Sweat Sensors Based on Laser-Scribed Graphene” and was submitted in September 2018 to the Faculty of Chemistry and Pharmacy at the University of Regensburg. As the new work done during the Ph.D. project relied on previous results and as these are presented in the published work, the combination is presented here as one chapter.

Lukas Wunderlich developed in the early phase the 2-electrode layout for the potentiometric sensor. He investigated the electrodeposition of the Ag/AgCl reference electrode and drop-coating of the ISE cocktail which was optimized by the author. In collaboration with Florian Weinzierl the finally used electrode layout for the impedance measurement was developed and tested. Florian Blaser measured the dose-response curves of the amperometric sensor for various pH values. Marcel Simsek provided the SEM images and Arne Behrent carried out the Raman measurements. Vanessa Tomanek created the graphical abstract. Axel Duerkop, Antje J. Baeumner, Yongjiu Lei and Husam N. Alshareef contributed with strategic discussions. The manuscript was written by the author and revised by LW, FW, AD, YL, HNA and AJB. AJB is corresponding author.

#### **Europium(III) Tetracycline as Probe for Detection of Hydrogen Peroxide in Microplate Assays (Chapter 4)**

Most of the experimental work was solely done by the author. Rahel Gruenberger and Laura Deml collected data in the scope of Bachelor Theses and an internship under supervision of the author. Some of the foils and solutions were prepared by Barbara Grotz and John Galligan and used by the author. Barbara Grotz, John Galligan, Axel Duerkop and Antje J. Baeumner contributed with strategic discussions. The manuscript was written by the author and will be revised by BG, JG, AD and AJB. AJB will be corresponding author.

#### **Combination of Europium(III) Tetracycline with Oxidase Enzymes in Biocompatible Hydrogels for Detection of Hydrogen Peroxide in Flow-Through Systems (Chapter 5)**

Most of the experimental work was solely done by the author. Some of the foils and solutions were prepared by Barbara Grotz and John Galligan and used by the author. Barbara Grotz, John Galligan, Axel Duerkop and Antje J. Baeumner contributed with strategic discussions. The manuscript was written by the author and will be revised by BG, JG, AD and AJB. AJB will be corresponding author.

#### **Conclusion and Perspectives (Chapter 6)**

The literature search and writing of the chapter was solely done by the author.

# Table of Contents

---

<b>ACKNOWLEDGEMENT .....</b>	<b>I</b>
<b>DECLARATION OF COLLABORATION .....</b>	<b>III</b>
<b>TABLE OF CONTENTS.....</b>	<b>V</b>
<b>SUMMARY.....</b>	<b>VIII</b>
<b>ZUSAMMENFASSUNG .....</b>	<b>XI</b>
<b>1 RELEVANCE AND STRUCTURE OF THE THESIS.....</b>	<b>1</b>
REFERENCES .....	6
<b>2 A CRITICAL REVIEW: POLYMER AND HYDROGEL DEPOSITION TECHNIQUES USED FOR PREPARATION OF OPTICAL AND ELECTROCHEMICAL BIOANALYTICAL SENSORS.....</b>	<b>10</b>
2.1 SHORT INTRODUCTION TO HYDROGELS AND POLYMERS .....	12
2.2 PRINCIPLES AND APPLICATIONS OF MEMBRANE DEPOSITION TECHNIQUES .....	13
2.2.1 <i>Drop-Coating</i> .....	13
2.2.2 <i>Solution Casting</i> .....	15
2.2.3 <i>Knife-Coating</i> .....	16
2.2.4 <i>Spray-Coating</i> .....	18
2.2.5 <i>Dip-Coating</i> .....	19
2.2.6 <i>Spin-Coating</i> .....	20
2.2.7 <i>Electrospinning</i> .....	22
2.2.8 <i>Electrochemical Deposition</i> .....	23
2.3 STRENGTHS AND WEAKNESSES OF THE DEPOSITION TECHNIQUES.....	25
2.4 CONCLUSION AND PERSPECTIVE .....	31
2.5 ACKNOWLEDGEMENT.....	31
2.6 REFERENCES.....	32

---

<b>3</b>	<b>ELECTROCHEMICAL MULTI-ANALYTE POINT-OF-CARE PERSPIRATION SENSORS USING ON-CHIP THREE-DIMENSIONAL GRAPHENE ELECTRODES.....</b>	<b>37</b>
3.1	INTRODUCTION.....	40
3.2	EXPERIMENTAL .....	42
3.2.1	<i>Materials</i> .....	42
3.2.2	<i>Methods</i> .....	44
3.3	RESULTS AND DISCUSSION .....	49
3.4	CONCLUSION .....	59
3.5	ACKNOWLEDGEMENT.....	59
3.6	REFERENCES .....	60
3.7	SUPPORTING INFORMATION .....	64
3.7.1	<i>Laser-Scribing Process</i> .....	64
3.7.2	<i>Optimization and Modification Process for Potentiometric Potassium Ion Sensor</i> .....	65
3.7.3	<i>Optimization of Impedance-based Electrolyte Sensor</i> .....	69
3.7.4	<i>Optimization of Amperometric Biosensors</i> .....	72
3.7.5	<i>Glucose Biosensor Performance on Skin</i> .....	78
3.7.6	<i>Lactate Biosensors' Performance Under Different Conditions</i> .....	79
3.7.7	<i>Characterization of Electrode Material</i> .....	80
<b>4</b>	<b>EUROPIUM(III) TETRACYCLINE AS PROBE FOR DETECTION OF HYDROGEN PEROXIDE IN MICROPLATE ASSAYS .....</b>	<b>82</b>
4.1	INTRODUCTION.....	84
4.2	EXPERIMENTAL .....	87
4.2.1	<i>Materials and Equipment</i> .....	87
4.2.2	<i>Preparation of Solutions</i> .....	87
4.2.3	<i>Methods</i> .....	92
4.2.4	<i>Statistics and Data Evaluation</i> .....	98
4.3	RESULTS AND DISCUSSION .....	99
4.3.1	<i>Detection of Hydrogen Peroxide, Glucose and Lactate</i> .....	99
4.3.2	<i>Interference Studies</i> .....	107
4.3.3	<i>Leakage Studies</i> .....	108
4.3.4	<i>Storage Stability Studies</i> .....	110
4.4	CONCLUSION .....	113
4.5	ACKNOWLEDGEMENT.....	114
4.6	REFERENCES .....	115
4.7	SUPPORTING INFORMATION .....	117
4.7.1	<i>Influence of Different Cutting Techniques</i> .....	117
4.7.2	<i>Interference Study</i> .....	118

<b>5</b>	<b>COMBINATION OF EUROPIUM(III) TETRACYCLINE WITH OXIDASE ENZYMES IN BIOCOMPATIBLE HYDROGELS FOR DETECTION OF HYDROGEN PEROXIDE IN FLOW-THROUGH SYSTEMS.....</b>	<b>119</b>
5.1	INTRODUCTION.....	121
5.2	EXPERIMENTAL .....	123
5.2.1	<i>Materials and Equipment</i> .....	123
5.2.2	<i>Preparation of Solutions</i> .....	124
5.2.3	<i>Methods</i> .....	127
5.2.4	<i>Statistics and Data Evaluation</i> .....	132
5.3	RESULTS AND DISCUSSION .....	134
5.3.1	<i>3-Layer System: D4-EuTc // LRP t 7016 // D4-GOx</i> .....	136
5.3.2	<i>Hydrogen Peroxide Detection</i> .....	138
5.3.3	<i>Glucose Detection</i> .....	139
5.3.4	<i>Leakage and Interference Study</i> .....	140
5.3.5	<i>Adjacently Placed Sensor Discs</i> .....	141
5.4	CONCLUSION .....	144
5.5	ACKNOWLEDGEMENT.....	144
5.6	REFERENCES.....	145
5.7	SUPPORTING INFORMATION .....	148
5.7.1	<i>Determination of Flow Speed of the Peristaltic Pump</i> .....	148
5.7.2	<i>3-Layered Sensor Discs in Flow Cell Setup</i> .....	148
5.7.3	<i>Determination of Eu(III) Content in 6 mm Disc via ICP-OES</i> .....	149
5.7.4	<i>General Investigations with 1 mM HP Solution in the Flow Cell</i> .....	150
5.7.5	<i>HP Detection</i> .....	152
5.7.6	<i>Leakage Study</i> .....	153
5.7.7	<i>Interference Study</i> .....	154
5.7.8	<i>Investigation of EuTc/GOx Ratio in Flow Cell Setup</i> .....	154
<b>6</b>	<b>CONCLUSION AND FUTURE PERSPECTIVES.....</b>	<b>157</b>
	REFERENCES .....	162
	<b>CURRICULUM VITAE.....</b>	<b>A</b>
	<b>PUBLICATIONS AND PRESENTATIONS.....</b>	<b>C</b>
	<b>EIDESSTÄTTLICHE ERKLÄRUNG.....</b>	<b>D</b>

# Summary

---

The main aspect of the thesis is the development of bio- and chemosensors for clinical and personal healthcare applications with new and common materials addressing important model analytes like glucose and lactate, but also potassium ions and electrolytes in general by optical and electrochemical detection methods. Since all developed bioanalytical sensors are exploiting different properties of hydrogels and polymers, a critical review highlights advantages and disadvantages of current polymer deposition techniques, and if a genuine commercialization of the presented sensor concepts is possible. It should also be mentioned that not just in the field of medical and point-of-care (POC) applications electrochemical and optical sensors and biosensors with polymeric layers are widely used, but for food safety and environmental issues, too.

A multianalyte sensor using exclusively laser-induced graphene (LIG)-based electrodes was developed for non-invasive eccrine sweat analysis. The relatively new material provides a 3-dimensional graphene-like structure, can be manufactured easier than any other carbon electrode also on industrial scale, and can be modified without large effort. Therefore, LIG is predestinated for affordable wearable POC sensors. It is demonstrated that LIG can address all three electrochemical sensing strategies (voltammetry, potentiometry, impedance) in a multianalyte system for sweat sensing.

A potentiometric potassium ion-selective electrode in combination with an electrodeposited Ag/AgCl reference electrode (RE) enabled the detection of potassium ions in the entire physiologically relevant range (1 mM to 500 mM) within seconds, unaffected by the presence of main interfering ions like chloride or sodium ions, and different sweat collecting materials. A kidney-shaped interdigitated unmodified LIG electrode allows the determination of the overall electrolyte concentration by electrochemical impedance spectroscopy at a fixed frequency. Enzyme-based strategies with amperometric detection share the common RE and were realized with Prussian blue as electron mediator and the biocompatible chitosan for enzyme immobilization and protection of the electrode. Using glucose and lactate oxidases, lower limits of detection of  $13.7 \pm 0.5 \mu\text{M}$  for glucose and  $28 \pm 3 \mu\text{M}$  for lactate were obtained, respectively. The sensor showed a good performance within the relevant pH range, with sweat collecting tissues, on a model skin system and furthermore in synthetic sweat as well as in artificial tear

fluid. Response time for each analytical cycle totals 75 seconds, and hence allows a quasi-continuous and simultaneous monitoring of all analytes. This multianalyte all-LIG system is therefore a practical, versatile, and most simple strategy for POC applications and has the potential to outcompete standard screen-printed electrodes.

The Europium(III) tetracycline complex (EuTc) is an optical probe for the sensitive detection of hydrogen peroxide (HP) at physiological relevant pH. In aqueous solution the inner coordination sphere of the  $\text{Eu}^{3+}$  central ion is surrounded by water molecules. This coordination leads to a quenched luminescence of the  ${}^5\text{D}_0 \rightarrow {}^7\text{F}_2$  transition of the lanthanide ion, detectable at 616 nm after an excitation at 405 nm. Reversible replacement of these water molecules by HP leads to an up to 16-fold enhancement of luminescence intensity. Combination of the probe with lactate oxidase (LOx) and glucose oxidase (GOx) forming HP as stoichiometric by-product during their catalytic reaction, enables the rapid and sensitive detection of the related substrates. The entrapment of the very selective enzyme and the sensitive luminescent probe within biocompatible hydrogels and polymers enlarges the thinkable bioanalytical applications enormously. The developed hydrogel-based sensor discs can be used in a microplate format as well as in flow-through systems for high-throughput detection and long-term monitoring.

Suitable hydrogels and polymers were investigated for the entrapment of the luminescent probe and the respective oxidase enzymes GOx and LOx. The polymer cocktails containing probe or enzyme were knife-coated with 30  $\mu\text{m}$  wet thickness on an in-house made coating device on transparent polyethylene terephthalate substrate sheets. Circular discs were hole-punched from the foils after drying and washing, and were stuck to a 96-well microplate. Within microplate assay approaches the systems were optimized regarding the used polymers and hydrogels, solvents, and the probe as well as the enzyme content.

A polyvinyl acetate/cellulose acetate (PVAc/CA) membrane was found as suitable for containing EuTc to detect HP. The probe was also embedded in a Hydromed® D4 layer protected by a PVAc/CA layer to reach a dynamic range from 10  $\mu\text{M}$  to 10 mM HP. Glucose samples up to 50 mM and lactate samples up to 20 mM are mixed with the respective enzyme and added to the discs in a 96-well plate. After 2 min to 5 min incubation time the luminescence is read out at 616 nm. D4-enzyme discs were produced and optimized to detect glucose and lactate under comparable conditions within the same dynamic range as mentioned above when the sample solution is mixed with EuTc solution in the microplate. The systems work at 25°C and 37°C. The discs can be stored light-protected for at least 6 months (probe discs) or up to 1 year (enzyme discs) at 4°C. They show no significant loss of probe or enzyme when in use for minimum 3 h at 37°C (probe discs) or 6 h at 25°C (enzyme discs). This fundamental work proves the reasonable application of EuTc and enzymes embedded in biocompatible

hydrogels for rapid hydrogen peroxide, glucose and lactate detection in a microplate format within physiological relevant concentrations and conditions and should be transferred into a flow-through system.

The combination of enzyme and probe in a one- or multilayer setup was investigated using different techniques since it simplifies the integration into a flow cell system, but up to now no satisfying solution was found. Therefore, the optimized EuTc and enzyme sensor discs were placed adjacently within the flow cell chamber to prove at least the fundamental concept of continuous monitoring. Some scope for further optimization regarding the perfect balance of probe/enzyme ratio and instrumental and experimental settings like flow speed and flow-cell geometry was left and discussed as future perspective.



# Zusammenfassung

---

Der Hauptaspekt dieser Dissertation ist die Entwicklung von Bio- und Chemosensoren für klinische und individuelle Gesundheitsanwendungen mit neuen und bekannten Materialien, die wichtige Modellanalyten wie Glucose und Lactat, aber auch Kaliumionen und Elektrolyte im Allgemeinen durch optische und elektrochemische Detektionsmethoden adressieren. Da alle entwickelten bioanalytischen Sensoren unterschiedliche Eigenschaften von Hydrogelen und Polymeren ausnutzen, hebt eine kritische Überprüfung die Vor- und Nachteile der aktuellen Polymerabscheidungstechniken hervor und ob eine echte Kommerzialisierung der vorgestellten Sensorkonzepte möglich ist. Erwähnenswert ist auch, dass elektrochemische und optische Sensoren sowie Biosensoren mit Polymerschichten nicht nur im Bereich der Medizin und Point-of-Care (POC)-Anwendungen weit verbreitet sind, sondern auch für Lebensmittelsicherheit und Umweltfragen.

Für die nicht-invasive Analyse von ekkrinem Schweiß wurde ein Multianalytensensor entwickelt, der ausschließlich auf laserinduzierten Graphen (LIG) Elektroden basiert. Das relativ neue Material bietet eine 3-dimensionale Graphen-ähnliche Struktur, lässt sich einfacher als jede andere kohlenstoffbasierte Elektrode auch im industriellen Maßstab herstellen und ohne großen Aufwand modifizieren und ist damit prädestiniert für erschwingliche Wearables and POC-Systeme. Es wird gezeigt, dass LIG alle drei elektrochemischen Messstrategien (Voltammetrie, Potentiometrie, Impedanz) in einem Multianalytensystem für die Detektion in Körperflüssigkeiten zusammenfassen kann.

Eine potentiometrische Kaliumionen-selektive Elektrode in Kombination mit einer galvanisch abgeschiedenen Ag/AgCl-Referenzelektrode (RE) ermöglicht den sekundenschnellen Nachweis von Kaliumionen im gesamten physiologisch relevanten Bereich (1 mM bis 500 mM), unabhängig von der Anwesenheit von Hauptstörionen wie Chlorid- oder Natriumionen und verschiedenen absorbierenden Materialien. Eine nierenförmig ineinandergreifende nichtmodifizierte LIG-Elektrode ermöglicht die Bestimmung der Gesamtelektrolytkonzentration durch elektrochemische Impedanzspektroskopie bei einer konstanten Frequenz. Die amperometrische Detektion mit enzymbasierten Strategien nutzt die gemeinsame RE. Die Arbeitselektrode wurde mit Berliner Blau als Elektronenmediator und einer biokompatiblen Chitosanschicht für die Enzymimmobilisierung und zum Schutz der Elektrode modifiziert. Unter

Verwendung von Glucoseoxidase (GOx) und Lactatoxidase (LOx) wurden untere Nachweisgrenzen von  $13,7 \pm 0,5 \mu\text{M}$  für Glucose bzw.  $28 \pm 3 \mu\text{M}$  für Lactat erzielt. Der Sensor zeigt eine gute Leistung im relevanten pH-Bereich, mit absorbierenden Geweben, auf einem Modellhautsystem und darüber hinaus in synthetischem Schweiß sowie in künstlicher Tränenflüssigkeit. Die Reaktionszeit für jeden Analysezyklus beträgt insgesamt 75 Sekunden und ermöglicht somit eine quasi-kontinuierliche und gleichzeitige Überwachung aller Analyten. Dieses Multianalyt-All-LIG-System ist daher eine praktische, vielseitige und einfachste Strategie für POC-Anwendungen und hat das Potenzial, standardmäßig genutzte siebgedruckte Elektroden zu übertreffen.

Der Europium(III)-Tetracyclin-Komplex (EuTc) ist eine optische Sonde zum sensitiven Nachweis von Wasserstoffperoxid (HP) bei physiologisch relevanten pH-Werten. In wässriger Lösung ist die innere Koordinationssphäre des  $\text{Eu}^{3+}$ -Zentralions von Wassermolekülen umgeben. Diese Koordination führt zu einer reduzierten Lumineszenz des  ${}^5\text{D}^0 \rightarrow {}^7\text{F}^2$ -Übergangs des Lanthanid-Ions, nachweisbar bei 616 nm nach einer Anregung bei 405 nm. Der reversible Austausch dieser Wassermoleküle durch HP führt zu einer bis zu 16-fachen Steigerung der Lumineszenzintensität. Die Kombination des Komplexes mit LOx und GOx, die bei ihrer katalytischen Reaktion HP als stöchiometrisches Nebenprodukt bilden, ermöglicht den schnellen und sensitiven Nachweis der jeweiligen Substrate. Der Einschluss des sehr selektiven Enzyms und der empfindlichen lumineszierenden Sonde in biokompatible Hydrogele und Polymere erweitert die denkbaren bioanalytischen Anwendungen enorm. Die entwickelten Hydrogel-basierten Sensor Discs können sowohl im Mikroplattenformat als auch in Durchflusssystemen zur Hochdurchsatzdetektion und Langzeitüberwachung eingesetzt werden.

Geeignete Hydrogele und Polymere wurden für den Einschluss der lumineszierenden Sonde und der entsprechenden Enzyme GOx und LOx untersucht. Die Polymercocktails, die die Sonde oder das Enzym enthielten, wurden mit einer Nassdicke von  $30 \mu\text{m}$  auf einer selbstentwickelten Beschichtungsvorrichtung auf transparente Polyethylenterephthalat-Substratfolien aufgetragen. Aus den Folien wurden nach dem Trocknen und Waschen kreisförmige Discs ausgestanzt und in eine 96-Well Microplate geklebt. Die Systeme wurden hinsichtlich der verwendeten Polymere und Hydrogele, Lösungsmittel sowie des Komplex- und Enzymgehalts innerhalb der Microplate Assays optimiert.

Eine Membran aus Polyvinylacetat/Celluloseacetat (PVAc/CA) wurde als geeignet gefunden, um EuTc sicher einzubetten und HP nachzuweisen. Die Sonde wurde auch in eine Hydromed® D4-Schicht eingebettet, die durch eine PVAc/CA-Schicht geschützt war, um einen dynamischen Messbereich zwischen  $10 \mu\text{M}$  bis  $10 \text{mM}$  HP zu erzielen. Glucoseproben bis  $50 \text{mM}$  und Lactatproben bis  $20 \text{mM}$  werden mit dem jeweiligen Enzym gemischt und auf die

Discs in einer 96-Well-Platte gegeben. Nach zwei bis fünf Minuten Inkubationszeit wird die Lumineszenzintensität bei 616 nm ausgelesen. D4-Enzym Discs wurden entwickelt und optimiert, um Glucose und Lactat unter vergleichbaren Bedingungen wie oben erwähnt nachzuweisen, wenn die Probenlösung mit EuTc-Lösung in der Microplate gemischt werden. Die Systeme funktionieren bei 25°C und 37°C. Die Discs können lichtgeschützt mindestens 6 Monate (EuTc Discs) bzw. bis zu 1 Jahr (Enzym Discs) bei 4°C gelagert werden. Die Discs zeigen keinen signifikanten EuTc- oder Enzymverlust, wenn sie über 3 h bei 37°C (EuTc Discs) oder 6 h bei 25 °C (Enzym Discs) verwendet werden. Diese Grundlagenarbeit beweist die sinnvolle Anwendung von EuTc und Enzymen eingebettet in biokompatible Hydrogele zum schnellen Nachweis von Wasserstoffperoxid, Glucose und Lactate im Microplate Format für physiologisch relevante Konzentrationen und unter ebensolchen Bedingungen. Die Discs sollen im weiteren Verlauf in ein Durchflusssystem überführt werden.

Die Kombination von Enzym und Sonde in einem ein- oder mehrschichtigen Aufbau wurde mit verschiedenen Techniken versucht zu realisieren, da dies die Integration in ein Durchflusssystem vereinfacht, aber bisher wurde keine zufriedenstellende Lösung gefunden. Deshalb wurden die optimierten EuTc Discs und Enzym Discs nebeneinander in der Durchflusszellenkammer platziert um zumindest das grundlegende Konzept der kontinuierlichen Überwachung beweisen zu können. Ein Spielraum für weitere Optimierungen hinsichtlich der perfekten Balance zwischen EuTc/Enzym-Verhältnis und instrumentellen und experimentellen Einstellungen wie Strömungsgeschwindigkeit und Strömungszellengeometrie bleibt weiterhin offen und wird, unter anderem, als Zukunftsaussichten diskutiert.

# 1 Relevance and Structure of the Thesis

---

The thesis focuses on the development of bio- and chemosensors for clinical and personal healthcare applications with new and common materials addressing mainly the important model analytes glucose and lactate, but also potassium ions and electrolytes in general by optical and electrochemical detection methods.

*Sentire*, Latin for “to perceive”, is the etymological origin of the word “sensor”. Generally spoken, a sensor is a device which responds to a stimulus, e.g. optical, electrical, physical, etc. and transmit it into a signal [1]. According to the IUPAC definition, “a biosensor is a device that uses specific biochemical reactions mediated by isolated enzymes, immunosystems, tissues, organelles or whole cells to detect chemical compounds usually by electrical, thermal or optical signals” [2]. Within the scope of the thesis, mainly enzyme-based biosensors, but also sensors in common understanding exploiting different polymers and hydrogels were investigated and optimized.

Nearly half a billion of people worldwide suffering from diabetes [3]. This disease is one of the leading causes of death all over the world as the World Health Organization states [3]. Therefore, the glucose sensor is still one of the most popular sensors and glucose, beside lactate and potassium ions, an acclaimed model analyte for the development of new sensors or sensor concepts [4] within the last two decades as a “Web of Science” record analysis discloses (**Figure 1.1 A**). Glucose sensors are available on electrochemical [5–9] and optical [10–13] detection platforms, with [5–7, 9, 12, 13] and without [10, 11] enzymes, whereby nearly always glucose oxidase (GOx) is used as biorecognition element.

Lactate level is important for athletics to adapt and improve their endurance and power training. It gives important insight into oxygen supply in tissue and the entire anaerobic metabolism in muscles [9]. During complicated surgeries or in septic patients controlling the lactate concentration helps to intervene in an early state, prevent septic shocks and reduce the mortality [14–16]. For lactate quantification, electrochemical [8, 9, 17] and optical [14, 15] biosensors are available which are mostly combined with lactate oxidase (LOx) or lactate dehydrogenase.

The most common electrolyte disturbance identified in clinical practice is an abnormal potassium ion level which affects primarily the cardiac, neuromuscular and gastrointestinal systems [18]. Therefore, the demand for developing sensors monitoring potassium ion concentration in blood or other body fluids is present over time and still rising (**Figure 1.1 A**). Since the very beginning in the 1960's as Pressman *et al* identified valinomycin as a selective ionophore for potassium transport in membranes [19, 20], it is used up to now for ion-selective electrodes (ISE) [9, 21–23] and optodes [24–26] in chemo- and biosensors. In any case, the valinomycin is entrapped in a polymeric film to allow almost solely potassium ions access to the transducer or recognition element through the membrane.

The use of hydrogels, polymers or other not further defined membranes in combination with a sensor in general or a biosensor in particular, has risen constantly within the last 30 years as a “Web of Science” record count analysis reveals (**Figure 1.1 B**) [4]. This trend is understandable regarding the numerous advantageous and adaptable properties of natural and synthetic polymers with regard to mesh size, stability, water retention ability, swelling behavior, degradability, sterilizability, and many more [27–32].

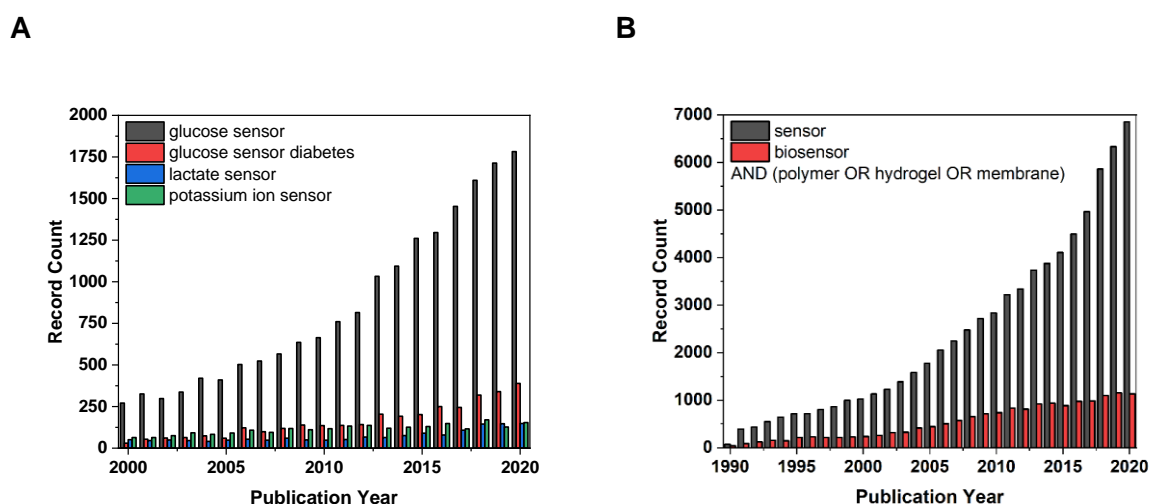


**Figure 1.1** Web of Science record count for **A** “glucose sensor”, “glucose sensor diabetes”, “lactate sensor” and “potassium ion sensor” between 2000 and 2021 and **B** “sensor AND (polymer OR hydrogel OR membrane)” and “biosensor AND (polymer OR hydrogel OR membrane)” between 1990 and 2020 [4].

Already in 1953, Clark *et al* used a platinum electrode with a cellophane protection layer for electrochemical determination of blood oxygen during cardiovascular surgeries [33]. He and his group were the pioneers in biosensor development. Just a few years later, in 1960, O. Wichterle and D. Lím discussed in a *Nature* article the relevance of biocompatible polymers with tunable properties for clinical and biomedical applications [34]. They stated the necessarily hydrophilic three-dimensional materials have a structure permitting the desired water content and allow permeability for metabolites. Important terminology for polymers and hydrogels was summarized in the year 1996 by Jenkins *et al* [35] and reflect the IUPAC

recommendations up to now: A macromolecule or polymer molecule is a molecule of high relative molecular mass structured from repetitive units of molecules of low relative molecular mass. It does not change the overall properties of the polymer if some of these smaller molecules or monomers are removed or added. The term hydrogel, first used in 1894 to describe a colloidal gel [36], is a special form of a polymer with remarkable hydrophilicity.

Since all the developed bioanalytical sensors were exploiting different properties of hydrogels and polymers, a critical review opens the thesis in following **Chapter 2**. Focus of the critical analysis is set on the polymer deposition techniques, if the polymers and hydrogels are suitable for the desired application, and if a genuine commercialization of the concept is possible. It should also be mentioned that not just in the field of medical and point-of-care (POC) applications sensors and biosensors with polymeric layers are widely used. Monitoring of seawater [37, 38] to observe the marine salt concentration or pH, checking wastewater [39] and soil [40] for pollutants and toxic compounds, or the detection of pesticides [41] on crops. These are just some examples for environmental and agri-food applications. Food safety is another very central topic and goes hand-in-hand with monitoring of the environment. Timely detection of spoiled food [42], especially sea food [43] or comprised toxins [44] and pathogens [45] can prevent many people from getting sick or even dying. Little noticed but a substantial worldwide humanitarian safety risk is caused by left behind buried landmines and explosives [46]. The fast and save detection of these can be realized with polymer-based biosensors [46]. Optical or electrochemical sensors are available in those fields, and even combined in sensors harnesses electrochemical luminescence [44, 45, 47] or bioluminescence [46].

Still most important for the detection or monitoring of the above named clinically relevant analytes glucose and lactate is blood or serum. But sampling is elaborately, cumbersome, and often painful for the patient. More affordable are non-invasive sampling techniques and therefore the analysis of other biological fluids like sweat [8, 9, 22, 48], tear fluid [9, 49], saliva [7], or urine [50, 51]. Even breath analyzers recognizing volatile organic compounds like acetone in diabetic patients are currently investigated [52]. Monitoring of those with a wearable, small, and ideally not recognizable device with a long lifetime is a growing trend within the last decades for POC and homecare nursery applications [9]. Smartphones can simplify the readout of many devices and deliver easy understandable results to the users without a medical background or special knowledge [10, 53].

An electrochemical multi-analyte platform for long-term monitoring with non-invasive sweat sampling technique is realized with modified graphene electrodes for a wearable device (**Chapter 3**). Laser-induced graphene (LIG) is presented and its advantages for POC applications are pointed out like the cost-effective mass production and easy modification of

the graphene-like electrode material. This relatively new material with its outstanding properties is suitable for wearable devices due to its stability and flexibility. Nearly every design can easily be realized and “printed” by a laser on a polymeric substrate like polyimide. Important information besides lactate and glucose levels are the hydration state and especially the potassium concentrations. Those can be gained from analyzing the eccrine sweat by wearable patches with and without more or less complex microfluidic systems [54–57].

An ISE is integrated in the wearable sweat-sensing device by drop-coating a valinomycin-polymer mixture on a circular LIG electrode for potentiometric potassium ion detection. Another circular LIG electrode is electrochemically modified with  $\text{AgNO}_3$  and  $\text{NaCl}$  solutions to obtain a sharable  $\text{Ag}/\text{AgCl}$  reference electrode. A polymeric protection membrane minimizes the cross-sensitivity towards chloride ions. The LIG working electrode of the multi-electrode setup was modified with a chemically deposited Prussian blue coating and drop-coated chitosan and enzyme layer to obtain the oxidase-based glucose and lactate sensors with amperometric detection of the stoichiometrically produced hydrogen peroxide. The counter electrode as well as the two kidney-shaped electrodes for impedimetric detection of the overall electrolyte concentration is completely unmodified LIG. The chapter shows the entire optimization process up to the final multianalyte sensor concept tested with artificial body fluid samples and filter paper as sweat collection pad on a skin model to prove the entire concept using LIG as commercially relevant POC electrode material of the future.

Since the early 2000's the concept of the hydrogen peroxide (HP) sensitive Europium(III) tetracycline (EuTc) complex is well-investigated by Wolfbeis, Dürkop, and others, and it is still an important luminescent probe for bioanalytical applications [58–62]. The complex is predestinated for applications at physiologically relevant pH levels in aqueous solutions due to its high sensitivity around pH 7 and its reversible luminescence intensity depending on the recent HP concentration. The combination of this sensitive lanthanide probe with the specific enzyme reactions of GOx and LOx producing stoichiometric amounts of HP opens a wide field of interesting and medical relevant applications for glucose and lactate detection. **Chapter 4** and **Chapter 5** focus on using the EuTc probe in a microplate format for POC applications and investigation and optimization of an approach for long-term monitoring in flow-through systems for clinical applications. The probe complex and the enzymes must be incorporated in a hydrogel or polymer to realize polymeric sensor discs for actually relevant applications in the future.

Analysis tools like simple microplate assays with fast optical readout by fluorescence techniques were investigated for hydrogen peroxide, glucose, and lactate detection as precursor strategy for online monitoring of glucose and lactate with the EuTc probe (**Chapter 4**). Biocompatible hydrogels and polymers were used for the entrapment of

the luminescent probe and the respective oxidase enzymes GOx and LOx. The polymer cocktails containing probe and enzyme were knife-coated with an in-house made coating device on transparent polyethylene terephthalate substrate sheets. Within the microplate assay approach the systems were optimized regarding the used polymers and hydrogels, solvents, and the probe as well as the enzyme content. Hydromed® D4, a polyurethane-based hydrogel dissolved in ethanol/water and a polyvinyl acetate/cellulose acetate mixture dissolved in dimethylformamide/water or cyclohexanone/water were found to offer a perfect environment for the probe and both enzymes. Furthermore, the sensor cocktails showed perfect knife-coating and film building properties.

As final aim, an integrated system ideally containing the probe and the enzyme within a single polymeric layer should be investigated since there is still no relevant optical system for glucose and lactate available continuously monitoring patients on the intensive care station or during complicated surgeries [63–66]. Now, samples are still drawn from the patient, send to an analytical laboratory in- or outside of the hospital or clinic, and the results are sent back to the treating physician. This time-consuming approach can cost lives because critical or even life-threatening conditions in the lactate or glucose household of the patient are realized too late. Many approaches to fulfill the ambitious demands for a working integrated sensor system by combination of the probe and enzyme layer were investigated, tested, and optimized in the microplate format, and are discussed in the beginning of **Chapter 5**.

A very promising 3-layer approach was found where a D4-EuTc layer is protected by a polylactic acid-based membrane (PLA) and separated from the top D4-GOx layer. The system was transferred to an in-house made flow cell system and tested with glucose samples whereas no reaction towards any concentration change was observed. It was found that the single membranes work in the flow through system, but the PLA layer compromises the complex. This led to an ascending background signal over time which was falsely interpreted as concentration-dependent luminescence increase. Therefore, the optimized EuTc and enzyme sensor discs were placed adjacently within the flow cell chamber to prove at least the fundamental concept within the main part of **Chapter 5** and let some scope for further optimization regarding the perfect balance of probe/enzyme ratio and instrumental and experimental settings like flow speed and flow-cell geometry.

Finally, in **Chapter 6** all relevant results are wrapped up briefly. A conclusion of the thesis and future perspectives of the investigated concepts are given emphasizing the advantages and disadvantages of the strategies.



## References

1. "Sensor." Merriam-Webster.com Dictionary, Merriam-Webster, <https://www.merriam-webster.com/dictionar>.
2. Gold V. The IUPAC Compendium of Chemical Terminology. Research Triangle Park, NC: International Union of Pure and Applied Chemistry (IUPAC); 2019.
3. WHO Health Topics - Diabetes. <https://www.who.int/health-topics/diabetes> (accessed January 14th, 2022).
4. Clarivate Analytics. Web of Science. <https://www.webofscience.com/>(accessed December 22th, 2021).
5. Zohourtalab A, Razmi H. Selective Determination of Glucose in Blood Plasma by Using an Amperometric Glucose Biosensor Based on Glucose Oxidase and a Chitosan/ Nafion/ IL/Ferrocene Composite Film. *Iranian Journal of Analytical Chemistry*. 2018;5:9–16.
6. Yezer I, Demirkol DO. Cellulose acetate–chitosan based electrospun nanofibers for bio-functionalized surface design in biosensing. *Cellulose*. 2020; <https://doi.org/10.1007/s10570-020-03486-y>
7. Arakawa T, Tomoto K, Nitta H, Toma K, Takeuchi S, Sekita T, Minakuchi S, Mitsubayashi K. A Wearable Cellulose Acetate-Coated Mouthguard Biosensor for In Vivo Salivary Glucose Measurement. *Anal Chem*. 2020; <https://doi.org/10.1021/acs.analchem.0c01201>
8. Lei Y, Zhao W, Zhang Y, Jiang Q, He J-H, Baeumner AJ, Wolfbeis OS, Wang ZL, Salama KN, Alshareef HN. A MXene-Based Wearable Biosensor System for High-Performance In Vitro Perspiration Analysis. *Small*. 2019; <https://doi.org/10.1002/smll.201901190>
9. Bauer M, Wunderlich L, Weinzierl F, Lei Y, Duerkop A, Alshareef HN, Baeumner AJ. Electrochemical multi-analyte point-of-care perspiration sensors using on-chip three-dimensional graphene electrodes. *Anal Bioanal Chem*. 2021; <https://doi.org/10.1007/s00216-020-02939-4>
10. Elsherif M, Hassan MU, Yetisen AK, Butt H. Wearable Contact Lens Biosensors for Continuous Glucose Monitoring Using Smartphones. *ACS Nano*. 2018; <https://doi.org/10.1021/acsnano.8b00829>
11. Guo J, Zhou B, Du Z, Yang C, Kong L, Xu L. Soft and plasmonic hydrogel optical probe for glucose monitoring. *Nanophotonics*. 2021; <https://doi.org/10.1515/nanoph-2021-0360>
12. Yu S, Ding L, Lin H, Wu W, Huang J. A novel optical fiber glucose biosensor based on carbon quantum dots-glucose oxidase/cellulose acetate complex sensitive film. *Biosens Bioelectron*. 2019; <https://doi.org/10.1016/j.bios.2019.111760>
13. Chen K-C, Li Y-L, Wu C-W, Chiang C-C. Glucose Sensor Using U-Shaped Optical Fiber Probe with Gold Nanoparticles and Glucose Oxidase. *Sensors (Basel)*. 2018; <https://doi.org/10.3390/s18041217>
14. Biswas A, Bornhoeft LR, Banerjee S, You Y-H, McShane MJ. Composite Hydrogels Containing Bioactive Microreactors for Optical Enzymatic Lactate Sensing. *ACS Sens*. 2017; <https://doi.org/10.1021/acssensors.7b00648>
15. Calabria D, Caliceti C, Zangheri M, Mirasoli M, Simoni P, Roda A. Smartphone-based enzymatic biosensor for oral fluid L-lactate detection in one minute using confined multilayer paper reflectometry. *Biosens Bioelectron*. 2017; <https://doi.org/10.1016/j.bios.2017.02.053>
16. Park MS. Recent lactate findings: is repeated serum lactate testing necessary in septic shock patients? *Acute Crit Care*. 2019; <https://doi.org/10.4266/acc.2019.00528>
17. Andrus LP, Unruh R, Wisniewski NA, McShane MJ. Characterization of Lactate Sensors Based on Lactate Oxidase and Palladium Benzoporphyrin Immobilized in Hydrogels. *Biosensors (Basel)*. 2015; <https://doi.org/10.3390/bios5030398>
18. Schaefer TJ, Wolford RW. Disorders of potassium. *Emerg Med Clin North Am*. 2005; <https://doi.org/10.1016/j.emc.2005.03.016>
19. Moore C, Pressman BC. Mechanism of action of valinomycin on mitochondria. *Biochemical and Biophysical Research Communications*. 1964; [https://doi.org/10.1016/0006-291X\(64\)90505-4](https://doi.org/10.1016/0006-291X(64)90505-4)

20. Pressman BC. Induced active transport of ions in mitochondria. *Proc Natl Acad Sci U S A*. 1965; <https://doi.org/10.1073/pnas.53.5.1076>
21. Parrilla M, Cuartero M, Padrell Sánchez S, Rajabi M, Roxhed N, Niklaus F, Crespo GA. Wearable All-Solid-State Potentiometric Microneedle Patch for Intradermal Potassium Detection. *Anal Chem*. 2019; <https://doi.org/10.1021/acs.analchem.8b04877>
22. Zhang S, Zahed MA, Sharifuzzaman M, Yoon S, Hui X, Chandra Barman S, Sharma S, Yoon HS, Park C, Park JY. A wearable battery-free wireless and skin-interfaced microfluidics integrated electrochemical sensing patch for on-site biomarkers monitoring in human perspiration. *Biosens Bioelectron*. 2021; <https://doi.org/10.1016/j.bios.2020.112844>
23. Wang L, Wang L, Zhang Y, Pan J, Li S, Sun X, Zhang B, Peng H. Weaving Sensing Fibers into Electrochemical Fabric for Real-Time Health Monitoring. *Adv. Funct. Mater*. 2018; <https://doi.org/10.1002/adfm.201804456>
24. Kassal P, Sigurnjak M, Steinberg IM. Paper-based ion-selective optodes for continuous sensing: Reversible potassium ion monitoring. *Talanta*. 2019; <https://doi.org/10.1016/j.talanta.2018.09.031>
25. Stelmach E, Maksymiuk K, Michalska A. Dual Sensitivity—Potentiometric and Fluorimetric—Ion-Selective Membranes. *Anal Chem*. 2021; <https://doi.org/10.1021/acs.analchem.1c03193>
26. Tribuser L, Borisov SM, Klimant I. Tuning the sensitivity of fluoroionophore-based K<sup>+</sup> sensors via variation of polymer matrix: A comparative study. *Sensors and Actuators B: Chemical*. 2020; <https://doi.org/10.1016/j.snb.2020.127940>
27. Fu J, Het Panhuis M in. Hydrogel properties and applications. *J Mater Chem B*. 2019; <https://doi.org/10.1039/c9tb90023c>
28. Sun X, Agate S, Salem KS, Lucia L, Pal L. Hydrogel-Based Sensor Networks: Compositions, Properties, and Applications-A Review. *ACS Appl Bio Mater*. 2021; <https://doi.org/10.1021/acsabm.0c01011>
29. Chen G, Tang W, Wang X, Zhao X, Chen C, Zhu Z. Applications of Hydrogels with Special Physical Properties in Biomedicine. *Polymers*. 2019; <https://doi.org/10.3390/polym11091420>
30. Mishra S, Rani P, Sen G, Dey KP. Preparation, Properties and Application of Hydrogels: A Review. In: Thakur VK, Thakur MK, editors. *Hydrogels. Recent Advances*. Singapore: Springer Singapore; 2018. pp. 145–173.
31. Bashir S, Hina M, Iqbal J, Rajpar AH, Mujtaba MA, Alghamdi NA, Wageh S, Ramesh K, Ramesh S. Fundamental Concepts of Hydrogels: Synthesis, Properties, and Their Applications. *Polymers*. 2020; <https://doi.org/10.3390/polym12112702>
32. Galante R, Pinto TJA, Colaço R, Serro AP. Sterilization of hydrogels for biomedical applications: A review. *J Biomed Mater Res B Appl Biomater*. 2018; <https://doi.org/10.1002/jbm.b.34048>
33. Clark LC, Wolf R, Granger D, Taylor Z. Continuous recording of blood oxygen tensions by polarography. *J Appl Physiol*. 1953; <https://doi.org/10.1152/jappl.1953.6.3.189>
34. Wichterle O, Lím D. Hydrophilic Gels for Biological Use. *Nature*. 1960; <https://doi.org/10.1038/185117a0>
35. Jenkins AD, Kratochvíl P, Stepto RFT, Suter UW. Glossary of basic terms in polymer science (IUPAC Recommendations 1996). *Pure and Applied Chemistry*. 1996; <https://doi.org/10.1351/pac199668122287>
36. Thakur S, Thakur VK, Arotiba OA. History, Classification, Properties and Application of Hydrogels: An Overview. In: *Hydrogels*: Springer, Singapore; 2018. pp. 29–50.
37. Müller BJ, Rappitsch T, Staudinger C, Rüschtz C, Borisov SM, Klimant I. Sodium-Selective Fluoroionophore-Based Optodes for Seawater Salinity Measurement. *Anal Chem*. 2017; <https://doi.org/10.1021/acs.analchem.7b01373>
38. Staudinger C, Strobl M, Breininger J, Klimant I, Borisov SM. Fast and stable optical pH sensor materials for oceanographic applications. *Sensors and Actuators B: Chemical*. 2019; <https://doi.org/10.1016/j.snb.2018.11.048>

39. Ashrafi, Sýs, Sedláčková, Farag, Adam, Přibyl, Richtera. Application of the Enzymatic Electrochemical Biosensors for Monitoring Non-Competitive Inhibition of Enzyme Activity by Heavy Metals. *Sensors*. 2019; <https://doi.org/10.3390/s19132939>
40. Bae JW, Seo HB, Belkin S, Gu MB. An optical detection module-based biosensor using fortified bacterial beads for soil toxicity assessment. *Anal Bioanal Chem*. 2020; <https://doi.org/10.1007/s00216-020-02469-z>
41. Roushani M, Nezhadali A, Jalilian Z. An electrochemical chlorpyrifos aptasensor based on the use of a glassy carbon electrode modified with an electropolymerized aptamer-imprinted polymer and gold nanorods. *Microchimica Acta*. 2018; <https://doi.org/10.1007/s00604-018-3083-0>
42. Abdalhai MH, Fernandes AM, Xia X, Musa A, Ji J, Sun X. Electrochemical Genosensor To Detect Pathogenic Bacteria (*Escherichia coli* O157:H7) As Applied in Real Food Samples (Fresh Beef) To Improve Food Safety and Quality Control. *J Agric Food Chem*. 2015; <https://doi.org/10.1021/acs.jafc.5b00675>
43. Yurova NS, Danchuk A, Mobarez SN, Wongkaew N, Rusanova T, Baeumner AJ, Duerkop A. Functional electrospun nanofibers for multimodal sensitive detection of biogenic amines in food via a simple dipstick assay. *Anal Bioanal Chem*. 2018; <https://doi.org/10.1007/s00216-017-0696-9>
44. Xiaosheng Shen, Mingli Liu, Cong Kong, Wenlei Zhai, Essy Kouadio Fodjo, Youqiong Cai. Chitosan and nafion assisted modification of enzyme-free electrochemical immunosensors for the detection of tetrodotoxin.
45. Chen S, Chen X, Zhang L, Gao J, Ma Q. Electrochemiluminescence Detection of *Escherichia coli* O157:H7 Based on a Novel Polydopamine Surface Imprinted Polymer Biosensor. *ACS Appl Mater Interfaces*. 2017; <https://doi.org/10.1021/acsami.6b12455>
46. Shemer B, Shpigel E, Hazan C, Kabessa Y, Agranat AJ, Belkin S. Detection of buried explosives with immobilized bacterial bioreporters. *Microb Biotechnol*. 2021; <https://doi.org/10.1111/1751-7915.13683>
47. Schuck A, Kim HE, Moreira JK, Lora PS, Kim Y-S. A Graphene-Based Enzymatic Biosensor Using a Common-Gate Field-Effect Transistor for L-Lactic Acid Detection in Blood Plasma Samples. *Sensors*. 2021; <https://doi.org/10.3390/s21051852>
48. Lin S, Wang B, Zhao Y, Shih R, Cheng X, Yu W, Hojaiji H, Lin H, Hoffman C, Ly D, Tan J, Chen Y, Di Carlo D, Milla C, Emaminejad S. Natural Perspiration Sampling and in Situ Electrochemical Analysis with Hydrogel Micropatches for User-Identifiable and Wireless Chemo/Biosensing. *ACS Sens*. 2020; <https://doi.org/10.1021/acssensors.9b01727>
49. Ruan J-L, Chen C, Shen J-H, Zhao X-L, Qian S-H, Zhu Z-G. A Gelated Colloidal Crystal Attached Lens for Noninvasive Continuous Monitoring of Tear Glucose. *Polymers*. 2017; <https://doi.org/10.3390/polym9040125>
50. Conte F, van Buuringen N, Voermans NC, Lefeber DJ. Galactose in human metabolism, glycosylation and congenital metabolic diseases: Time for a closer look. *Biochim Biophys Acta Gen Subj*. 2021; <https://doi.org/10.1016/j.bbagen.2021.129898>
51. Wang Q, Liu Y, Campillo-Brocal JC, Jiménez-Quero A, Crespo GA, Cuartero M. Electrochemical biosensor for glycine detection in biological fluids. *Biosens Bioelectron*. 2021; <https://doi.org/10.1016/j.bios.2021.113154>
52. Worrall AD, Qian Z, Bernstein JA, Angelopoulos AP. Water-Resistant Polymeric Acid Membrane Catalyst for Acetone Detection in the Exhaled Breath of Diabetics. *Anal Chem*. 2018; <https://doi.org/10.1021/acs.analchem.7b03808>
53. Banik S, Melanthota SK, Arbaaz, Vaz JM, Kadambalithaya VM, Hussain I, Dutta S, Mazumder N. Recent trends in smartphone-based detection for biomedical applications: a review. *Anal Bioanal Chem*. 2021; <https://doi.org/10.1007/s00216-021-03184-z>
54. Chung M, Fortunato G, Radacsi N. Wearable flexible sweat sensors for healthcare monitoring: a review. *J R Soc Interface*. 2019; <https://doi.org/10.1098/rsif.2019.0217>
55. Hoekstra R, Blondeau P, Andrade FJ. IonSens: A Wearable Potentiometric Sensor Patch for Monitoring Total Ion Content in Sweat. *Electroanalysis*. 2018; <https://doi.org/10.1002/elan.201800128>

56. Karpova EV, Shcherbacheva EV, Galushin AA, Vokhmyanina DV, Karyakina EE, Karyakin AA. Noninvasive Diabetes Monitoring through Continuous Analysis of Sweat Using Flow-Through Glucose Biosensor. *Anal Chem.* 2019; <https://doi.org/10.1021/acs.analchem.8b05928>
57. Nyein HYY, Tai L-C, Ngo QP, Chao M, Zhang GB, Gao W, Bariya M, Bullock J, Kim H, Fahad HM, Javey A. A Wearable Microfluidic Sensing Patch for Dynamic Sweat Secretion Analysis. *ACS Sens.* 2018; <https://doi.org/10.1021/acssensors.7b00961>
58. Wolfbeis OS, Dürkop A, Wu M, Lin Z. A Europium-Ion-Based Luminescent Sensing Probe for Hydrogen Peroxide. *Angew. Chem. Int. Ed.* 2002; [https://doi.org/10.1002/1521-3773\(20021202\)41:23<4495:AID-ANIE4495>3.0.CO;2-I](https://doi.org/10.1002/1521-3773(20021202)41:23<4495:AID-ANIE4495>3.0.CO;2-I)
59. Wolfbeis OS, Schäferling M, Dürkop A. Reversible Optical Sensor Membrane for Hydrogen Peroxide Using an Immobilized Fluorescent Probe, and its Application to a Glucose Biosensor. *Microchimica Acta.* 2003; <https://doi.org/10.1007/s00604-003-0090-5>
60. Wu M, Lin Z, Dürkop A, Wolfbeis OS. Time-resolved enzymatic determination of glucose using a fluorescent europium probe for hydrogen peroxide. *Anal Bioanal Chem.* 2004; <https://doi.org/10.1007/s00216-004-2785-9>
61. Dürkop A, Wolfbeis OS. Nonenzymatic direct assay of hydrogen peroxide at neutral pH using the Eu<sub>3</sub>Tc fluorescent probe. *J Fluoresc.* 2005; <https://doi.org/10.1007/s10895-005-2984-6>
62. Courrol L, Samad R. Applications of Europium Tetracycline Complex: A Review. *CPA.* 2008; <https://doi.org/10.2174/157341208786306216>
63. Ganter M, Zollinger A. Continuous intravascular blood gas monitoring: development, current techniques, and clinical use of a commercial device. *Br J Anaesth.* 2003; <https://doi.org/10.1093/bja/aeg176>
64. Gelsomino S, Lorusso R, Livi U, Romagnoli S, Romano SM, Carella R, Lucà F, Billè G, Matteucci F, Renzulli A, Bolotin G, Cicco G de, Stefano P, Maessen J, Gensini GF. Assessment of a continuous blood gas monitoring system in animals during circulatory stress. *BMC Anesthesiol.* 2011; <https://doi.org/10.1186/1471-2253-11-1>
65. Kuster N, Bargnoux AS, Badiou S, Dupuy A-M, Piéroni L, Cristol JP. Multilevel qualification of a large set of blood gas analyzers: Which performance goals? *Clin Biochem.* 2019; <https://doi.org/10.1016/j.clinbiochem.2019.09.005>
66. Philani Buthelezi E, Rampota E, Mphogo M, Marule F, Moshen Tanyanyiwa D. Point of Care Blood Gas Analyser Verification at the Largest Academic Hospital in Southern Hemisphere Revived by Coronavirus Calls for Tests to Be Verified. *PLM.* 2020; <https://doi.org/10.11648/j.plm.20200402.11>

## 2 A Critical Review: Polymer and Hydrogel Deposition Techniques Used for Preparation of Optical and Electrochemical Bioanalytical Sensors

---

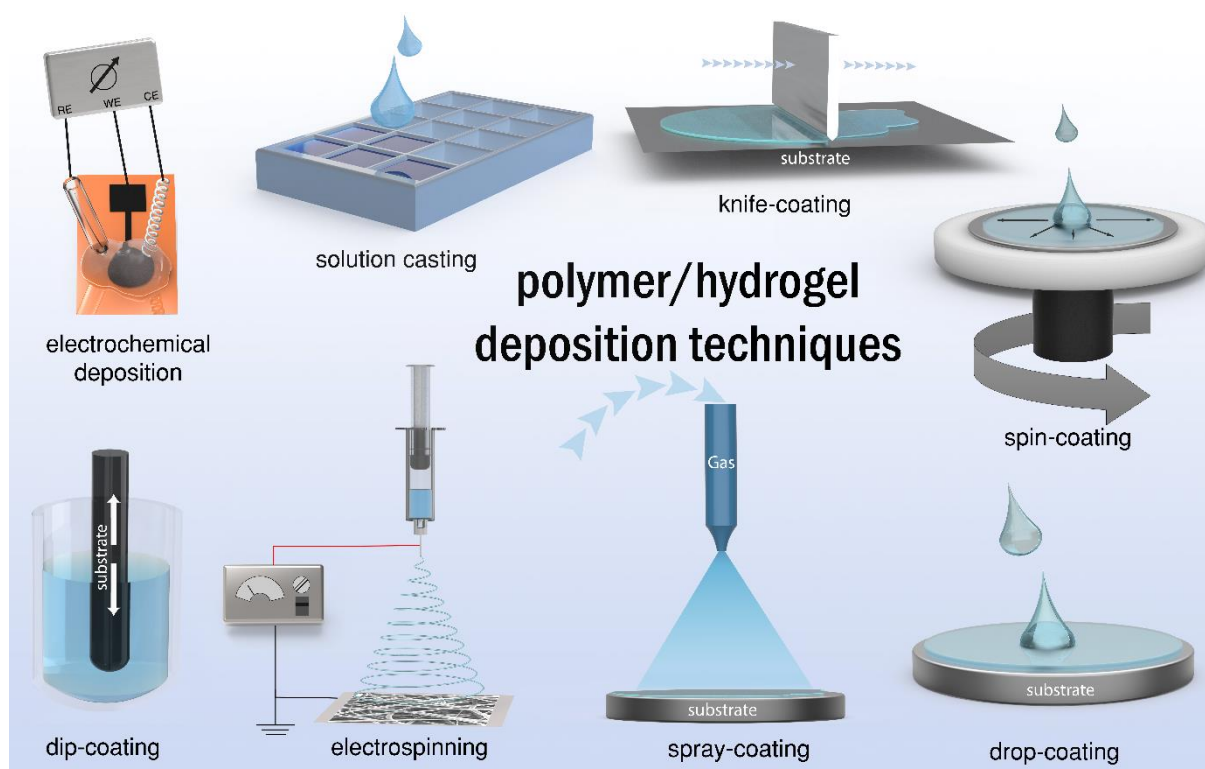
### Abstract

Sensors, ranging from *in vivo* through to single-use systems, employ protective membranes or hydrogels to enhance sample collection or serve as filters, to immobilize or entrap probes or receptors, or to stabilize and enhance a sensor's lifetime. Furthermore, many applications demand specific requirements such as biocompatibility and non-fouling properties for *in vivo* applications, or fast and inexpensive mass production capabilities for single-use sensors. We critically evaluated how membrane materials and their deposition methods impact optical and electrochemical systems with special focus on analytical figures of merit and potential toward large scale production.

Over the course of the last five years, most sensing applications within healthcare diagnostics included glucose, lactate, uric acid, O<sub>2</sub>, H<sup>+</sup> ions, and some specific metabolites and markers. In the case of food safety and environmental monitoring, the choice of analytes was much more comprehensive regarding a variety of natural and synthetic toxicants like bacteria, pesticides, or pollutants and other relevant substances.

**Keywords:** critical review, optical and electrochemical (bio)sensors, hydrogels and polymers, deposition techniques, commercialization

## Graphical Abstract



**A shortened version of this chapter will be submitted as critical review.**

## Author contributions

The manuscript was solely written by the author and partly revised by Antje J. Bäumner and Axel Duerkop. AJB will be corresponding author. The graphical abstract was drawn by Vanessa Tomanek.

## **2.1 Short Introduction to Hydrogels and Polymers**

The use of hydrogels, polymers or other not further defined membranes in combination with a sensor in general has risen constantly within the last 30 years from below 100 to nearly 7,000 publications per year as a “Web of Science” record count analysis reveals [1]. This trend is understandable regarding the numerous advantageous and adaptable properties of natural and synthetic polymers with regard to mesh size, stability, water retention ability, swelling behavior, degradability, sterilizability, and many more for the immobilization and protection of the recognition elements [2–8].

Polymers and hydrogels can be classified by their properties or by categories like their origin. Some of the hydrogels are derived from natural sources like polysaccharides (e.g. alginates or chitosan derivatives), or protein-based polymers like collagen [9]. Prominent examples for hydrogels assembled from synthetic building blocks are polyethylene glycol (PEG), polyvinyl chloride (PVC), polyurethanes (PU) or Nafion®, a perfluorinated polymer which can be used as cation-selective and conductive membrane [8, 10]. The large 3D network provides an enhanced surface area and consists of physically (like hydrogen bonding,  $\pi$ - $\pi$ -stacking or hydrophobic interactions) or chemically (covalently) cross-linked monomers [11]. Further classification can be made by the charge of the hydrogel (anionic, cationic, ampholytic, or uncharged). The number, type, and charge of the active groups of the monomers strongly affects the interaction of the hydrogel and the recognition element or also the analyte. For stimuli-responsive hydrogels which are often charged networks, no recognition elements or labels are necessary. The hydrogel itself reacts directly to the changed environment e.g. increasing or decreasing pH, ionic strength or temperature by adapting its network structure by swelling or deswelling [12].

The active groups of the hydrogel and the net density play a major role for the choice of the respective immobilization technique [13]. The recognition element can be bound covalently and irreversibly via different coupling techniques like click-chemistry [14–16], or it is just entrapped within the network structure. One disadvantage of covalent binding is especially for protein-based labels, a structural change which induces a reduced or generally changed activity. Also, the polymer properties can change depending on the amount of immobilized label. The large advantage of this method is surely the enhanced stability and lifetime of the sensor due to the reduced risk of loss of the recognition element over time. The non-covalent incorporation into a polymeric structure does not affect the properties or activity in such a drastic way but offers the risk of leakage if the hydrogel network is not perfectly balanced for the demanded application. In other cases, the reversible embedding of a molecule is desired, and the hydrogel serves just as carrier [17]. The loaded molecule should be released when a trigger or target molecule interacts with the hydrogel or the label.

On the one hand side polymers derived from natural sources are usually known as biocompatible and show in best case no toxicity. On the other hand, some of the polymers tend to adhere to biological material like cells and proteins or lead to allergic reactions due to irreconcilable impurities [9, 13]. Non-fouling hydrogels are predestinated for in-vivo applications whereas others are better candidates for single-use sensors without direct contact to human tissue or skin. The properties can be adapted by changing or mixing different monomer blocks or combine natural with synthetic hydrogels to exploit the advantages from both sides and overcome the disadvantages [18].

## **2.2 Principles and Applications of Membrane Deposition Techniques**

While the importance of the material is obvious, it is less known that the deposition method itself has an as relevant effect on the sensors' performance. It influences the film's surface morphology, density, thickness, and attachment to the substrate. At the same time, the deposition technique is affected by the substrate, the solvents used, receptor elements, and the polymer itself within the precursor cocktail. Most important techniques include drop-coating and solution-casting, knife-, blade- or bar-coating, spray-coating, dip-coating, spin-coating, electrospinning, and electrochemical deposition. Each method comes with unique parameters influencing the performance of the membrane (**Table 2.1**), so that it is advisable to carry out a thorough evaluation of the materials and receptor elements used with respect to the immobilization techniques and fabrication methods to optimize the resulting sensor. Combinations of different techniques and materials are a common strategy to overcome disadvantages and exploit the beneficial effects of the individual polymer and deposition method. Considering the purpose of sensors as mass product, their original academic development ought to keep a later mass production in mind. This also holds true for membrane deposition methods as some are significantly better suited for upscaling compared to others.

### **2.2.1 Drop-Coating**

Drop-coating or drop-casting is a most simple and fast technique to deposit a polymeric layer on a surface and modify it with a receptor element. Especially on lab scale it is the easiest approach for surface modification that generates essentially no waste material. On industrial scale this technique can be realized by large plotters. It is best suited for coating of a small and defined area, because for larger areas controlling thickness, porosity, and uniformity of the film is more difficult [19]. The general process includes the mixing of recognition elements such as enzymes [20–23], DNA derivatives [24, 25], or probes such as fluorescent dyes, luminophores [26] or nanoparticles [27, 28] with an evaporable solvent and a binder (e.g. hydrogels, polymers, or cross-linkers like glutaraldehyde), followed by application of this cocktail to the desired surface. In addition to the cocktail composition and surface conditions, drying time, annealing temperature and the applied volume are contributing factors toward the



final homogeneity and morphology of the deposited material. Here, the coffee-ring-effect phenomenon presents a significant limitation on the reproducibility of drop-casted surfaces and requires partly complex strategies to be overcome [29]. While mainly organic solvents and binders are used, water-based solvents are needed for the entrapment of fragile biological molecules such as enzymes.

The sheer simplicity of the approach ensures wide-spread use with mixtures based on Nafion, chitosan (CS), cellulose acetate (CA) or conducting polymers like poly(3,4-ethylenedioxythiophene) (PEDOT) and other hydrogels and polymers for electrochemical detection of glucose [20, 21], lactate [22], and uric acid [30] in different body fluids like sweat, blood, and tears, tetrodotoxin in seafood samples [27], heavy metals in wastewater [21], HIV-1-gene in blood [24] and pH values of various aqueous solutions [26].

Cui *et al* drop-coated a acetylcholinesterase/bovine serum albumin (AChE/BSA) mixture on top of an electrodeposited TiO<sub>2</sub>/chitosan film which is immobilized by electrostatic interactions due to the oppositely charged materials for detection of pesticides in food samples [31]. Wang *et al* drop-coated a mixture of their ssDNA/EDC/NHS for covalent bonding on an electrodeposited PEDOT for electrochemical detection of tumor markers [32]. Gong *et al* drop-coated simply a Nafion solution on a pretreated glassy carbon electrode (GCE) and let it dry under ambient conditions [24]. The membrane was used for immobilization of ssDNA for electrical impedance spectroscopic (EIS) detection of HIV-1 gene in blood samples. It was found that Nafion could not only stabilize graphene but also increase the dispersion of graphene applied without using a more complex deposition technique [24]. Due to the self-assembling behavior of the ssDNA on the surface the straightforward drop-coating method does not seem problematic regarding homogeneous covering of the surface.

Zohourtalab and Razmi used this simple technique for application of all layers of their amperometric glucose sensor with a chitosan/Nafion/ionic liquid (IL)/ferrocene composite film on top of a carbon electrode [20]. The group around Ashrafi *et al* used comparable materials like chitosan and Nafion and the simple-drop coating technique for modification of a GCE with multi-wall carbon nanotubes and GOx to use it as glucose sensor, and furthermore for the detection of heavy metals by non-competitive inhibition of the enzyme activity [21]. Besides the simple and suitable film application, the chitosan membrane based sensor is probably not suitable for the detection of the positively charged metal ions since chitosan's mainly positively charged surface will repel the heavy metals impairing the sensor's performance [31]. Using another neutral or negatively charged hydrogel or polymer would be better and may increase the sensitivity.

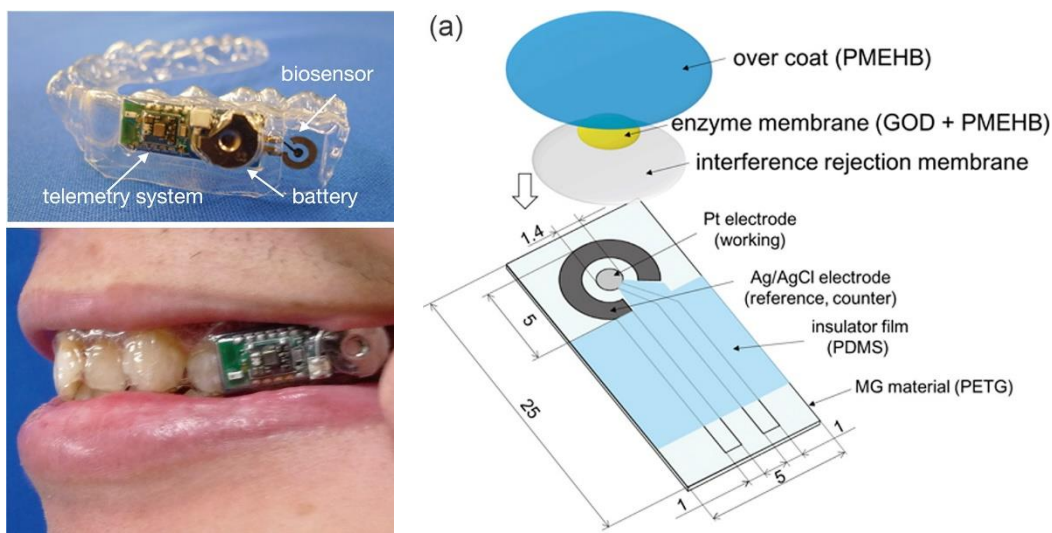


**Figure 2.1** Arakawa *et al* demonstrated a biocompatible glucose sensor placed within a mouthguard using the straightforward drop-coating method since film thickness and morphology are irrelevant for the performance (reprinted with permission from [33]. Copyright © 2020 American Chemical Society.)

A really innovative electrochemical glucose sensing system exploiting different properties of the used polymers is presented by Arakawa *et al* [33]. An already existing mouthguard is simply drop-coated with polyethylene terephthalat glycol (PETG) as biocompatible supporting structure due to its good adhesion to the sputtered metals which serve as Pt WE and Ag CE/RE (**Figure 2.1**). Thickness of the drop-coated layers does not play any role. The electrode strains are insulated by drop-coated polydimethylsiloxane (PDMS) before the Ag electrode is chloridized electrochemically. Drop-coating is here the simplest method since no special film thickness or surface morphology is needed. The GOx as recognition element is mixed with a PMEHB solution and drop-coated on an additional interference rejection membrane made from CA on top of the WE. After drying und UV-light indicated cross-linking of the enzyme, the entire area is again drop-coated by another layer of PMEHB to avoid leakage of the enzyme and the adsorption of proteins in saliva on the electrodes. All used polymeric materials are highly biocompatible and approved for human in-vivo use. PMEHB avoids adsorption of proteins from the saliva. Therefore, the combination of the used materials with the simple drop-coating technique is an adequate solution for realizing this proof-of-concept saliva glucose sensor.

### 2.2.2 Solution Casting

For solution casting methods, the polymeric solution can be poured and dried in a mold or between glass plates to obtain a defined thickness or shape. Film morphology and its quality in general mainly depend on the homogeneity of the cocktail, its concentration, solvents used, temperature, and pressure applied during evaporation or annealing [19, 34]. It is a common technique for casting PDMS generating specific sensor shapes with low demands toward the substrate. Importantly, casting of larger areas can be accomplished on an industrial scale, but

just as a batch process. Continuous approaches are difficult for film productions but have been demonstrated successfully for castings of small molds in special shapes.

As one example a temperature-sensitive PDMS layer based on Eu-complexes is named, developed and optimized by the group of Gaspar *et al* [35]. The PDMS-complex mixture is molded in a Teflon petri dish to obtain a circular layer. By adaption of the chemically bonded Eu(III)  $\beta$ -diketonate complexes different temperature ranges between 25°C and 110°C can be covered with high sensitivity by luminescence lifetime measurements. The luminescent optical probe is highly soluble within the polymeric cocktail to avoid inhomogeneities within the casted sensor. Furthermore, PDMS offers high thermal conductivity and stability which makes it the ideal candidate for this application in combination with the casting method [35].

Another example for casting polymeric solutions for sensing applications is the fiber optic ratiometric fluorescence pH sensor for monitoring corrosion in concrete, presented by Bartelmess *et al* [36]. A hydrogel D4/thymol blue (TB) cocktail is filled in a ceramic tube with Teflon plugs and dried layer-by-layer. After removing the inner Teflon plug, a polystyrene cocktail containing quantum dots is filled in and dried in the hollow D4-TB to obtain the ratiometric bi-layered sensing optode. The unique design of their sensor enables the long-term monitoring of concrete to avoid degradation-initiated breaks and therefore severe accidents in civil engineering. The preparation process is laborious and takes a lot of time due to the different drying step after filling the molds, but it is the only technique to obtain this special shaped sensor heads on a lab scale as a proof of principle. On industrial scale casting methods for large films are realizable easier but just as batch production. Continuous approaches are difficult to realize for film production but useful for casting of small forms in special shapes.

### 2.2.3 Knife-Coating

Knife-coating, also known as spread coating, bar coating or blade coating, is a simple and fast coating technique for large areas on a flexible substrate without a defined surface pattern [19]. This technique can easily be adapted to industrial scale (role-to-role fabrication) which enables a continuous and cost-effective high-throughput production [37, 38]. Usually, the knife or blade is fixed, and the substrate is moved underneath at a certain distance to define the wet layer thickness. There is low waste of the coating material and therefore the method is also useful for expensive coatings. On lab scale, typically the supporting material is fixed, and the blade or knife is moved with a defined gap over the substrate [38]. Other approaches use a bar [39] or rod twined around with a wire of stated thickness to define the gap between the substrate and the moving part, and subsequently the layer thickness [34]. Tape or other spacer materials are similarly used at lab scale to define the distance between substrate and blade. Commonly, the resulting film thickness can be regulated by the gap size between substrate and knife, the viscosity of the coated cocktail which is mainly influenced by its composition and temperature,

the coating speed, surface tension and wetting properties of the substrate and the amount of volatile solvent contained in the cocktail [37, 38]. Therefore, cleaning and perhaps a pre-treatment step of the substrate is necessary to obtain a smooth, even, and lasting film. But most critically, this method is unsuitable for making sub-micro scale films, and furthermore, controlling the micrometric precision of the blade is difficult or restricted by the thickness of the used spacers [19, 40]. Furthermore, drying, or annealing processes after the actual deposition process can influence the film building and must be optimized or automated to obtain reproducible films.

However, knife-coating has received least attention in electrode fabrication but is a low-cost and straightforward process for fabrication of optical sensor membranes like many research groups showed. Important examples are optical sensors for pH [39, 41], oxygen [41, 42], gaseous sulfur mustard [43] and ammonia [44]. Many groups use Hydromed D4, a polyurethane based hydrogel as 5 wt% or 10 wt% solution in ethanol/water mixtures for knife-coating on flexible substrates due to its superb film-building properties [39, 43, 44] but also polystyrene [42] and Nafion [39] solutions are suitable candidates for knife-coating. The active components are dissolved or suspended homogeneously within the polymeric solution. This cocktail is then coated with a defined layer thickness to obtain even and homogeneous films without special surface morphology containing enzymes, probes, or fluorescent dyes. Additional cross-linking agents like glutaraldehyde (GA) fix soluble components within the hydrogel network by covalent cross-linking. Additionally, GA crosslinking can also serve to form molecular imprints in the polymer to form unique biomimetic materials working as receptors for recognition and binding of target molecules [45, 46].

Maierhofer *et al* investigated knife-coated dual-lifetime referencing ammonia sensors with tunable sensitivity and limit of detection (LOD) based on the respective hydrogel/polymer mixtures [44]. Polymers, solvents, and dyes are perfectly balanced regarding hydrophilicity that allow coating layer-by-layer without influencing the lower layer. The hydrophobic layer on top of the membrane ensemble enables the gaseous compounds to enter but prevents the recognition elements from leaching. The reference dye in each sensor membrane overcame the not optimum reproducibility of layer thickness for each coated sensor foil. Jiang *et al* harnessed knife-coating to obtain high spatial resolution and improved a similar oxygen sensor system by introduction of an optical isolation layer containing carbon black to minimize wavelength-dependent backscattering and reflections from any background [41]. This strategy can be found in many optical sensors applied to real-world samples.

Dalfen *et al* demonstrated bar-coating for composite films. D4 was chosen to provide a near aqueous environment for the entrapped pH-sensitive diazaoxotriangulenium (DAOTA) dyes whereas Nafion virtually eliminates negative influence of anions like chloride and nitrate [39].

Since the highly charged matrix affected the  $pK_a$  values of the embedded dye negatively, the group concluded that covalent attachment to the polymer support may be needed. This suggests though, that another membrane deposition method must be chosen to enable high surface-to-volume ratios to provide high dye-immobilization densities. Also Tribuser *et al* demonstrated how properties like sensitivity or quantum yield of a  $K^+$  fluoroionophore change depending on the chosen polyurethane-based hydrogel matrix with different hydrophilicity using knife-coating technique for film preparation [47].

Bidmanova *et al* demonstrated that knife-coating is highly suitable for the deposition of polymers onto sensing materials [43]. Specifically, commercially available pH stripes were layered with D4 fixed with GA vapor to prevent probe leakage and to enhance the long-term stability. The haloalkane dehalogenase LinB was co-immobilized with bovine serum albumin (BSA) using different techniques. While this proof-of-principle could have been accomplished using drop-coating on lab scale, the demonstrated knife-coating suggests the applicability for mass production especially due to the commercially pH stripes and the polymer material chosen.

#### **2.2.4 Spray-Coating**

Spray-coating is a commonly used, simple and low-cost technique for the deposition of films in large areas. It can be performed in batch production on lab and industrial scales or as roll-to-roll process in industry. It is a contactless deposition procedure that makes it an optimal coating process for sensitive substrate surfaces and materials. The coating fluid is atomized to droplets within a spray nozzle by pressurized air or gases like nitrogen or argon, and transferred on the substrate [34, 37, 38].

Although, it is a simple method, many process parameters are crucial to determine surface morphology and layer thicknesses like nozzle configurations, pressure and composition of the carrier gas, coating speed, work distance, temperature and number of sprayed layers [19, 37, 48–50]. Furthermore, the liquid properties of the coating solution or suspension like surface tension, viscosity, density, and vapor pressure influence the quality of the sprayed coating layer [19, 51]. Disadvantageous could be harmful exposure to the aerosols of the spray mist and the difficulty of preventing the nozzle from clogging which requires a sophisticated and careful cleaning processes of the nozzles. The method is especially useful for coating of full and large areas. When masks or templates are used, much waste may be produced and often low edge resolution is observed [37, 51]. On the other hand, complicated sensor shapes become accessible, easily. As a main advantage the method enables a simple generation of thick films via layer-by-layer applications [49, 52].

Skin-mountable microelectronics are a promising technique for personalized medicine applications and biointegrated devices [53]. Cai *et al* presented a fully flexible electrode array using MXene-polypyrrole nanowires mixture as interconnecting components which was fabricated via a shadow mask–assisted spray coating [53]. Nishinaka *et al* use spray-coating for the deposition of a thick and uniform PEDOT:PSS layer as organic electrochemical transistor (OECT) for monitoring electrophysiological activities [49]. The group compared the application to spin coating where production of thick films is more difficult. Chen *et al* exploits the technique for application of silver nanoparticle composite [52]. The morphology and self-assembly of AgNPs mixed with cellulose nanofibrils is emphasized as positive effect of the layer-by-layer application via spray-coating (**Figure 2.2**). AgNP coating be used for hydrophilic antifouling coverings and label-free biosensors. Struchkov *et al* us spray-coating for the application of thin graphene oxide (GO) films [48]. They emphasize that especially the low substrate heating temperature preserves most of the oxygen-containing functional groups and is therefore an optimal method for application of GO films.

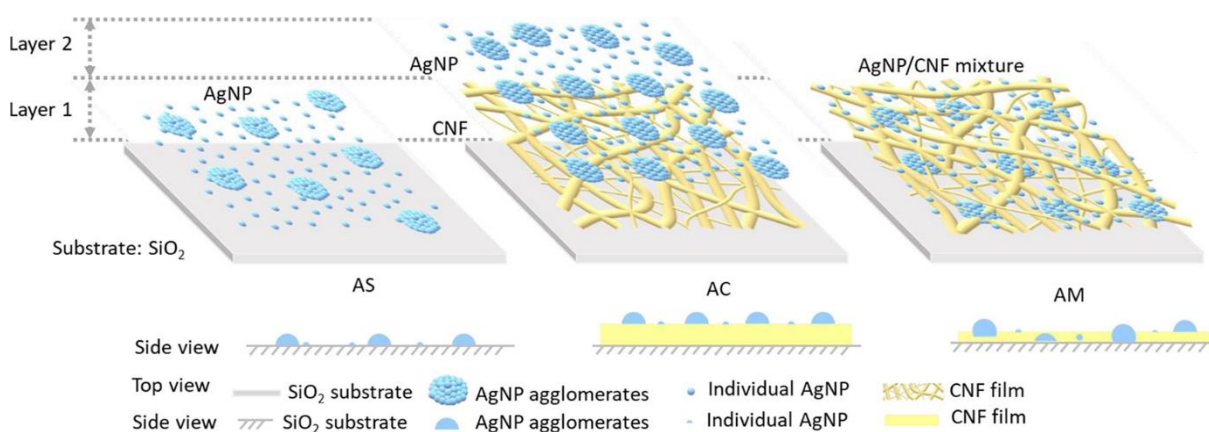


**Figure 2.2** Chen *et al* presented the self-assembling of spray-coated Ag nanoparticles (AgNP) on blank SiO<sub>2</sub> substrate (AS), with cellulose nanofibrils (CNFs) as bottom layer (AC) and applying both within a mixture (AM) on the SiO<sub>2</sub> substrate. They demonstrate the modification of the surface contact angle and suppose their potential as antifouling coating or use as label-free biosensors. (reprinted with permission from [50]. Copyright © 2021 The Authors. Published under a Creative Common Attribution CC-BY License.)

### 2.2.5 Dip-Coating

Dip-coating is a common technique used on lab and industrial scale for thin-film coatings and involves four stages: immersion, dwelling, withdrawal, and drying [34]. Surface morphology and thickness of the layer is influenced mainly by the properties of the dip solution and the substrate to be treated, like similar polarity, and furthermore from process parameters like process temperature, dwelling time, dipping and withdrawal speed, and finally drying time and temperature. The method does not require any special equipment [34] and can also be carried out as batch or continuous process on industrial scale [54]. Preferably, controlled conditions are applied since the method is susceptible to defects caused by contamination, aggregation

of precursors, microscopic air bubbles in the solution, and irregularities in the supporting substrate surface [55]. Repeating the process for several times can also minimize the defects but results in increased thickness. Dip-coating can coat membranes and substrates by adding layers with 100 nm to 100  $\mu\text{m}$  thickness and with pore sizes ranging between 1 nm and 5  $\mu\text{m}$  [55]. Best thin film building can be observed for high-viscosity solutions and cocktails with high surface tension [37, 38].

While classical dip-coating may waste material covering front and backsides of substrates, Ceratti *et al* demonstrated a novel process coating large areas on just one side with a high uniformity [56], which also largely impacts multi-layer processes. Further refined deposition of material is also possible as demonstrated by Xiong *et al* [57] where the distal end of a fiber optic is appended with a carbon quantum dots/cellulose acetate (CQDs/CA) mixture enabling the formation of a highly adrenaline sensitive sensor for continuous and real-time detection via fluorescence quenching within physiological relevant concentration ranges. Similarly, the end of a quartz fiber was dip-coated with a CQDs/glucose oxidase (GOx)/CA composite material to obtain a highly selective glucose sensor [58]. Finally, also electrochemical concepts have been demonstrated such as the wearable motion sensors using a spandex strand dip-coated with graphene nanoplatelets and shielded by silicon rubber that are used as electrical conductive yarn [59]. Common to all these approaches is the use of relatively inexpensive materials, the avoidance of material waste and limiting the applications solely for single-layer coatings.

### **2.2.6 Spin-Coating**

Spin-coating is a technique used for spreading a uniform thin film layers on a substrate by centrifugal forces. The method can be performed on laboratory scale in small benchtop devices which is a fast and cheap method. On industrial scale, spin-coating is used in batch processes since it is not suitable for continuous roll-to-roll processes. In general, an excess amount of the solution is placed in the middle of the substrate and is rapidly spread during the spinning process to the edges of the fast-rotating substrate. Film thickness can be empirically controlled by spin speed, time, temperature, volume of added substrate, composition, and viscosity of the applied solution as well as the wetting properties of the substrate [19]. Spin coating can coat membranes with thickness in the range of 70 to 500 nm and pore size varies continuously from 4 to 200 nm [55]. Reproducibility issues limit this technique to a few substrates and goes along with some waste of the coating solution unless spun-off solution can be safely re-used [51]. Drying or annealing of the spin-coated material is necessary and influences quality and thickness of the applied layer. A very flat substrate surface is required to obtain a homogeneous film thickness over the entire area and to avoid streaks. Usually, the spinning itself is done within seconds but the annealing and drying may take hours or days.



Biring *et al* used spin coating for the preparation of an optical dual gas sensor for the simultaneous detection of oxygen and ammonia [60]. The oxygen sensitive Pt porphyrin derivative complex was mixed with ethyl cellulose in THF and spin coated on one side of a glass slide. The backside was spin-coated with a cellulose acetate membrane containing the ammonia sensitive eosin Y dye. Coating process itself was done within 20 seconds but the membranes must be dried for 24 h at ambient conditions for each side. The group around Kenney *et al* spin-coated fluorescein-containing D4-hydrogel on a PET support to obtain an optical pH sensor for paper-based cell cultures [61]. The multiple sensor layers are shown in **Figure 2.3**. Spinning process was executed for just 10 seconds on 18 mm PET circles, and the films are dried overnight and rehydrated for 48 hours in buffer before UV-sterilization. None of them fixed their recognition element after the deposition process and simply presume that dyes stay inside the membranes.

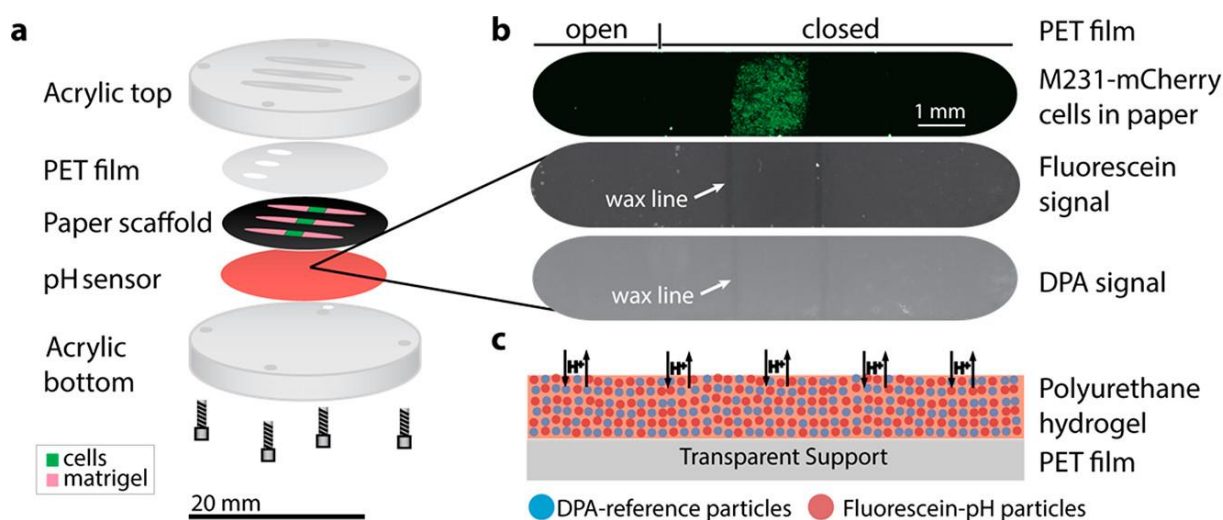


**Figure 2.3** Kenney *et al* presented an optical pH sensor for mapping spatiotemporal gradients in three-dimensional paper-based cell cultures. The D4 membrane contains the pH sensitive fluorescein dye and diphenylanthracene (DPA) as reference dye. The respective polymer cocktail was spin-coated on a transparent PET support (reprinted with permission from [61]. Copyright © 2018 American Chemical Society.)

Also, for electrochemical sensors spin coating is advantageous including polymers and composite materials of polymers and nanoparticles. For example, Yoon *et al* presented a flexible Kapton® polymer electrode with sputtered gold and spin coated MoS<sub>2</sub> nanoparticles with chemically bound GOx for glucose sensing [62]. They emphasize especially their fabrication process as simple and fast. The covalently bound enzyme promises a long-lasting and non-leaching recognition element. Gao *et al* uses spin-coating for the entrapment of uricase immobilized in SiO<sub>2</sub> mesoporous foams and SiNPs in a polyethylene glycol/polyvinyl alcohol (PEG/PVA) composite gel on a gold surface to create a surface plasmon resonance biosensor for detection of uric acid [63]. Spin-coating seems here the best choice of deposition method since a very flat and thin surface film can be created. A comparison of their work with



an SPR sensor for uric acid by Kant *et al* [64] who used dip-coating for functionalization reveals that Gao group's LOD is nearly two orders of magnitude lower.

### 2.2.7 Electrospinning

Electrospinning is an electrodynamic one-step process which uses electrical potential differences to produce ultrafine, long and continuous nanofibers with diameters at micro to nanoscale on a conductive collector substrate [19, 34, 65]. Electrospun nanofibers are favorable for applications where a large and porous surface area with high functionalization ability is beneficial [66]. Therefore, electrospinning is a predestinated technique for sensor film coatings with subsequent immobilization steps. Beside other techniques for generating nanofiber networks on surfaces [65], electrospinning appears as a simple inexpensive process which is controllable via many process parameters like temperature, air humidity, potential, distance between collector and nozzle, and the properties of the spinning solution itself [67]. But on lab scale, it can be difficult to keep temperature and air humidity constant which are critical parameters for reproducibility. Furthermore, clogging of the polymeric solution within the syringe and nozzle must be avoided by optimizing the cocktail composition and parameters like feed speed. Electrospinning on a conductive but non-transparent material can lead in case of optical approaches to the necessity of an additional transfer step to a transparent substrate. Enzymes, dyes, nanoparticles or other transducers can be directly entrapped within the fiber by dispersing or dissolving them within the spinning solution or can be afterwards immobilized either on the fiber surface or on top of the porous network by different techniques [66, 68]. Hardware requirements are more complex than for the other techniques regarding especially the high-voltage power supply safety restrictions, [69] however, a large number of natural and synthetic polymers can be spun, the morphology of the nanofibers and the collected mats can be tailored toward special features and the method is easily scalable [70] albeit with still relatively slow production rates [71]. Through the spinning parameters, the thickness of the nanofibers can be influenced, but generating nanofibers with diameters below 10 nm is challenging [19]. Compared to the other methods, electrospinning enables easy production of very thin films with a large surface-to-volume ratio due to the extended porosity [34].

Yurova and Mobarez *et al* used functionalized electrospun nanofibers for optical sensing of biogenic amines in food samples as a simple dipstick format [72, 73]. CA and the respective dyes are dissolved in acetic acid/acetone mixtures and the fiber mats were deposited on indium tin oxide (ITO) substrate. They emphasize that the sensors based on electrospun fiber mats offer a one order of magnitude enhanced linear range and LOD compared to sensors based on simple polymer films although a lower sample volume is required for their sensor. El-Moghazy *et al* even showed a replacement of conventionally casted membranes by their electrospun cellulose membranes increased the active surface area on the working electrode

of a screen-printed three-electrode sensor by more than two times, and consequently enhancing the fabricated aptamer sensor performance detecting ochratoxin A in coffee samples [15].

The group around Yezer *et al* uses CA-chitosan mixtures for electrospinning and show an easy production process for highly biocompatible sensors and straightforward covalent immobilization of the model enzyme GOx within the porous network [74]. They characterized their CA–chitosan electrospun NFs on detail based on the composition of the solution and process parameters like spinning time to show the influence of these parameters on the sensor performance. Furthermore, they cross-linked the GOx with the polymeric network afterwards with GA to avoid leakage of the enzyme.

### **2.2.8 Electrochemical Deposition**

Electrochemical deposition, also known as electrodeposition, electrophoretic deposition, or electroplating, is a traditional and inexpensive process used for thin-film coating of polymers and metal-based nanostructures on a conductive or semiconductive support such as indium tin oxide, gold or carbon-based materials by an electrical current or redox reaction [19, 55]. It has been the method of choice for the functionalization of electrochemical sensors and deposition of conductive polymers such as poly(acetylene), PEDOT, poly(thiophene), poly(p-phenylene vinylene), poly(pyrrole) and poly(aniline) [75, 76]. A simple two or three electrode setup is dipped into the precursor solution. An appropriate potential is applied, typically through cyclic voltammetry or chronoamperometry causing sufficient current flow to initiate the polymerization of the polymeric precursors directly on the electrode surface by oxidation of the monomers to form reactive radicals [77–79]. The characteristics of the polymeric film, i.e. thickness, porosity, and uniformity can be controlled by the applied potential, current flow, and scanning speed as well as by additives within the precursor solution, temperature, and pH and ionic strength of the solution. Within a single step this technique allows the growth of a conductive film from nanometers up to several hundreds of microns [55]. General characteristics of the electrode surface such as surface morphology, wettability and electrical properties are equally influential [19, 75, 77, 78]. In contrast to most other methods, parameters change throughout the process, which is not limited to the concentration of the precursor molecules but especially also the conductivity in dependence of the increasing layer thickness. Overall, electrochemical deposition allows a highly controllable formation of the structure and properties of the conductive polymeric layer.

Many groups use electrodeposited conductive polymers for improving their electrochemical bio- and chemosensors. Mello and Mulato presented in 2018 their studies about optimized polyaniline (PANI) thin films as optical and potentiometric pH sensor [80]. For galvanostatic electrodeposition they used a simple two-electrode system with a Pt-counter electrode and

fluorine-doped tin oxide substrate as WE. By variation of process parameters like the deposition time, they showed the influence on thickness, morphology, and reflectance of the deposited PANI films. Following, the sensitivity of the resulting extended-gate field-effect-transistor (EGFET) and optical reflectance chemical sensors can easily be adapted based on these properties. Wang *et al* developed an anti-fouling ultrasensitive DNA sensor for the electrochemical detection of breast cancer marker BRCA1 in serum based on electrochemically deposited PEDOT membranes [32]. The PEDOT layer was deposited from a 3,4-ethylenedioxythiophene/sodium citrate solution on a GCE whereas the citrate ions incorporate carboxyl groups for the subsequent immobilization of the antifouling peptide by Ni(II)-ions via Ni-O coordination [76]. The simple and easy production of the highly sensitive and selective sensor is achievable thanks to the deposition method for the conductive PEDOT polymer and would not be easy to realize with other deposition methods. They improved their LOD from 1.72 fM to 0.03 fM compared to previous works.

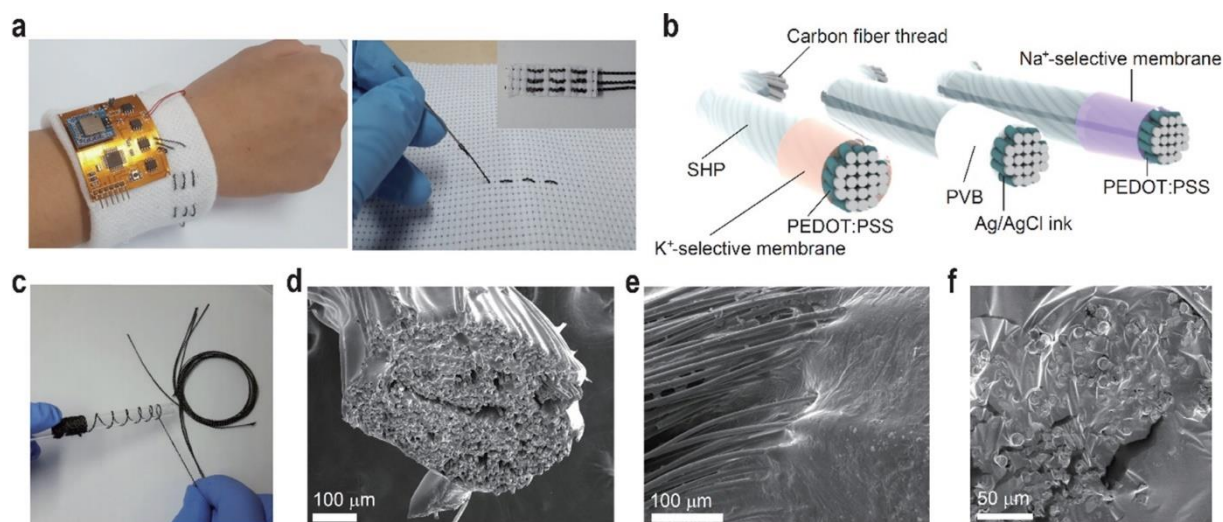


**Figure 2.4** Yoon *et al* present an electrodeposited PEDOT:PSS based biocompatible polymer that is capable of self-healing via hydrogen bonding. Combination with carbon fiber thread (c) and ion-selective membranes (b) makes it a versatile new toolset for a wearable perspiration sensor which can be directly knitted into textiles (a). Via scanning electron microscopy images (d to f) the group proved the self-healing properties. (reprinted with permission from [79]. Copyright © 2021 American Chemical Society.)

The group around Yoon *et al* investigated autonomous self-healing sensors based on electrodeposited PEDOT:PSS carbon fiber threads for the preparation of wearable  $K^+$  and  $Na^+$  sweat sensors [79] like shown in **Figure 2.4**. The conductive polymer plays the role of a solid contact transducer converting charge carriers from ions to electrons by the redox process of PEDOT:PSS. The afterwards applied ion selective membrane is applied via dip coating into the respective ionophore polymer cocktails based on PVC with bis(2-ethylhexyl) sebacate (DOS) as plasticizer in THF. Interestingly, Cui *et al* used the electrochemical technique for the deposition of a chitosan layer on a chitosan- $TiO_2$  sol-gel film on a reduced graphene oxide (rGO) modified GCE for detection of organophosphate pesticides with immobilized AChE [31].

The non-conductive CS film is positively charged after the deposition and therefore the negatively charged AChE/BSA mixture can be easily drop-coated on top. The probe is then adsorbed homogeneously on the surface by the electrostatic interactions due to the different charges. Further advantageous properties of the mesoporous TiO<sub>2</sub>/CS layer are named with large specific surface area, non-toxicity, semi-conductivity, and excellent biocompatibility, offering effective AChE loading and high electrocatalytic activity [31]. All groups showed that the combination of different deposition techniques is very useful to get access to the different advantages of the respective method.

### **2.3 Strengths and Weaknesses of the Deposition Techniques**

The overall purpose and goal of any sensor modification through a film (gel or membrane) is to enable or improve its performance. Deposition techniques foremostly affect the film's surface morphology and thickness and hence have to be wisely chosen. Furthermore, they determine the overall coating area and shapes achievable, which influences their potential for the production of large quantities of sensors such as in a commercialized product. Each method has its own strengths and weaknesses with respect to these parameters, which is summarized in **Table 2.1**. The other relevant properties of the polymer and hydrogel films are more determined by their chemical nature, such as mechanical stability, mesh size and cross-linking degree, concentration of the active ingredients, and adherence to their substrate.

Surface morphology plays a role regarding contact angle and therefore wettability of the sensor membrane, and may also influence resistance against fouling processes, albeit this property is most often addressed through additional protective membranes. The three methods of greatest interest here are solution casting, electrospinning and electrodeposition as in for each case the surface morphology can be influenced and even designed toward specific outcomes. Film thickness influences sample molecule accumulation, diffusion and hence reaction kinetics. Most techniques allow for easy adjustment of thicknesses in the nanometer to micrometer range, with the exception of knife coating where sub-micrometer heights are difficult to achieve. In the case of affordability, lab vs. production scale, drop-coating for small flat areas like electrodes and dip-coating for fibers and sensor stripes remain the best for inexpensive lab-scale fabrication. Both are very simple without special equipment needed and useful for demonstrating a new sensor concept and prove its fundamental functionality. Drop-coating on lab scale is the right choice when no special morphology is needed, and the film thickness does not play a large role.

For increased production purposes and the fabrication of large areas, knife-coating, spray-coating and spin-coating offer a straightforward approach when no special surface morphology is needed, and will support role-to-role production. Thickness of the prepared films can be

adapted easily and ranges between lower sub-micron region for spray-coating and spin-coating and hundreds of micron whereas for knife-coating it is difficult to reach the sub-micron range [49, 52, 55]. These techniques are preferable for preparing optical sensor membranes since it is lavish to coat small electrode areas using masks or templates. Disadvantages like inhomogeneity of the foils or batch-to-batch reproducibility especially on lab scale can be overcome by embedding reference dyes and measure ratiometrically at two different wavelengths.

In the case of multi-layer films, a combination of the deposition methods may be advantageous rather than sticking with one method, albeit the latter is easier on large scale production. However, often times combinations of the more refined methods such as solution casting, electrospinning or electrodeposition may be combined with the simpler methods for generating additional protective layers.

Solution casting enables the creation of special forms and shapes by using molds and can be realized on all scales in batch processes. Interestingly, a support or carrier material is not necessary since the dried or tempered casting represents the sensor shape itself. But it can be a lavish preparation and production process if more than one mold or layer is needed each requiring drying or tempering steps in-between [36].

Electrochemical deposition is a precise and well-tunable deposition technique with the opportunity to adapt the resulting surface morphology and thickness by instrumental parameters [19, 55]. But it is limited to conductive substrates and therefore best suited for electrochemical sensors. A thorough evaluation of the instrumental parameters is necessary since the surface is changing its properties like conductivity with progressive deposition time. It is not mandatory to apply the polymeric solution exactly and solely on the electrode area because the polymerization just takes place on the conductive structure of the substrate.

Electrospinning should be the method of choice when a high surface-to-volume ratio is inevitable which is realized by creating a highly porous network of nanofibers on a collector substrate [66]. Although reproducibility is not ideal on lab scale and safety requirements are high the method provides the most pronounced surface structure of the deposited polymeric material on nanoscale which can be further processed [81]. Due to the extended surface area small sensors with high sensitivity can be obtained.

The combination of the different techniques is a mighty tool to overcome drawbacks and exploit solely the advantages of each individual deposition method to open decent possibilities for polymeric film generation. A deeper knowledge about and understanding of the influence of the deposition method on the quality of the polymeric film and the general properties of the used polymers and hydrogels is essential for a successful application of those in a

commercialized sensing system. Additionally, it must be evaluated which properties of the membrane are relevant for the targeted sensing application. As an example, an anti-fouling but negatively charged Nafion membrane is the worst choice for the detection of e.g. anions since the sensitivity will be reduced unintentionally. But Nafion or comparable polymers with negatively charged surface groups like sulfonate will be an excellent option for pH sensing in a matrix with anionic interferences like sweat or seawater. Blending polymers and hydrogels to adjust their properties at a certain degree and influence the properties of the active compound is a conceivable compromise regarding selectivity, sensitivity, and other indicators of a sensor. Simple and straightforward techniques with the possibility for role-to-role production like knife-coating can prepare an inexpensive substrate for the deposition of an additional layer by another technique with better surface morphology control like spray-coating or spin-coating. A conductive electrode surface can be treated by electrochemical deposition in a first way to modify solely the conductive areas where the redox reactions take place. Following in a second step, a protective membrane can be deposited without the need of an accurate or precise limitation of the exact electrode area like knife-coating, dip-coating, or spray-coating.

Therefore, the choice of the suitable polymer or hydrogel mixture, the support material and specially the respective deposition method should not be underestimated but chosen rather deliberately for each sensor type and its intended application. More criteria must be considered than one may think if a genuine commercialization for a long-living, stable, and reliable and reasonable end-consumer product is envisaged.

**Table 2.1** Overview of herein reviewed polymeric film deposition techniques with their most important key facts as well as advantages and disadvantages to enable a suitable choice of a fitting technique for sensor development.

Technique	Principle	Simplicity and Apparatus Effort	Film Morphology	Potential for Commercialization	Advantages	Disadvantages	Ref
<b>Drop-Coating</b>	defined volume of polymeric cocktail is transferred with a pipette onto the substrate and dried/annealed	very simple, very small instrumental demand, no special equipment needed, pipette is sufficient	no special morphology but self-assembling layers can be fabricated	roll-to-roll fabrication possible with large plotters, but also batch production	<input checked="" type="checkbox"/> easiest method for proof of sensor concept	<input checked="" type="checkbox"/> just for small and defined areas <input checked="" type="checkbox"/> coffee ring effect <input checked="" type="checkbox"/> reproducibility regarding film morphology and thickness	[20, 21, 24, 31, 32]
<b>Solution Casting</b>	the polymeric cocktail is poured in a mold or special form and then dried/annealed	medium simplicity, small apparatus effort, molds and forms are needed	special morphology can be obtained by (nano)structured molds	batch production for defined shapes, but also continuous process possible	<input checked="" type="checkbox"/> special forms and shapes accessible without substrate	<input checked="" type="checkbox"/> laborious and time-consuming since more steps are necessary for multi-layered sensors <input checked="" type="checkbox"/> preparing of the mold is required previously	[35, 36]
<b>Knife-Coating</b>	the polymeric cocktail is spread with a knife, blade, bar, or rod with defined distance over the substrate and dried/annealed	simple, small apparatus effort, can be realized with very simple tools like tape or wire and doctor's blade/bar/rod	no special morphology, smooth and even surface	roll-to-roll fabrication is already a standard technique in industry	<input checked="" type="checkbox"/> large areas can be coated fast and easy <input checked="" type="checkbox"/> good for film thicknesses within entire $\mu\text{m}$ range	<input checked="" type="checkbox"/> reproducibility on lab scale <input checked="" type="checkbox"/> membrane thickness is restricted to spacer material or must be adjusted by sensor cocktail composition <input checked="" type="checkbox"/> sub-micron layers difficult to achieve	[39, 41, 43, 44]

Technique	Principle	Simplicity and Apparatus Effort	Film Morphology	Potential for Commercialization	Advantages	Disadvantages	Ref
<b>Spray-Coating</b>	the polymeric cocktail is applied as very small droplets via pressurized air/gases through a nozzle on the substrate	simple, medium apparatus effort, spray-chamber with aspiration, pressurized air/gas supply for even and uniform spray mist	no special morphology, smooth and even surface, self-assembling layers and layer-by-layer buildups can be produced	roll-to-roll fabrication already standard method but also batch production possible	<input checked="" type="checkbox"/> easy layer-by-layer deposition for large areas <input checked="" type="checkbox"/> special forms and shapes easily accessible <input checked="" type="checkbox"/> film thicknesses between lower nm and upper $\mu\text{m}$ range	<input checked="" type="checkbox"/> for small areas masks or templates required <input checked="" type="checkbox"/> waste of material by coating of undesired areas <input checked="" type="checkbox"/> not suitable for viscous polymer cocktails	[32–34, 37]
<b>Dip-Coating</b>	the substrate is dipped into the polymeric cocktail with subsequent annealing/drying	very simple, no apparatus effort, simply a suitable vessel	no special morphology, smooth and even surface	roll-to-roll fabrication already standard method but also batch production possible	<input checked="" type="checkbox"/> very simple and easy <input checked="" type="checkbox"/> sophisticated methods available for precise film control	<input checked="" type="checkbox"/> waste of material by coating of undesired areas like backside or masks with simple methods	[41–43]
<b>Spin-Coating</b>	an excess polymeric cocktail is placed in the middle of the substrate which is rotated fast at a defined speed to spread the polymeric solution homogeneously by centrifugal forces	simple, medium apparatus effort, a commercial or in-house made spin-coating device with adjustable reproducible spinning speed is necessary	no special morphology, smooth and even surface	just batch production and no continuous approach	<input checked="" type="checkbox"/> smooth and even films on lab scale and industrial scale <input checked="" type="checkbox"/> film thicknesses from nm up to $\mu\text{m}$ region accessible	<input checked="" type="checkbox"/> waste of material since an excess must be applied on the substrate	[44, 45, 47]



Technique	Principle	Simplicity and Apparatus Effort	Film Morphology	Potential for Commercialization	Advantages	Disadvantages	Ref
<b>Electro-spinning</b>	the polymeric cocktail is deposited in form of nanofibers via electrical potential difference between a spray nozzle and a grounded collector substrate	medium simplicity, large apparatus effort, high voltage supply safety restrictions, pump with very homogeneous feed rate	very defined surface morphology, porous networks and structures can be realized easily	batch-to-batch production and continuous process, but still too slow for market-relevant applications on industrial scale	<input checked="" type="checkbox"/> conductive and non-conductive substrates possible <input checked="" type="checkbox"/> very high surface-to-volume ratio of deposited film	<input checked="" type="checkbox"/> apparatus effort and safety requirements <input checked="" type="checkbox"/> worse reproducibility on lab-scale	[56–58]
<b>Electro-chemical Deposition</b>	the polymeric precursor cocktail is applied on the conductive substrate and a voltage/current is applied to start the polymerization process by reduction/oxidation of the precursors	simple, medium apparatus effort, potentiostat and RE (e.g. Ag/AgCl) and/or CE (e.g. Pt wire) is necessary	surface morphology can be adjusted by electrical settings	batch-to-batch production thinkable	<input checked="" type="checkbox"/> deposition occurs just on defined area <input checked="" type="checkbox"/> highly reproducible also on lab-scale <input checked="" type="checkbox"/> film thicknesses from nm to $\mu\text{m}$ range accessible with medium apparatus effort	<input checked="" type="checkbox"/> just suitable for conductive and semi-conductive substrates	[17, 63–65]

## 2.4 Conclusion and Perspective

Hydrogels and polymers are essential components of most sensors enabling *in vivo*, continuous and rapid analysis in an analyte's original (most complex) sample matrix. Much research is hence put toward the development of new, sophisticated and customized polymers and hydrogels [82]. Also, layered and blended polymer cocktails are investigated to provide an optimal sensing environment. Yet, the importance of the deposition method is too often underestimated and may in fact become the sole reason why lab-scale sensors will not be easily adaptable to large-scale production as critical sensor performance may rely on the special features obtained through the deposition method chosen.

Therefore, initial screening of various production methods is advisable already during the initial sensor development phase. Common characterization methods for of the polymeric layers include scanning electron microscopy, atomic force microscopy, and contact angle measurements [83, 84] providing important information about the surface morphology and surface-to-volume-ratio where applicable, and the wetting properties of the deposited films. Testing the basic functionality of each sensor prototype to determine crucial characteristics like sensitivity and selectivity helps to make an appropriate decision for the right deposition technique.

Similarly, some dead-end research studies especially in bioanalytical sensor development are preventable where the interplay between solvents needed for special polymers, for an effective deposition technique and the delicate nature of the biorecognition element may not be well balanced. A change in deposition techniques may instead rapidly provide new avenues to be followed.

To sum up, this review offers a critical summary of popular thin and thick film deposition techniques with application examples in the field of bioanalytical sensors. Hopefully, more people get aware of the delicate choice of a convenient membrane deposition technique with the appropriate polymers, hydrogels, and substrates for the envisaged sensor application by a critical evaluation of the strengths and weaknesses of each method ahead of or at least in the early phase of their sensor development.

## 2.5 Acknowledgement

The author acknowledges Vanessa Tomanek for drawing the graphical abstract.

## 2.6 References

1. Clarivate Analytics. Web of Science. <https://www.webofscience.com/>(accessed December 22th, 2021).
2. Fu J, Het Panhuis M in. Hydrogel properties and applications. *J Mater Chem B*. 2019; <https://doi.org/10.1039/c9tb90023c>
3. Sun X, Agate S, Salem KS, Lucia L, Pal L. Hydrogel-Based Sensor Networks: Compositions, Properties, and Applications-A Review. *ACS Appl Bio Mater*. 2021; <https://doi.org/10.1021/acsabm.0c01011>
4. Chen G, Tang W, Wang X, Zhao X, Chen C, Zhu Z. Applications of Hydrogels with Special Physical Properties in Biomedicine. *Polymers*. 2019; <https://doi.org/10.3390/polym11091420>
5. Mishra S, Rani P, Sen G, Dey KP. Preparation, Properties and Application of Hydrogels: A Review. In: Thakur VK, Thakur MK, editors. *Hydrogels. Recent Advances*. Singapore: Springer Singapore; 2018. pp. 145–173.
6. Bashir S, Hina M, Iqbal J, Rajpar AH, Mujtaba MA, Alghamdi NA, Wageh S, Ramesh K, Ramesh S. Fundamental Concepts of Hydrogels: Synthesis, Properties, and Their Applications. *Polymers*. 2020; <https://doi.org/10.3390/polym12112702>
7. Galante R, Pinto TJA, Colaço R, Serro AP. Sterilization of hydrogels for biomedical applications: A review. *J Biomed Mater Res B Appl Biomater*. 2018; <https://doi.org/10.1002/jbm.b.34048>
8. Kulkarni T, Slaughter G. Application of Semipermeable Membranes in Glucose Biosensing. *Membranes (Basel)*. 2016; <https://doi.org/10.3390/membranes6040055>
9. Catoira MC, Fusaro L, Di Francesco D, Ramella M, Boccafoschi F. Overview of natural hydrogels for regenerative medicine applications. *J Mater Sci: Mater Med*. 2019; <https://doi.org/10.1007/s10856-019-6318-7>
10. Kusoglu A, Weber AZ. New Insights into Perfluorinated Sulfonic-Acid Ionomers. *Chem Rev*. 2017; <https://doi.org/10.1021/acs.chemrev.6b00159>
11. Guo Y, Bae J, Fang Z, Li P, Zhao F, Yu G. Hydrogels and Hydrogel-Derived Materials for Energy and Water Sustainability. *Chem Rev*. 2020; <https://doi.org/10.1021/acs.chemrev.0c00345>
12. Lucío MI, Cubells-Gómez A, Maquieira Á, Bañuls M-J. Hydrogel-based holographic sensors and biosensors: past, present, and future. *Anal Bioanal Chem*. 2022; <https://doi.org/10.1007/s00216-021-03746-1>
13. Jose M. Guisan, editor. Immobilization of Enzymes and Cells. *Methods in Biotechnology*, vol. 22. 2nd edition. Totowa, New Jersey: Humana Press; 2006.
14. Devaraj NK, Finn MG. Introduction: Click Chemistry. *Chem Rev*. 2021; <https://doi.org/10.1021/acs.chemrev.1c00469>
15. El-Moghazy AY, Amaly N, Istamboulie G, Nitin N, Sun G. A signal-on electrochemical aptasensor based on silanized cellulose nanofibers for rapid point-of-use detection of ochratoxin A. *Microchimica Acta*. 2020; <https://doi.org/10.1007/s00604-020-04509-y>
16. Andrus LP, Unruh R, Wisniewski NA, McShane MJ. Characterization of Lactate Sensors Based on Lactate Oxidase and Palladium Benzoporphyrin Immobilized in Hydrogels. *Biosensors (Basel)*. 2015; <https://doi.org/10.3390/bios5030398>
17. Ma C, Shi Y, Pena DA, Peng L, Yu G. Thermally Responsive Hydrogel Blends: A General Drug Carrier Model for Controlled Drug Release. *Angew Chem Int Ed Engl*. 2015; <https://doi.org/10.1002/anie.201501705>
18. Zhang K, Feng Q, Fang Z, Gu L, Bian L. Structurally Dynamic Hydrogels for Biomedical Applications: Pursuing a Fine Balance between Macroscopic Stability and Microscopic Dynamics. *Chem Rev*. 2021; <https://doi.org/10.1021/acs.chemrev.1c00071>
19. Ahmad R, Wolfbeis OS, Hahn Y-B, Alshareef HN, Torsi L, Salama KN. Deposition of nanomaterials: A crucial step in biosensor fabrication. *Materials Today Communications*. 2018; <https://doi.org/10.1016/j.mtcomm.2018.09.024>

20. Zohourtalab A, Razmi H. Selective Determination of Glucose in Blood Plasma by Using an Amperometric Glucose Biosensor Based on Glucose Oxidase and a Chitosan/ Nafion/ IL/Ferrocene Composite Film. *Iranian Journal of Analytical Chemistry*. 2018;5:9–16.
21. Ashrafi, Sýs, Sedláčková, Farag, Adam, Přebyl, Richtera. Application of the Enzymatic Electrochemical Biosensors for Monitoring Non-Competitive Inhibition of Enzyme Activity by Heavy Metals. *Sensors*. 2019; <https://doi.org/10.3390/s19132939>
22. Schuck A, Kim HE, Moreira JK, Lora PS, Kim Y-S. A Graphene-Based Enzymatic Biosensor Using a Common-Gate Field-Effect Transistor for L-Lactic Acid Detection in Blood Plasma Samples. *Sensors*. 2021; <https://doi.org/10.3390/s21051852>
23. Wang Q, Liu Y, Campillo-Brocal JC, Jiménez-Quero A, Crespo GA, Cuartero M. Electrochemical biosensor for glycine detection in biological fluids. *Biosens Bioelectron*. 2021; <https://doi.org/10.1016/j.bios.2021.113154>
24. Gong Q, Wang Y, Yang H. A sensitive impedimetric DNA biosensor for the determination of the HIV gene based on graphene-Nafion composite film. *Biosens Bioelectron*. 2017; <https://doi.org/10.1016/j.bios.2016.02.045>
25. Baghbaderani SS, Noorbakhsh A. Novel chitosan-Nafion composite for fabrication of highly sensitive impedimetric and colorimetric As(III) aptasensor. *Biosensors and Bioelectronics*. 2019; <https://doi.org/10.1016/j.bios.2019.01.059>
26. Waleed Al-Qaysi W, Duerkop A. A luminescent europium complex for wide-range pH sensors and sensor microtiterplates. *Analyst*. 2018; <https://doi.org/10.1039/c8an00775f>
27. Xiaosheng Shen, Mingli Liu, Cong Kong, Wenlei Zhai, Essy Kouadio Fodjo, Youqiong Cai. Chitosan and nafion assisted modification of enzyme-free electrochemical immunosensors for the detection of tetrodotoxin.
28. Liu Q, Bai W, Guo Z, Zheng X. Enhanced electrochemiluminescence of Ru(bpy)<sub>3</sub><sup>2+</sup>-doped silica nanoparticles by chitosan/Nafion shell@carbon nanotube core-modified electrode. *Luminescence*. 2021; <https://doi.org/10.1002/bio.3979>
29. Kaliyaraj Selva Kumar A, Zhang Y, Li D, Compton RG. A mini-review: How reliable is the drop casting technique? *Electrochemistry Communications*. 2020; <https://doi.org/10.1016/j.elecom.2020.106867>
30. Xu Z, Song J, Liu B, Lv S, Gao F, Luo X, Wang P. A conducting polymer PEDOT:PSS hydrogel based wearable sensor for accurate uric acid detection in human sweat. *Sensors and Actuators B: Chemical*. 2021; <https://doi.org/10.1016/j.snb.2021.130674>
31. Cui H-F, Wu W-W, Li M-M, Song X, Lv Y, Zhang T-T. A highly stable acetylcholinesterase biosensor based on chitosan-TiO<sub>2</sub>-graphene nanocomposites for detection of organophosphate pesticides. *Biosens Bioelectron*. 2018; <https://doi.org/10.1016/j.bios.2017.07.068>
32. Wang G, Han R, Su X, Li Y, Xu G, Luo X. Zwitterionic peptide anchored to conducting polymer PEDOT for the development of antifouling and ultrasensitive electrochemical DNA sensor. *Biosens Bioelectron*. 2017; <https://doi.org/10.1016/j.bios.2016.10.088>
33. Arakawa T, Tomoto K, Nitta H, Toma K, Takeuchi S, Sekita T, Minakuchi S, Mitsubayashi K. A Wearable Cellulose Acetate-Coated Mouthguard Biosensor for In Vivo Salivary Glucose Measurement. *Anal Chem*. 2020; <https://doi.org/10.1021/acs.analchem.0c01201>
34. Fu Y, Dudley EG. Antimicrobial-coated films as food packaging: A review. *Compr Rev Food Sci Food Saf*. 2021; <https://doi.org/10.1111/1541-4337.12769>
35. Gaspar RDL, Fortes PR, Mazali IO, Sigoli FA, Raimundo IM. Optical Temperature Sensors Based On Europium(III) Beta-Diketonate Complexes Chemically Bonded To Functionalized Polydimethylsiloxane. *ChemistrySelect*. 2018; <https://doi.org/10.1002/slct.201801373>
36. Bartelmess J, Zimmek D, Bartholmai M, Strangfeld C, Schäferling M. Fibre optic ratiometric fluorescence pH sensor for monitoring corrosion in concrete. *Analyst*. 2020; <https://doi.org/10.1039/c9an02348h>
37. Søndergaard RR, Hösel M, Krebs FC. Roll-to-Roll fabrication of large area functional organic materials. *J. Polym. Sci. B Polym. Phys*. 2013; <https://doi.org/10.1002/polb.23192>

38. Park J, Shin K, Lee C. Roll-to-Roll Coating Technology and Its Applications: A Review. *Int. J. Precis. Eng. Manuf.* 2016; <https://doi.org/10.1007/s12541-016-0067-z>
39. Dalfen I, Dmitriev RI, Holst G, Klimant I, Borisov SM. Background-Free Fluorescence-Decay-Time Sensing and Imaging of pH with Highly Photostable Diazaotriangulenium Dyes. *Anal Chem.* 2019; <https://doi.org/10.1021/acs.analchem.8b02534>
40. Xie K, Fu Q, Qiao GG, Webley PA. Recent progress on fabrication methods of polymeric thin film gas separation membranes for CO<sub>2</sub> capture. *Journal of Membrane Science.* 2019; <https://doi.org/10.1016/j.memsci.2018.10.049>
41. Jiang Z, Yu X, Hao Y. Design and Fabrication of a Ratiometric Planar Optode for Simultaneous Imaging of pH and Oxygen. *Sensors (Basel).* 2017; <https://doi.org/10.3390/s17061316>
42. Moßhammer M, Scholz VV, Holst G, Kühl M, Koren K. Luminescence Lifetime Imaging of O<sub>2</sub> with a Frequency-Domain-Based Camera System. *J Vis Exp.* 2019; <https://doi.org/10.3791/60191>
43. Bidmanova S, Steiner M-S, Stepan M, Vymazalova K, Gruber MA, Duerkop A, Damborsky J, Prokop Z, Wolfbeis OS. Enzyme-Based Test Strips for Visual or Photographic Detection and Quantitation of Gaseous Sulfur Mustard. *Anal Chem.* 2016; <https://doi.org/10.1021/acs.analchem.6b01272>
44. Maierhofer M, Rieger V, Mayr T. Optical ammonia sensors based on fluorescent aza-BODIPY dyes- a flexible toolbox. *Anal Bioanal Chem.* 2020; <https://doi.org/10.1007/s00216-020-02891-3>
45. Sudjarwo WAA, Dobler MT, Lieberzeit PA. QCM-based assay designs for human serum albumin. *Anal Bioanal Chem.* 2022; <https://doi.org/10.1007/s00216-021-03771-0>
46. Tse Sum Bui B, Auroy T, Haupt K. Fighting Antibiotic-Resistant Bacteria: Promising Strategies Orchestrated by Molecularly Imprinted Polymers. *Angewandte Chemie.* 2022; <https://doi.org/10.1002/ange.202106493>
47. Tribuser L, Borisov SM, Klimant I. Tuning the sensitivity of fluoroionophore-based K<sup>+</sup> sensors via variation of polymer matrix: A comparative study. *Sensors and Actuators B: Chemical.* 2020; <https://doi.org/10.1016/j.snb.2020.127940>
48. Struchkov NS, Alexandrov EV, Romashkin AV, Silakov GO, Rabchinskii MK. Uniform graphene oxide films fabrication via spray-coating for sensing application. *Fullerenes, Nanotubes and Carbon Nanostructures.* 2020; <https://doi.org/10.1080/1536383X.2019.1686623>
49. Nishinaka M, Jinno H, Jimbo Y, Lee S, Wang J, Lee W, Yokota T, Someya T. High-Transconductance Organic Electrochemical Transistor Fabricated on Ultrathin Films Using Spray Coating. *Small Structures.* 2021; <https://doi.org/10.1002/sstr.202000088>
50. Chen Q, Brett CJ, Chumakov A, Gensch M, Schwartzkopf M, Körstgens V, Söderberg LD, Plech A, Zhang P, Müller-Buschbaum P, Roth SV. Layer-by-Layer Spray-Coating of Cellulose Nanofibrils and Silver Nanoparticles for Hydrophilic Interfaces. *ACS Appl. Nano Mater.* 2021; <https://doi.org/10.1021/acsanm.0c02819>
51. Sampaio PGV, González MOA, Oliveira Ferreira P, Cunha Jácome Vidal P, Pereira JPP, Ferreira HR, Oprime PC. Overview of printing and coating techniques in the production of organic photovoltaic cells. *Int J Energy Res.* 2020; <https://doi.org/10.1002/er.5664>
52. Layer-by-Layer Assembled Semipermeable Membrane for amperometric glucose sensors, R. Tipnis et al, *Journal of Diabetes Science and Technology*, 2007, 1, 2.
53. Cai Y, Shen J, Yang C-W, Wan Y, Tang H-L, Aljarb AA, Chen C, Fu J-H, Wei X, Huang K-W, Han Y, Jonas SJ, Dong X, Tung V. Mixed-dimensional MXene-hydrogel heterostructures for electronic skin sensors with ultrabroad working range. *Sci Adv.* 2020; <https://doi.org/10.1126/sciadv.abb5367>
54. Neacșu IA, Nicoară AI, Vasile OR, Vasile BȘ. Inorganic micro- and nanostructured implants for tissue engineering. In: Grumezescu AM, editor. *Nanobiomaterials in hard tissue engineering.* Amsterdam, Boston, Heidelberg: WA William Andrew an imprint of Elsevier; 2016. pp. 271–295.
55. Mavukkandy MO, McBride SA, Warsinger DM, Dizge N, Hasan SW, Arafat HA. Thin film deposition techniques for polymeric membranes– A review. *Journal of Membrane Science.* 2020; <https://doi.org/10.1016/j.memsci.2020.118258>

56. Ceratti DR, Louis B, Paquez X, Faustini M, Grosso D. A New Dip Coating Method to Obtain Large-Surface Coatings with a Minimum of Solution. *Advanced Materials*. 2015; <https://doi.org/10.1002/adma.201502518>
57. Xiong H, Ding L, Xu B, Liang B, Yuan F. A Versatile Optical Fiber Sensor Comprising an Excitation-Independent Carbon Quantum Dots/Cellulose Acetate Composite Film for Adrenaline Detection. *IEEE Sensors J*. 2021; <https://doi.org/10.1109/JSEN.2021.3054410>
58. Yu S, Ding L, Lin H, Wu W, Huang J. A novel optical fiber glucose biosensor based on carbon quantum dots-glucose oxidase/cellulose acetate complex sensitive film. *Biosens Bioelectron*. 2019; <https://doi.org/10.1016/j.bios.2019.111760>
59. Montazerian H, Rashidi A, Dalili A, Najjaran H, Milani AS, Hoorfar M. Graphene-Coated Spandex Sensors Embedded into Silicone Sheath for Composites Health Monitoring and Wearable Applications. *Small*. 2019; <https://doi.org/10.1002/smll.201804991>
60. Biring S, Sadhu AS, Deb M. An Effective Optical Dual Gas Sensor for Simultaneous Detection of Oxygen and Ammonia. *Sensors (Basel)*. 2019; <https://doi.org/10.3390/s19235124>
61. Kenney RM, Boyce MW, Whitman NA, Kromhout BP, Lockett MR. A pH-Sensing Optode for Mapping Spatiotemporal Gradients in 3D Paper-Based Cell Cultures. *Anal Chem*. 2018; <https://doi.org/10.1021/acs.analchem.7b05015>
62. Yoon J, Lee SN, Shin MK, Kim H-W, Choi HK, Lee T, Choi J-W. Flexible electrochemical glucose biosensor based on GOx/gold/MoS<sub>2</sub>/gold nanofilm on the polymer electrode. *Biosens Bioelectron*. 2019; <https://doi.org/10.1016/j.bios.2019.111343>
63. Gao J, Yuan Y, Liang L, Yang M. A Refractometric Uric Acid Biosensor Based on Immobilized Uricase and PVA+PEG Composite Hydrogels. *IEEE Sensors J*. 2020; <https://doi.org/10.1109/JSEN.2020.3027672>
64. Kant R, Tabassum R, Gupta BD. Fiber Optic SPR-Based Uric Acid Biosensor Using Uricase Entrapped Polyacrylamide Gel. *IEEE Photon. Technol. Lett*. 2016; <https://doi.org/10.1109/LPT.2016.2571722>
65. Alghoraibi I, Alomari S. Different Methods for Nanofiber Design and Fabrication. In: Barhoum A, Bechelany M, Makhoulf ASH, editors. *Handbook of Nanofibers*. Cham: Springer; 2019. pp. 1–46.
66. Matlock-Colangelo L, Baeumner AJ. Biologically inspired nanofibers for use in translational bioanalytical systems. *Annual review of analytical chemistry (Palo Alto, Calif.)*. 2014; <https://doi.org/10.1146/annurev-anchem-071213-020035>
67. Alam AKMM, Ewaldz E, Xiang C, Qu W, Bai X. Tunable Wettability of Biodegradable Multilayer Sandwich-Structured Electrospun Nanofibrous Membranes. *Polymers*. 2020; <https://doi.org/10.3390/polym12092092>
68. Xue J, Wu T, Dai Y, Xia Y. Electrospinning and Electrospun Nanofibers: Methods, Materials, and Applications. *Chem Rev*. 2019; <https://doi.org/10.1021/acs.chemrev.8b00593>
69. Reddy SM, Vadgama P. Entrapment of glucose oxidase in non-porous poly(vinyl chloride). *Analytica Chimica Acta*. 2002; [https://doi.org/10.1016/S0003-2670\(02\)00246-5](https://doi.org/10.1016/S0003-2670(02)00246-5)
70. Munteanu BS, Sacarescu L, Vasiliu A-L, Hitruc GE, Pricope GM, Sivertsvik M, Rosnes JT, Vasile C. Antioxidant/Antibacterial Electrospun Nanocoatings Applied onto PLA Films. *Materials (Basel)*. 2018; <https://doi.org/10.3390/ma11101973>
71. Persano L, Camposeo A, Tekmen C, Pisignano D. Industrial Upscaling of Electrospinning and Applications of Polymer Nanofibers: A Review. *Macromol. Mater. Eng*. 2013; <https://doi.org/10.1002/mame.201200290>
72. Yurova NS, Danchuk A, Mobarez SN, Wongkaew N, Rusanova T, Baeumner AJ, Duerkop A. Functional electrospun nanofibers for multimodal sensitive detection of biogenic amines in food via a simple dipstick assay. *Anal Bioanal Chem*. 2018; <https://doi.org/10.1007/s00216-017-0696-9>
73. Mobarez SN, Wongkaew N, Simsek M, Baeumner AJ, Duerkop A. Dipsticks with Reflectometric Readout of an NIR Dye for Determination of Biogenic Amines. *Chemosensors*. 2020; <https://doi.org/10.3390/chemosensors8040099>

74. Yezer I, Demirkol DO. Cellulose acetate–chitosan based electrospun nanofibers for bio-functionalized surface design in biosensing. *Cellulose*. 2020; <https://doi.org/10.1007/s10570-020-03486-y>
75. Aydemir N, Malmström J, Travas-Sejdic J. Conducting polymer based electrochemical biosensors. *Phys Chem Chem Phys*. 2016; <https://doi.org/10.1039/c5cp06830d>
76. Wang Y, Liu A, Han Y, Li T. Sensors based on conductive polymers and their composites: a review. *Polym Int*. 2020; <https://doi.org/10.1002/pi.5907>
77. Tonelli D, Scavetta E, Gualandi I. Electrochemical Deposition of Nanomaterials for Electrochemical Sensing. *Sensors (Basel)*. 2019; <https://doi.org/10.3390/s19051186>
78. Kim S, Jang LK, Park HS, Lee JY. Electrochemical deposition of conductive and adhesive polypyrrole-dopamine films. *Sci Rep*. 2016; <https://doi.org/10.1038/srep30475>
79. Yoon JH, Kim S-M, Eom Y, Koo JM, Cho H-W, Lee TJ, Lee KG, Park HJ, Kim YK, Yoo H-J, Hwang SY, Park J, Choi BG. Extremely Fast Self-Healable Bio-Based Supramolecular Polymer for Wearable Real-Time Sweat-Monitoring Sensor. *ACS Appl Mater Interfaces*. 2019; <https://doi.org/10.1021/acsami.9b16829>
80. Mello HJNPD, Mulato M. Influence of galvanostatic electrodeposition parameters on the structure-property relationships of polyaniline thin films and their use as potentiometric and optical pH sensors. *Thin Solid Films*. 2018; <https://doi.org/10.1016/j.tsf.2018.04.022>
81. Wongkaew N, Simsek M, Arumugam P, Behrent A, Berchmans S, Baeumner AJ. A Robust strategy enabling addressable porous 3D carbon-based functional nanomaterials in miniaturized systems. *Nanoscale*. 2019; <https://doi.org/10.1039/c8nr09232j>
82. Ahmadi Y, Kim K-H. Functionalization and customization of polyurethanes for biosensing applications: A state-of-the-art review. *TrAC Trends in Analytical Chemistry*. 2020; <https://doi.org/10.1016/j.trac.2020.115881>
83. Azeera M, Vaidevi S, Ruckmani K. Characterization Techniques of Hydrogel and Its Applications. In: Mondal MIH, editor. *Cellulose-Based Superabsorbent Hydrogels*. Cham: Springer International Publishing; 2019. pp. 737–761.
84. Rahman MS, Islam MM, Islam MS, Zaman A, Ahmed T, Biswas S, Sharmeen S, Rashid TU, Rahman MM. Morphological Characterization of Hydrogels. In: Mondal MIH, editor. *Cellulose-Based Superabsorbent Hydrogels*. Cham: Springer International Publishing; 2019. pp. 819–863.

### 3 Electrochemical Multi-Analyte Point-of-Care Perspiration Sensors Using On-Chip Three-Dimensional Graphene Electrodes

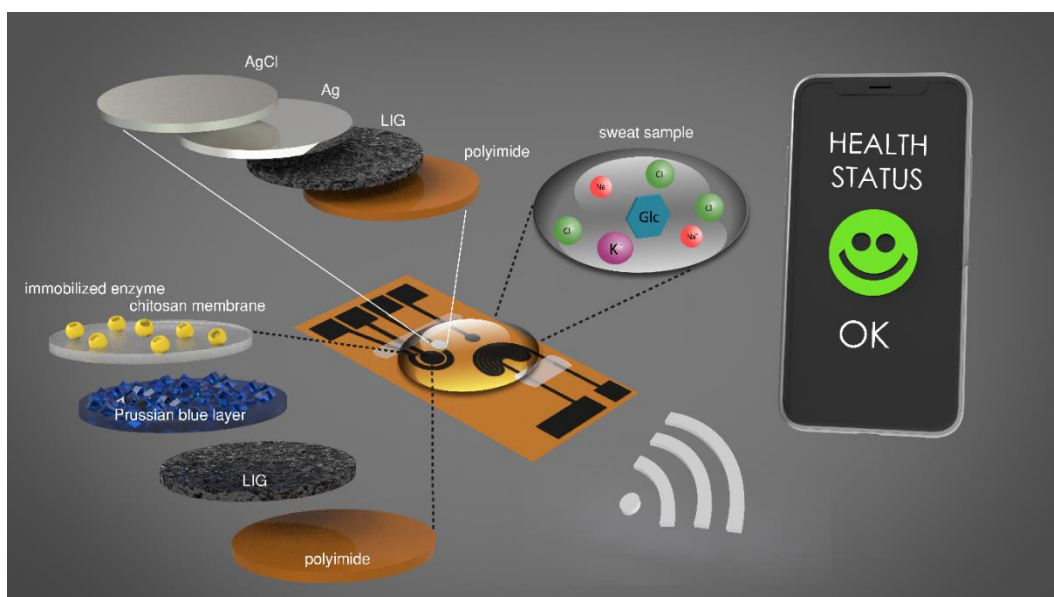
---

#### Abstract

Multianalyte sensing using exclusively laser-induced graphene (LIG)-based planar electrode systems was developed for sweat analysis. LIG provides 3D structures of graphene, can be manufactured easier than any other carbon electrode also on large scale, and in form of electrodes: hence, it is predestinated for affordable, wearable point-of-care sensors. Here, it is demonstrated that LIG facilitates all three electrochemical sensing strategies (voltammetry, potentiometry, impedance) in a multianalyte system for sweat analysis. A potentiometric potassium ion-selective electrode in combination with an electrodeposited Ag/AgCl reference electrode (RE) enabled the detection of potassium ions in the entire physiologically relevant range (1 mM to 500 mM) with a fast response time, unaffected by the presence of main interfering ions and sweat collecting materials. A kidney-shaped interdigitated LIG electrode enabled the determination of the overall electrolyte concentration by electrochemical impedance spectroscopy at a fixed frequency. Enzyme-based strategies with amperometric detection share the common RE and were realized with Prussian blue as electron mediator and the biocompatible chitosan for enzyme immobilization and protection of the electrode. Using glucose and lactate oxidases, lower limits of detection of  $13.7 \pm 0.5 \mu\text{M}$  for glucose and  $28 \pm 3 \mu\text{M}$  for lactate were obtained, respectively. The sensor showed a good performance at different pH, with sweat collecting tissues, on a model skin system and furthermore in synthetic sweat as well as in artificial tear fluid. Response time for each analytical cycle totals 75 seconds, and hence allows a quasi-continuous and simultaneous monitoring if all analytes. This multianalyte all-LIG system is therefore a practical, versatile and most simple strategy for point-of-care applications and has the potential to outcompete standard screen-printed electrodes.



## Graphical Abstract



**This chapter has been published.**

M. Bauer, L. Wunderlich, F. Weinzierl, Y. Lei, A. Duerkop, H. N. Alshareef, A. J. Baeumner; *Analytical and Bioanalytical Chemistry* **2021**, 413, 763-777

### Author contributions

Most of the experimental work was solely done by the author. Data plots, other images and text passages which are already published within the scope of the author's Master's Thesis (in whole or in part) are marked with an asterisk [\*] after the respective sentence or paragraph or in the respective caption. The Master's thesis is entitled "Development of Wearable, Electrochemical Sweat Sensors Based on Laser-Scribed Graphene" and was submitted in September 2018 to the Faculty of Chemistry and Pharmacy at the University of Regensburg. As the new work done during the Ph.D. project relied on previous results and as these are presented in the published work, the combination is presented here as one chapter.

Lukas Wunderlich developed in the early phase the 2-electrode layout for the potentiometric sensor. He investigated the electrodeposition of the Ag/AgCl reference electrode and drop-coating of the ISE cocktail which was optimized by the author. In collaboration with Florian Weinzierl the finally used electrode layout for the impedance measurement was developed and tested. Florian Blaser measured the dose-response curves of the amperometric sensor for various pH values. Marcel Simsek provided the SEM images and Arne Behrent carried out

the Raman measurements. Vanessa Tomanek created the graphical abstract. Axel Duerkop, Antje J. Baeumner, Yongjiu Lei and Husam N. Alshareef contributed with strategic discussions. The manuscript was written by the author and revised by LW, FW, AD, YL, HNA and AJB. AJB is corresponding author.

### **3.1 Introduction**

The pursuit of developing bio- and chemosensors has long been driven by the realization that these sensors have a powerful potential to address the analytical challenges of on-site, rapid, accurate, simple, and inexpensive detection. Through miniaturization, advancements in biorecognition elements, in coating chemistries, and signal amplification new sensor designs indeed keep proving exactly this potential. A quite current trend in on-site diagnostics seeks to develop wearable sensors not only for clinical diagnostics but also for monitoring of fitness or health state [1]. Here, the miniaturization of electronic components and development of new materials are equally key to advance wearable sensing technology further, as can be evidenced by products ranging from smart watches and wristbands which monitor heartbeat or body temperature through adhesive stickers and screen-printed tattoos to smart textiles and contact lenses which are capable of collecting more information than physical vital signs [2].

In the year 1953 Paul di Sant' Agnese *et al.* published the first article on the detection of cystic fibrosis, a genetic disorder, in context of increased salt concentration in sweat and saliva [3, \*]. Thus, standard test procedures for sodium chloride content in sweat for the immediate detection of the pernicious disease were developed [4, \*]. Sweat also contains many different electrolytes, and other relevant biomarkers like organic acids, metal ions, amino acids, carbohydrates, and vitamins which can be used for drawing conclusions on an individual's health status [5, 6, \*]. Therefore, besides the sensitivity of the respective detection method for biomarkers in lower concentration ranges, the selectivity of the receptor of the sensor is very important for reliable measurements [\*].

Easy accessibility of sweat at any time with non-invasive collecting methods qualify sweat as a perfect bio matrix for point-of-care (POC) diagnostics and long-term health monitoring. In general, many factors like environment, activity level, hormones, sympathetic nervous system, and also the individual diet, induce perspiration [7, \*]. Eccrine sweat is generated easily over the entire body during physical activities or without exercising in warmer surroundings to regulate the body temperature [8, \*]. For subjects at rest, the sweat rate may be too low for continuous monitoring. However, perspiration can be stimulated simply with heat or by iontophoretic techniques using low electrical currents in combination with agonists like pilocarpine [9, \*]. The analysis of sweat is predestined to be realized in a wearable device for continuous monitoring over a long-term period [\*]. As such, reliable glucose level diagnosis by sweat analysis would improve millions of diabetics' daily live routine in a significantly more comfortable way [\*]. Studies reveal promising results that the glucose concentration in sweat correlates with blood glucose level and contains no glucose from the environment, albeit studies indicate that blood and interstitial analysis are more reliable [7, 10].

A light-weighted and in the best case not noticeable wearable sweat sensor is the favorable way to perform real-time monitoring of body conditions for medical home-care applications or during physical activity [\*]. Hydration level, the related electrolyte content and concentrations of biomolecules give a good overview of the current state of the user's physiological conditions [\*]. Potassium ions in general are required for correct nerve transmission and an oversupply as well as a lack thereof can cause several effects up to an abnormal heart rhythm and finally death [11, \*]. An increased electrolyte content in sweat during workout is a direct indication for dehydration [12, \*]. Lactate is an important biomarker for providing information on the oxygen supply in tissue and the entire anaerobic metabolism in muscles. Its concentration in sweat correlates directly with the concentration in blood [13, \*]. If anomalies in these biomarker concentrations are detected in a timely manner a fast-acting electrolyte or drug intake can prevent malfunctions of the body like muscle cramps or much more threatening consequences occurring due to nutrient deficits [14, \*].

Sweat analysis of such analytes can easily be performed through electrochemical detection. Furthermore, inexpensive mass production possibilities, miniaturization, integration into fluidic systems and with flexible circuit boards, makes electrochemical detection a preferred technology for sweat analysis. In fact, carbon-based electrodes dominate the electrochemical point-of-care market [15–20] and advances and better understanding of graphene suggests that it is a highly favorable transducer material [\*].

In search of economic and straight-forward synthesis routes for graphene, Lin *et al.* reported the new concept of laser-induced graphene (LIG) also termed laser-scribed graphene (LSG) by others [21–23, \*]. It was made from commercial polymers such as polyimide (PI) derivatives in 2014 by exposing those to a computer-controlled CO<sub>2</sub> infrared laser which generates 3D-graphene layers under ambient conditions [24, \*]. This economic and reagent-free one-step synthesis of porous graphene on a polymer substrate opened incredible new applications for bioanalytical demands [21–23, 25–28, \*]. It was thus studied here as a material for sweat-based sensing. Of special interest was to demonstrate that an all-LIG sensor can be generated for multi-analyte detection, employing the three important electrochemical detection strategies of voltammetry, potentiometry and conductometry. Through LIG surface modifications enzyme-based biosensors for glucose and lactate, an ion-selective chemosensor for potassium ions, and a simple conductometric electrolyte setup were developed. The multi-analyte performance was evaluated to prove that it functioned well within the physiological ranges of all analytes in sweat, was tested on skin and in artificial sweat samples.

## 3.2 Experimental

### 3.2.1 Materials

#### *Chemicals*

All solid and liquid chemicals were of at least analytical grade and purchased from Sigma-Aldrich (Sigma-Aldrich Chemie GmbH, Taufkirchen, Germany), Fluka (Fluka Chemie GmbH, Buchs, Switzerland), VWR (VWR International GmbH, Darmstadt, Germany), Merck (Merck KGaA, Darmstadt, Germany) or Roth (Carl Roth GmbH + Co. KG, Karlsruhe, Germany). Chitosan from crab shells (practical grade) was purchased from Sigma-Aldrich. All reagents were used without further purification. Millipore water was used for preparation of all aqueous solutions. [\*]

#### *Enzymes*

Lactate oxidase (LOx) type II (from *aerococcus viridans*, 36.0 U·mg<sup>-1</sup> powder) was purchased from Hölzel Diagnostika (Hoelzel Diagnostika Handels GmbH, Cologne, Germany). Glucose oxidase (GOx) type VII (from *aspergillus niger*, 168.8 kU·mg<sup>-1</sup> powder) was purchased from Sigma-Aldrich. [\*]

#### *Other Materials*

Polyimide film with a thickness of 125 µm was purchased from CMC Klebetechnik (CMC Klebetechnik GmbH, Frankenthal, Germany). As sweat collecting pads the following materials were used: Kimtech Science labor tissues (Kimberly-Clark GmbH, Koblenz, Germany), Whatman® 595 filter paper (Schleicher & Schuell, Dassel, Germany), gauze (EAZ GmbH, Boeblingen, Germany). Chicken leg was purchased from local supermarkets. Different nail polishes, kitchen towels and artificial tear fluid were purchased from local drug stores. [\*]

#### *Equipment and Accessories*

The following equipment with suitable software and accessories were used: Keithley 175 autoranging multimeter (Keithley Instruments Inc., Cleveland, Ohio, USA), CHI 650 A potentiostat (CH Instruments Inc., Austin, Texas, USA), portable bipotentiostats/galvanostats µStat400 (Methrom DropSens, Filderstadt, Germany), PalmSens4 and EmStatBlue (PalmSens BV, GA Houten, Netherlands). The handheld plating device was purchased from Conrad Electronic (Conrad Electronic SE, Hirschau, Germany). Commercially available Ag/AgCl reference electrodes (Bioanalytical Systems Inc., West Lafayette, IN, USA) and a Pt wire (Goodfellow GmbH, Hamburg, Germany) were used. A Dino Lite digital USB microscope with suitable software DinoCapture 2.0 was used to capture magnified images of the modified LIG electrodes (Dunwell Tech, Inc, Torrance, CA, USA). For all laser-scribing processes a

laser-engraving device VLS 2.30 equipped with a 30 W CO<sub>2</sub> laser ( $\lambda = 10.6 \mu\text{m}$ ) from Universal Laser Systems (Universal Laser Systems Inc., Scottsdale, Arizona, USA) was used. [\*]

For imaging the morphology and structure of the laser-induced graphene, a scanning electron microscope (SEM) LEO 1530 from Zeiss (Carl Zeiss AG, Oberkochen, Germany) was used. Raman spectroscopy was performed with a DXR Raman microscope from Thermo Fisher (Thermo Fisher Scientific GmbH, Dreieich, Germany).

#### *Preparation of Solutions and Buffers*

1X PBS (phosphate buffered saline) solution with pH 7.4, 0.1 mol·L<sup>-1</sup> citrate buffers with pH 4 and 5, 0.1 mol·L<sup>-1</sup> phosphate buffers with pH 6 and 7 and a potassium free phosphate buffer (0.1 mol·L<sup>-1</sup>, pH 7.4) for the multianalyte-sensor was prepared with and without 1 mmol·L<sup>-1</sup> glucose. All buffers were stored at 4 °C. [\*]

A potassium chloride stock solution with concentration of 1 mol·L<sup>-1</sup> was prepared in water and diluted to concentrations ranging between  $1 \cdot 10^{-7}$  and 0.5 mol·L<sup>-1</sup>. For the interfering cation study, MgCl<sub>2</sub>, CaCl<sub>2</sub> and NaCl stock solutions with a concentration of 0.1 mol·L<sup>-1</sup> were prepared in 10 mmol·L<sup>-1</sup> KCl solution and diluted with 10 mmol·L<sup>-1</sup> KCl solution. AgNO<sub>3</sub> solution for silver deposition with mass concentration  $\beta = 400 \text{ mg} \cdot \text{mL}^{-1}$  in water was prepared. For the K<sup>+</sup>-selective membrane two precursor solutions were made: solution A: 270 mg polyvinylchloride (PVC) were dissolved in 2.7 mL of tetrahydrofuran (THF). Solution B: 520  $\mu\text{L}$  dibutylsebacat (DBS) as plasticizer were mixed with 50  $\mu\text{L}$  of valinomycin solution ( $\beta = 80 \text{ mg} \cdot \text{mL}^{-1}$  in methanol). Solution B was continuously stirred while solution A was added. The membrane solution contained 16 mg of valinomycin ionophore per gram PVC. A second PVC cocktail without valinomycin was prepared as described before as protection membrane for the reference electrode. These solutions were stored in a THF atmosphere at 4 °C and have to be stirred for at least 1 hour at room temperature before use. Nafion solution was mixed with an excess of solid KCl and continuously stirred to obtain a saturated solution. [\*]

For Prussian blue deposition on the working electrode two 10 mmol·L<sup>-1</sup> iron (III) salt solutions (precursor solutions) were prepared from FeCl<sub>3</sub> and K<sub>3</sub>[Fe(CN)<sub>6</sub>]. Both were dissolved in a 0.1 mol·L<sup>-1</sup> HCl solution containing 0.1 mol·L<sup>-1</sup> KCl. Storage at 4 °C in the dark is recommended. A 0.1% weight chitosan solution was prepared by dissolving chitosan in 0.1 mol·L<sup>-1</sup> acetic acid. A 100 mmol·L<sup>-1</sup> hydrogen peroxide (HP) stock solution was freshly prepared before use. Dilution series of HP in buffer ranging between 1  $\mu\text{mol} \cdot \text{L}^{-1}$  and 10 mmol·L<sup>-1</sup> were prepared. Synthetic sweat solution according to DIN 53160-2 was prepared by dissolving 5 g NaCl and 1 g urea in 1 L water and its pH was adjusted with 1% NH<sub>4</sub>OH solution to 6.5. For the biosensor assays 100 mmol·L<sup>-1</sup> D-glucose and sodium L-lactate stock solutions

were prepared and diluted with the respective buffers to a concentration range between  $1 \mu\text{mol}\cdot\text{L}^{-1}$  and  $10 \text{mmol}\cdot\text{L}^{-1}$ . D-glucose solutions were allowed to mutarotate overnight. Lactate solutions in concentrations ranging between  $10 \mu\text{mol}\cdot\text{L}^{-1}$  and  $10 \text{mmol}\cdot\text{L}^{-1}$  were additionally prepared in synthetic sweat and artificial tear fluid. Lyophilized enzymes were dissolved in PBS. The activity of the solution of glucose oxidase was  $4 \text{U}\cdot\mu\text{L}^{-1}$ . For lactate oxidase, an activity of  $5 \text{U}\cdot\mu\text{L}^{-1}$  was adjusted. [\*]

### **3.2.2 Methods**

#### *Laser-Scribing Process and General Electrode Treatment*

The desired electrode structures were drawn in original size with the vector graphic software CorelDRAW 17 (Corel Corporation, Ottawa, Ontario, Canada) The CorelDRAW data are compatible with the software of the used laser-engraving device VLS 2.30 (Universal Laser Systems Inc., Scottsdale, Arizona, USA) and needs no further conversion. The electrodes were fabricated on a  $125 \mu\text{m}$  thick polyimide film. The scribing was performed by exposing the film to a 30 W  $\text{CO}_2$  laser with 1% laser power and 10% scribing speed (maximum speed is  $0.127 \text{m}\cdot\text{s}^{-1}$ ). The image density parameter was set to level 7, representing 1,000 laser pulses per inch (PPI) in x-direction and 2,000 PPI in y-direction. **SI Figure 3.1** shows the schematic procedure of the laser-scribing process. Further optimizations of the scribing process are explained in the SI. The electrodes were cleaned with water and isopropyl alcohol and dried with compressed air to remove dust traces around the pattern. The strands were isolated with two layers of nail polish. Connection pads were protected with copper tape or silver paint. [\*]

#### *Characterization of Electrode Material*

Morphology and graphene-like characteristics of the LIG were determined by SEM and Raman spectroscopy (see supporting information (SI), **SI Figure 3.23**). Morphology was studied by SEM at 5.0 kV. The samples have been cut with a scissor and gold sputtered for 30 s ( $\approx 7 \text{nm}$  layer thickness) after placing them on specimen stubs. Raman spectra from  $50 \text{cm}^{-1}$  to  $3500 \text{cm}^{-1}$  were collected on a Raman microscope with a 532 nm laser set to 8 mW power and a 50X objective with an estimated focal spot diameter of  $0.7 \mu\text{m}$ . 16 scans were averaged per spot.

#### *Fabrication of the Potentiometric Sensor*

A simple design with two circular electrodes was used.  $8 \mu\text{L}$  of the ISE-membrane cocktail were deposited onto one electrode to coat the whole electrode area. The membrane was dried overnight at ambient conditions. For RE fabrication,  $20 \mu\text{L}$  of  $\text{AgNO}_3$  solution ( $\beta = 400 \text{mg}\cdot\text{mL}^{-1}$ ) were dropped on the RE and equilibrated on the electrode for 5 min. A commercial handheld plating device with a voltage of 3 V and a current of 300 mA was used. The plating process

was carried out for 1 minute. The electrode was immersed into a saturated KCl solution and a 0.8 V (vs. Ag/AgCl) DC voltage was applied for 200 s to receive the silver chloride layer on top. [\*] The entire modification process is schematically shown in **SI Figure 3.9**. For further information regarding the optimization process, see SI.

#### *Design of the Impedance Sensor*

An applicable design with interdigitated two-electrode structure was developed and optimized (see SI). The sensor needed no further modifications.

#### *Amperometric Biosensor with Layered Working Electrode*

A three-electrode setup based on commercially available planar sensor systems was chosen. 2  $\mu\text{L}$  of each iron salt precursor solution were applied exclusively onto the working electrode (WE) area and allowed to react there for 20 minutes under ambient conditions. The formed PB layer is stabilized for 2 h at 100 °C. The chitosan membrane was applied by drop-coating 2  $\mu\text{L}$  of the chitosan solution on the PB-modified WE. The membrane was dried for 90 minutes under ambient conditions. 2  $\mu\text{L}$  of the respective enzyme solution were applied to the dried chitosan membrane. For incubation, the electrodes were stored at least two hours at ambient conditions, or overnight at 4 °C. A scheme of the entire buildup of the modified WE is shown in **Figure 3.1**. Reference electrode (RE) and counter electrode (CE) were made from unmodified LIG. After cleaning with a few droplets of buffer solution, the sensors were ready to use. [\*]

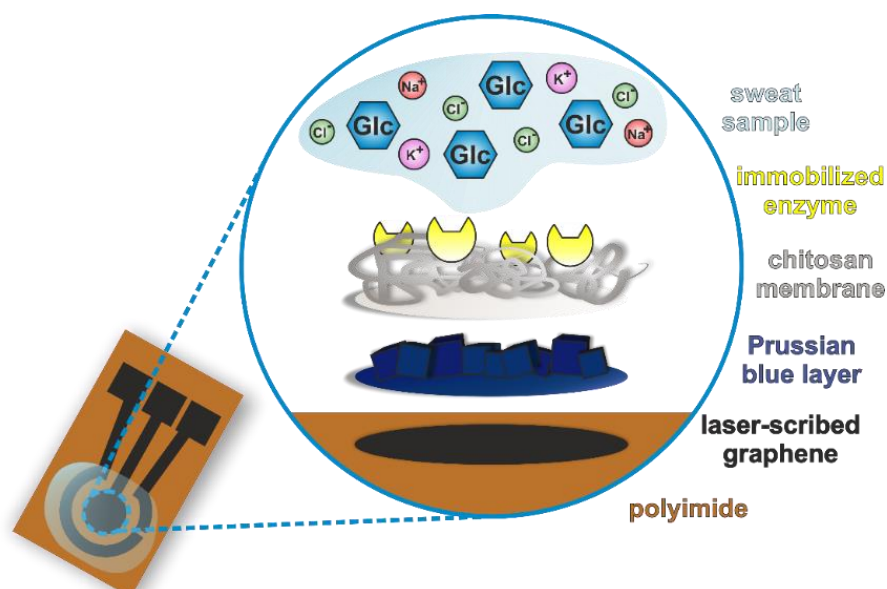


**Figure 3.1** Scheme of the WE of the amperometric biosensor after all modification steps. The laser-induced graphene on the flexible PI substrate is the base for the chemical deposited PB layer. The chitosan membrane fixes the PB layer while providing the polymer network on which the enzyme is immobilized. The sweat sample or any other solution is applied on top [\*]



### *Multi-Analyte Design*

The three single-analyte sensor designs were combined so that the amperometric and potentiometric sensors share a circular RE with electrodeposited Ag/AgCl layer like shown in **Figure 3.2 c**.

### *General Procedures and Instrumental Settings*

For potentiometric measurements, both electrodes were connected to a multimeter, 30  $\mu\text{L}$  of sample solution were applied, and the potential was read off immediately. The sensor was carefully swabbed with tissue and the next solution was applied. The same procedure was performed with all other sample solutions. Sample application without using sweat collection pads is herein called droplet method. In case of using filter paper or gauze as sample collection pad, sample volume was doubled. [\*]

For impedance measurements, 100  $\mu\text{L}$  of the respective ion solution were applied and the measurement was started at a fixed frequency of 1000 Hz with an AC amplitude of 10 mV and DC potential of 0 V, immediately. After the measurement was finished, the solution was carefully swabbed away with a paper towel and the respective following solution with increasing analyte concentration was applied. [\*]

The amperometric sensor was connected to a commercial software-controlled potentiostat. For the general procedure, a droplet of 30  $\mu\text{L}$  of the respective sample solution was applied to the biosensor (with and without filter paper as sweat collection substrate) and the measurement was started immediately. Different experimental setups are shown in **Figures 3.2 a** and **3.2 b**. The working range of the sensors was determined by measuring a cyclic voltammogram (CV) of PBS between 0.85 V and -0.95 V vs. LIG with a scan speed of 50  $\text{mV}\cdot\text{s}^{-1}$ . The CVs showed usually four characteristic peaks of the respective reduction and oxidation steps of the PB mediator layer. A potential in the decay of the first oxidation peak, usually between -0.1 V and 0.1 V vs. LIG, was chosen for the amperometric determinations. If the Ag/AgCl RE was used, the CV settings were adjusted to a slightly higher potential. With the same experimental setup, the chronoamperometric measurements were performed with a run time of 60 seconds and the potential determined from the CV. To equilibrate the sensor, buffer was measured for at least five times. The measurement was started immediately after sample application without further incubation time. The droplet on the electrode was carefully absorbed with a paper towel and the next sample solution was applied. [\*]

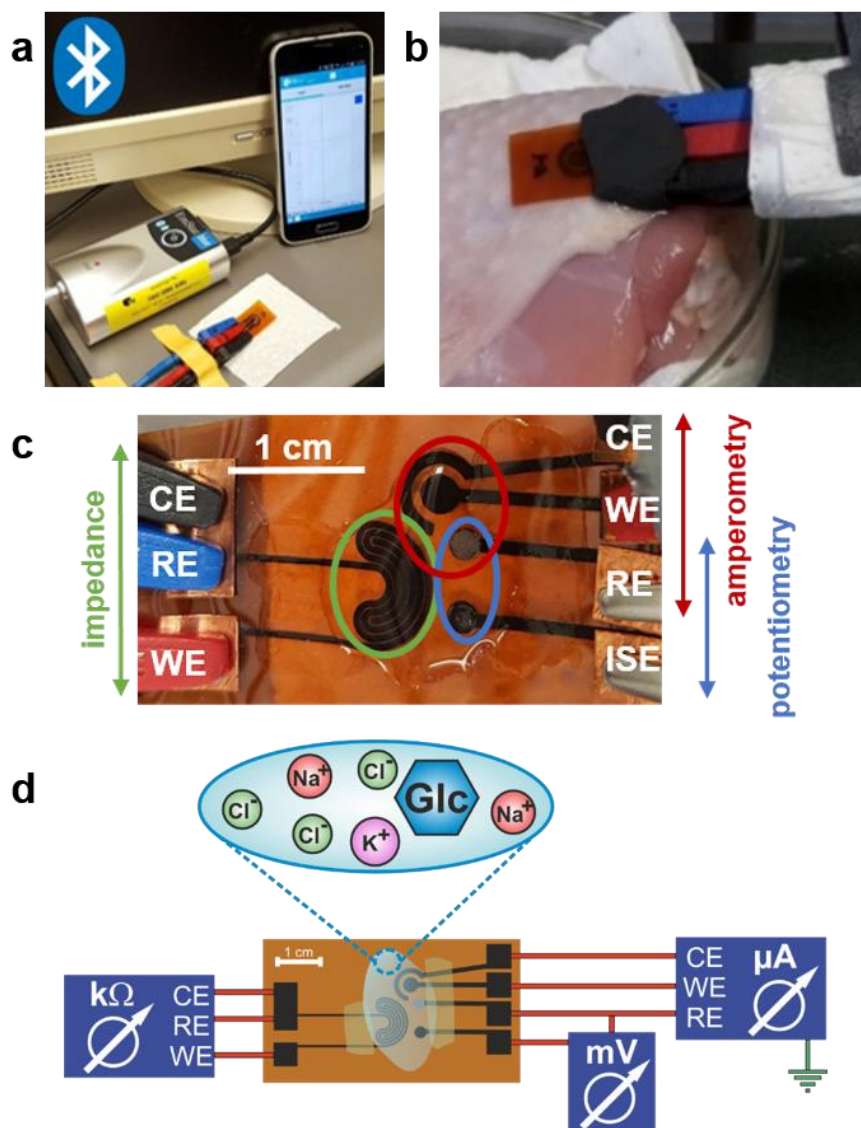


**Figure 3.2** **a** Sensor connected to the EmStatBlue potentiostat via three crocodile clamps attached to the connection pads. For planar setup, a sample droplet of 30  $\mu\text{L}$  which covers all three electrodes was added. There is a wireless connection of the potentiostat via Bluetooth<sup>®</sup> to the software application installed on a smartphone. [\*] **b** Experimental setup for detection of glucose and lactate with amperometric measurements on a chicken leg to simulate human skin and to provide a biological substrate. A piece of filter paper is used as simulated sweat collection pad. Modelling clay protects the contacts from moisture due to the shortened strands. The sensor is in a fixed position whereas the chicken substrate with the applied sample can be moved up and down. [\*] **c** Combined LIG sensor. Connection pads are protected with adhesive copper tape against abrasion through the crocodile clamps. The strands are isolated by nail polish. 150  $\mu\text{L}$  to 200  $\mu\text{L}$  of sample solution are suitable to cover the active electrode area. **d** Schematic view of the combined LIG biosensor on polyimide substrate connected to two potentiostats and a multimeter. 150  $\mu\text{L}$  to 200  $\mu\text{L}$  of mixed samples containing all potential analytes are applied and can be measured quasi simultaneously after calibration of the single sensors

For the multianalyte sensor, 150  $\mu\text{L}$  of sample solution containing different amounts of each analyte were applied to the multi-electrode system. For a quasi-simultaneous acquisition, the potential difference of the ISE was read out first after sample application. Then, the impedance was measured and as last step, the amperometric detection was done. In summary, one

analytical cycle takes approximately 75 seconds. A schematic experimental setup is shown in **Figures 3.2 c** and **3.2 d**.

Some measurements were performed with filter paper or gauze as sweat collection pad and on a chicken leg with skin to simulate detection under more real conditions (see **Figure 3.2 b** for the experimental setup). Moreover, lactate quantification was performed in synthetic sweat solution according to DIN 53160-2 and in artificial tear fluid. [\*]

#### *Statistics and Data Evaluation*

All calculation, especially the arithmetic mean values and standard deviation (SD) were calculated with Microsoft Excel 2016 (Microsoft Corporation, Redmond, Washington, USA). Usually, measurements were performed at least in triplicate ( $n = 3$ ). Suspicious values were removed after failing the outlier Q-test. SD is represented by error bars in y-direction. [\*]

Linear and non-linear regression curves were accomplished with following equations (1) and (2). Lower limit of detection (LOD) and lower limit of quantification (LOQ) for linear calibration curves were calculated with equations (3) and (4). To calculate the LOD and LOQ from a sigmoidal fit curve, the equations (5) and (6) were used. [\*]

linear curve fit:	$y = m \cdot x + b$	(1)	
			<i>m ... slope</i>
sigmoidal curve fit:	$y = \frac{A_1 - A_2}{1 + \left(\frac{x}{x_0}\right)^p} + A_2$	(2)	<i>b ... y – axis intercept</i>
			<i>A<sub>1</sub> ... initial value</i>
			<i>A<sub>2</sub> ... final value</i>
LOD (linear fit):	$LOD = \frac{3 \cdot \sigma_{blank}}{m}$	(3)	<i>x<sub>0</sub> ... center</i>
			<i>p ... power</i>
LOQ (linear fit):	$LOQ = \frac{10 \cdot \sigma_{blank}}{m}$	(4)	<i>σ<sub>blank</sub> ... SD of blank (or</i>
LOD (sigmoidal fit):	$LOD = A_1 - 3 \cdot \sigma_{blank}$	(5)	<i>lowest measured value)</i>
LOQ (sigmoidal fit):	$LOQ = A_1 - 10 \cdot \sigma_{blank}$	(6)	

### 3.3 Results and Discussion

The development strategy of the multi-analyte all-LIG sensor is based on an initial study of each single sensing principle separately. Electrode layout, laser-scribing conditions and all other depending parameters and procedures were optimized to serve all three sensing concepts well. The key was to demonstrate that an all-LIG concept is possible for all three electroanalytical detection strategies and that those can easily be combined for multi-analyte detection.

#### *Potentiometric Sensor for Potassium Ion Quantification*

The LIG-based sensor for potentiometric determination of potassium ions consists of an ion-selective electrode with valinomycin embedding PVC membrane and an electro-deposited Ag/AgCl reference electrode. The potential of the reference electrode fabricated via galvanic silver plating and subsequent electrochemical oxidation in saturated KCl solution was measured vs. a silver chloride coated silver wire. A difference below 1 mV indicated a well-working production process. A planar design with circular electrodes was chosen considering a future application as sweat sensor worn on skin. Size, distance, and shape of the electrodes were optimized for best performance (see SI, **SI Figures 3.3-3.9**) resulting in a well-working all-LIG sensor with relative errors below 4% (**Figure 3.3**). Specifically, K<sup>+</sup> detection worked within a concentration range of 1·10<sup>-5</sup> mol·L<sup>-1</sup> to 1 mol·L<sup>-1</sup> KCl when covering the electrodes with a single droplet of sample solution. Using filter paper as simulated sweat collection pad, the lower linear range limit increased to 1 mmol·L<sup>-1</sup> KCl indicating an expected direct negative impact on the ion diffusion profile to the sensor surface. As the median range of interest for K<sup>+</sup> analysis in sweat is fluctuating around 5 mmol·L<sup>-1</sup> with peak values up to 38 mmol·L<sup>-1</sup> [5, 29, 30], the dynamic range of the sensor is an excellent fit. Furthermore, due to valinomycin a good selectivity towards K<sup>+</sup> ions was demonstrated compared to the main interfering cations Na<sup>+</sup>, Mg<sup>2+</sup> and Ca<sup>2+</sup> as shown in **SI Figure 3.5**.

As can be seen in **Figure 3.3 a** and **Figure 3.3 b**, the slopes of the dose response curves are around 95 mV·dec<sup>-1</sup> in case of using the electrodeposited Ag/AgCl RE. This indicates that our pseudo Ag/AgCl reference electrode contributes to the signal and responds to the chloride ions of the KCl standards accordingly. This was demonstrated by simply performing the same experiments with KNO<sub>3</sub>, NaCl and KH<sub>2</sub>PO<sub>4</sub> (**Figure 3.3 c**) whereas the other electrolytes showed just half of the slope in contrast to the dose-response curve for KCl.

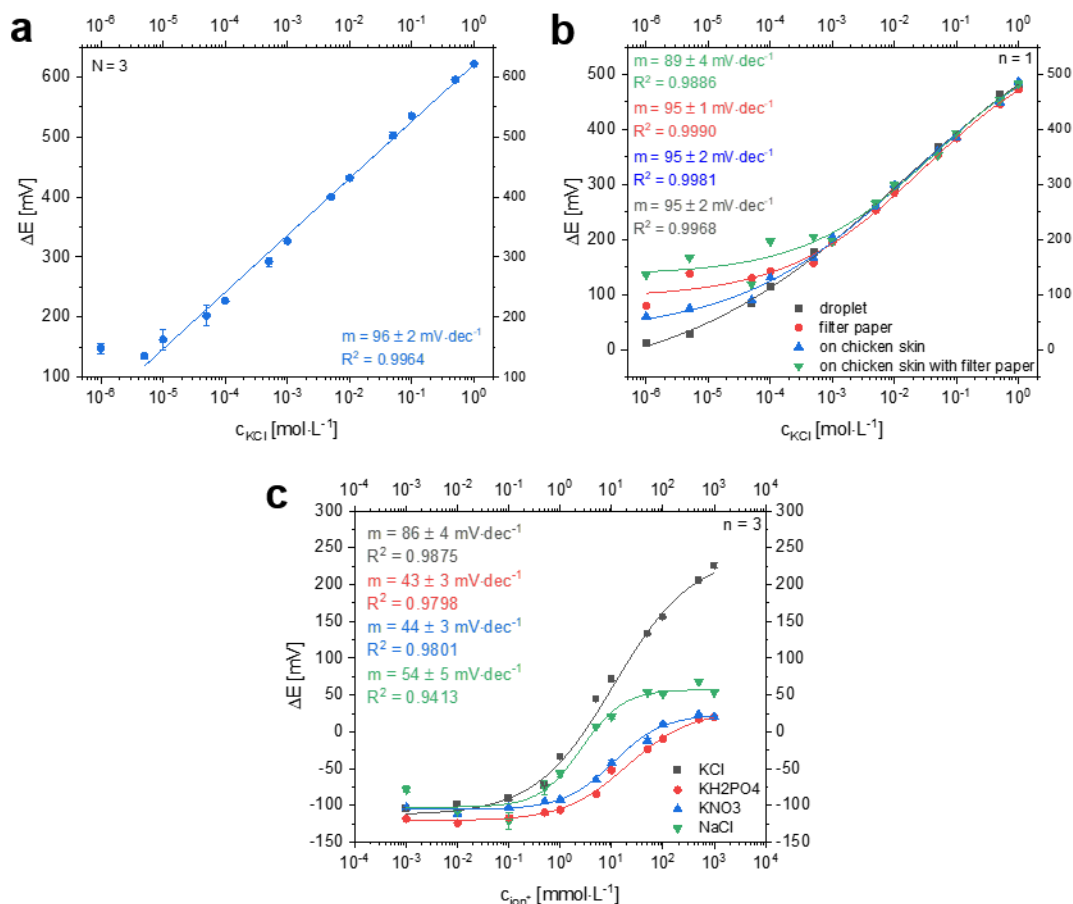


**Figure 3.3** **a** Dose-response-curve of a potentiometric, planar LIG based sensor with Ag/AgCl RE measuring KCl concentrations ranging from  $10^{-6}$  to  $1 \text{ mol} \cdot \text{L}^{-1}$  with the droplet method ( $N_{\text{sensor}} = 3$ ). The linear range goes down to  $1 \cdot 10^{-5} \text{ mol} \cdot \text{L}^{-1}$  KCl and the slope is  $96 \pm 2 \text{ mV} \cdot \text{dec}^{-1}$ . The small standard deviation, represented as error bars, especially in the linear range, indicates a reproducible electrode fabrication procedure. [\*] **b** Dose-response curves of the potentiometric LIG sensor with Ag/AgCl RE. KCl samples were measured by application of droplets (grey boxes), using a filter paper as sweat collection pad (red circles), measuring sample droplets on chicken skin (blue triangle) and on chicken skin with filter paper (green triangle) [\*] **c** Dose-response curves of one sensor when different electrolytes containing  $K^+$  and  $Cl^-$  ions, are measured to demonstrate the sensor's sensitivity towards both species (grey boxes: KCl, red circles  $\text{KH}_2\text{PO}_4$ , blue triangles:  $\text{KNO}_3$  green triangles: NaCl)

In theory, a 118 mV slope (i.e. 2x Nernstian slope of 59 mV) would be expected for KCl additions. However, the pre-deposition of AgCl on the pseudo reference electrode likely prevents that. For actual  $K^+$  ion quantification in sweat, two strategies can be used. Either, a simple LIG electrode can be applied as reference material or the pseudo RE will be covered with a Nafion/KCl/PVC membrane (**Figure 3.4**). The additional membrane keeps chloride concentration at the RE constant and prevents  $Cl^-$  ions from the sample to interfere. Besides the reduced sensitivity caused by the increased resistance, both strategies show a suitable way to minimize the influence of chloride ions within the relevant range. Moreover, we expect that the unprotected Ag/AgCl electrode in combination with another RE works as simple chloride ion sensor.

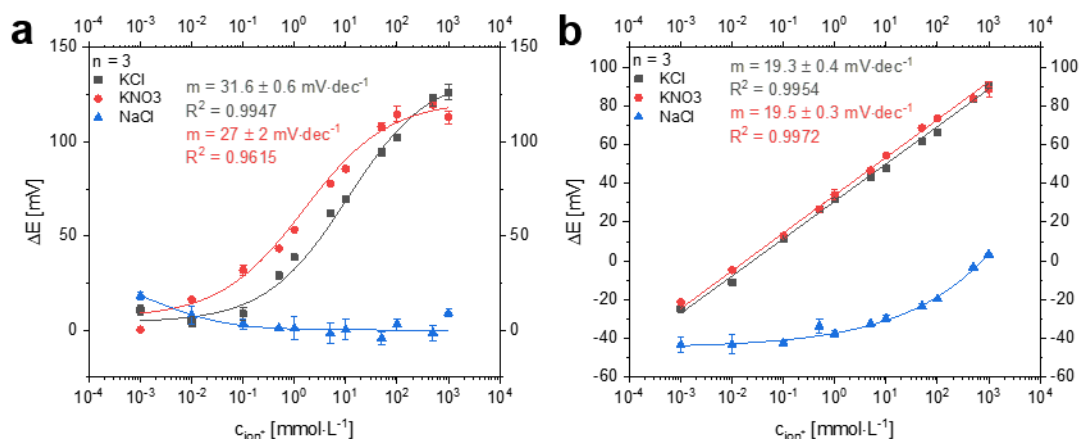


**Figure 3.4** Dose-response curves of all-LIG potentiometric sensors with an ISE versus different RE **a** Ag/AgCl pseudo-RE was protected by a Nafion/KCl/PVC layer and **b** an unmodified LIG was used as RE material to minimize the influence of chloride ions (grey boxes: KCl, red circles KNO<sub>3</sub>, blue triangles: NaCl;  $n = 3$ )

It should be pointed out that the overall fabrication of the potentiometric sensors is reliable even on lab-scale as shown by minimal differences in slopes and low standard deviations (**Figures 3.3, 3.4** and **3.8**). However, it can also be seen that each change in sensor set-up creates additional resistance layers which is reflected in the varying slopes observed in these data sets, i.e. sensors without Nafion layer follow a Nernstian behavior, as those with additional PVC and Nafion layers, or when mechanically disturbed by filter paper or gauzes show an overall decrease in slope.

#### *Impedance Sensor for Electrolyte Quantification*

EIS was used to quantify the overall electrolyte content in sweat. Electrolyte concentration in sweat is an important indicator for the hydration level of the body. Therefore, an interdigitated LIG electrode structure was designed and optimized (see SI, **Figures 3.10 – 3.15**). The impedance measurement with the kidney-shaped sensor was performed at constant frequency of 1 kHz with a fixed amplitude of 10 mV to enable a fast response of the sensor. Application of KCl solutions to the sensor with and without filter paper as sweat collection pad showed small standard deviations and similar curve shapes in the physiological relevant electrolyte concentration range of 1 mmol·L<sup>-1</sup> to 1 mol·L<sup>-1</sup> [5, \*] (see **Figure 3.5**). Ion concentrations in sweat range from lower millimolar concentrations up to peak values over 0.5 mol·L<sup>-1</sup> which is well within the reliable detection range of this sensor [5, 12, \*].

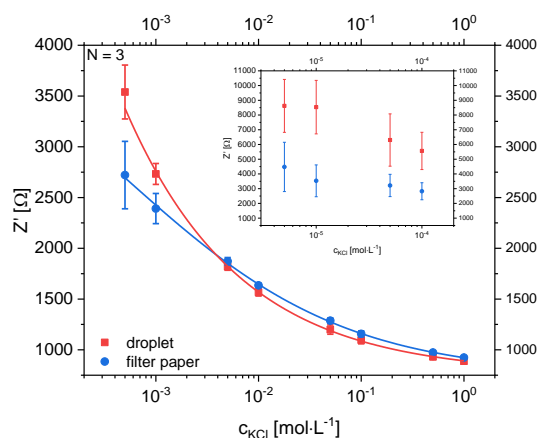


**Figure 3.5** Dose-response curve of impedance measurements of KCl solutions with concentrations ranging between  $5 \cdot 10^{-4}$  and  $1 \text{ mol} \cdot \text{L}^{-1}$  in a planar all LIG setup ( $N_{\text{sensor}} = 3$ ) with the droplet method (blue circles) and Whatman® 595 filter paper (red boxes) to simulate a sweat collection pad. The inset shows a zoomed-in section for the concentration range below the relevant range. Instrumental settings: fixed frequency of 1000 Hz with an AC amplitude of 10 mV and DC potential of 0 V [\*]

### Amperometric Glucose and Lactate Biosensors

Enzyme-based biosensors were developed for the amperometric detection of glucose and lactate. Glucose oxidase and lactate oxidase were used as their reaction with the respective analytes produce  $\text{H}_2\text{O}_2$ , which can easily be detected on Prussian blue-coated carbon electrodes. Chitosan membranes were selected as protection membranes and scaffolds for enzyme immobilization due to their wide-spread and established performance in such enzyme sensors [1, 2, 31–37]. Here, these well-established concepts were established on the LIG electrodes. Enzyme immobilization, Prussian blue coating, chitosan membrane protection as well as acquisition and incubation time were optimized (see SI, **Figures 3.16 – 3.20**). For most of the optimizations steps, hydrogen peroxide (HP) sensors (without immobilized enzyme) were used and the characteristics of the underlying  $\text{H}_2\text{O}_2$ -sensor are shown in **Table 3.1**. Subsequently, the glucose sensor was tested in solution by dropping sample volumes onto the electrodes (**Figure 3.6**), with a simulated sweat collection pad (wipe) and on chicken skin (**Table 3.1**). In the case of the droplet method, a limit of detection (LOD) of  $13.7 \pm 0.5 \mu\text{mol} \cdot \text{L}^{-1}$  and a limit of quantification (LOQ) of  $42 \pm 2 \mu\text{mol} \cdot \text{L}^{-1}$  were calculated from dose-response curves with an upper limit of the dynamic range around  $2 \text{ mmol} \cdot \text{L}^{-1}$  and a sensitivity of  $20.0 \pm 0.8 \mu\text{A} \cdot \text{L} \cdot \text{mmol}^{-1} \cdot \text{cm}^{-2}$ . For the application intended, the detectable concentration range is appropriate, as glucose concentrations in sweat are in the range between  $6 \mu\text{mol} \cdot \text{L}^{-1}$  and  $2.2 \text{ mmol} \cdot \text{L}^{-1}$  with a median value of  $170 \mu\text{mol} \cdot \text{L}^{-1}$  reported [5].

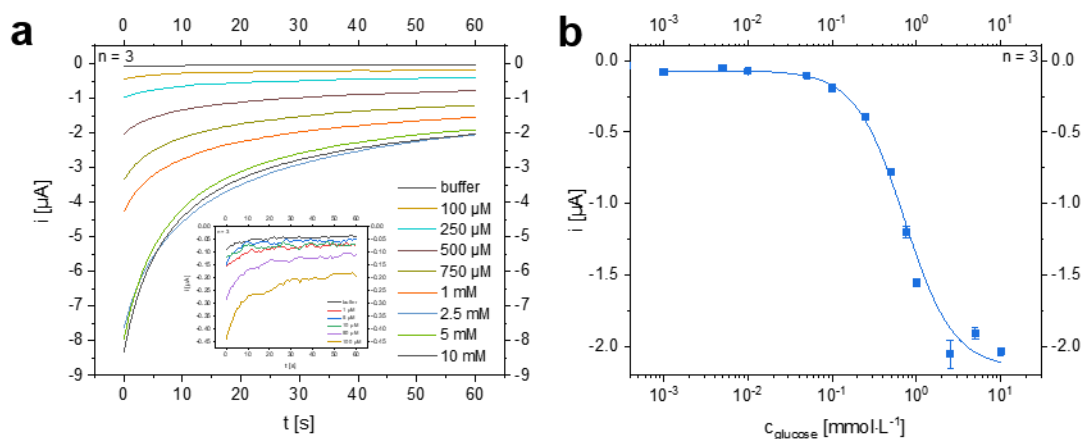


**Figure 3.6 a** Exemplary time versus current curves of chronoamperometric characterization of a modified glucose biosensor with chemical deposited Prussian blue layer, 0.1% chitosan membrane and theoretical GOx activity of  $1 \text{ U}\cdot\text{mm}^{-2}$  ( $n = 3$ , error bars are hidden for clarity). The applied potential was  $-50 \text{ mV vs. LIG}$ . Run time was 60 seconds and the sample was applied as a droplet. The magnified cutout demonstrates that low glucose solutions can be distinguished from each other. [\*] **b** Dose-response curve ( $n = 3$ , SD represented by error bars, droplet method) resulting from the respective  $I$  vs.  $t$  curve after a run time of 60 seconds on half-logarithmic scale. LOD is  $13.7 \pm 0.5 \mu\text{mol}\cdot\text{L}^{-1}$  and LOQ is  $42 \pm 2 \mu\text{mol}\cdot\text{L}^{-1}$  [\*]

In the case of filter paper and chicken skin analyses, LOD and LOQ are increased by a factor of nine to  $120 \pm 4 \mu\text{mol}\cdot\text{L}^{-1}$  and  $365 \pm 11 \mu\text{mol}\cdot\text{L}^{-1}$ , respectively. The sensitivity of the sensor decreased by a factor of five to  $4.5 \pm 0.1 \mu\text{A}\cdot\text{L}\cdot\text{mmol}^{-1}\cdot\text{cm}^{-2}$  (**SI Figure 3.21 b**). We therefore suggest to change the sweat collection to other strategies in the future, such as macro-collection channels as published by Lei *et al.* [38], as also indicated by further CV analyses (**SI Figure 3.21 a**). This strategy would provide better analyte diffusion profiles and hence create conditions similar to those established in the droplet method.

Due to the broad pH range of sweat based on different factors like collection point, extent of activity or fitness level of the individuals [6, 39], dose-response curves for glucose were recorded between pH 4 and pH 7. Each curve was measured on one sensor with an applied potential of  $0 \text{ V vs LIG}$ . The resulting dose-response curves and the calculated sensor specifications are comparable (**Figure 3.7**). The dose-response curves were normalized due to the varying sensitivities of the different sensors. If the manual modification steps are replaced by an automated method, we assume that the reproducibility of the sensitivity can be increased. Currently, a two-point calibration for the lowest and highest concentration and normalization is a satisfying procedure for comparison.



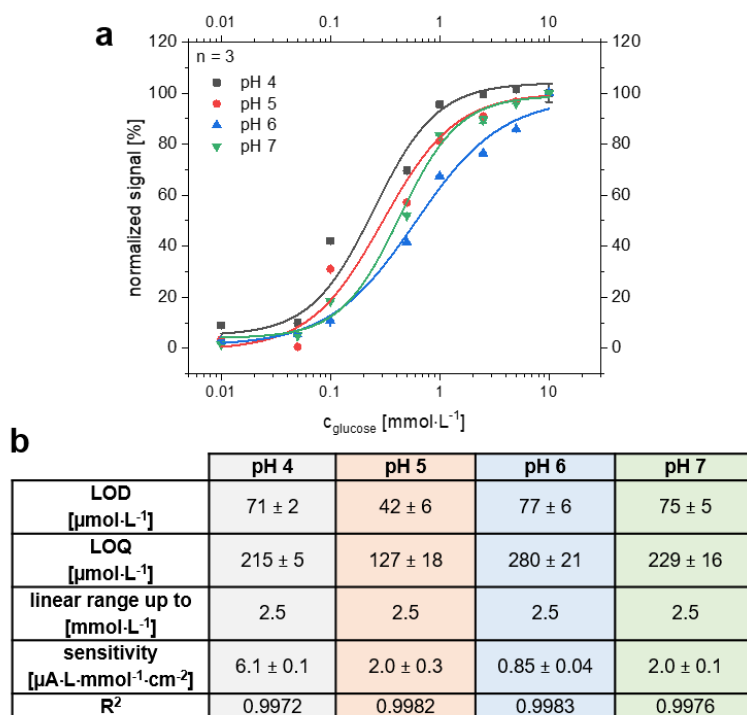


**Figure 3.7 a** Normalized dose-response curves of glucose in phosphate/citrate buffers at different physiological relevant pH values (between 4 and 7). For each pH value, a new sensor was taken. A potential of  $E = 0$  V vs. *LIG* was applied for all chronoamperometric measurements. All curves have a highly comparable shape independent of pH. Normalization of the signals from different sensors is necessary due to the varying sensitivity of the manually fabricated sensors. **b** Summary of important characteristics for the glucose sensors at different physiological relevant pH ranges

Upon simply exchanging the enzyme from glucose to lactate oxidase, the strength of the sensor concept became obvious. No further optimization experiments were required. The lactate detection in the droplet format was performed within a concentration range from  $10 \mu\text{mol}\cdot\text{L}^{-1}$  to  $5 \text{mmol}\cdot\text{L}^{-1}$ . A LOD of  $28 \pm 3 \mu\text{mol}\cdot\text{L}^{-1}$  and a LOQ of  $86 \pm 8 \mu\text{mol}\cdot\text{L}^{-1}$  were obtained with a sensitivity of  $16 \pm 1 \mu\text{A}\cdot\text{L}\cdot\text{mmol}^{-1}\cdot\text{cm}^{-2}$  (**Table 3.1**). Interestingly, the sensor is too sensitive for lactate concentrations in sweat, which ranges from  $3.7$  up to  $50 \text{mmol}\cdot\text{L}^{-1}$  [5, 40]. This high level is a well-known challenge for oxidase-based biosensors in literature [5, 29, 41]. To overcome this challenge, perforated membranes could be used as demonstrated previously by our groups [38]. Experiments with gauze for sweat collection showed the same trend as previously seen for glucose detection. LOD and LOQ declined nearly by a factor of five compared to the droplet method to  $133 \pm 1 \mu\text{mol}\cdot\text{L}^{-1}$  and  $415 \pm 3 \mu\text{mol}\cdot\text{L}^{-1}$ , respectively, with a sensitivity of  $1.75 \pm 0.01 \mu\text{A}\cdot\text{L}\cdot\text{mmol}^{-1}\cdot\text{cm}^{-2}$ . In the case of lactate, the *LIG*-lactate sensor performs well within the lower physiological relevant range. At the same time, materials other than gauze should be investigated in the future such as specialized polymer sponges, hydrophobic fibers or microfluidic channels [41–46].

In the case of lactate as analyte, measurements in synthetic sweat matrix (DIN 53160-2) and in artificial tear fluid were also performed using the droplet method. Data plots for lactate measurements are shown in **SI Figure 3.22**. The values of sensitivity, LOD and LOQ are summarized and compared to all other amperometric determinations in **Table 3.1**.

**Table 3.1** Comparison of important sensor characteristics determined with droplet method and sweat collecting substrate for chronoamperometric detection of the respective analytes hydrogen peroxide, glucose and lactate in 1X PBS pH 7.4 as well as in synthetic sweat solution according to DIN 53160-2 and artificial tear fluid with droplet application

analyte	H <sub>2</sub> O <sub>2</sub>	glucose		lactate			
sample application via	droplet	droplet	filter on skin	droplet	synthetic sweat solution droplet	artificial tear fluid droplet	gauze
LOD [ $\mu\text{mol}\cdot\text{L}^{-1}$ ]	121 $\pm$ 6	13.7 $\pm$ 0.5	120 $\pm$ 4	28 $\pm$ 3	25 $\pm$ 4	82 $\pm$ 1	133 $\pm$ 1
LOQ [ $\mu\text{mol}\cdot\text{L}^{-1}$ ]	367 $\pm$ 2	42 $\pm$ 2	365 $\pm$ 11	86 $\pm$ 6	76 $\pm$ 11	249 $\pm$ 2	415 $\pm$ 3
linear range up to [ $\text{mmol}\cdot\text{L}^{-1}$ ]	5	1.5	1.5	1	5	1	2.5
sensitivity [ $\mu\text{A}\cdot\text{L}\cdot\text{mmol}^{-1}\cdot\text{cm}^{-2}$ ]	3.0 $\pm$ 0.1	20.0 $\pm$ 0.8	4.5 $\pm$ 0.1	16 $\pm$ 1	6.1 $\pm$ 0.4	4.5 $\pm$ 0.6	1.75 $\pm$ 0.01
adj. R <sup>2</sup>	0.9736	0.9860	0.9895	0.9633	0.9377	0.9989	0.9864

The enzymatic sensors show at least comparable or even better LOD/LOQ and sensitivity than the underlying HP sensor. As the HP is produced directly on the sensor surface in the case of the enzyme sensors, dependence on HP diffusion is minimized and therefore the sensitivity can be improved. The sensor's performances prove their applicability for the detection of glucose and lactate in the respective fluids representing real samples. While LOD and upper detection limit are shifted to higher values in comparison to their performance in buffer solution, the sensors are a suitable platform for quantification within the physiological range of lactate in eccrine sweat (3.7 - 50  $\text{mmol}\cdot\text{L}^{-1}$  [5]) and tear fluid (1  $\text{mmol}\cdot\text{L}^{-1}$  to 5  $\text{mmol}\cdot\text{L}^{-1}$  [47]). As indicated in **Table 3.1**, various filter papers were studied to function as sweat collection material. Depending on the ability to hold aqueous solution on top of the sensor surface, more or less hindrance of the detection itself was observed. Materials similar to simple filter paper work well in most instances as indicated by the filter paper, Kimwipe tissue and gauze data shown. Moreover, all favorable data obtained from the single-parameter sensors suggested to combine the sensors to a miniaturized POC multi-analyte sensing platform for a reliable and affordable sweat analysis.

### *Combined Multi-Analyte Sensor*

For the multi-analyte concept, the first challenge was to minimize the sensor area to provide reliable responses with analyte volumes as low as possible. Therefore, the Ag/AgCl reference electrode is successfully shared by the potentiometric and the amperometric setup (**Figures 3.2 c** and **3.2 d**). Cross talk of the electrodes is minimized by choosing a semi-simultaneous measurement approach in which sensors are turned on and off consecutively within a short time. Each analytical cycle (potentiometry, impedance, and chronoamperometry) requires only 75 seconds, and hence allows a quasi-continuous and simultaneous monitoring of all analytes. In this format, dynamic ranges and LOD/LOQ are comparable to the characteristics obtained for the single-parameter sensors (**Figure 3.8**). This indicates that the changed layout and electrode geometry do not affect the performance. Most interestingly, it proves that multianalyte sensing in an all-LIG format using any of the desirable electrochemical techniques can be realized and easily adapted to other analytes of interest to which ionophores or enzymes are available.

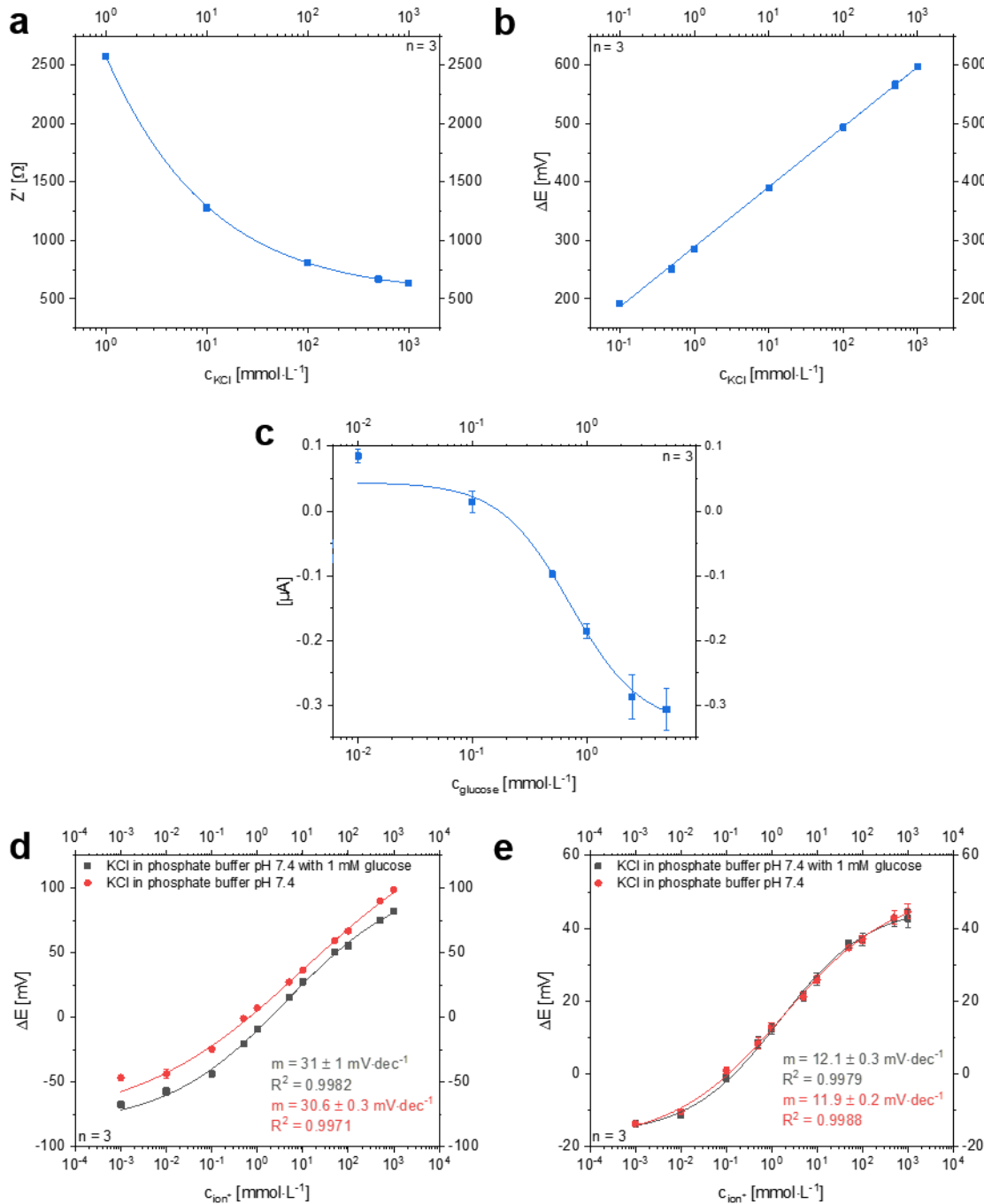


**Figure 3.8** Dose-response curves of combined multi-analyte sensor for three determination methods under the same conditions as for the single-analyte sensor. All techniques show a comparable response as the single-analyte sensors **a** The all-electrolyte concentration with the impedance measurement is highly reliable in the physiological relevant range from 1 to 500  $\text{mmol}\cdot\text{L}^{-1}$  **b** A similar reliability within the relevant range is provided for the detection of potassium concentrations with the potentiometric sensor. The slope of the linear fit is  $103 \pm 1 \text{ mmol}\cdot\text{dec}^{-1}$  **c** Glucose determination with the amperometric setup. LOD of  $135 \pm 5 \mu\text{mol}\cdot\text{L}^{-1}$  and LOQ of  $410 \pm 15 \mu\text{mol}\cdot\text{L}^{-1}$  were obtained Potentiometric determinations were performed with a **d** Nafion/KCl/PVC protected RE and a **e** LIG RE

**Table 3.2** shows similar sweat sensing platforms in comparison to important key characteristics of our presented work. Our all-LIG multi-analyte sweat sensor scores well or even better than most comparable works, especially with respect to the simplicity of the fabrication process and the flexibility of introducing new analytes by changing ionophores or enzymes.

**Table 3.2** Overview of comparable sweat sensing devices (single analyte and multi-detection systems) in comparison to our work

analyte	detection method	electrode material	LOD	detection range	sensitivity	response time	year
glucose	amperometric, enzymatic (GOx)	rGO on PI with Au/Pt NPs + chitosan	5 $\mu$ M	0–2.4 mM	48 $\mu$ A/mM $\text{cm}^2$	20 s	2018 [48]
glucose	amperometric, enzymatic (GOx)	SPE, graphite/Ag in microfluidic PET patch	11 $\mu$ M	50–200 $\mu$ M	1 nA/ $\mu$ M	1 min	2019 [49]
K <sup>+</sup>	potentiometric, ISE (valinomycin)		-	5–40 mM	51.3 mV/dec	-	
glucose	amperometric, enzymatic (GOx)	photo lithography on flexible PET; Ag/AgCl RE and CE, PB/chitosan/CNT on WE; PVB-RE, carbon/PEDOT:PSS	-	0-200 $\mu$ M	2.35 nA/ $\mu$ M	1 min	2016 [29]
K <sup>+</sup>	potentiometric, ISE (valinomycin)		-	1–32 mM	61.3 mV/dec	-	
lactate	amperometric, enzymatic (LOx)		-	0-30 mM	220 nA/ $\mu$ M	1 min	
lactate	amperometric, enzymatic (LOx)	SPE, Ag/AgCl, CNT, TTF, chitosan, on temporary tattoo	-	up to 30 mM	10.31 $\mu$ A/mM $\text{cm}^2$	1 min	2013 [50]
lactate	amperometric, enzymatic (LOx)	SPE, PB/graphite, Ag/AgCl, Carbon, chitosan	0.39 mM	0-14 mM	-	30 s	2017 [34]
K <sup>+</sup>	potentiometric, ISE (valinomycin)		10 <sup>-3.9</sup> M	0-100 mM	58.0 mV/dec	20 s	
glucose	amperometric, enzymatic (GOx)	LIG, PtNPs, chitosan	< 300 nM	up to 2.1 mM	4.622 $\mu$ A/mM	-	2020 [51]
glucose	amperometric, enzymatic (GOx/LOx)	all LIG-based, drop-coated/electro-deposited/chemical deposited Ag/AgCl RE, LIG RE possible, PB/chitosan WE	13.5 $\mu$ M	up to 1.5 mM	20.0 $\mu$ A/mM $\text{cm}^2$	60 s	This work
lactate			28 $\mu$ M	up to 5 mM	16 $\mu$ A/mM $\text{cm}^2$		
K <sup>+</sup>	potentiometric, ISE (valinomycin)		10 <sup>-4.5</sup> M	up to 1 M	96 mV/dec	1 s	
electrolytes	impedance		10 <sup>-3.5</sup> M	1 mM-1 M	-	5 s	

GOx: glucose oxidase; LOx: lactate oxidase; ISE: ion-selective electrode; PI: polyimide rGO: reduced graphene; NPs: nanoparticles; SPE: screen-printed electrodes; PET: polyethylene terephthalate; RE: reference electrode, CE: counter electrode; WE: working electrode; PB: Prussian blue; CNT: carbon nanotubes; PVB: polyvinyl butyral; PEDOT:PSS: poly(3,4-ethylenedioxythiophene) polystyrene sulfonate; TTF: tetrathiafulvalene; LIG: laser-induced graphene

### **3.4 Conclusion**

Laser-induced graphene (LIG) is a reasonably new, alternate graphene-like 3D carbon material investigated for electrochemical sensing, supercapacitors and fuel cells [21, 27, 52]. Its simple fabrication requires a polyimide foil (such as commercially available Kapton sheets used herein), and a CO<sub>2</sub>-laser [24]. No additional pastes, substrates, gas environments, cleanroom conditions or special know-how is needed, which catapults LIG electrodes into a category of most-easy-to-prepare electrochemical transducers from small lab-scale to large-scale production, easily amenable also to roll-to-roll fabrication. In this study, we demonstrated an all-LIG multianalyte sensing platform, employing the three relevant electrochemical principles used in point-of-care sensors (i.e. voltammetry, potentiometry, impedance) and addressing a relevant analytical challenge by applying it to sweat analysis. The inherent mechanical flexibility of the LIG substrate paired with the electroanalytical performance of the 3D graphene-like network enabled the detection of all chosen analytes (electrolyte, potassium ion, glucose and lactate) in their relevant physiological range. Furthermore, most recent work demonstrated the non-toxicity of the LIG electrodes [53] and previous studies using aptamers indicated that highly sensitive bioanalytical sensors are feasible [21, 54]. Interestingly, when using more advanced substrates, such as polyimide nanofiber mats, new strategies are possible that create nanoparticle-embedding LIG-nanofibers [55]. Similar strategies may be feasible when generating polyimide-nanoparticle blends and spin-coating those onto flat surfaces prior to pyrolysis via the laser. We predict that LIG electrodes will play a major role in future electroanalytical systems, not only applied to the point-of-care, but also to other low-cost analytical challenges such as food and environmental monitoring, since the all-LIG sensing platform is feasible and can easily be fabricated even under resource-limited conditions.

### **3.5 Acknowledgement**

The authors acknowledge partial funding and availability of the laser scribe through a grant by the King Abdullah University of Science and Technology (KAUST) Sensor Initiative (Grant # CRF-2015-SENSOR-2709). We further acknowledge Marcel Simsek for recording the SEM images, Arne Behrent for the Raman measurements and Vanessa Tomanek for drawing the graphical abstract.

### 3.6 References

1. Bhandodkar AJ, Wang J. Non-invasive wearable electrochemical sensors: a review. *Trends Biotechnol* 2014;32:363–371.
2. Tricoli A. Wearable and Miniaturized Sensor Technologies for Personalized and Preventive Medicine. *Adv Funct Mater*. 2017;27:1–19.
3. Di Sant'Agnese PA, Darling RC, Perera GA, Shea E. Abnormal electrolyte composition of sweat in cystic fibrosis of the pancreas; clinical significance and relationship to the disease. *Pediatrics* 1953;12(5):549–563.
4. Mishra A, Greaves R, Massie J. The Relevance of Sweat Testing for the Diagnosis of Cystic Fibrosis in the Genomic Era. *The Clinical biochemist. Reviews / Australian Association of Clinical Biochemists*. 2005;26(4):135–153.
5. Harvey CJ, LeBouf RF, Stefaniak AB. Formulation and stability of a novel artificial human sweat under conditions of storage and use. *Toxicol Vitro*. 2010;24(6):1790–1796.
6. Vautz W, Seifert L, Mohammadi M, Klinkenberg IAG, Liedtke S. Detection of axillary perspiration metabolites using ion mobility spectrometry coupled to rapid gas chromatography. *Anal Bioanal Chem*. 2020;412(1):223–232.
7. Jadoon S, Karim S, Akram MR, Kalsoom Khan A, Zia MA, Siddiqi AR, Murtaza G. Recent developments in sweat analysis and its applications. *Int J Anal Chem*. 2015; <https://doi.org/10.1155/2015/164974>
8. Anastasova S, Crewther B, Bemnowicz P, Curto V, Ip HM, Rosa B, Yang G-Z. A wearable multisensing patch for continuous sweat monitoring. *Biosens. Bioelectron*. 2017;93:139–145
9. Simmers P, Li SK, Kasting G, Heikenfeld J. Prolonged and localized sweat stimulation by iontophoretic delivery of the slowly-metabolized cholinergic agent carbachol. *J. Dermatol. Sci*. 2018;89(1):40–51.
10. Moyer J, Wilson D, Finkelshtein I, Wong B, Potts R. Correlation between sweat glucose and blood glucose in subjects with diabetes. *Diabetes Technol. Ther*. 2012;14(5):398–402.
11. Halperin ML, Kamel KS. Potassium. *Lancet*. 1998;352(9122):135–140.
12. Gengchen L, Smith K, Kaya T. Implementation of a microfluidic conductivity sensor - a potential sweat electrolyte sensing system for dehydration detection. Conference proceedings : ... Annual International Conference of the IEEE Engineering in Medicine and Biology Society. IEEE Engineering in Medicine and Biology Society. Annual Conference 2014:1678–1681.
13. Sakharov DA, Shkurnikov MU, Vagin MY, Yashina EI, Karyakin AA, Tonevitsky AG. Relationship between lactate concentrations in active muscle sweat and whole blood. *Bull. Exp. Biol. Med*. 2010;150(1):83–85.
14. Soar J, Perkins GD, Abbas G, Alfonzo A, Barelli A, Bierens JJLM, Brugger H, Deakin CD, Dunning J, Georgiou M, Handley AJ, Lockey DJ, Paal P, Sandroni C, Thies K-C, Zideman DA, Nolan JP. European Resuscitation Council Guidelines for Resuscitation 2010 Section 8. 2010;81(10):1400–1433.
15. Ahammad AS, Islam T, Hasan MM. Graphene-Based Electrochemical Sensors for Biomedical Applications. *Biomedical Applications of Graphene and 2D Nanomaterials*. Elsevier. 2019:249–282.
16. Brownson DAC, Banks CE (eds). *The Handbook of Graphene Electrochemistry*. Springer London. 2014.
17. Taniselass S, Arshad MKM, Gopinath SCB. Graphene-based electrochemical biosensors for monitoring noncommunicable disease biomarkers. *Biosens. Bioelectron*. 2019;130:276–292
18. Rakhi RB, Nayak P, Xia C, Alshareef HN. Novel amperometric glucose biosensor based on MXene nanocomposite. *Sci. Rep*. 2016. <https://doi.org/10.1038/srep36422>
19. Hammond JL, Formisano N, Estrela P, Carrara S, Tkac J. Electrochemical biosensors and nanobiosensors. *Essays Biochem*. 2016;60(1):69–80.

20. Zhang C, Zhang Z, Yang Q, Chen W. Graphene-based Electrochemical Glucose Sensors: Fabrication and Sensing Properties. *Electroanalysis*. 2018;30(11):2504–2524.
21. Fenzl C, Nayak P, Hirsch T, Wolfbeis OS, Alshareef HN, Baeumner AJ. Laser-Scribed Graphene Electrodes for Aptamer-Based Biosensing. *ACS Sens.*. 2017;2(5):616–620.
22. Nayak P, Jiang Q, Kurra N, Wang X, Buttner U, Alshareef HN. Monolithic laser scribed graphene scaffolds with atomic layer deposited platinum for the hydrogen evolution reaction. *J. Mater. Chem. A*. 2017;5(38):20422–20427.
23. Nayak P, Kurra N, Xia C, Alshareef HN. Highly Efficient Laser Scribed Graphene Electrodes for On-Chip Electrochemical Sensing Applications. *Adv. Electron. Mater.* 2016;2(10):1600185.
24. Lin J, Peng Z, Liu Y, Ruiz-Zepeda F, Ye R, Samuel ELG, Yacaman MJ, Yakobson BI, Tour JM. Laser-induced porous graphene films from commercial polymers. *Nat. Commun.* 2014;5:5714–5722.
25. Cao L, Zhu S, Pan B, Dai X, Zhao W, Liu Y, Xie W, Kuang Y, Liu X. Stable and durable laser-induced graphene patterns embedded in polymer substrates. *Carbon*. 2020;163:85–94.
26. Lee S-H, Kim JH, Yoon J-R. Laser Scribed Graphene Cathode for Next Generation of High Performance Hybrid Supercapacitors. *Sci. Rep.* 2018; <https://doi.org/10.1016/j.ijhydene.2018.12.038>
27. Ye R, James DK, Tour JM. Laser-Induced Graphene: From Discovery to Translation. *Adv. Mater.* 2019; <https://doi.org/10.1002/adma.201803621>
28. Aparicio-Martínez E, Ibarra A, Estrada-Moreno IA, Osuna V, Dominguez RB. Flexible electrochemical sensor based on laser scribed Graphene/Ag nanoparticles for non-enzymatic hydrogen peroxide detection. *Sens. Actuators B Chem.* 2019; <https://doi.org/10.1016/j.snb.2019.127101>
29. Gao W, Emaminejad S. Fully integrated wearable sensor arrays for multiplexed in situ perspiration analysis. *Nature*. 2016;529:509–513.
30. Shirreffs SM, Maughan RJ. Whole body sweat collection in humans: an improved method with preliminary data on electrolyte content. *J. Appl. Physiol.* 1997;82(1):336–341.
31. Hartig D, Hacke S, Ott L, Gabrielczyk J, Müller C, Jördening H-J, Scholl S. Diffusion Studies of Glucose and Sucrose in Chitosan Membranes and Beads for Enzymatic Production Processes. *Chem. Eng. Technol.* 2018;41(7):1433–1440.
32. Kang X, Wang J, Wu H, Aksay IA, Liu J, Lin Y. Glucose Oxidase–graphene–chitosan modified electrode for direct electrochemistry and glucose sensing. *Biosens. Bioelectron.* 2009;25(4):901–905.
33. Zhu J, Zhu Z, Lai Z, Wang R, Guo X, Wu X, Zhang G, Zhang Z, Wang Y, Chen Z. Planar Amperometric Glucose Sensor Based on Glucose Oxidase Immobilized by Chitosan Film on Prussian Blue Layer. *Sensors*. 2002;2(4):127–136.
34. Sempionatto JR, Nakagawa T, Pavinatto A, Mensah ST, Imani S, Mercier P, Wang J. Eyeglasses based wireless electrolyte and metabolite sensor platform. *Lab. Chip*. 2017;17(10):1834–1842.
35. Kulkarni T, Slaughter G. Application of Semipermeable Membranes in Glucose Biosensing. *Membranes*. 2016;6(4):55–75.
36. Shiwaku R, Matsui H, Nagamine K, Uematsu M, Mano T, Maruyama Y, Nomura A, Tsuchiya K, Hayasaka K, Takeda Y, Fukuda T, Kumaki D, Tokito S. A Printed Organic Circuit System for Wearable Amperometric Electrochemical Sensors. *Sci. Rep.* 2018; <https://doi.org/10.1038/s41598-018-24744-x>.
37. Bandodkar AJ, Jia W, Yardımcı C, Wang X, Ramirez J, Wang J. Tattoo-based noninvasive glucose monitoring: a proof-of-concept study. *Anal. Chem.* 2015;87(1):394–398.
38. Lei Y, Zhao W, Zhang Y, Jiang Q, He J-H, Baeumner AJ, Wolfbeis OS, Wang ZL, Salama KN, Alshareef HN. A MXene-Based Wearable Biosensor System for High-Performance In Vitro Perspiration Analysis. *Small*. 2019; <https://doi.org/10.1002/smll.201901190>
39. Schmid-Wendtner M-H, Korting HC. The pH of the skin surface and its impact on the barrier function. *Skin Pharmacol Physiol.* 2006;19(6):296–302.



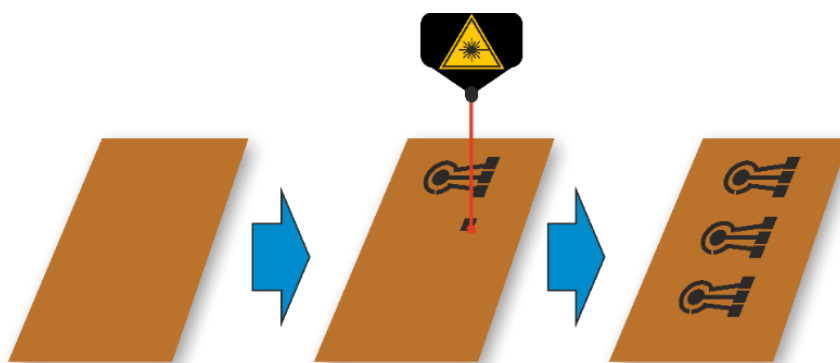
40. Derbyshire PJ, Barr H, Davis F, Higson SPJ. Lactate in human sweat: a critical review of research to the present day. *J. Physiol. Sci.* 2012;62(6):429–440.
41. Lei Y, Sun R, Zhang X, Feng X, Jiang L. Oxygen-Rich Enzyme Biosensor Based on Superhydrophobic Electrode. *Adv. Mater.* 2016;28(7):1477–1481.
42. Khattab TA, Dacrory S, Abou-Yousef H, Kamel S. Smart microfibrillated cellulose as swab sponge-like aerogel for real-time colorimetric naked-eye sweat monitoring. *Talanta.* 2019; <https://doi.org/10.1016/j.talanta.2019.120166>
43. Huang X, Liu Y, Chen K, Shin W-J, Lu C-J, Kong G-W, Patnaik D, Lee S-H, Cortes JF, Rogers JA. Stretchable, wireless sensors and functional substrates for epidermal characterization of sweat. *Small.* 2014;10(15):3083–3090
44. Kim SB, Zhang Y, Won SM, Bhandodkar AJ, Sekine Y, Xue Y, Koo J, Harshman SW, Martin JA, Park JM, Ray TR, Crawford KE, Lee K-T, Choi J, Pitsch RL, Grigsby CC, Strang AJ, Chen Y-Y, Xu S, Kim J, Koh A, Ha JS, Huang Y, Kim SW, Rogers JA (2018) Super-Absorbent Polymer Valves and Colorimetric Chemistries for Time-Sequenced Discrete Sampling and Chloride Analysis of Sweat via Skin-Mounted Soft Microfluidics. *Small.* 2018; <https://doi.org/10.1002/sml.201703334>
45. Ding R, Lisak G. Sponge-based microfluidic sampling for potentiometric ion sensing. *ACA.* 2019;1091:103–111.
46. Liu C, Xu T, Wang D, Zhang X. The role of sampling in wearable sweat sensors. *Talanta.* 2020; <https://doi.org/10.1016/j.talanta.2020.120801>
47. van Haeringen NJ. Clinical biochemistry of tears. *Surv. Ophthalmol.* 1981;26(2):84–96.
48. Xuan X, Yoon HS, Park JY. A wearable electrochemical glucose sensor based on simple and low-cost fabrication supported micro-patterned reduced graphene oxide nanocomposite electrode on flexible substrate. *Biosens. Bioelectron.* 2018;109:75–82.
49. Nyein HYY, Bariya M, Kivimäki L, Uusitalo S, Liaw TS, Jansson E, Ahn CH, Hangasky JA, Zhao J, Lin Y, Happonen T, Chao M, Liedert C, Zhao Y, Tai L-C, Hiltunen J, Javey A. Regional and correlative sweat analysis using high-throughput microfluidic sensing patches toward decoding sweat. *Sci. Adv.* 2019; <https://doi.org/10.1098/rsif.2019.0217>
50. Jia W, Bhandodkar AJ, Valdés-Ramírez G, Windmiller JR, Yang Z, Ramírez J, Chan G, Wang J. Electrochemical tattoo biosensors for real-time noninvasive lactate monitoring in human perspiration. *Anal. Chem.* 2013;85(14):6553–6560.
51. Yoon H, Nah J, Kim H, Ko S, Sharifuzzaman M, Barman SC, Xuan X, Kim J, Park JY. A chemically modified laser-induced porous graphene based flexible and ultrasensitive electrochemical biosensor for sweat glucose detection. *Sens. Actuators B Chem.* 2020; <https://doi.org/10.1016/j.snb.2020.127866>
52. Zhang F, Zhang W, Guo J, Lei Y, Dar MA, Almutairi Z, Alshareef HN. All-Carbon Hybrid Mobile Ion Capacitors Enabled by 3D Laser Scribed Graphene. *Energy Technol.* 2020; <https://doi.org/10.1002/ente.202000193>
53. Puetz P, Behrent A, Baeumner AJ, Wegener J. Laser-scribed graphene (LSG) as new electrode material for impedance-based cellular assays. *Sens. Actuators B Chem.* 2020; <https://doi.org/10.1016/j.snb.2020.128443>
54. Yagati AK, Behrent A, Beck S, Rink S, Goepferich AM, Min J, Lee M-H, Baeumner AJ. Laser-induced graphene interdigitated electrodes for label-free or nanolabel-enhanced highly sensitive capacitive aptamer-based biosensors. *Biosens. Bioelectron.* 2020; <https://doi.org/10.1016/j.bios.2020.112272>
55. Wongkaew N, Simsek M, Arumugam P, Behrent A, Berchmans S, Baeumner AJ. A Robust strategy enabling addressable porous 3D carbon-based functional nanomaterials in miniaturized systems. *Nanoscale.* 2019;11(8):3674–3680.
56. Timmer B, Sparreboom W, Olthuis W, Bergveld P, van den Berg A. Optimization of an electrolyte conductivity detector for measuring low ion concentrations. *Lab Chip.* 2020;2(2):121–124.
57. Ricci F, Moscone D, Palleschi G. Procedure 17 Preparation of Prussian blue-modified screen-printed electrodes via a chemical deposition for mass production of stable hydrogen peroxide sensors. *Compr. Anal. Chem.* 2007;49: e119-e124.

58. Jiang Y, Zhang X, Shan C, Hua S, Zhang Q, Bai X, Dan L, Niu L. Functionalization of graphene with electrodeposited Prussian blue towards amperometric sensing application. *Talanta*. 2011;85(1):76–81.
  59. Jia W-Z, Wang K, Xia X-H. Elimination of electrochemical interferences in glucose biosensors. *Trends Analyt. Chem.* 2010;29(4):306–318.
  60. Zhang X, Wang J, Ogorevc B, Spichiger UE. Glucose Nanosensor Based on Prussian-Blue Modified Carbon-Fiber Cone Nanoelectrode and an Integrated Reference Electrode. *Electroanalysis*. 1999;11(13):945–949.
- \* Bauer M. Development of Wearable, Electrochemical Sweat Sensors Based on Laser-Scribed Graphene. Master's Thesis. 2018.

### 3.7 Supporting Information

#### 3.7.1 Laser-Scribing Process

The general laser-scribing process is schematically shown in the following **SI Figure 3.1**. Flexible PI substrate is exposed to a commercial infrared CO<sub>2</sub> laser. The desired pattern can be “printed” on the substrate using suitable power and speed settings to obtain the porous graphene-like material.

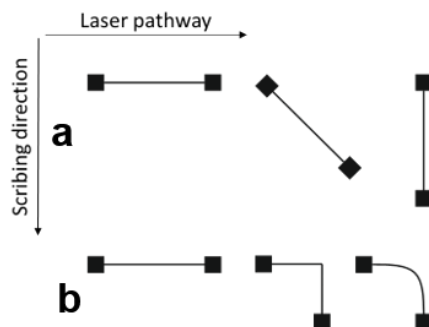


**SI Figure 3.1** Scheme of the laser-scribing process: a polyimide foil (orange) as flexible substrate for the desired pattern is exposed to a commercial infrared CO<sub>2</sub> laser ( $\lambda = 10.6 \mu\text{m}$ ) with suitable laser power settings and scribing speed under ambient conditions to provide a porous 3D graphene material (black) with properties appropriate for electrochemical analysis [\*]

LIG electrodes produced with the VLS 2.30 laser scriber show different performance depending on the orientation during the scribing process. The scribing direction is always along the Y-axis, the laser pathway is always perpendicular to the scribing direction along the X-axis. Primitive designs were created that consisted only of two contact pads connected by a conductive strand. A design with a linear connection was produced; once orientated perpendicular to the scribing direction, once rotated by 45°, and another one parallel to the scribing direction (**SI Figure 3.2 a**). The resistance of the designs (N = 3) was measured from the middle of one pad to the middle of the other pad with a commercial voltmeter (distance of 5 cm).

While orientated in scribing direction, the resistance was  $594 \pm 27 \Omega$  and therefore the lowest. If produced in a 45° angle, an increase in resistance by 76 % could be observed ( $1048 \pm 13 \Omega$ ). Production perpendicular to the scribing direction leads to an increase by 128 % ( $1353 \pm 37 \Omega$ ).

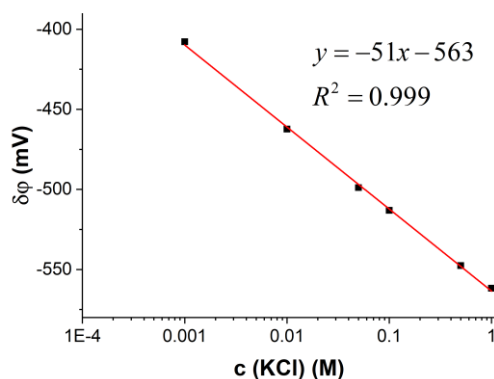
All structures that are not aligned to the scribing direction increase the resistance of an electrode significantly. A second set of designs was created with the same length and thickness as before but once with a 90° bend and once with the kink smoothed to a curve. (**SI Figure 3.2 b**) The design with the 90° bend showed an increase in resistance by 65 % ( $982 \pm 19 \Omega$ ), introducing the curve leads to an increase of 54 % ( $916 \pm 9 \Omega$ ).



**SI Figure 3.2** **a** Linear designs for resistance measurements; **b** Designs with kink or curve

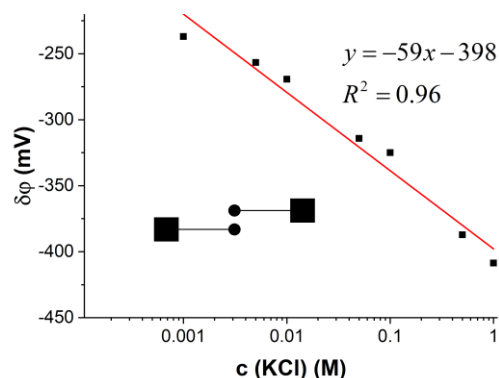
### 3.7.2 Optimization and Modification Process for Potentiometric Potassium Ion Sensor

To prove the measurement principle, at first a simple potentiometric setup was tested in bulk solution by using the ion selective membrane modified LIG electrode (diameter  $d = 2.5$  mm) versus a commercial external Ag/AgCl electrode. As can be seen in **SI Figure 3.3**, the dose-response curve shows the expected trend over a large concentration range. The slope of 51 mV is quite close to the theoretically expected value of 59 mV. Changes in ionic strength did not influence the potential between an unmodified LIG electrode and the commercial Ag/AgCl RE.



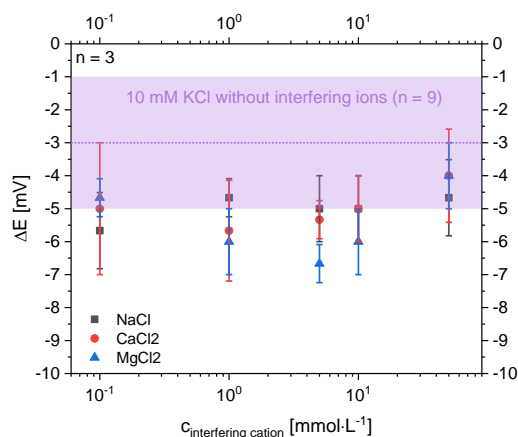
**SI Figure 3.3** Dose-response curve of a LIG electrode with a valinomycin doped membrane, using a standard Ag/AgCl electrode as reference in bulk solution. Coherence which shows LIG potassium selective electrode is suitable ( $n = 1$ ).

Since the initial measurements were performed by dipping the electrodes into solution, the setup was changed to a planar LIG electrodes on one flexible substrate. To enable a planar electrode setup a new design had to be found. Therefore, both electrodes had to be closer together, to enable a full coating of both electrodes with just one drop of sample solution. The setup used for measurements shown in **SI Figure 3.4** is the best compromise between analogy to the real wearable setup and working convenience.



**SI Figure 3.4** Dose response curve of a valinomycin coated electrode versus a planar Ag/AgCl-coated LIG reference electrode. The corresponding electrode design is shown as inset. The measurements were performed by depositing a drop of potassium chloride solution on the planar electrode. Since the curve shows a linear behavior the measurement principle was approved working ( $n = 1$ ).

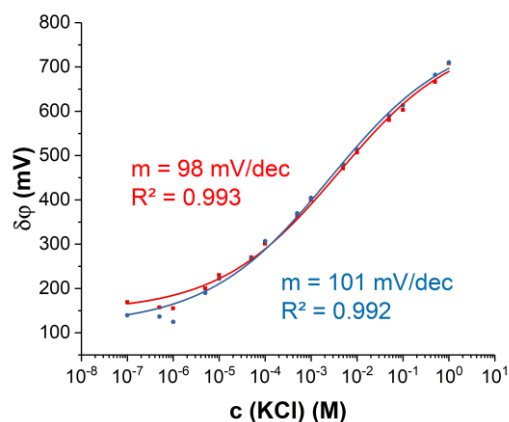
The thickness of the ion-selective membrane was about 70  $\mu\text{m}$  (measured by optical light microscopy) and the concentration of the ionophore in the membrane solution was 16 mg per gram PVC. Both parameters might have potential to be optimized, but as the slope of the calibration curve is close to the theoretical value no other combinations have been tested. Furthermore, valinomycin selectivity towards  $\text{K}^+$  ions was demonstrated against to the main interfering cations  $\text{Na}^+$ ,  $\text{Mg}^{2+}$  and  $\text{Ca}^{2+}$  as shown in **SI Figure 3.5**. Potassium ion concentration was constant at 10  $\text{mmol}\cdot\text{L}^{-1}$  whereas the interfering cation concentrations were varied between 0.1 and 50  $\text{mmol}\cdot\text{L}^{-1}$ .



**SI Figure 3.5** 10 mM KCl solution in water were measured (mean value with standard deviation is shown as violet box,  $n = 9$ ). 10 mM KCl solutions with main interfering cation concentrations between 0.1 and 50 mM were measured. They show a small signal decrease to the sample solution without interfering ions. **Grey boxes** NaCl **red circles**  $\text{CaCl}_2$  **blue triangles**  $\text{MgCl}_2$  solutions were measured with the planar design using the drop-coated ISE vs. unmodified LIG electrode

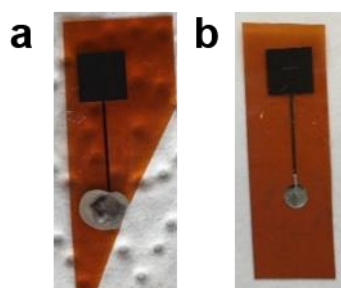
The dose-response curve reveals that the principle will work on LIG electrodes. The signal changes upon changing the concentration were measured immediately after sample

application and after 60 seconds with the silver paste based Ag/AgCl RE. Both resulted in stable and reproducible values (**SI Figure 3.6**).



**SI Figure 3.6** Dose-response-curve the potentiometric, planar LIG based sensor, measuring a KCl concentration ranging from  $10^{-7}$  to 1 M. In this case the reference electrode was synthesized using a conductive silver paste ( $n = 3$ ). The linear range goes down to  $10^{-4}$  M KCl. The red curve shows the potential directly after sample application with a slope of 98 mV per decade, whereas the blue curve shows the potential after 60 s with a slope of 101 mV per decade, respectively. For both times the curves show good coherence

As a next step, to further improve the LIG based electrode setup, a different planar reference electrode was used. Up to now a conductive silver paste with deposited silver chloride was used (**SI Figure 3.7 a**), which was suitable for initial measurements, but since the deposition of this paste cannot be performed reproducibly and it is not known which additional ingredients are contained in this paste, the reference electrode needed further improvement.

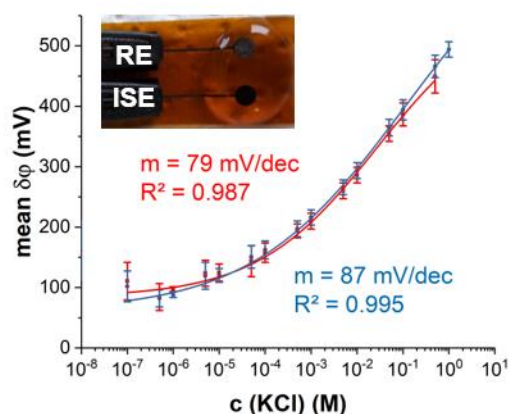


**SI Figure 3.7 a** LIG based reference electrode, using a conductive silver paste. **b** Ag/AgCl RE which was made by using a plating device and  $\text{AgNO}_3$  electrolyte. The improved procedure, using a plating device, enables a much more reproducible fabrication process

Therefore, first Ag should be electrodeposited with from a silver nitrate solution and, in a second step, the surface layer oxidized to silver chloride. A commercially available handheld plating device was used for deposition with a  $\text{AgNO}_3$  solutions, mass concentration ranging between  $200 \text{ mg}\cdot\text{mL}^{-1}$  and  $1000 \text{ mg}\cdot\text{mL}^{-1}$ . One drop of electrolyte, between 10 and  $50 \mu\text{L}$ , was deposited on the LIG. For a uniform deposition it was needed to equilibrate the silver nitrate solution on the LIG. Different equilibration times between 1 minute and 15 minutes were tested

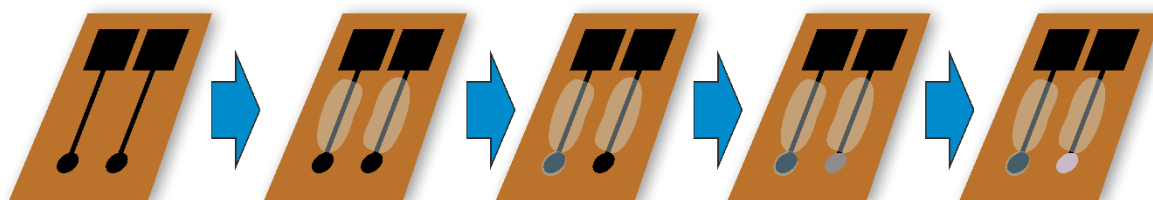
and the uniformity after the plating process was evaluated by naked eye. The actual plating was executed between a few seconds and 2 minutes. An immediate formation of a silver layer on the LIG could be observed. To form the silver chloride coating, the silver-plated electrode was immersed into a saturated KCl solution and a DV voltage of 800 mV was applied for 60 seconds up to 200 seconds. A slight darkening of the silver layer could be seen (**SI Figure 3.7 b**).

In a  $10^{-2}$  M KCl solution this new planar LIG based reference electrode shows a potential of 2 mV versus a silver wire coated with silver chloride, which indicates that the coated LIG electrode should be suitable as reference electrode. As can be seen in **SI Figure 3.8** the improved LIG-based RE decreases the linear range of the potentiometric potassium selective sensor down to  $10^{-5}$  M KCl.



**SI Figure 3.8** Dose-response-curve the potentiometric, planar LIG based sensor, measuring a KCl concentration ranging from  $10^{-7}$  to 1 M. In this case the Ag/AgCl RE was electrodeposited with a plating device. The sensor design is shown as inset. The linear range goes down to  $10^{-5}$  M KCl. The red curve shows the potential after 0 s with a slope of 79 mV per decade, whereas the blue curve shows the potential after 60 s with a slope of 87 mV per decade, respectively. For both times the curves show good coherence

Finalized parameters are summarized in the experimental section. The final modification procedure to obtain a potentiometric LIG sensor is shown in the following **SI Figure 3.9**.



**SI Figure 3.9** The entire modification process for the potentiometric sensor is shown schematically from left to right starting with the raw LIG pattern, followed by the insulation of the strands and drop-coating of the ion-selective membrane cocktail on the left electrode. Afterwards, on the right electrode, a silver layer is plated and in the last drawing the formed AgCl layer is shown [\*]

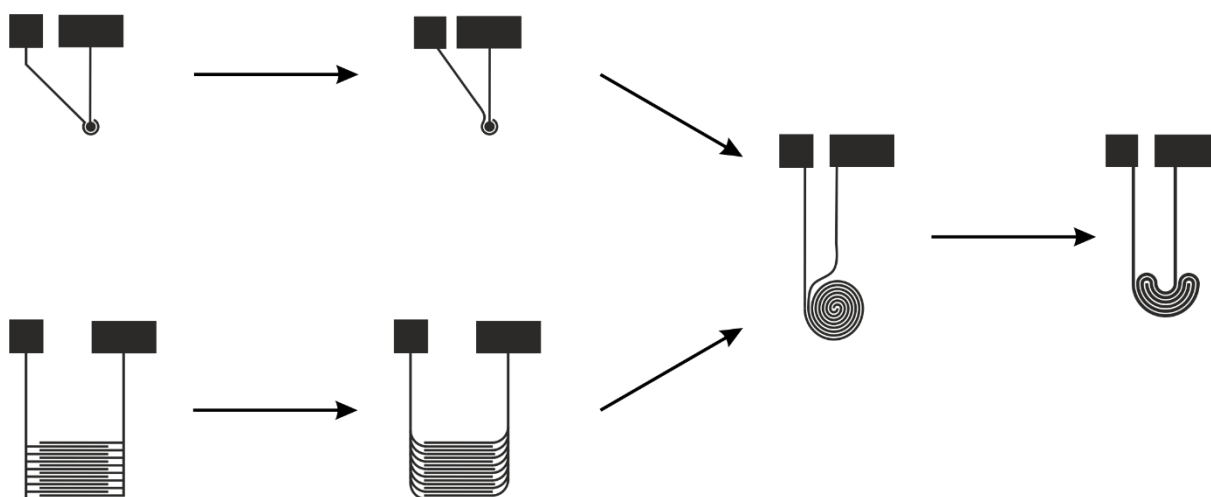
### 3.7.3 Optimization of Impedance-based Electrolyte Sensor

Cell constants for the interdigitated structure are calculated from the ratio of the space  $S$  between two fingers and the width  $W$  of one finger. According to literature [56] an optimized cell constant is obtained for a  $S/W$  ratio of 0.54. Furthermore, the length  $L$  and the number  $N$  of the electrode fingers are important characteristics, and both should be as large as possible to improve the cell constant. In a first attempt,  $L$  was set to 6 mm and  $N$  was set to 10, which results in a total electrode size of approximately 15 mm height and 8 mm width.



**SI Figure 3.10** Layout of an interdigitated Laser-Induced-Graphene electrode on polyimide substrate

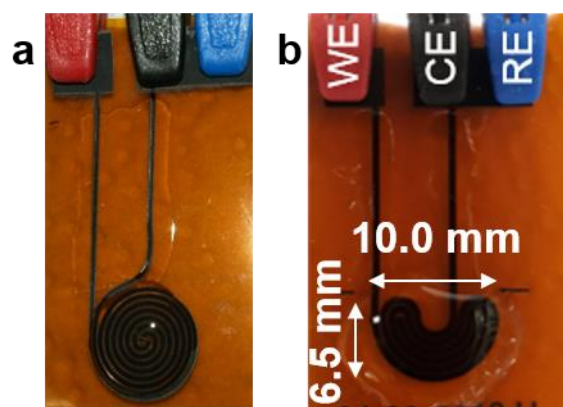
The electrode layout needed further improvements with regard to respective scribing conditions. Right angles and lines perpendicular to the scribing direction should be avoided as explained above. The evolution of the layout is shown in **SI Figure 3.11** where we finally ended up with the kidney-shaped design which was used for all investigations in the main part. For all designs, the line width of the electrodes is 0.5 mm and spacing between the electrodes is 0.2 mm.



**SI Figure 3.11** Optimization of LIG electrode layout for impedance measurements. Since right angles increase the electrode resistance, the design was created with the least numbers of right angles. It turned out, that an interdigitated design with a higher electrode area showed better results. Horizontal structures show decreased resistance since they are orientated in the scribing direction.

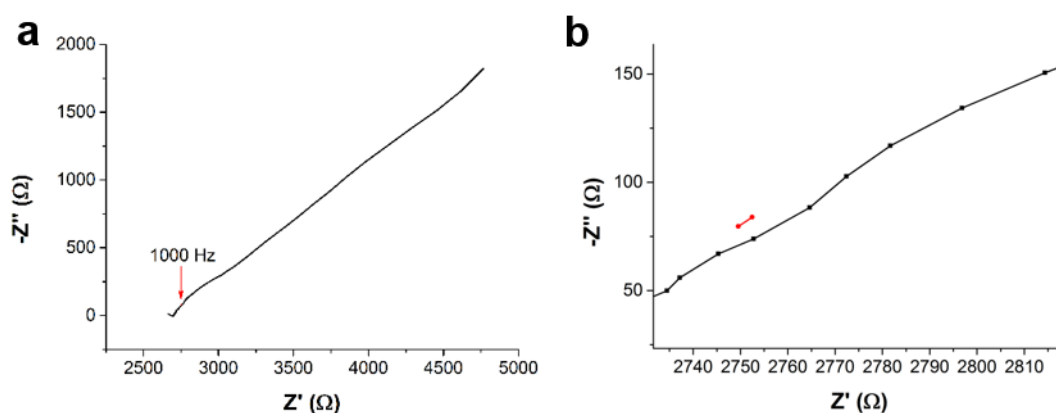
The in following described optimization procedures were performed with the previously developed spiral design (**SI Figure 3.12 a**). These procedures are concerning especially the instrumental settings and sample application techniques. For the measurements shown in the main part of the work the kidney-shaped design (**SI Figure 3.12 b**) was used.





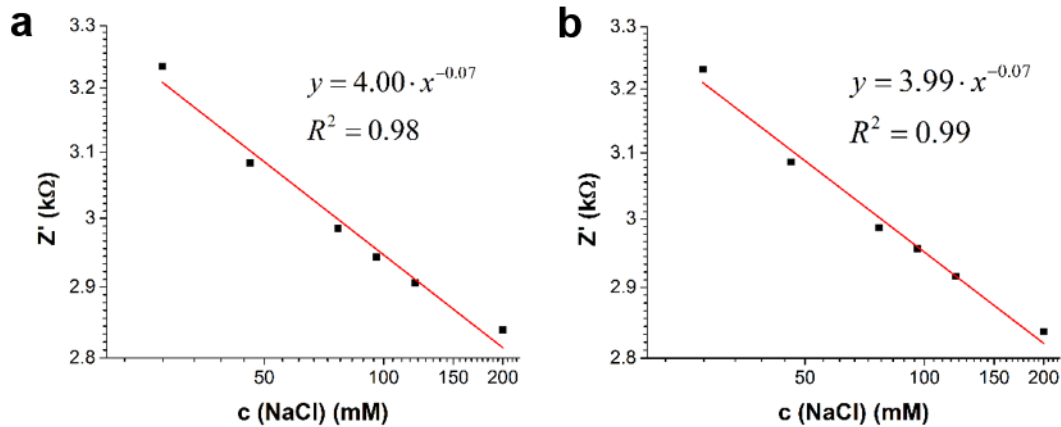
**SI Figure 3.12** **a** Spiral electrode design for impedance measurement as previous version of the finally used kidney-shaped design shown in **b**. Line width is 0.5 mm; line spacing between the electrodes is 0.2 mm [\*]

A full impedance spectrum of a LIG electrode was measured at  $E_{DC} = 0$  V,  $E_{AC} = 0.1$  V, from 100 kHz to 1 Hz for a 0.5 M NaCl solution (**SI Figure 3.13 a**). The full spectrum is compared to a measurement at a fixed frequency at 1000 Hz (**SI Figure 3.13 b**). It can be seen, that the impedance value of the fixed frequency matches the value obtained out of the full spectrum. Measuring at a fixed frequency of 1000 Hz reduces sensor's response time from minutes to a few seconds.



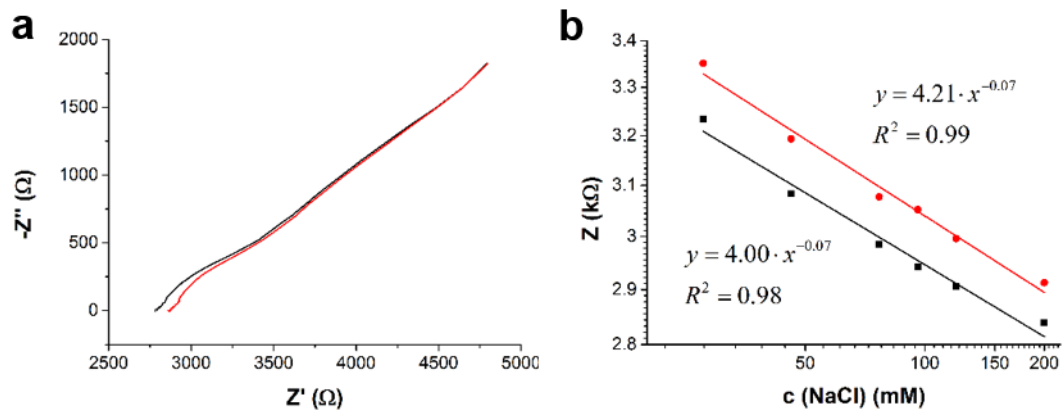
**SI Figure 3.13** Spiral design was used for all measurements. **a** Impedance spectrum of a LIG electrode measured at  $E_{DC} = 0$  V,  $E_{AC} = 0.1$  V, from 100 kHz to 1 Hz immersed into a 0.5 M NaCl solution. **b** Comparison of the full spectrum (black, magnified cut-out from **a**) with a measurement at a fixed frequency of 1000 Hz (red). It can be seen, that the impedance value of the fixed frequency matches the value obtained out of the full spectrum

Next, the dose-response curves are shown. NaCl solution in a concentration range between 28 and 200 mM were measured. The data shown in **SI Figure 3.14 a** were derived from a full spectrum measurement. The values were taken at a frequency of 1 kHz. Data shown in **SI Figure 3.14 b** were obtained from a measurement of the same samples at fixed frequency of 1 kHz. There is no significant difference between both. A measurement at fixed frequency is much faster and therefore preferable.



**SI Figure 3.14** Dose-response-curves of LIG electrodes, measured at  $E_{DC} = 0$  V,  $E_{AC} = 0.1$  V, from 100 kHz to 1 Hz for NaCl concentrations ranging from 28 mM to 200 mM. Impedance values at 1000 Hz are taken from **a** a full spectrum and **b** a measurement at fixed frequency was performed with the same samples

**SI Figure 3.15 a** shows full impedance spectra, measured at  $E_{DC} = 0$  V,  $E_{AC} = 0.1$  V, from 100 kHz to 1 Hz for a 0.2 M NaCl solution. The black spectrum was measured by immersing the electrode into solution, whereas for obtaining the red spectrum a drop of salt solution was deposited on the electrode structure. **SI Figure 3.15 b** shows the corresponding dose-response-curves for NaCl concentrations ranging between 28 mM and 200 mM. The impedance value was taken out of the full spectra at 1000 Hz. The curves do not match; therefore, one application mode must be chosen.



**SI Figure 3.15 a** Impedance spectra, measured at  $E_{DC} = 0$  V,  $E_{AC} = 0.1$  V, from 100 kHz to 1 Hz for a 0.2 M NaCl solution. The black spectrum was measured by immersing the electrode into solution, whereas for obtaining the red spectrum a drop of salt solution was deposited on the electrode structure **b** Corresponding dose-response-curves for NaCl concentrations ranging from 28 mM to 200 mM. The impedance value was taken out of the full spectra at 1000 Hz. The curves do not match; therefore, one mode of application should be chosen

### 3.7.4 Optimization of Amperometric Biosensors

Two different methods for PB deposition were investigated [57, 58]. Subsequently, differently concentrated chitosan solutions for drop-coating a suitable membrane were applied using literature conditions [35, 59]. Furthermore, the electrodeposited and well-reproducible Ag/AgCl RE was compared to a LIG reference electrode. Reproducibility and complexity of production were also taken into account for the decisions. During these fundamental optimization steps a suitable run time for the amperometric measurement was determined, which meets the requirements with regard to accuracy and time effort. Last step was optimization of enzyme immobilization and incubation time. [\*]

#### *Electrodeposition of Prussian Blue*

An often-reported method for PB deposition on a graphene or carbon-based surface is the electrochemical deposition using cyclic voltammetry [58, 60]. The electrodeposition was investigated with different experimental setups and electrodes. In the beginning a vertical three-electrode setup with an external Ag/AgCl RE and a platinum wire CE was used. Later, the electrodeposition was performed in the planar all-LIG setup with a LIG reference electrode and the self-made electrodeposited Ag/AgCl RE, respectively. Different scan speeds and number of cycles were investigated. [\*]

First, the planar sensor with the electrodeposited Ag/AgCl reference electrode was tested. Depositing PB solely on the LIG WE was not possible using the sensor layout. After drop-coating the PB precursor solution, without applying a potential or current, a redox reaction started forming a clearly visible blue PB layer on the Ag/AgCl surface. Therefore, the sequence of electrode modification was swapped. The PB layer was deposited first in vertical setup using an external RE and in the second step the Ag/AgCl deposition procedure was performed. It is important to ensure the silver nitrate solution does not touch the PB layer due to the spontaneous formation of silver on the WE surface. [\*]

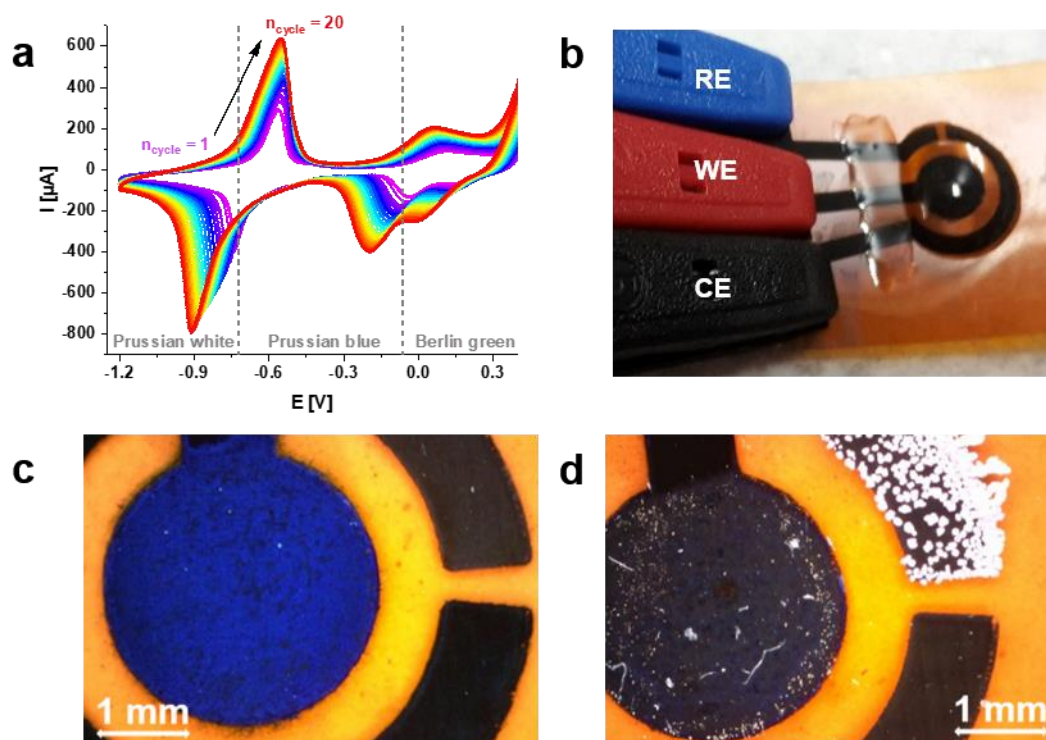
The unmodified sensor and both external electrodes were fixed and immersed into the deoxygenated and freshly mixed precursor solution. After a few CV scans, independent of scan rate and potential step width, a dark blue layer on the WE was recognizable with the naked eye. After at least ten cycles the PB layer was distinctive visible and furthermore PB was precipitated in the precursor solution. During removing the sensor from the setup and also during electrode cleaning with water, a large part of the blue layer dropped off. This vertical setup proved soon to be a laborious method where a large amount of the precursor solution is needed. Therefore, the planar setup was tested again with the unmodified LIG as reference electrode. **SI Figure 3.16 a** shows the resulting CV scans during the electrodeposition process

of Prussian blue versus a LIG reference electrode in a planar setup (**SI Figure 3.16 b**). The resulting PB layer before cleaning with water is shown in **SI Figure 3.16 c**. [\*]

Compared with literature data measured in conventional cells under similar conditions (pH, buffer, concentrations, instrumental settings), the shape of the single CVs and also the observation with increasing repetitions are similar [58, 60]. With every additional scan the peak currents increase whereas a slight potential shift, especially for the reduction peaks, is observed. The characteristic four main peaks of both redox couples Prussian blue/Prussian white and Prussian blue/Berlin green are clearly differentiable. For a reproducible sensor production and also with regard to instrumental effort, the electrochemical deposition of PB was not the best option. The formed PB layer was rather sensitive and even got damaged during rinsing to remove the excess PB precursor solutions.[\*]

#### *Chemical Deposition of Prussian Blue*

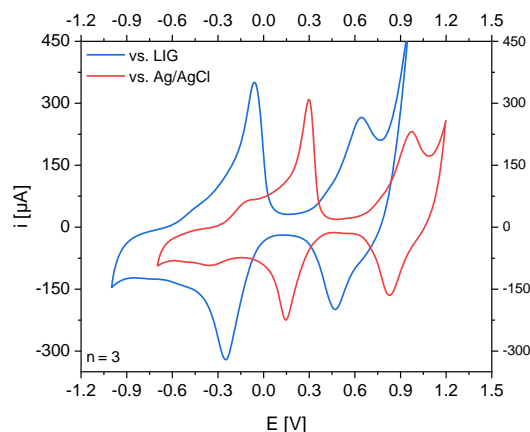
Ricci *et al.* described a simple procedure for the modification of screen-printed graphite electrodes via chemical deposition of PB [57]. The protocol was varied to increase the reproducibility of the redox mediator layer. Therefore, the PB precursor solutions are mixed exclusively on the WE area ( $d = 3 \text{ mm}$ ) and soaked in the porous graphene layer for 20 minutes at ambient conditions. Afterwards, the layer was stabilized and activated for 2 hours at  $100 \text{ }^\circ\text{C}$ . To avoid an undefined loss of PB, the chitosan membrane was drop-coated before the final washing step was performed. An image of the modified sensor was captured with a handheld digital microscope and is shown in **SI Figure 3.16 d**. Due to the comparable performance of the sensors and the straightforward production process, which is also more compatible with the Ag/AgCl deposition, the chemical deposition was chosen. [\*]



**SI Figure 3.16** **a** CV scans of Prussian blue electrodeposition on the LIG working electrode. The CV was performed from 0.5 to -1.2 V vs. LIG ( $20 \text{ mV}\cdot\text{s}^{-1}$ ) in a planar setup [\*] **b** with applied PB precursor solutions. [\*] **c** The WE area modified with electrodeposited PB. The electrochemical deposition was used in a planar setup vs. LIG RE and the image was captured before washing steps. The LIG counter electrode is unmodified [\*] **d** PB layer on the WE was chemically deposited. To avoid an undefined loss of PB, the chitosan membrane was drop-coated before the final washing step was performed. On the RE the Ag/AgCl layer was electrodeposited after PB deposition. The CE is unmodified. (The magnified images were captured with Dino Lite digital USB microscope with suitable software Dino Capture 2.0 [\*])

#### Ag/AgCl and LIG as Reference Electrode Material

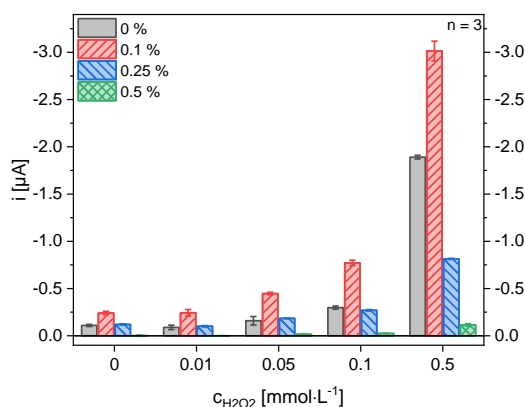
CVs of pure buffer were measured in the planar setup versus internal RE. The sensors were prepared with chemical deposited Prussian blue and 0.5% chitosan solution. Representative cyclic voltammograms are shown for both setups in **SI Figure 3.17**. The whole CV versus Ag/AgCl is shifted by around 0.4 V to higher potentials in comparison to the LIG reference electrode. Using a LIG reference electrode is favorable because the sensor's working range is near 0 V. The peak currents are higher than the ones using the Ag/AgCl electrode that promises an increased sensitivity of the sensor. Furthermore, the practically nonexistent modification step pleads also for LIG as RE material. A large drawback of the LIG RE was the occurring potential shift during repeated CV scans as well as during the amperometric detection. Therefore, the RE modification is necessary. [\*]



**SI Figure 3.17** Comparison of representative CVs (PBS; scan speed  $50 \text{ mV}\cdot\text{s}^{-1}$ ) were determined in a planar sensor setup with droplet method. The PB layer was chemically deposited and covered by a chitosan membrane (0.5% chitosan solution). CVs were measured versus internal LIG (blue) and versus electrodeposited Ag/AgCl reference electrode (red). Dependent on the RE used the peak potentials are shifted [\*]

#### Optimization of Chitosan Membrane Thickness

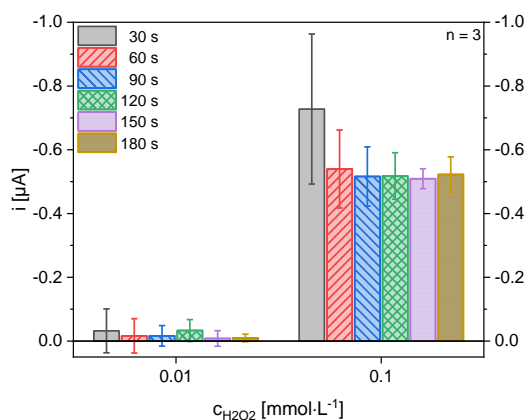
Same volumes of chitosan solutions with concentrations of 0.1%, 0.25% and 0.5% were applied to the WE area and dried overnight at ambient conditions. After buffer measurements, four  $\text{H}_2\text{O}_2$  solutions in a concentration range from 10 to  $500 \mu\text{mol}\cdot\text{L}^{-1}$  were applied three times. Chronoamperometry was run for 60 s at the respective suitable potential. The resulting currents and the signal-to-noise ratio are shown and compared in **SI Figure 3.18**. The sensor with the lowest chitosan concentration (0.1%) applied, showed for all hydrogen peroxide (HP) concentrations the highest current. It is plausible that the lower concentrated chitosan solutions result in a thinner membrane than higher concentrated ones when the same volume was applied. Therefore, the diffusion of the analyte but also interfering compounds, is less hindered in a thinner membrane. On the other hand, with the 0.5% chitosan membrane for HP concentrations of  $50 \mu\text{mol}\cdot\text{L}^{-1}$  and above, a significant increased S/N was obtained. The thicker membrane increases the selectivity but reduces the sensitivity. Experiments were continued with 0.1% and 0.5% chitosan membranes but subsequently the 0.1% chitosan solution was used solely. The later immobilized biorecognition element increases the selectivity and therefore the higher sensitivity of the thin membrane is preferable. [\*]



**SI Figure 3.18** Different concentrated chitosan solutions (0%, 0.1%, 0.25%, 0.5%) were drop-coated on the WE of hydrogen peroxide sensors with chemical deposited PB layer ( $n = 3$ ). The signals, which were obtained 60 s after application of HP solutions in 1X PBS pH 7.4, were compared [\*]

### Optimization of Chronoamperometric Response Time

During all the modification and optimization steps a suitable chronoamperometric run time was determined. Chronoamperometry was run for 180 s. Every 30 seconds the responded data were evaluated with regard to signal and principally stability. Results for 10 and 100  $\mu\text{mol}\cdot\text{L}^{-1}$   $\text{H}_2\text{O}_2$  solutions are shown in **SI Figure 3.19**. The signal is almost stable after 60 seconds for 0.1  $\text{mmol}\cdot\text{L}^{-1}$  HP solutions. All signals of lower concentration are similar within the error bars. The standard deviations of the three-fold determinations are slightly decreasing for both  $\text{H}_2\text{O}_2$  concentrations with increasing response times. With regard to real-time monitoring, a short run time is preferable. Therefore, 60 seconds acquisition time is a suitable compromise between response time and reliability of the signal. [\*]



**SI Figure 3.19** 10 and 100  $\mu\text{M}$  hydrogen peroxide solutions were applied onto the sensor and the chronoamperometric measurements were run for 180 s ( $n = 3$ ). Every 30 seconds the response data were evaluated. Signal and signal stability (refers to standard deviation) were considered to find a compromise between response time and reliability of the signal [\*]



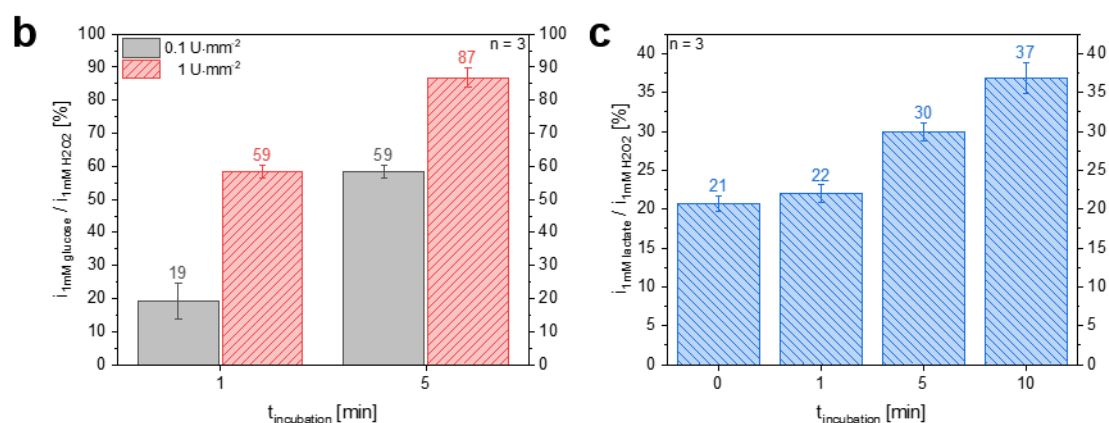
### Immobilization of Enzyme, Activity and Incubation Time Experiments

For the amperometric sensor, different enzyme immobilization strategies found in literature [29, 33, 34] were adapted and tested. The sensors' performances were compared, and the results are shown summarized in **SI Figure 3.20 a**. A reason for failing of the immobilization strategies a) and b) is the acidic milieu of the chitosan solution. Chitosan is only soluble in acidic aqueous solution that is no suitable medium for the sensitive enzymes over a longer period. Therefore, extended contact with the acetic solution probably inactivated or damaged the glucose oxidase. Applying the enzyme solution on top of the chitosan network, could lead to a loose entrapment within the polymer structure. [\*]

The same volume of GOx aliquots (theoretically calculated activity of 0.4 and 4 U· $\mu\text{L}^{-1}$ ) was applied onto the chitosan membrane. The resulting GOx activities therefore were 0.1 and 1 U· $\text{mm}^{-2}$  on the working electrode, assuming a planar surface. Incubation times of 1 and 5 minutes were tested and the respective signals were compared (**SI Figure 3.20 b**). To compare different sensors directly with each other, the signal of glucose was normalized to the signal of the respective  $\text{H}_2\text{O}_2$  solution. As expected, higher enzyme activity within the same incubation time provided a higher signal (50 % higher for the 5 min incubation example shown in **SI Figure 3.20 b**). Similarly, longer incubation resulted in higher signals. The incubation time experiment was repeated with 5 U· $\mu\text{L}^{-1}$  LOx instead of GOx solutions (**SI Figure 3.20 c**). Also here, longer incubation times provide a higher normalized signal. With regard to the later application as continuous sensing device long incubation times are not preferable. Therefore, the application of a high enzyme amount is favorable. [\*]

**a**

immobilization strategy		performance
1)	enzyme covered with chitosan solution [34]	no measurable response
2)	enzyme premixed with chitosan solution [29]	no reproducible results
3)	enzyme applied onto chitosan membrane [33]	reliable signals



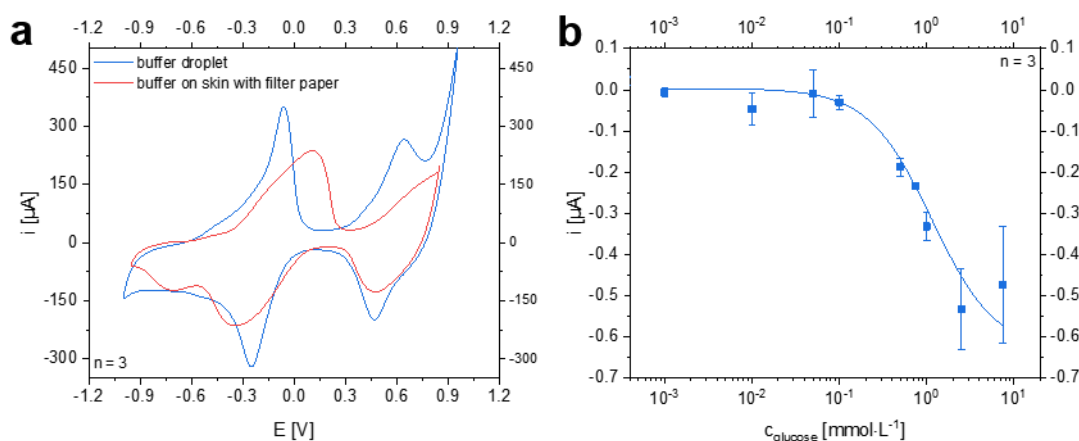
**SI Figure 3.20 a** Different immobilization strategies with chitosan as enzyme-friendly material were adapted and tested. The sensor performances suggested an enzyme application on top of the chitosan



layer [\*] **b** 2  $\mu\text{L}$  of two different GOx solutions ( $0.4 \text{ U}\cdot\mu\text{L}^{-1}$  and  $4 \text{ U}\cdot\mu\text{L}^{-1}$ ) were applied on top of the sensors and incubated overnight at  $4^\circ\text{C}$ . The resulting enzyme activities at the WE were calculated as  $0.1 \text{ U}\cdot\text{mm}^{-2}$  (grey) and  $1 \text{ U}\cdot\text{mm}^{-2}$  (red). The signals are normalized to the signal of  $1 \text{ mM}$  hydrogen peroxide solution [\*] **c** Enzyme incubation experiments were also performed with a  $5 \text{ U}\cdot\mu\text{L}^{-1}$  lactate oxidase solution drop-coated on top of a chitosan/PB modified WE (each  $n = 3$ ) [\*]

### 3.7.5 Glucose Biosensor Performance on Skin

To proof the sensors functionality on biological substrates, the experiments were repeated on chicken skin using filter paper as sweat collecting tissue. Detection on the blank chicken skin was not possible. Poor conductivity and a blocked electrode surface were observed, but the reasons therefore were not further investigated. With a sweat absorbing substrate layer between electrodes and chicken skin the sensors performance was recovered. A noticeable difference to the droplet method was the shift of sensor's suitable working potential to a higher potential as shown in **SI Figure 3.21 a**. Especially, in the anodic current region the peaks were distorted compared to CVs obtained with droplet method. Thus, the peak separations were significantly increased indicating a restricted electron transfer. Glucose concentrations between  $1 \mu\text{mol}\cdot\text{L}^{-1}$  and  $10 \text{ mmol}\cdot\text{L}^{-1}$  were measured three times on chicken skin with filter paper at a slightly increased potential compared to droplet method. The resulting calibration curve is shown in **Figure 3.21 b**. Due to the previous obtained results during potassium sensor characterization, higher LOD and LOQ were expected. Indeed, both values are increased by a factor of nine to  $120 \pm 4 \mu\text{mol}\cdot\text{L}^{-1}$  and  $365 \pm 11 \mu\text{mol}\cdot\text{L}^{-1}$  compared to droplet method. Sensor sensitivity decreased by a factor of five to  $4.5 \pm 0.1 \mu\text{A}\cdot\text{L}\cdot\text{mmol}^{-1}\cdot\text{cm}^{-2}$ . [\*]



**SI Figure 3.21 a** CVs of glucose sensor in buffer ( $50 \text{ mV}\cdot\text{s}^{-1}$  vs. LIG) with droplet method (blue) and measured on chicken with filter paper as sweat collection pad (red) [\*] **b** Dose-response curve ( $n = 3$ , SD represented by error bars) of amperometric detection of glucose on chicken skin with filter paper as sweat collection pad at a potential of  $0.2 \text{ V}$  vs. LIG, acquisition time of  $60 \text{ s}$  and no further incubation time. A slope of  $-0.32 \pm 0.01 \mu\text{A}\cdot\text{L}\cdot\text{mmol}^{-1}$  and an adjusted  $R^2$  value of  $0.9895$  were calculated. The LOD is  $120 \pm 4 \mu\text{mol}\cdot\text{L}^{-1}$  and the LOQ is  $365 \pm 11 \mu\text{mol}\cdot\text{L}^{-1}$  [\*]

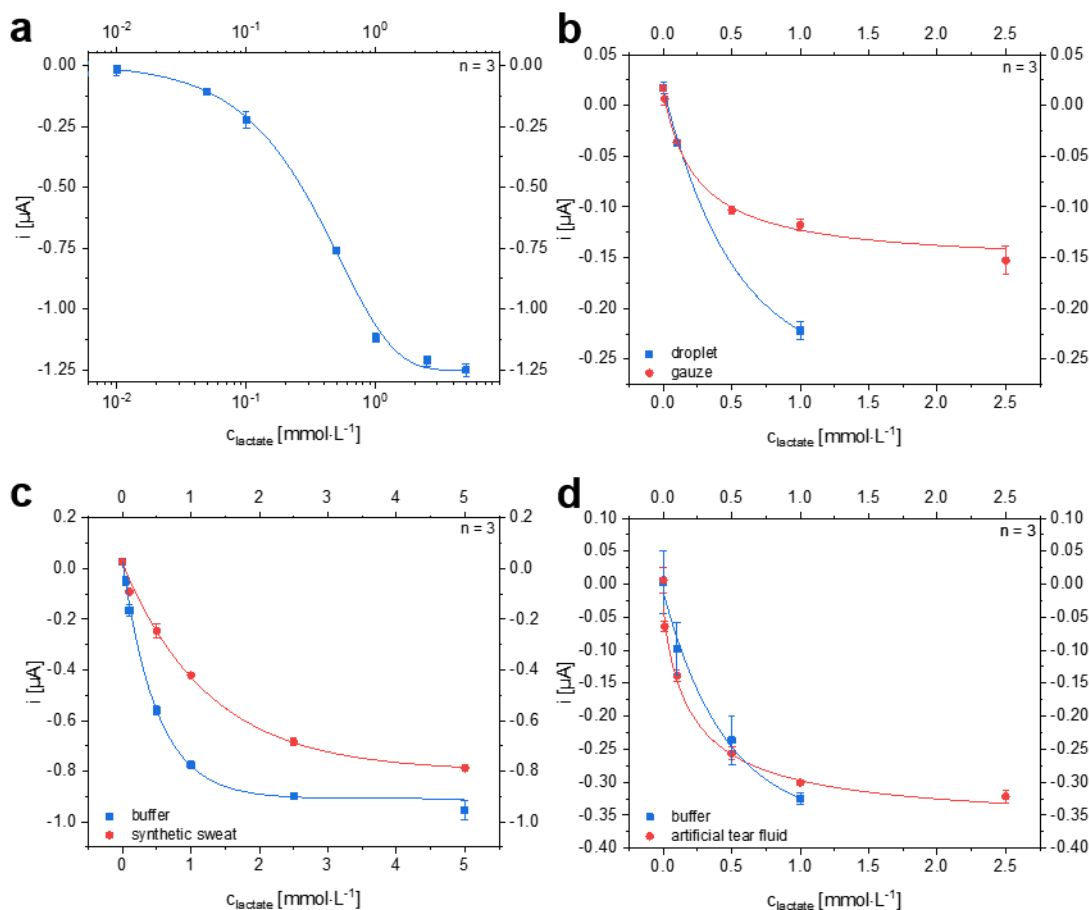
### 3.7.6 Lactate Biosensors' Performance Under Different Conditions

The simple exchangeability of the enzyme was proven by replacing GOx with LOx. The lactate detection with LOx immobilized was performed within a concentration range of 10  $\mu\text{mol}\cdot\text{L}^{-1}$  and 5  $\text{mmol}\cdot\text{L}^{-1}$ . The resulting calibration curve for lactate detection with droplet method is shown in **SI Figure 3.22 a**. A LOD of  $28 \pm 3 \mu\text{mol}\cdot\text{L}^{-1}$  and a LOQ of  $86 \pm 8 \mu\text{mol}\cdot\text{L}^{-1}$  were reached. The obtained sensitivity is  $16 \pm 1 \mu\text{A}\cdot\text{L}\cdot\text{mmol}^{-1}\cdot\text{cm}^{-2}$ . Especially the lower quantification limit is completely satisfying for sensing in sweat. [\*]

Gauze was tested as sweat collecting material due to the unsatisfying results with filter paper as soaking material. It was necessary to use 60  $\mu\text{L}$  of sample solution to wet the whole gauze pad. The results of a triple measurement on one sensor in comparison to droplet method are shown in **SI Figure 3.22 b**. [\*]

A triple measurement of different lactate concentrations ranging between 0.1 and 5  $\text{mmol}\cdot\text{L}^{-1}$  in pure buffer and in a synthetic sweat matrix according to DIN 53160-2 was performed on one sensor, respectively. Droplet method was used for both investigations. The resulting dose-response curves are shown in **SI Figure 3.22 c**. The curve shapes of both data sets are very similar. The curve of synthetic sweat spiked with lactate is shifted parallel to lower currents compared to the measurements of lactate in 1X PBS pH 7.4. [\*]

Lactate is also present in human tears. Therefore, lactate determination was performed in an artificial tear fluid. The used commercial eye drops contain 0.15% sodium hyaluronate and sodium chloride in a citrate buffer around pH 7. The pure solution was used as solvent for different lactate concentrations between 0.01  $\text{mmol}\cdot\text{L}^{-1}$  and 2.5  $\text{mmol}\cdot\text{L}^{-1}$ . The results in comparison to lactate in 1X PBS pH 7.4 are shown in **SI Figure 3.22 d**. Both determinations were performed on the same sensor to enable a direct comparison of the curves. The curve shapes of both data sets are related and comparable. [\*]

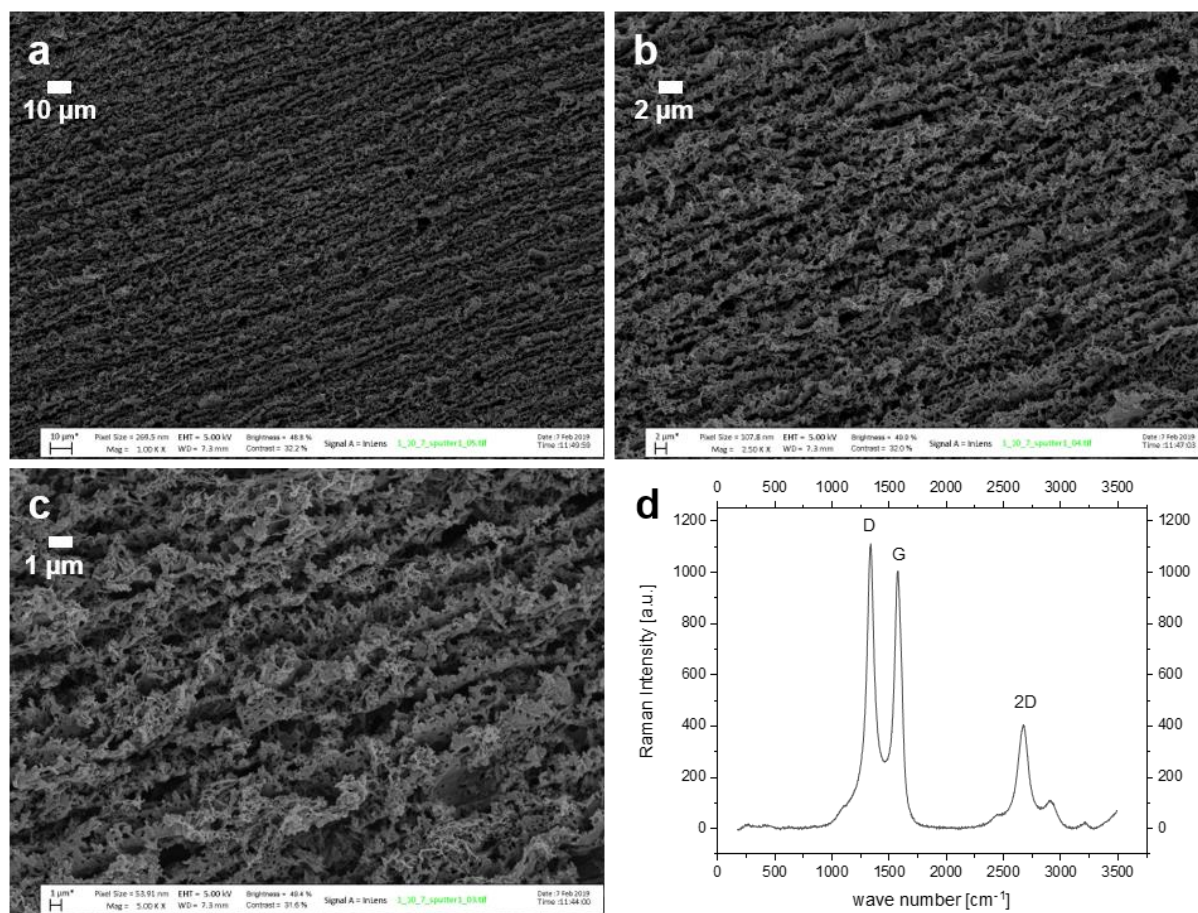


**SI Figure 3.22** **a** Dose-response curve ( $n = 3$ , SD represented by error bars, droplet method) for amperometric detection of lactate at a potential of  $-20$  mV vs. LIG and an acquisition time of 60 s on half-logarithmic scale. The biosensor was modified with chemical deposited Prussian blue and a 0.1% chitosan membrane. LOx activity on the WE was  $1.4 \text{ U}\cdot\text{mm}^{-2}$ . There was no further incubation time [\*] **b** Lactate determination in 1X PBS pH 7.4 with the droplet method (blue boxes) and gauze as sweat collecting pad (red circles). Chronoamperometry was performed at a potential of  $-20$  mV vs. LIG. The tests were performed three times for each concentration ( $n = 3$ ) on the same sensor to compare the results directly [\*] **c** Triplicate measurement of lactate in pure 1X PBS pH 7.4 (blue boxes) and dilutions in synthetic sweat solution pH 6.5 (red circles) according to DIN 53160-2 with the same lactate sensor at  $E = -50$  mV vs. LIG [\*] **d** Lactate determination with the droplet method in 1X PBS pH 7.4 (blue boxes) and in artificial tear fluid (red circles). Tests were performed three times for each concentration on the same sensor to compare the results directly [\*]

### 3.7.7 Characterization of Electrode Material

Surface morphology and graphene-like characteristics of the LIG was determined by SEM imaging and Raman spectroscopy. The SEM images (**Figures 3.23 a**, **3.23 b** and **3.23 c**) show the same spot of the LIG with different magnifications. One can clearly see the roughness and porosity of the three-dimensional material. Furthermore, thin sheets and flakes are visible. For further characterization, Raman spectra were recorded (**SI Figure 3.23 d**). The pronounced 2D peak at around  $2700 \text{ cm}^{-1}$  is comparable with the one in single-layer graphene. The 2D

band profile can be typically found in 2D graphite with randomly stacked graphene layers along the c-axis [24].



**SI Figure 3.23** SEM images (magnification factors **a** 1,000 **b** 2,500 **c** 5,000). The porous and rough structure of the LIG is clearly visible. **d** Raman spectra of the LIG structure ( $n = 16$ , error bars are hidden for clarity, 532 nm laser, set at 8 mW, 50  $\mu\text{m}$  slit aperture, 50 X objective)

## 4 Europium(III) Tetracycline as Probe for Detection of Hydrogen Peroxide in Microplate Assays

---

### Abstract

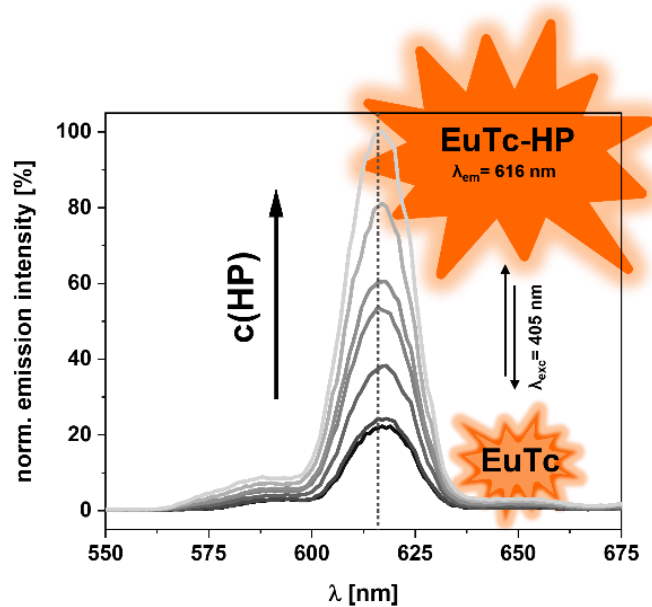
Many biological relevant reactions release or depends on hydrogen peroxide (HP). Therefore, HP is a very important model analyte in the field of (bio)medical applications. Europium(III) tetracycline complex (EuTc) coordinates reversible with HP at physiological relevant pH. This coordination leads to an increase of luminescence intensity of the  ${}^5D_0 \rightarrow {}^7F_2$  transition of the  $\text{Eu}^{3+}$  ion, detectable at 616 nm after an excitation at 405 nm. The mechanism behind this phenomenon is the replacement of the quenching water molecules from the inner coordination sphere around the  $\text{Eu}^{3+}$  central ion by the HP molecules.

Including oxidase enzymes, where HP is formed as a stoichiometric by-product, enables the rapid and sensitive detection of the related substrates like glucose with glucose oxidase (GOx) and lactate with lactate oxidase (LOx) with EuTc. The entrapment of the very selective enzyme and the sensitive luminescent probe within biocompatible hydrogels and polymers enlarges the thinkable bioanalytical applications enormously, not just in a microplate format. The assembling of sensor discs in a microplate by factory side enables a simple assay type for rapid detection of large numbers of samples.

Herein, we present a polyvinyl acetate/cellulose acetate (PVAc/CA) membrane containing EuTc to detect hydrogen peroxide. Furthermore, the probe was embedded in a D4 layer protected by a PVAc/CA layer to reach a dynamic range from 10  $\mu\text{M}$  to 10 mM. Glucose samples up to 50 mM and lactate samples up to 20 mM are mixed with the respective enzyme and added to the discs in a 96-well plate. After 2 min to 5 min incubation time the luminescence is read out at 616 nm. Hydromed® D4-GOx and D4-LOx discs were produced and optimized to detect glucose and lactate under comparable conditions within the same dynamic range as mentioned above when the sample solution is mixed with EuTc solution in the microplate. All systems work at 25°C and 37°C. The discs can be stored light-protected for at least 6 months (probe discs) or up to 1 year (enzyme discs) at 4°C. They show no significant loss of probe or enzyme when in use for minimum 3 h at 37°C (probe discs) or 6 h at 25°C (enzyme discs).

This fundamental work proves the reasonable application of EuTc and enzymes embedded in biocompatible hydrogels for rapid hydrogen peroxide, glucose and lactate detection in a microplate format within physiological relevant concentrations and conditions.

### Graphical Abstract



This chapter or at least parts of it are intended for submission but currently kept under seal due to patent claims by Terumo Cardiovascular Systems Corporation, Ann Arbor, MI 48103-9300 USA.

### Author contributions

Most of the experimental work was solely done by the author. Rahel Gruenberger, Julia Ciechocińska and Laura Deml collected data under supervision of the author. Some of these data sets are presented in the **Figure 4.7**, **Figure 4.8**, **Figure 4.9**, **Figure 4.11** and **SI Figure 4.2**. Some of the foils were prepared by Barbara Grotz and John Galligan and used by the author. Barbara Grotz, John Galligan, Axel Duerkop and Antje J. Baeumner contributed with strategic discussions. The manuscript was written by the author and revised by BG, JG, AD and AJB. AJB is corresponding author.

## 4.1 Introduction

Since hydrogen peroxide (HP) plays a large role throughout physiological processes, it is one of the most popular analytes, not just for medical applications [1]. Many assays and sensors were developed over time [2]. Modification of existing HP sensors with biorecognition elements like enzymes increases the scope of this sensor type enormously [3]. In many oxidase-catalyzed reactions HP is released as stoichiometric byproduct and therefore an indirect determination of the respective substrate is possible [4]. The other way round application of an assay format for the reliable quantification of an enzyme is thinkable [5]. Especially electrochemically based sensors are popular and were continuously improved since amperometric or potentiometric determination methods are fast and sufficient. The best-known indirect hydrogen peroxide sensor is still the glucometer, a small point-of-care (POC) device for the reliable determination of blood glucose by amperometry [6]. A small blood droplet applied on the sophisticated single-use electrode provides within seconds the current glucose concentration in a understandable way for the user [7]. This is fine for single determinations, performed by the patient itself or clinic staff for a controllable number of samples. As soon as the sample throughput rises the requirements for the technical effort and equipment increases. Besides the advantages of microfluidic systems like the economical mass production of the chips themselves, the development of the sophisticated microfluidics is time-consuming and expensive, the staff needs special training or even experts are required for the operation of the complex devices to run the microfluidic chip in a reliable way [8]. Samples cannot be prepared in the run-up, thus one chip after another must be loaded with sample and applied to the machine.

Therefore, the development of simple optical microtiter plate (MTP) assays is a convenient way to overcome at least some of the named challenges of the electrochemical screening of samples. A prominent example for MTP assays is the enzyme-linked immunosorbent assay (ELISA) which was already carried out in the 1970's by Voller *et al* for the detection of toxoplasma antibodies [9]. MTPs are standardized in size, bottom-shape, and number of wells and therefore each standard plate reader device with a suitable optic and detector can be used for the read-out. The wells of a 96-well MTP can easily be pretreated or coated with the respective reagents by adsorption, through covalent bonds, or the chemicals are embedded in polymers or hydrogels [10]. All wells can be filled with sample solution at once with multichannel pipettes. Further, the entire plate is scanned in one step within seconds by the reader. With an internal calibration or reference, a fast, simple, and convenient method for determination of hydrogen peroxide or other analytes in a large number of multiple samples can be offered [11].

Absorbance and luminescence, including fluorescence, bio- and chemiluminescence, measurements are suitable methods for straightforward MTP assays. The methods have some advantages and disadvantages whereas the most pronounced advantage for the fluorescence is the generally around 1,000 times higher sensitivity and the thereof resulting lower detection limits [12]. Another factor against absorbance measurements in microplates is the limited pathway in the well. Furthermore, especially in the field of medical applications, absorbance at many wavelengths is not very specific or nearly impossible in highly concentrated serum or blood samples. Excitation and emission wavelengths can be better tuned by the choice of a suitable fluorophore. For the sake of completeness must be said that organic fluorophores and fluorescent proteins suffer from photobleaching, strong background autofluorescence in the visible spectrum and the broad emission bands often results in significant spectral overlapping, too [13–15]. But luminophores and luminescent dyes exist in a large variety and a suitable compound with the right detection technique like time-resolved measurements for metal–organic complexes can be found to outnumber matrix effects and background fluorescence [13, 16].

With the exception of La(III) and Lu(III), all of the Ln(III) ions are luminescent and their narrow f–f emission lines cover the entire spectrum, from ultraviolet (UV) like Gd(III) to visible (e.g. Eu(III) or Tb(III)) and near-infrared (NIR, e.g. Er(III) or Yb(III)) ranges with long lifetimes [17]. The lanthanide ions show generally a small Stokes shift which explains the partial overlap of excitation and emission band [18]. But with organic ligands as sensitizer the energy absorbance band of the complex can be shifted to the absorbance band of the organic ligand. The from the organic molecule absorbed energy is transferred via intersystem crossing mechanisms to the excited states of the central ion. The Ln(III) relaxes to the ground state and the energy is emitted in form of light. This results in strong emission intensities with a large pseudo-Stokes shift up to [13, 19].

Since 2002, Wolfbeis *et al* and other research groups have reported using Eu(III)-based complexes as probe for different analytes and in particular the Europium(III) tetracycline (EuTc) complex for selective and sensitive detection of HP or related compounds in microplate assays and flow-through systems [20–26]. The organo-metal complex coordinates with hydrogen peroxide at physiological relevant pH range. This coordination leads to an increase of luminescence intensity of the  $^5D_0 \rightarrow ^7F_2$  transition of the  $\text{Eu}^{3+}$  ion, detectable at 616 nm [17]. The mechanism behind the possible detection of HP is the reversible replacement of quenching water molecules from the inner coordination sphere around the  $\text{Eu}^{3+}$  central ion by non-quenching HP molecules [20, 21]. Replacing the water molecules by HP leads to a strong concentration-dependent increase of the emission intensity like shown in **Figure 4.1**.



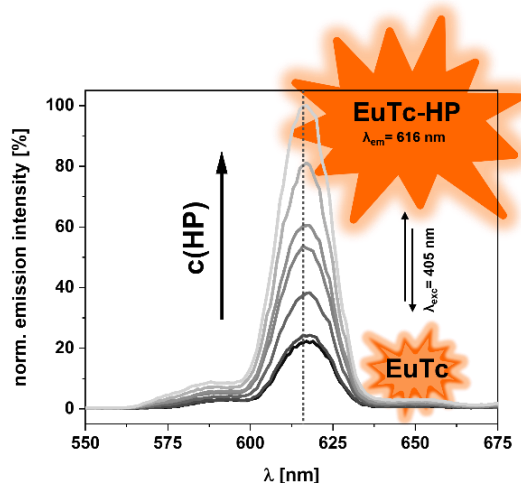


**Figure 4.1** The luminescence intensity of the  ${}^5D_0 \rightarrow {}^7F_2$  transition of the  $\text{Eu}^{3+}$  ion, detectable at 616 nm, is increased when quenching water molecules, coordinating the inner sphere of the  $\text{Eu}(\text{III})$  tetracycline complex are replaced by hydrogen peroxide molecules.

As mentioned in the beginning, many biological relevant reactions include oxidase enzymes, where HP is formed as by-product. The HP concentration correlates consequently with the related substrate concentration. Important model substrates for medical applications are still glucose and lactate and the associated enzymes glucose oxidase (GOx) and lactate oxidase (LOx). Combination of the very selective enzyme reactions with the sensitive luminescent probe EuTc opens a wide field of interesting and important bioanalytical and medical applications.

Homogeneous as well as heterogeneous assay formats are thinkable in the microplate. Generally, luminescent probes as well as enzymes can be entrapped within suitable membranes and hydrogels to obtain optical sensors or optodes for detection of the related metabolites [13, 22, 27–29]. For a microplate assay the probes and enzymes can already be immobilized within the wells to obtain a feasible detection system. Two polymers or polymer mixtures have very promising properties regarding biocompatibility and diffusion. A mixture of polyvinyl acetate (PVAc) and cellulose acetate (CA) was already used in 1983 by Tsuchida *et al* for a multi-enzyme membrane electrode used in human serum for detection of creatinine and creatine [30]. Hydromed® D4, a polyurethane-based hydrogel with a water content of around 50 % is an often used material for the entrapment of enzymes or organic dye molecules for chemo- and biosensor applications [23, 31–33] and enables a fast hydrogen peroxide diffusion [34]. Fully optimized biocompatible probe-enzyme-hydrogel systems for implantable optical sensors and therefore long-term, real-time and continuous monitoring of arbitrary analytes are hence possible and the future perspective of this work.

## 4.2 Experimental

### 4.2.1 Materials and Equipment

For all experiments bi-distilled water (just referred as water) is used.

*Following chemicals are used without further purification:*

Hydromed® D4 was purchased from AdvanSource Biomaterials ([www.advbiomaterials.com](http://www.advbiomaterials.com)). Europium trichloride hexahydrate  $\text{EuCl}_3 \cdot 6 \text{H}_2\text{O}$  (99.9 %), tetracycline HCl ( $\geq 95\%$ ), polyvinyl acetate (average  $M_w \approx 100,000$ ), cellulose acetate (average  $M_n \approx 30,000$ ), cyclohexanone (p.a.;  $\geq 99.5\%$ ), glucose oxidase from *Aspergillus Niger* (type VII, lyophilized powder,  $\geq 100,000$  units / g solid), sodium hydroxide (p.a.;  $\geq 98\%$ ), hydrogen peroxide solution (35 %) ethanol (p.a.;  $\geq 99.8\%$ ), sodium lactate (p.a.;  $\geq 99.0\%$ ), sodium chloride (p.a.;  $\geq 99.0\%$ ) and monosodium phosphate dihydrate (p.a.;  $\geq 99.0\%$ ) were purchased from Sigma-Aldrich (<https://www.sigmaaldrich.com>). HEPES (4-(2-hydroxyethyl)-1-piperazineethanesulfonic acid) (for biochemistry) was purchased from VWR (<https://www.vwr.com>). D(+)-glucose monohydrate (for microbiology) and sodium azide  $\text{NaN}_3$ , (extra pure), were purchased from Merck (<https://www.merckmillipore.com>). Lactate oxidase from *Aerococcus Viridans* (type II, lyophilized powder, 36.0 U/mg powder) was purchased from Hölzel Diagnostika HandelsGmbH (<https://www.hoelzel-biotech.com>).

*Following other materials are used:*

Mylar® (bi-axial oriented poly-terephthalate foils with 125  $\mu\text{m}$  thickness) was purchased from GoodFellow GmbH (<http://www.goodfellow.com>). Adhesive tape (tesa® Verlegebond) was purchased from tesa SE (<https://www.tesa.com>). Aluminum foil purchased from local stores was used for light protection.

*Following further equipment and accessories are used:*

FLUOstar Omega from BMG LABTECH GmbH (<https://www.bmg-labtech.com>) and Synergy Neo2 Hybrid Multi-Mode Reader from BioTek Instruments ([www.biotek.de](http://www.biotek.de)) with 96-well microtiter plates, white, medium binding, flat bottom, purchased from greiner BIO-ONE, product# 655075 (<https://www.gbo.com>). Laser-engraving device VLS 2.30 equipped with a 30 W  $\text{CO}_2$  laser ( $\lambda = 10.6 \mu\text{m}$ ) and two optical lens systems (2.0 lens and High-Power Density Focusing Optics (HPDFO)) from Universal Laser Systems (<https://www.ulsinc.com>). Toggle press HK 800 for hole-punching with different-sized circular cutting tools from Berg & Schmid (<https://www.bergundschmid.de>).

### 4.2.2 Preparation of Solutions

In general, all weights and volumes can be adapted proportionally if higher or lower number of samples, foils or discs must be prepared.

#### **4.2.2.1 0.1 M HEPES pH 7.4**

119.16 g  $\pm$  1.12 g HEPES are dissolved in approx. 4.75 L water in a 5 L volumetric flask while stirring with a magnetic stirring bar. NaOH pellets are added under strong stirring to reach a pH value of 7.40  $\pm$  0.05. Volume is filled up to 5 L with water. After mixing, pH value is checked and noted. If necessary, 0.50  $\pm$  0.05 g NaN<sub>3</sub> are added and dissolved by shaking. The solution can be stored up to 12 months at ambient conditions in a glass bottle. If the buffer is prepared without sodium azide, it should be stored not longer than 4 weeks at ambient conditions.

#### **4.2.2.2 Chloride and Phosphate Solutions for Interference Study**

584.4 mg  $\pm$  5.8 mg are dissolved in 50 ml buffer to obtain a 200 mM chloride stock solution. The stock solution is diluted to 150 mM, 100 mM and 50 mM chloride with buffer. The dilutions are used for the interference studies.

156.0 mg  $\pm$  1.6 mg are dissolved in 50 ml buffer to obtain a 20 mM phosphate stock solution. The stock solution is diluted to 2 mM, 1 mM and 0.5 mM phosphate with buffer. The dilutions are used for the interference studies.

#### **4.2.2.3 Hydrogen Peroxide Solutions**

To obtain a 100 mM HP stock solution, 5190  $\mu$ L buffer is mixed with 45  $\mu$ L of 35 % HP solution in a 10 mL glass vial by shaking. The respective dilutions with HP concentrations of 0, 0.1, 0.5, 1, 5 and 10 mM for the standard assay are prepared by diluting the stock solution or the respective other solution with buffer in 15 mL plastic tubes. 1:10 dilutions are prepared by mixing 1.5 mL 100 mM HP stock solution with 13.5 mL buffer. 1:2 dilution to obtain the 5 mM HP solution is prepared by mixing 7.5 mL of 10 mM HP solution with the same volume of buffer. The samples must be used within 24 h and must be stored at 4°C. The sample volume is suitable for the measurement of 96 wells. 0 mM HP refers to pure buffer.

#### **4.2.2.4 Glucose and Lactate Solutions**

To obtain a 100 mM glucose stock solution, 1981.7  $\pm$  2.0 mg glucose monohydrate is weighed in a 100 mL volumetric flask and dissolved in approx. 75 mL buffer.

To obtain a 100 mM lactate stock solution, 1120.6  $\pm$  1.1 mg sodium lactate is weighed in a 100 mL volumetric flask and dissolved in approx. 75 mL buffer.

Then the volume is filled up to 100 mL and the solution is mixed by shaking. The stock solution is diluted with buffer like shown in the following **Table 4.1**. The sample volume is suitable for the measurement of 4 x 96 wells. 0 mM glucose or lactate sample refers to pure buffer. The samples can be stored over 6 months at ambient conditions when sodium azide is contained.

**Table 4.1** Dilution scheme for glucose or lactate samples with the respective final glucose or lactate concentrations.

<b>C<sub>sample</sub></b> <b>[mM]</b>	<b>V<sub>buffer</sub></b> <b>[mL]</b>	<b>V<sub>stock solution</sub></b> <b>[mL]</b>
50.0	25.0	25.0
25.0	37.5	12.5
20.0	40.0	10.0
10.0	45.0	5.0
5.0	47.5	2.5
2.5	48.75	1.25
1.0	49.5	0.5
0.5	49.75	0.25
0.0	50.0	0.0

**4.2.2.5 Eu<sup>3+</sup> Stock Solution**

1832.1 ± 0.9 mg of EuCl<sub>3</sub>·6 H<sub>2</sub>O is dissolved in approx. 5 mL of water using a 10.0 mL volumetric flask. Volume is filled up to 10 mL volume with water. The solution is split into aliquots of 400 µL. These can be stored for at least 6 months under light protection at 4°C.

**4.2.2.6 Tetracycline Stock Solution**

31.84 ± 0.06 mg of tetracycline HCl is dissolved in 4.0 mL of water in a glass flask. The solution must be used within 30 minutes and must be stored light protected.

**4.2.2.7 EuTc Solution for Functionality Test**

500 µL of the tetracycline stock solution (**chapter 4.2.2.6**) is mixed with 50 µL of the Eu<sup>3+</sup> stock solution (**chapter 4.2.2.5**) in 4.45 mL water in an amber 50 mL plastic tube. 45.0 mL of 0.1 M HEPES pH 7.4 is added, and the solution is mixed by shaking shortly. The solution must be used within 6 h and must be stored light protected.

**4.2.2.8 Glucose/EuTc and Lactate/EuTc Solutions**

Sample solutions containing glucose and EuTc or lactate and EuTc are prepared by mixing 6 mL of the EuTc solution for functionality test (**chapter 4.2.2.7**) and 6 mL of the respective glucose or lactate samples (**chapter 4.2.2.4**). Additionally, a 0 mM glucose/EuTc or lactate/EuTc sample is prepared. Following **Table 4.2** gives an overview of the final glucose concentration and the concentration of the used glucose or lactate samples. The solutions must be used within 6 h and must be stored light protected. The sample volume is suitable for the measurement of 96 wells.

**Table 4.2** Glucose or lactate concentrations in the used glucose or lactate samples and the final glucose or lactate concentration in the glucose/EuTc or lactate/EuTc samples in mM.

<b>C<sub>glucose/lactate sample</sub></b> <b>[mM]</b>	<b>C<sub>sample final</sub></b> <b>[mM]</b>
100.0	50.0
50.0	25.0
20.0	10.0
10.0	5.0
5.0	2.5
1.0	0.5
0.0 (= 0.1 M HEPES pH 7.4)	0.0

#### 4.2.2.9 Enzyme Solutions for Homogeneous Assays

To obtain a GOx stock solution with a theoretical activity of 1 U/ $\mu$ L, 2.0  $\pm$  0.2 mg of GOx is dissolved by gentle shaking within 450  $\mu$ L of buffer in a 500  $\mu$ L plastic reaction tube until no lumps are visible. To obtain a LOx stock solution with a theoretical activity of 1 U/ $\mu$ L, 2.0  $\pm$  0.2 mg of LOx is dissolved by gentle shaking within 72  $\mu$ L of buffer in a 200  $\mu$ L plastic reaction tube until no lumps are visible. The enzyme stock solution can be stored light-protected at 4°C for up to at least 6 months but it is recommended to use it within 4 weeks. To obtain 40 mU/ $\mu$ L enzyme solutions, the stock solutions are diluted 1:25 (v/v) with buffer.

#### 4.2.2.10 Polymer Cocktails

##### 10 wt% D4 in EtOH/H<sub>2</sub>O

90.0  $\pm$  0.9 mL ethanol is mixed with 10.0  $\pm$  0.1 mL. 10.0  $\pm$  0.1 g Hydromed D4 is dissolved in 90.0  $\pm$  0.9 g of EtOH/water in a 100 mL glass flask under strong stirring with a magnetic stirring bar until no lumps are visible (preferable overnight (ON) stirring). Temperature should be between 20°C and 50°C.

##### 10 wt% PVAc/CA in CHon/H<sub>2</sub>O

99.0  $\pm$  0.1 mL CHon is mixed with 1.00  $\pm$  0.01 mL water. 7.92  $\pm$  0.08 g CA and 0.080  $\pm$  0.008 g PVAc are dissolved in 72.0  $\pm$  0.7 g CHon/H<sub>2</sub>O in a 100 mL glass flask under strong stirring with a magnetic stirring bar until no lumps are visible (preferable ON stirring). Temperature should be between 20°C and 50°C.

##### 10 wt% PVAc/CA in DMF/H<sub>2</sub>O

90.0  $\pm$  0.1 mL DMF is mixed with 10.0  $\pm$  0.1 mL water. 7.92  $\pm$  0.08 g CA and 0.080  $\pm$  0.008 g PVAc are dissolved in 72.0  $\pm$  0.7 g DMF/H<sub>2</sub>O in a 100 mL glass flask under strong stirring with a magnetic stirring bar until no lumps are visible (preferable ON stirring). Temperature should be between 20°C and 50°C.

#### **4.2.2.11 EuTc Stock Solution for Sensor Cocktails**

6.97 ± 0.06 mg tetracycline HCl are weighed in a 500 µL plastic reaction tube and dissolved under strong shaking in 75 µL of the Eu<sup>3+</sup> stock solution (**chapter 5.2.2.5**). The solution must be used immediately and cannot be stored.

#### **4.2.2.12 Sensor Cocktails**

##### *EuTc in 10 wt% D4 in EtOH/H<sub>2</sub>O*

A 5 mL glass vial with plastic snap cap is used. 1.499 ± 0.015 g of the 10 wt% D4 in ethanol/H<sub>2</sub>O are weighed in. To obtain a 0.1 wt% EuTc cocktail, 10 µL of the EuTc stock solution are added. To obtain a 0.2 wt% EuTc cocktail, 20 µL of the EuTc stock solution are added. To obtain a 0.5 wt% EuTc cocktail, 50 µL of the EuTc stock solution are added. The vial is sealed tightly with Parafilm. The cocktail is stirred 10 ± 1 minutes at ambient conditions. It is recommended to use the cocktail as soon as possible. The volume is suitable for the preparation of up to 6 to 8 foils.

##### *EuTc in 10 wt% PVAc/CA in DMF/H<sub>2</sub>O*

A 5 mL glass vial with plastic snap cap is used. 1.499 ± 0.015 g of the 10 wt% PVAc/CA in DMF/H<sub>2</sub>O are weighed in. To obtain a 0.1 wt% EuTc cocktail, 10 µL of the EuTc stock solution are added. The vial is sealed tightly with Parafilm. The cocktail is stirred 70 ± 10 minutes at ambient conditions. It is recommended to use the cocktail as soon as possible. The volume is suitable for the preparation of up to 6 foils.

#### **4.2.2.13 Enzyme Stock Solutions for Enzyme Cocktails**

To obtain an enzyme stock solution for 0.25 wt% enzyme cocktails, 6.0 ± 0.1 mg of the enzyme is dissolved within 80 µL of 0.1 M HEPES pH 7.4 in a 500 µL plastic reaction tube until no lumps are visible. To obtain an enzyme stock solution for 0.5 wt% enzyme cocktails, 9.0 ± 0.1 mg of the enzyme is dissolved within 60 µL of 0.1 M HEPES pH 7.4 in a 500 µL plastic reaction tube until no lumps are visible. A thermal cycler set at 35 ± 1 °C and 500 rpm is used for 12.5 ± 2.5 min. The solution can be stored light-protected overnight at 4°C but it is recommended to use it immediately.

#### **4.2.2.14 Enzyme Cocktails**

Two methods were tested and optimized and lead to the same performance of the discs.

##### *Method A (With Enzyme Stock Solution)*

A 5 mL glass vial with plastic snap cap is used. 1.499 ± 0.015 g of the 10 wt% D4 cocktail in EtOH/H<sub>2</sub>O are weighed in. 50 µL of the enzyme stock solution for 0.25 wt% enzyme cocktails are added to obtain a 0.25 wt% enzyme cocktail. 50 µL of the enzyme stock solution for

0.5 wt% enzyme cocktails are added to obtain a 0.5 wt% enzyme cocktail. The vial is sealed tightly with Parafilm. The cocktail is stirred 1.5 to 2 hours at 37°C until a homogeneous suspension is obtained. It is recommended to use the cocktail within 1 h. The volume is suitable for the preparation of up to 6 to 8 foils.

#### *Method B (Without Enzyme Stock Solution)*

A 5 mL glass vial with plastic snap cap is used. To obtain a 0.25 wt% enzyme cocktail,  $5.0 \pm 0.1$  mg of the enzyme is dissolved within 200  $\mu\text{L}$  of 0.1 M HEPES pH 7.4. 1800  $\mu\text{L}$  of ethanol and 0.20  $\pm$  0.02 g Hydromed D4 polymer is added under strong stirring. To obtain a 0.5 wt% enzyme cocktail,  $7.5 \pm 0.1$  mg of the enzyme is dissolved within 150  $\mu\text{L}$  of 0.1 M HEPES pH 7.4. 1350  $\mu\text{L}$  of ethanol and 0.149  $\pm$  0.015 g Hydromed D4 polymer is added under strong stirring. The vial is sealed tightly with Parafilm. The cocktail is stirred 6 to 8 hours at 37°C until a homogeneous suspension is obtained. It is recommended to use the cocktail immediately within 1 to 2 h. The volume is suitable for the preparation of up to 6 to 8 foils.

### 4.2.3 Methods

#### 4.2.3.1 Knife-Coating

An in-house made knife-coater device (**Figure 4.2 A**) is used for production of all sensor and enzyme foils. The schematic (not-to-scale) side-view of the application of a first layer on the support material is shown in **Figure 4.2 B**.

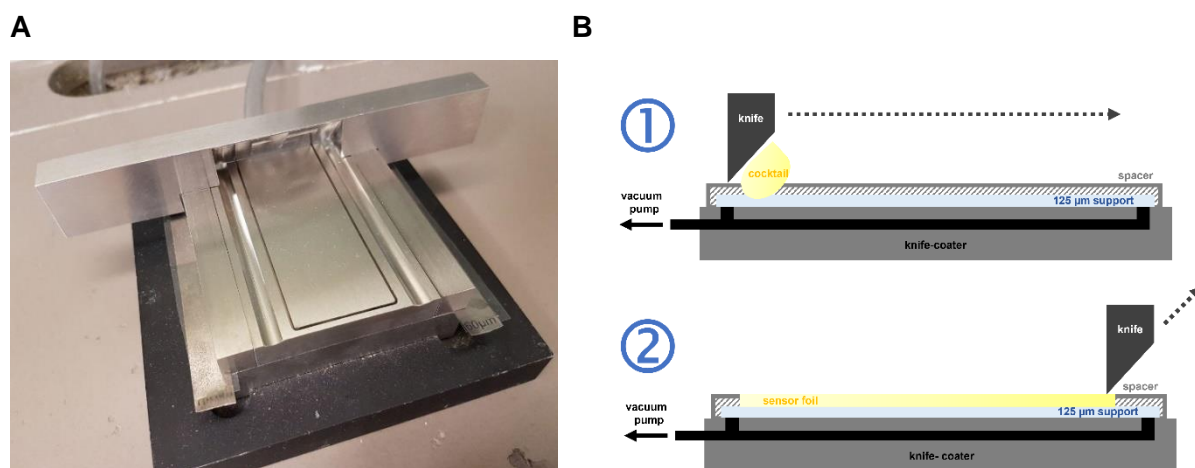


**Figure 4.2** **A** An in-house made knife-coating device for preparation of foils with a maximum size of approx. 5.5 x 11.0 cm **B** Schematic side-view of the knife-coating process for the first layer (not to scale).

#### *Application of First Layer*

The 30  $\mu\text{m}$  or 60  $\mu\text{m}$  spacers and pieces of Mylar support are placed in the knife-coater at both sides to define the wet layer thickness. If not mentioned otherwise, usually 30  $\mu\text{m}$  spacers were used. A planar, rectangular Mylar substrate (approx. 5.5 cm x 11.0 cm) is placed on the

knife-coating device and fixed by turning on the vacuum pump. The sheet is cleaned by using a wipe soaked with ethanol and rubbing. After the rubbing alcohol is completely evaporated, 200  $\mu$ L to 300  $\mu$ L of the respective sensor, enzyme or polymer cocktail is pipetted as a homogeneous line on the starting point of the Mylar substrate. The knife is pulled slowly to the end of the substrate to obtain an even film. After around 30 seconds, the vacuum pump is turned off and the foils are moved to the oven on an even plate for drying. The foils are dried for  $2.5 \pm 0.5$  h at  $39 \pm 1$  °C. A second layer can be applied immediately after the drying time.

If no second layer is applied, the sheets are washed for  $15 \pm 1$  minutes in an excess of buffer on an orbital shaker (300 to 350 rpm) to remove unbound complex or enzyme and organic solvent residues, and to rehydrate the hydrogel after drying. The sheets can then be stacked carefully and stored light-protected in a closed zipper bag at 4°C until sensor disc preparation.

#### *Application of Further Layers*

The 30  $\mu$ m or 60  $\mu$ m spacers and pieces of Mylar support are placed in the knife-coater at both sides to define the wet layer thickness for the second or third layer. If not mentioned otherwise, usually 30  $\mu$ m spacers were used. The Mylar substrate with the dried layer(s) on top is placed on the knife-coater and fixed by turning on the vacuum pump. 250  $\mu$ L to 300  $\mu$ L of the respective second layer cocktail is pipetted as a homogeneous line on the starting point of the Mylar substrate. The knife is pulled slowly to the end of the substrate to obtain an even film that covers the first layer(s). After around 30 seconds, the vacuum pump is turned off and the foils are moved to the oven on an even plate. The foils are dried for  $2.5 \pm 0.5$  h at  $39 \pm 1$  °C. A further layer can be applied immediately after the drying time.

If no further layer is applied, the sheets are washed for  $15 \pm 1$  minutes in an excess of buffer on an orbital shaker (300 to 350 rpm) to remove unbound complex or enzyme and organic solvent residues, and to rehydrate the hydrogel after drying. The sheets can then be stacked carefully and stored light-protected in a closed zipper bag at 4°C until sensor disc preparation.

#### **4.2.3.2 Sensor Disc Preparation**

On the backside of the Mylar support (= the uncoated side), double-adhesive tape is applied. With a toggle press, discs with a diameter of 6 mm are punched out of the foil. Elsewise, the laser cutter can be used (100% laser power, 70% speed, 1000 ppi). It must be avoided to take discs from nearby the edges, a distance to the edges of at least 2 mm is recommended. Furthermore, all applied polymer and hydrogel layers should overlap completely in the used area. After removing the protective cover of the adhesive tape, the sensor discs are fixed on the bottom of the MTP wells. Usually,  $n = 4$  or  $n = 8$  discs are used for an assay. The prepared MTPs are covered with a plastic lid and can be stored light protected at 4°C until a functionality test is performed, or they can be used immediately.



### 4.2.3.3 Assay Types

Within this chapter, all performed assay types within the microplate are described. If not stated otherwise in the captions or Results and Discussion part, all experiments were performed like described in following with the same settings.

#### 4.2.3.3.1 Homogeneous Assays without Discs

In general, every assay was performed by mixing 50  $\mu\text{L}$  of EuTc solution for functionality test (**chapter 5.2.2.7**) with 50  $\mu\text{L}$  of buffer for blank measurement or sample solution (glucose or lactate) and adding 1  $\mu\text{L}$  of the respective enzyme solution (theoretical activity of 1 U/ $\mu\text{L}$ ) or 50  $\mu\text{L}$  of the respective enzyme solution (theoretical activity of 40 mU/ $\mu\text{L}$ ) before starting the measurement.

Following settings (**Table 4.3**) of the plate reader FLUOstar Omega from BMG LABTECH GmbH are used for the within this chapter described assay types (if not stated otherwise):

**Table 4.3** Parameters and the respective settings of the used FLUOstar Omega plate reader for the homogeneous assays.

parameter	15 min	10 min
protocol name	EuTc_kinetic_15min	EuTc_kinetic_10min
no. of multichromatics	1	
excitation filter	405/10 nm	
emission filter	615/10 nm	
gain	1200	
well scan	none	
optic	top optic	
settling time	0.2 s	
no. of kinetic windows	1	
no. of cycles	16	11
measurement start time	0.0 s	
no. of flashes	20	
cycle time	60 s	
pause before cycle	no	
shaking 1	shake between reading; double orbital @300 rpm	
shaking 2	shake before first cycle, double orbital @300 rpm for 5 s	

Temperature is set to  $25.0 \pm 0.5$  °C,  $30.0 \pm 0.5$  °C or  $37.0 \pm 0.5$  °C and the measurements can be started when the desired temperature is reached. For measurements at 25°C, the samples are not prewarmed. For 30°C and 37°C measurements, the samples are prewarmed in a tempered water bath at the desired temperature.

## 4.2.3.3.2 Heterogeneous Assays with Discs

Following settings (**Table 4.4**) of the plate reader FLUOstar Omega from BMG LABTECH GmbH are used for the within this chapter named assay types (if not stated otherwise):

**Table 4.4** Parameters and the respective settings of the used FLUOstar Omega plate reader for each assay type. Glucose/EuTc and glucose assay are equally used for the respective lactate/EuTc and lactate assay.

parameter	washing step	HP assay	glucose/EuTc assay	glucose assays
<i>protocol name</i>	EuTc_wash _15min	EuTc_6min _kinetic	EuTc_10min _kinetic	EuTc_10min _kinetic
<i>no. of multichromatics</i>	1			
<i>excitation filter</i>	405/10 nm			
<i>emission filter</i>	615/10 nm			
<i>gain</i>	1200			
<i>well scan</i>	none			
<i>optic</i>	top optic			
<i>settling time</i>	0.2 s			
<i>no. of kinetic windows</i>	1			
<i>no. of cycles</i>	2	7	11	11
<i>measurement start time</i>	0.0 s			
<i>no. of flashes</i>	20			
<i>cycle time</i>	900 s	60 s		
<i>pause before cycle</i>	no			
<i>shaking 1</i>	shake between reading; double orbital @300 rpm			
<i>shaking 2</i>	shake before first cycle, double orbital @300 rpm for 5 s			

Temperature is set to  $25.0 \pm 0.5$  °C,  $30.0 \pm 0.5$  °C or  $37.0 \pm 0.5$  °C and the measurements can be started when the desired temperature is reached. For measurements at 25°C, the samples are not prewarmed. For 30°C and 37°C measurements, the samples are prewarmed in a tempered water bath at the desired temperature. The washing procedure is performed for all discs in the very beginning.

#### *Washing Procedure for All Disc Types*

100 µL buffer is added with an 8-channel pipette to each sensor disc and is washed for 15 minutes in the plate reader. Therefore, a kinetic measurement is started for 15 minutes. During the washing procedure, the samples are shaken orbitally by the plate reader at 300 rpm. The samples are excited at 405/10 nm and the emission intensity is measured at 615/10 nm at the beginning and in the end at  $25.0 \pm 0.5$  °C or  $37.0 \pm 0.5$  °C (protocol for “washing step” shown in **Table 4.4**). Washing solution is removed completely by flipping the MTP over the sink and pounded the MTP on a tissue for three times.

*Functionality Test 1 (HP Assay with EuTc Discs in MTP)*

100  $\mu\text{L}$  of 0 mM HP sample is added with the multichannel pipette to each sensor discs. The plate is shaken for 5 seconds before the kinetic measurement is started for 6 minutes (protocol for “HP assay” shown in **Table 4.4**; 10 minutes is possible, too). During the measurement, the samples are shaken orbitally by the plate reader at 300 rpm. The samples are excited at 405/10 nm and the emission intensity is measured at 615/10 nm at regular intervals (usually 1 min) at defined temperature. When the kinetic measurement is finished, the MTP is flipped over to remove the sample solutions. The MTP is pounded three times on a tissue to completely remove all remaining solution. The described procedure is repeated with the same discs for the next higher concentrated HP sample.

*Functionality Test 2 (Glucose/EuTc and Lactate/EuTc Assay with Enzyme Discs in MTP)*

100  $\mu\text{L}$  of 0 mM glucose/EuTc or lactate/EuTc sample is added with the multichannel pipette to each sensor discs. The plate is shaken for 5 seconds before the kinetic measurement is started for 10 minutes (protocol for “glucose/EuTc assay” shown in **Table 4.4**). During the measurement, the samples are shaken orbitally by the plate reader at 300 rpm. The samples are excited at 405/10 nm and the emission intensity is measured at 615/10 nm at regular intervals (usually 1 min) at defined temperature. When the kinetic measurement is finished, the MTP is flipped over to remove the sample solutions. The MTP is pounded three times on a tissue to completely remove all remaining solution. The described procedure is repeated with the same discs for the next higher concentrated glucose/EuTc or lactate/EuTc sample.

*Functionality Test 3 (Glucose and Lactate Assay with Enzyme/EuTc Discs in MTP)*

100  $\mu\text{L}$  of 0 mM glucose or lactate sample is added with the multichannel pipette to each sensor discs. The plate is shaken for 5 seconds before the kinetic measurement is started for 10 minutes (detailed protocol for “glucose assay” shown in **Table 4.4**). During the measurement, the samples are shaken orbitally by the plate reader at 300 rpm. The samples are excited at 405/10 nm and the emission intensity is measured at 615/10 nm at regular intervals (usually 1 min) at defined temperature. When the kinetic measurement is finished, the MTP is flipped over to remove the sample solutions. The MTP is pounded three times on a tissue to completely remove all remaining solution. The described procedure is repeated with the same discs for the next higher concentrated glucose or lactate sample.

*Functionality Test 4 (Glucose/GOx and Lactate/LOx Assay with EuTc Discs in MTP)*

100  $\mu\text{L}$  of 0 mM glucose or lactate sample is added with the multichannel pipette to each sensor discs. Then, 1  $\mu\text{L}$  of the respective enzyme solution (theoretical activity of 1 U/ $\mu\text{L}$ ) or 50  $\mu\text{L}$  of the respective enzyme solution (theoretical activity of 40 mU/ $\mu\text{L}$ ) is added immediately

before start. The plate is shaken for 5 seconds before the kinetic measurement is started for 10 minutes (detailed protocol for “glucose assay” shown in **Table 4.4**). During the measurement, the samples are shaken orbitally by the plate reader at 300 rpm. The samples are excited at 405/10 nm and the emission intensity is measured at 615/10 nm at regular intervals (usually 1 min) at defined temperature. When the kinetic measurement is finished, the MTP is flipped over to remove the sample solutions. The MTP is pounded three times on a tissue to completely remove all remaining solution. The described procedure is repeated with the same discs for the next higher concentrated glucose or lactate sample. Same amount of the respective enzyme is added.

#### **4.2.3.4 Interference Study**

PVAc/CA-EuTc discs are measured with 100  $\mu$ L buffer with and without interfering ions (chloride and phosphate) like described for a regular HP assay (Functionality Assay 1) at 25°C. Instead of increasing HP concentrations, the respective next higher concentrated interference solution is added to the discs.

#### **4.2.3.5 Leakage Study**

##### *EuTc Discs*

Functionality assays were performed as described above with EuTc and blank discs. The supernatant solutions from each sample concentration are not discarded after the runtime of the assay is over but collected in another microplate. The supernatants are mixed with 1  $\mu$ L of 100 mM HP solution to obtain a 1 mM HP concentration per well. The samples were excited at 405 nm and the emission intensity was measured at 615 nm every 60 seconds within 10 minutes (detailed protocol for “glucose assay” shown in **Table 4.4**). Intensities are compared to the mean values of the supernatants obtained from blank discs without EuTc.

##### *Enzyme Discs*

Substrate/EuTc assays were performed like described above with the enzyme and blank discs. D4-enzyme discs and blank discs were shaken at 350 rpm with 100  $\mu$ L of buffer. The buffer is changed in regular time intervals (e.g., within 6 hours: 4x15 min, 2x30 min, 4x60 min). The supernatant solutions were transferred to another MTP and mixed with 100  $\mu$ L of glucose/EuTc solution (100 mM glucose solution mixed 1:1 (v/v) with EuTc solution). The measurement was started immediately. The samples were excited at 405 nm and the emission intensity was measured at 615 nm every 60 seconds within 10 minutes (detailed protocol for “glucose assay” shown in **Table 4.4**). The substrate/EuTc assay was repeated with the washed discs. Results are compared to the initial performance of the discs.

#### 4.2.3.6 Storage Stability Study

The ready-to-use sensor or enzyme discs are stuck and stored within microplates. 200  $\mu\text{L}$  of 0.1 M HEPES pH 7.4 (contains 0.01 wt% sodium azide) is added to half of the discs in each prepared plate. The entire plate is sealed with adhesive protection foil and covered with aluminum foil for light protection. One plate is stored at 22°C, the other one at 4°C. After the respective storage times (between 1 and 52 weeks), the storage buffer is removed completely by flipping the plate and pounding it three times on tissue. The plate can be used immediately for the next step, performing an assay by starting with the washing procedure.

#### 4.2.4 Statistics and Data Evaluation

All calculation, especially the arithmetic mean values and standard deviation (SD) were calculated with Microsoft Excel 2016 (Microsoft Corporation, Redmond, Washington, USA) or by the respective plate reader software MARS Data Analysis Software from BMG LABTECH GmbH (<https://www.bmglabtech.com>) and Gen5 Microplate Reader and Imager Software from BioTek Instruments ([www.biotek.de](http://www.biotek.de)). Measurements were performed at least in triplicate ( $n \geq 3$ ). Suspicious values were removed after failing the outlier Q-test. Calculated SD is represented by error bars in y-direction.

Linear and non-linear regression curves were accomplished with following equation (1) and equation (2).

$$\text{linear curve fit:} \quad y = m \cdot x + b \quad (1) \quad \begin{array}{l} m \dots \text{slope} \\ b \dots y - \text{axis intercept} \end{array}$$

$$\text{sigmoidal curve fit:} \quad y = \frac{A_1 - A_2}{1 + \left(\frac{x}{x_0}\right)^p} + A_2 \quad (2) \quad \begin{array}{l} A_1 \dots \text{initial value} \\ A_2 \dots \text{final value} \\ x_0 \dots \text{center} \\ p \dots \text{power} \end{array}$$

### 4.3 Results and Discussion

As mentioned in the introduction part, our and other groups developed already well-established assays for the detection of HP using Europium(III) tetracycline as metal-organic probe. But these assays are optimized for concentrations below 1 mM HP. Best performance of the luminescent probe was obtained when Eu(III) ions and tetracycline are mixed in molar ratio of 3:1 and at a pH value of 6.9 [20, 21]. First step of the presented work is to prove if the EuTc probe is suitable for higher concentrations and other pH to enable a broader application area. Therefore, a suitable probe concentration for the detection of hydrogen peroxide samples in the range from 50  $\mu$ M to 10 mM in 0.1 M HEPES pH 7.4, representing the regular blood pH [35], was established. The next step was to find a suitable enzyme concentration to realize a glucose and lactate detection in the physiological relevant ranges as well as for exceptional situation like hypo- and hyperglycemia or -lactatemia. Assays are performed at 25°C and 37°C to investigate the impact of temperature on the assay performance through changes in enzyme activity or luminescence intensity.

The entrapment of enzymes and probe were realized in simple one-component and one- or two-layer hydrogel or polymer discs to show the functionality regarding future applications for fully implantable sensors. The capability of retaining the enzyme and the probe within the hydrogel or polymer structure was tested in leakage experiments. Furthermore, the storage stability of the GOx and EuTc discs were investigated at two temperatures in dried state and incubated in buffer.

#### 4.3.1 Detection of Hydrogen Peroxide, Glucose and Lactate

##### 4.3.1.1 Homogeneous Assays

The already existing protocols from Dürkop and Wolfbeis *et al* [20–22] were adapted by increasing the EuTc concentration for the assays. Furthermore, instead of MOPS buffer at pH 6.9, a 0.1 M HEPES pH 7.4 for simulating the blood pH were used for the further optimization steps and assays.

The following **Figure 4.3** shows collected emission spectra of homogeneous HP/EuTc mixtures in a 96-well microplate after an excitation at 405 nm. The inset shows the deviated signal intensities at 616 nm plotted versus the HP concentration as dose-response curve. The system is still more sensitive for HP concentration below 1 mM. But it is possible to make semi-quantitative statements for HP concentrations above 1 mM. Luminescence increases with rising HP concentration. Combination of the EuTc probe with the right amount of enzyme activity makes it a powerful tool for glucose and lactate detection in a homogeneous assay in a plate format. This knowledge works as proof of concept for the following experiments, and this simple HP assay was not further optimized.

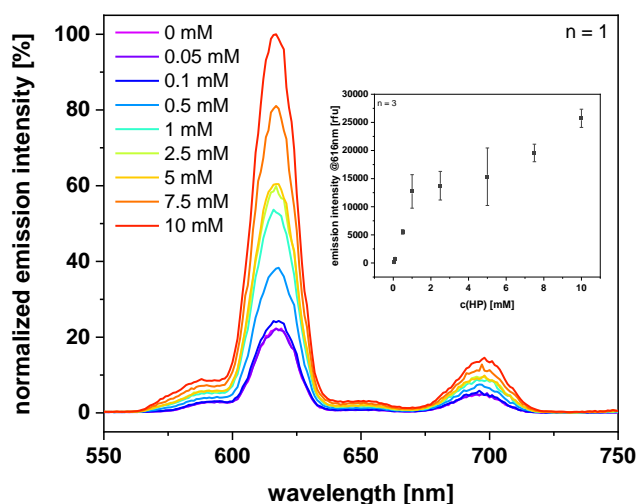


**Figure 4.3** The emission spectra of EuTc solution with and without HP was measured between 550 nm and 750 nm. The pronounced emission peak around 616 nm represents the  ${}^5D_0 \rightarrow {}^7F_2$  transition of the  $\text{Eu}^{3+}$  ion. With increasing HP concentration, the intensity of the emission peak rises due to the reversible exchange of quenching water molecules by the HP molecules. Inlet: Dose-response curve obtained from the emission values at 616 nm from three separately recorded spectra (BioTek plate reader,  $\lambda_{\text{exc}}=405/8$  nm, scan from 550 nm to 750 nm with step width of 1 nm,  $n = 1-3$ , gain 85,  $25^\circ\text{C}$ , 10 min incubation time).

The following dose-response curves shown in **Figure 4.4** were obtained from homogeneous assays. An EuTc solution was mixed with the same volume of lactate or glucose samples in buffer at pH 7.4. A suitable volume of the respective enzyme solution is added to obtain a theoretical activity of 1 U/well. The dose-response curves were obtained from the kinetic measurements after 2.5 minutes at  $25^\circ\text{C}$  and  $37^\circ\text{C}$  to investigate the temperature dependency of the assay. On the one hand side, the luminescence of the EuTc is reduced with increasing temperature [19], but on the other hand side enzyme activity increases with temperature [36]. These opposite effects are assumed to outnumber each other fully or at least in parts.

In case of glucose, the assumption was not confirmed, and the sensitivity of the assay is reduced at higher temperature. The homogeneous assay for glucose should be carried out at ambient temperature. Lactate oxidase outnumbers the negative temperature effect on the luminescence properties of the EuTc complex at higher temperature. As the dose-response curves of the lactate assay reveals the sensitivity of the assay is the same at  $25^\circ\text{C}$  and  $37^\circ\text{C}$ . Furthermore, at high temperature the signal intensity for the added lactate concentrations above 20 mM is higher than for the same concentrations measured at ambient temperature. Apparently, the enzyme activity is improved at higher temperature and comes over the negative temperature effect.

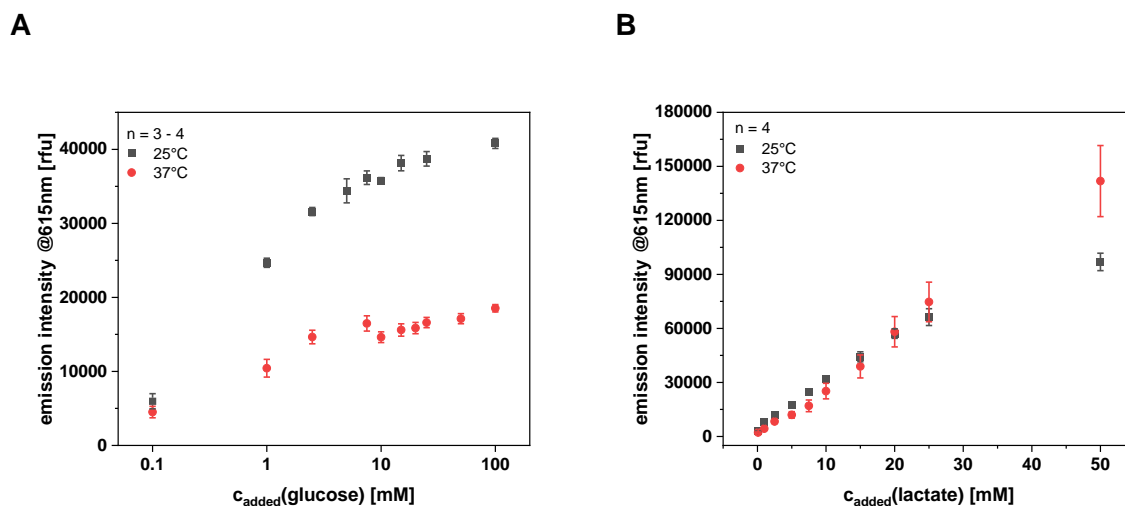


**Figure 4.4** Blank corrected dose-response curves of 50  $\mu\text{L}$  EuTc solution mixed with 50  $\mu\text{L}$  of sample solution (0-100 mM) and 1  $\mu\text{L}$  of the respective enzyme solution (1 U/ $\mu\text{L}$ ) at 25°C and 37°C. All solutions were prepared in 0.1 M HEPES pH 7.4 **A** glucose **B** lactate (FluoStar  $\Omega$ ,  $\lambda_{\text{exc}}=405/10$  nm,  $\lambda_{\text{em}}=615/10$  nm,  $n = 3-4$ , gain 1200, 25°C and 37°C, 5 min incubation time)

Nevertheless, an appropriate temperature monitoring is highly recommended in every case to obtain reliable and reproducible results. Calibration of the system or the assay should always be carried out at the same temperature at the later assay is performed. As proof of concept the shown dose-response curves support the possibility of a successful heterogeneous assay where the probe and/or the enzyme are entrapped within a hydrogel or polymer.

#### 4.3.1.2 Heterogeneous Assays with Probe Discs

Two polymer or polymer mixtures have very promising properties regarding biocompatibility and diffusion properties, and the knife-coating process gives smooth and even sensor foils with suitable solvent mixtures. A combination of one mass equivalent polyvinyl acetate (PVAc) and 99 mass equivalents cellulose acetate (CA) dissolved in a cyclohexanone/acetone mixture was already used in 1983 by Tsuchida *et al* for the preparation of a multi-enzyme membrane electrode [30]. Hydromed® D4, a polyurethane-based hydrogel with a water content of around 50 % is an often used material for the entrapment of enzymes, organic dyes or other probes for chemo- and biosensor applications [23, 31–33] and enables a fast hydrogen peroxide diffusion [34].

10 wt% of the respective polymer mixture or hydrogel are dissolved in a suitable solvent mixture. For PVAc/CA, cyclohexanone/water (CHon/ $\text{H}_2\text{O}$ , 99:1, v/v) and dimethyl formamide/water (DMF/ $\text{H}_2\text{O}$ , 9:1, v/v) mixtures are appropriate to dissolve both polymers. If the EuTc complex or enzyme should be entrapped within the polymer, a water content of 10 vol% is recommended. Low water content seems to hinder the formation of the EuTc complex. Acetone as solvent should be avoided in case of EuTc entrapment. It is assumed from initial solvent experiments that acetone irreversibly forms a complex with Eu(III) and



makes it impossible to detect hydrogen peroxide. For D4, 10 wt% polymer cocktails can be obtained with ethanol/water mixtures (EtOH/H<sub>2</sub>O, 9:1, v/v). Other short-chained alcohols like 2-propanol and *tert*-butanol are appropriate, too. Using them for the preparation of sensor or polymer cocktails results in higher viscosity of the cocktail and therefore an impeded knife-coating process. It would be necessary to warm the cocktail up to 40°C or even higher to decrease the viscosity to obtain smooth foils during the knife-coating process. An increased cocktail temperature is always a risk for destabilization or destruction of the suspended enzyme or the dissolved EuTc complex. Furthermore, the used solvents evaporate faster at higher temperature. This can lead to cracks or other irregularities on the surface of the sensor and enzyme foils.

The EuTc content is optimized for both hydrogels and polymer mixtures. Sensor cocktails with 10 wt% polymer and EuTc contents between 0.01 wt% and 1.0 wt% were prepared, sensor foils with a wet thickness of 30 µm were coated, dried, and washed. The discs obtained from these foils were stuck into a microplate by adhesive tape to prevent them from moving around or swimming up. A heterogeneous HP assay was performed. The resulting dose-response curves after 5 min of incubation time at 25°C are shown in the following **Figure 4.5**.

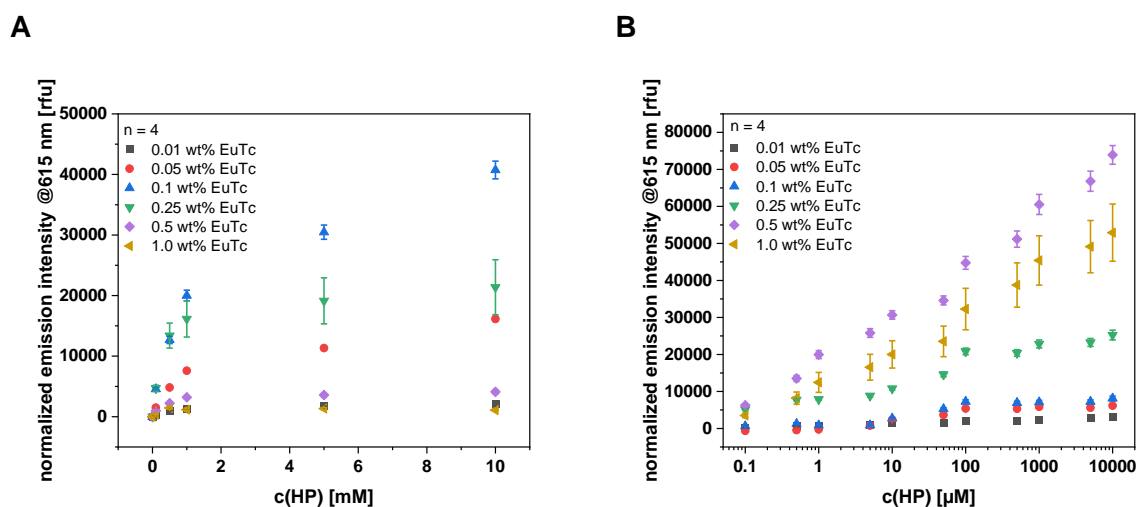


**Figure 4.5** Normalized dose-response curves obtained from sensor discs incubated for 5 min with the respective HP samples. **A** PVAc/CA-EuTc sensor discs were obtained from sensor cocktails with 10 wt% PVAc/CA and x.y wt% EuTc in DMF/H<sub>2</sub>O **B** D4-EuTc // PVAc/CA sensor discs were obtained from sensor cocktails with 10 wt% D4 and x.y wt% EuTc in EtOH/H<sub>2</sub>O covered with a protection layer obtained from a polymer cocktail containing 10 wt% PVAc/CA in CHon/H<sub>2</sub>O (FluoStar Ω, λ<sub>exc</sub>=405/10 nm, λ<sub>em</sub>=615/10 nm, n = 4, gain 1200, 25°C, 5 min incubation time)

For both tested polymer and hydrogel systems, the optimum EuTc is different. For PVAc/CA polymer mixture, the most sensitive dose-response curve for HP detection was obtained for discs with 0.1 wt% complex in the initial sensor cocktail. Using D4 as immobilizing hydrogel with a PVAc/CA protection layer to prevent EuTc from leakage, 0.5 wt EuTc in the initial sensor cocktail is recommended to get the most sensitive dose-response curve for HP detection. For

higher or lower EuTc content, the sensitivity of the dose-response behavior especially for HP concentrations above 1 mM decreases rapidly. A dynamic range for HP detection between 0.1  $\mu$ M and 10 mM is shown with D4-EuTc discs protected by a PVAc/CA membrane.

Therefore, for all further experiments and follow-up optimizations, PVAc/CA-EuTc discs obtained from 10 wt% PVAc/CA with 0.1 wt% EuTc in a DMF/water mixture were used. Furthermore, D4-EuTc discs were obtained from 10 wt% D4 with 0.5 wt% EuTc in an ethanol/water mixture. As protection layer, a 10 wt% PVAc/CA polymer cocktail dissolved in 99:1 (v/v) CH<sub>3</sub>OH/water is applied on top.

Different cutting techniques for the sensor discs were tested. From an exemplary PVAc/CA-EuTc sensor discs were cut with a laser-engraving machine with two different optics, and hole-punched with a toggle press. Laser cutting offers beside the fastness an assumed welding of the different polymer layers. The influence of the cutting technique on the discs' performance is illustrated by emission scans of the discs with and without HP. The cut sensor foil and the normalized emission scans are shown in the SI part (**SI Figure 4.1**). There is a drastic difference in the emission intensity patterns of the sensor discs. Especially the discs cut by laser show a worse response towards the added HP. It is assumed that the released heat during the cutting process destroys the complex by oxidation. The oxidized tetracycline molecule is not functional as antenna and therefore the energy transfer from the organic ligand to the central metal ion is repealed. Without this energy transfer the luminescence is strongly decreased. Therefore, the discs are hole-punched manually with the toggle press for all further experiments to reduce the risk of diminished activity by oxidation processes during the laser cutting process.

Another important parameter which must be investigated for the sensor discs is the temperature. It is known that luminescence is a temperature-dependent process. With increasing temperature, the probability of radiation-free relaxation of excited states increases whereas the probability for internal energy transfer from the antenna ligand to the central ion decreases [17, 19]. Both effects lead to a reduced luminescence intensity at higher temperature. For PVAc/CA-EuTc sensor discs spectra were collected at temperatures between 25°C and 40°C. The excitation and emission spectra and the resulting emission intensity at 616 nm plotted versus the temperature are shown in the following **Figure 4.6**.

Emission intensity decreases linearly by over 50 % within the observed temperature range of 25°C to 40°C. Therefore, it must be kept in mind that the calibration of the system is just valid at one set temperature. For measurements at any other temperature, the system needs another calibration beforehand, or the obtained results must be re-calculated internally by an

implanted software for the current temperature. Subsequently, a reliable temperature monitoring system must be added if the system is used for implantable sensors in the future.

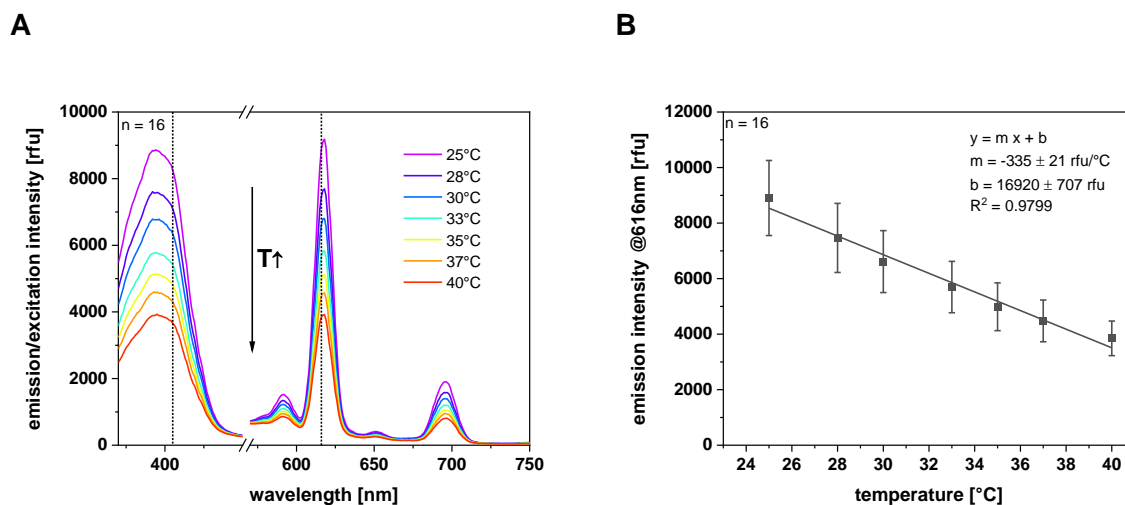


**Figure 4.6** **A** Mean value of emission and excitation spectra of PVAc/CA-EuTc discs (10 wt% PVAc/CA and 0.1 wt% EuTc in DMF/H<sub>2</sub>O) are shown at different temperatures between 25°C and 40°C. **B** The emission intensity at 616 nm was plotted versus temperature. A linear decrease by over 50 % of the signal intensity can be observed by increasing the temperature from 25°C to 40°C. (BioTek plate reader,  $\lambda_{exc}=405/8$  nm,  $\lambda_{em}=616/8$  nm,  $n = 16$ , gain 100, 25°C to 40°C).

Combination of the luminescent system with an enzyme introduces an antagonist about temperature dependency. Usually, enzyme catalysis, as well as many other chemical reactions, are accelerated by rising temperature [36]. The PVAc/CA-EuTc discs were incubated with substrate/enzyme mixtures and the kinetic curves are recorded. Deviated from the kinetics after 2.5 minutes, the dose-response curves for glucose and lactate detection at 25°C and 37°C are shown in the following **Figure 4.7**. Theoretical enzyme activity is 2 U/well.

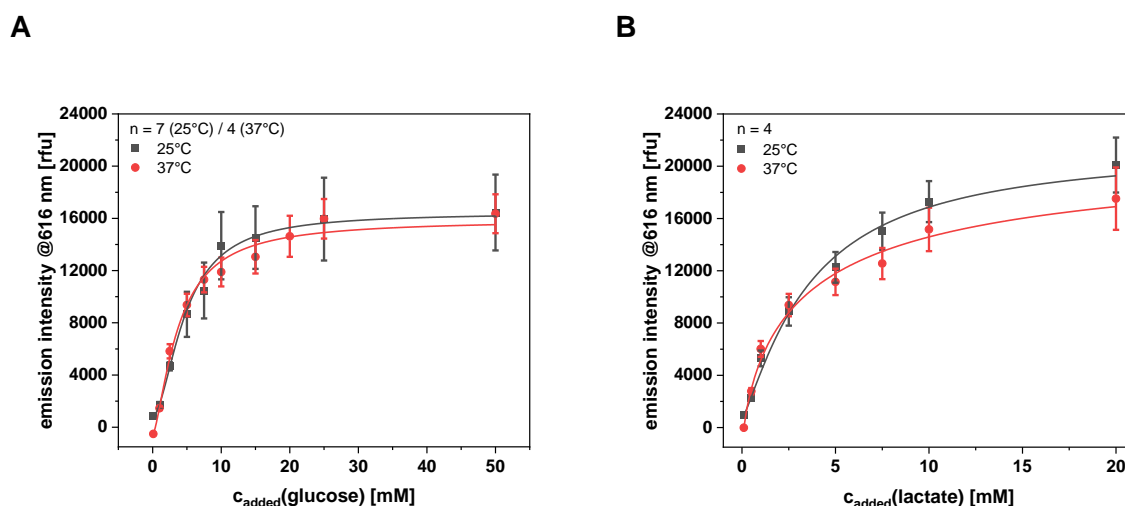


**Figure 4.7** Normalized dose-response curves obtained from kinetic assays including discs made from 10 wt% PVAc/CA with 0.1 wt% EuTc (cocktail prepared in DMF/water). 100  $\mu$ L of the respective sample solution and 50  $\mu$ L of 40 mU/ $\mu$ L enzyme solution are added. **A** glucose/GOx assay **B** lactate/LOx assay (BioTek plate reader,  $\lambda_{exc}=405/8$  nm,  $\lambda_{em}=616/8$  nm,  $n = 4/7$ , gain 80, 25°C/37°C, 2.5 min incubation time)

Within standard deviations, there is no significant difference between the assays' sensitivity at different temperatures. As discussed previously, two opponent effects, namely the decreased luminescence and the increased enzyme activity, are affecting the performance of the assay, also in case of PVAc/CA-EuTc sensor discs. But the luminescence decrease is lower than it was observed in the homogeneous assays for glucose determination (**Figure 4.4 A**) or for the blank PVAc/CA-EuTc discs (**Figure 4.6**). These are promising results for the future application as implantable sensor for continuous monitoring. Within the PVAc/CA membrane the EuTc performance is less affected by temperature changes than in case of homogeneous assays used for detection of glucose and lactate. Nevertheless, temperature control or monitoring is recommended also for the heterogeneous assay types to obtain reliable results.

In summary, a simple optical sensing approach is realized by physical entrapment of the HP-sensitive probe EuTc within a one- or two-layer system of biocompatible hydrogels and polymers. The discs are stuck into a microplate. By adding the sample solution and the respective enzyme, within less than 5 minutes reliable results in up to 96 samples can be obtained simultaneously.

#### **4.3.1.3 Heterogeneous Assays with Enzyme Discs**

Next step was to realize the entrapment of GOx and LOx within a hydrogel or polymer layer. It is preferable to use the same biocompatible hydrogels as for the EuTc discs due to their excellent properties regarding the future applications as implantable optode. Production process should be as simple as possible and comparable to the production of the probe discs to have a consistent procedure for all processes.

Therefore, polymer cocktails with relatively mild organic solvents were tested for getting suitable enzyme cocktails. Most promising is 10 wt% D4 in EtOH/water for lactate oxidase and glucose oxidase. A highly concentrated enzyme stock solution is added to the polymer cocktail and the enzyme is carefully dispersed under stirring at slightly elevated temperature for 1 to 2 hours. Enzyme foils and discs are made and prepared for the microplate assays. Enzyme cocktails with 0.2 wt%, 0.5 wt% and 1.0 wt% of the respective enzyme were prepared. The respective substrate is mixed with EuTc solution and added to enzyme discs. The luminescence at 615 nm is monitored over time and dose-response curves are derived usually after 5 minutes of kinetic measurements. The assays were performed 25°C, 30°C and 37°C to investigate the influence of temperature on enzyme activity and luminescence quenching. The normalized dose-response curves of D4-GOx discs derived from kinetic measurements with glucose/EuTc solutions are shown in the following **Figure 4.8**.

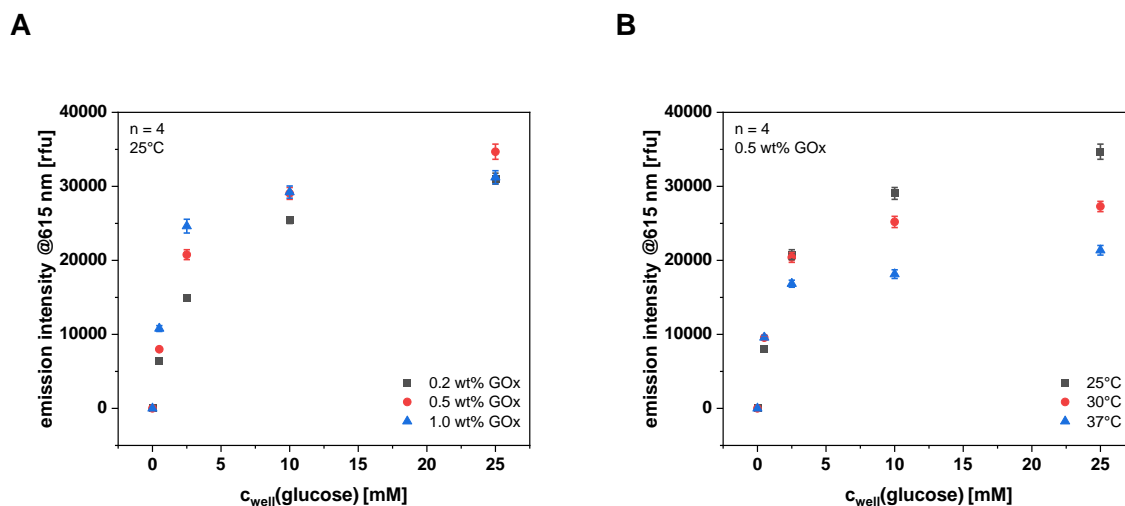


**Figure 4.8** Normalized dose-response curves of D4-GOx discs (10 wt% D4 in EtOH/buffer) after 5 min of incubation time with glucose/EuTc solutions. The resulting glucose concentrations per well are ranging between 0.5 mM and 25 mM ( $c_{added}$  between 1 mM and 50 mM) **A** Discs were prepared from enzyme cocktails with 0.2 wt%, 0.5 wt% and 1.0 wt% GOx and measured at 25°C **B** Discs were prepared from enzyme cocktail with 0.5 wt% GOx and measured at 25°C, 30°C and 37°C (FluoStar  $\Omega$ ,  $\lambda_{exc}$ =405/10 nm,  $\lambda_{em}$ =615/10 nm,  $n = 4$ , gain 1200, 25°C, 30°C, 37°C)

**Figure 4.8 A** shows how the different enzyme amount changes the performance and therefore the sensitivity of the assay. For the highest tested GOx amount (1.0 wt% GOx in the enzyme cocktail) the signal change is higher for lower concentrations. But there is no great difference in the signal of 10 mM and 25 mM glucose recognizable. The lowest tested enzyme amount (0.2 wt% GOx) has a good sensitivity over the entire range. But the best performance at 25°C is obtained for discs derived from enzyme cocktails containing 0.5 wt% GOx. The luminescence intensity especially for 10 mM and 25 mM of final glucose concentration is well distinguishable in the assay for those discs. Therefore, D4-GOx discs obtained from 0.5 wt% GOx cocktails were used for further experiments.

**Figure 4.8 B** shows the dose-response curves of D4-GOx discs obtained from 0.5 wt% enzyme cocktails within glucose/EuTc assays at three different temperatures. As mentioned earlier, it is assumed that the accelerated substrate conversion at elevated temperature can somehow outnumber the negative temperature effect on the luminescence intensity. For low and medium glucose concentrations up to 5 mM (results in final concentration of 2.5 mM per well) this may be true but especially for higher concentrations the sensitivity of the assay decreases with temperature and best results are obtained at 25°C. Same observations were made for the other tested enzyme concentrations.

The fundamental investigations were repeated under same conditions but GOx was replaced by the same amount of LOx. Lactate/EuTc solutions were added to the D4-enzyme discs and the assay was performed like described in the Experimental section. The derived dose-response curves after 5 minutes are shown for discs with three different LOx in amounts in

**Figure 4.9 A.** The respective dose-response curves at 25°C, 30°C and 37°C for discs obtained from cocktails with 0.2 wt% LOx are shown in **Figure 4.9 B.**

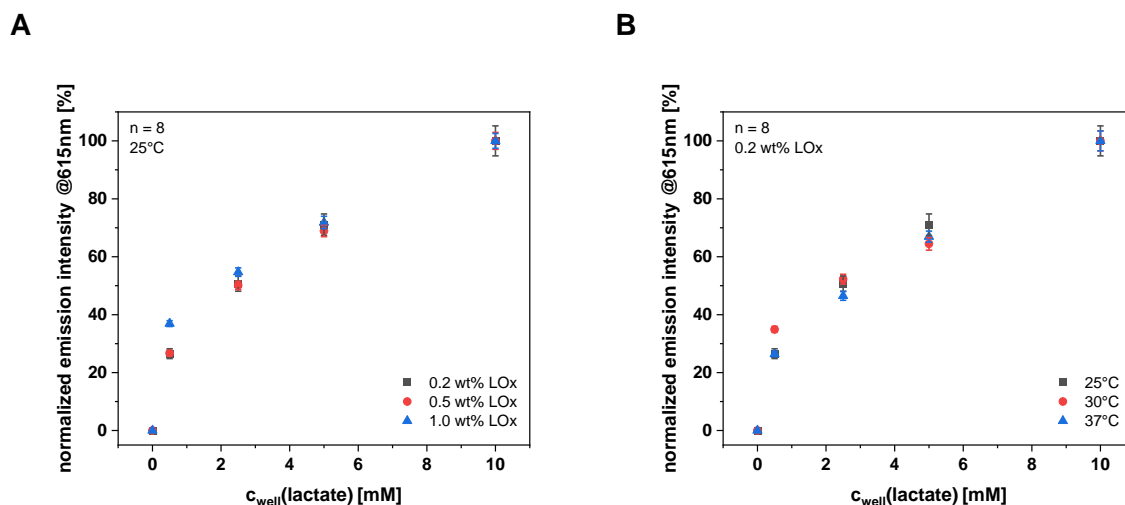


**Figure 4.9** Normalized dose-response curves of D4-LOx discs (10 wt% D4 in EtOH/buffer) after 5 min of incubation time with lactate/EuTc solutions. The resulting lactate concentrations per well are ranging between 0.5 mM and 10 mM ( $C_{\text{added}}$  between 1 mM and 20 mM) **A** Discs were prepared from enzyme cocktails with 0.2 wt%, 0.5 wt% and 1.0 wt% LOx and measured at 25°C **B** Discs were prepared from enzyme cocktail with 0.2 wt% LOx and measured at 25°C, 30°C and 37°C (FluoStar  $\Omega$ ,  $\lambda_{\text{exc}}=405/10$  nm,  $\lambda_{\text{em}}=615/10$  nm,  $n = 4$ , gain 1200, 25°C, 30°C, 37°C)

There is no great difference in performance or sensitivity for the tested LOx amount within the D4 hydrogel discs. Just discs obtained from the cocktail with 1.0 wt% LOx show a higher signal for the lowest lactate concentration of 0.5 mM compared to the discs with the lower enzyme content. With respect to economy, further experiments were focused on discs with 0.2 wt% or 0.5 wt% LOx in the initial cocktails. Lactate/EuTc assays are performed at 25°C, 30°C and 37°C with these discs. The three dose-response plots are very similar, and it can be assumed that the increased LOx activity outnumbers the negative temperature effect at higher temperature.

To sum up, a GOx amount of 0.5 wt% within the initial 10 wt% D4 cocktail in EtOH/water or EtOH/buffer leads to best performance of the assay at 25°C. The assay can also be conducted at 30°C or 37°C but sensitivity is significantly decreased for added glucose concentrations above 5 mM. In case of D4-LOx discs, an initial amount of 0.2 wt% within the enzyme cocktail is suitable to obtain highly sensitive discs. The negative effect on the luminescence intensity can be outnumbered by the increased enzyme activity at elevated temperature. The lactate/EuTc with D4-LOx discs assay can be performed without loss of sensitivity at temperatures up to 37°C in the microplate format.

#### 4.3.2 Interference Studies

The probe EuTc is not just very sensitive but highly specific for HP as Dürkop and Wolfbeis *et al* reported previously. The luminescence is not affected by alkali and ammonium

ions. Chloride, sulfate, and nitrate ions in concentrations up to 100 mM do not interfere with the probe. However, citrate and phosphate are known to lead to an increase of the luminescence. Furthermore, proton concentration has an influence on the charge of the organic ligand and therefore on the luminescence intensity. Strongest luminescence is observed within a pH window of 6.6 and 7.2 and drops rapidly outside of this range [20].

Therefore, the PVAc/CA-EuTc discs were tested in a small interference assay. The discs were incubated with buffer samples without interfering ions and with a physiological relevant low, medium, and high phosphate or chloride concentration. The resulting data are shown in the following **SI Figure 4.2**. Neither chloride anions, as assumed, nor phosphate ions within the physiological relevant range interfere significantly with the probe complex entrapped in the PVAc/CA membrane. Regarding the future aim of getting a fully implantable system, more interferences beside ions like other metabolites in blood or serum components will be tested as well as chemicals which are usually used during surgeries.

### **4.3.3 Leakage Studies**

The sensor and enzyme discs were tested for their capability to entrap the probe or protein safely without leakage and ensures a reliable functionality for long-term monitoring. Regarding the pursued future application, the implantable optical sensor system, leakage of all compounds should be avoided to prevent the chemicals from entering a patient's blood circuit. But for non-implantable sensors, a leakage of the recognition element or probe also leads to reduced shelf-life and diminish the sensitivity of the system over time.

For the PVAc/CA-EuTc system derived from sensor cocktails with 10 wt PVAc/CA and 0.1 wt% EuTc in DMF/H<sub>2</sub>O, the regular HP and glucose/GOx or lactate/LOx assays were performed at 25°C and 37°C. The supernatant solutions were collected every 15 min, mixed with HP in case of glucose and lactate and after a short incubation time, the luminescence intensities were compared to sample solutions incubated with blank PVAc/CA discs under the same conditions. Exemplary bar charts are shown in the following **Figure 4.10** for an initial HP assay at 25°C (**A**) for 1.5 h and an extended glucose/EuTc assay at 37°C (**B**) for over 3 h in the microplate format.

For the first trial, six different HP solutions (from 0 mM to 10 mM) were added to the sensor discs and shaken for 15 min at 25°C. None of the investigated supernatants show a significant difference to the blank signals. This means there is no washed out EuTc present in the supernatant solutions. The experiment was repeated with the probe discs but at elevated temperature and with extended number of samples. Within 3 h at 37°C and fresh solution in certain intervals, there is no significant leakage of the probe complex from the PVAc/CA membrane.

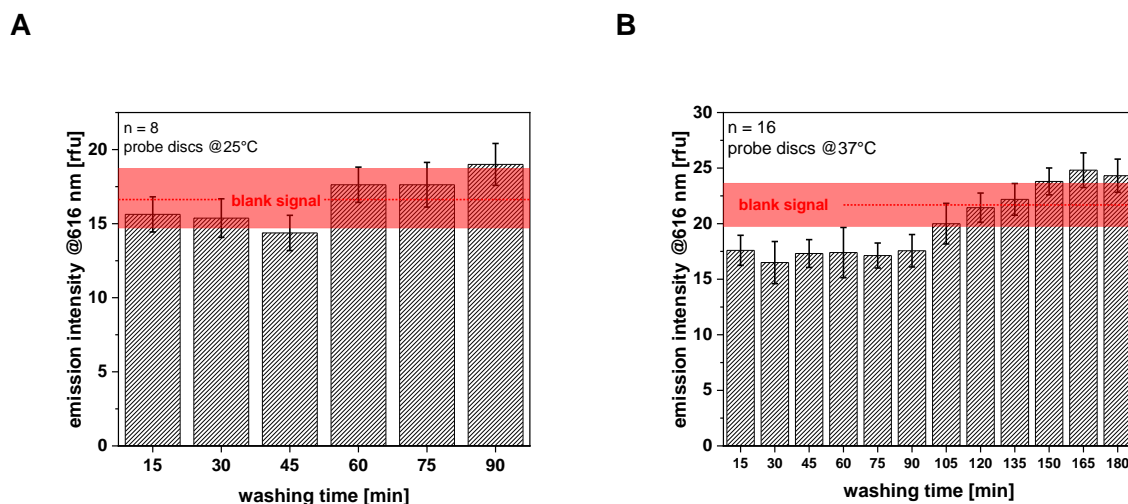


**Figure 4.10** Supernatants from glucose/GOx assays with PVAc/CA-EuTc discs (10 wt% polymer mixture and 0.1 wt% EuTc were dissolved in DMF/H<sub>2</sub>O for the sensor cocktail) were collected, incubated with HP and the luminescence after 5 min was compared to the mean signal of all supernatant solutions collected from blank PVAc/CA discs. The glucose/GOx assays were performed at **A** 25°C and at **B** 37°C (BioTek plate reader,  $\lambda_{exc}=405/8$  nm,  $\lambda_{em}=616/8$  nm,  $n = 8/16$ , gain 80, 25°C)

The study was repeated for the D4-enzyme discs. Therefore, D4-GOx and D4-LOx discs (obtained from enzyme cocktails with 10 wt% D4 and 0.5 wt% enzyme dissolved in EtOH/HEPES) were investigated regarding the ability to retain the enzyme. The experimental trial was adapted to check the discs' performance before and after intensive washing procedure to prove the enzyme is retained within the hydrogel structure. The results from those investigations are shown in the following **Figure 4.11** for D4-GOx (**A**) and D4-LOx (**B**). Both disc types were obtained from cocktails containing 10 wt% D4 and 0.5 wt of the respective oxidase dissolved in ethanol/buffer mixture.

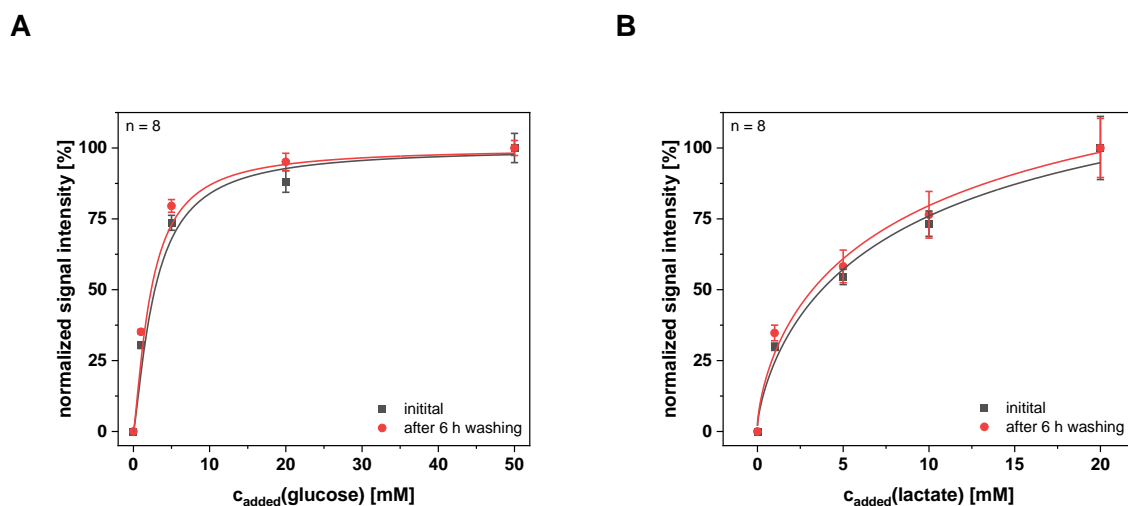


**Figure 4.11** Normalized dose-response curves of initially tested enzyme discs (grey squares) and after 6 h of intensive washing tested (red dots). Data sets from 5 minutes assay time were taken for **A** D4-GOx and **B** D4-LOx discs. Discs were obtained from cocktails with 10 wt% D4 and 0.5 wt% enzyme in EtOH/HEPES (FluoStar  $\Omega$ ,  $\lambda_{exc}=405/10$  nm,  $\lambda_{em}=615/10$  nm,  $n = 8$ , gain 1200, 25°C)



First, the initial performance of the discs was determined by a substrate/EuTc assay. Afterwards, the discs were incubated in 100  $\mu$ L buffer in the microplate and shaken up to 6 h. The buffer solution was exchanged by fresh buffer solution in regular time intervals (4x15 min, 2x30 min and 4x60 min). The supernatants were collected, and possible enzyme leakage was determined by detection of produced HP. There was no enzyme activity detected in any supernatant solutions of each assay.

Following, the D4-enzyme discs were used again in a substrate/EuTc assay and showed comparable results to the initial assay performance like shown in **Figure 4.11 A** for GOx and **Figure 4.11 B** for LOx. Comparing the normalized data to each other, the dose-response curves look identical within standard deviation. Therefore, a significant enzyme leakage can be excluded based on the data sets. To sum up, both enzymes stay inside the D4 hydrogel also during a 6-hour long-term study. The enzymes are still functional after that time and shows a comparable performance as initially was observed.

Concluding the leakage study, no significant loss of EuTc from PVAc/CA membranes was observed, neither with HP at ambient conditions nor with substrate/enzyme samples at 37°C over a period of over 3 hours. The enzyme discs were washed for over 6 h whereas the washing solutions was changed in defined intervals. It is assumed that no leakage occurs over this time because the initial and after the intensive washing procedure derived dose-response curves are highly comparable. These are promising results for all tested disc types in the microplate format. A successful adaption to a flow-through system can be expected based on the data.

#### **4.3.4 Storage Stability Studies**

With respect to future commercialization of the assay, a shelf storage or lifetime determination of the sensor and enzyme discs is mandatory. The sensor and enzyme discs were stored sealed and light-protected at 4°C and 22°C within the microplate. Half of the discs were covered with 0.1 M HEPES pH 7.4 containing sodium azide to prevent microbiological growth. The other discs were stored in dried state. The initial performance was determined with the respective assay type and compared with the dose-response plots after certain time intervals.

**Figure 4.12** shows the recovered signals over a time frame of nearly 6 months obtained from PVAc/CA-EuTc discs (10 wt% PVAc/CA and 0.1 wt% EuTc in DMF/H<sub>2</sub>O) for 1 mM (**A**) and 10 mM (**B**) hydrogen peroxide samples.

Within standard deviation, nearly all recoveries range between  $\pm 12.5\%$  or even  $\pm 5\%$  compared to the initial signal response. After 3 weeks and 4 weeks, the recoveries of the discs stored at 4°C in dried state are still not higher than 125% recovery for both tested concentrations. Due to the large number of needed discs, different foils were used for the

stability study, but the recoveries are always calculated back to the initial value of the same foil to overcome possible foil-to-foil variations. Changing recoveries are a sign for leakage of the probe from the hydrogel, oxidation of the tetracycline ligand or other not further specified degradation processes within the probe complex or the hydrogel. Especially in solution a weak stability of the complex was reported by Wolfbeis *et al* [20, 22] but within the PVAc/CA layer and under the named conditions, it is shown that the probe complex is stabilized over time. The complex shows a comparable signal to the initial measurements independent of the used storage conditions and temperature for at least 24 weeks.

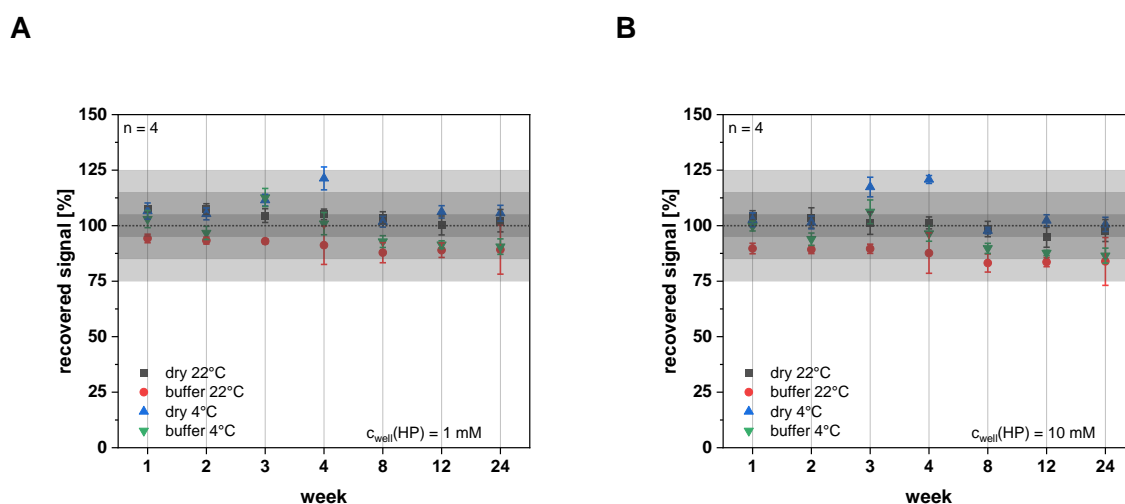


**Figure 4.12** PVAc/CA-EuTc (10 wt% PVAc/CA and 0.1 wt% EuTc in DMF/H<sub>2</sub>O discs were stored light-protected with and without 0.1 M HEPES pH 7.4 at 4°C and 22°C. HP assays were performed after defined time intervals and the signal intensity was compared to the initial ones. **A** 1 mM and **B** 10 mM HP concentration per disc (FluoStar  $\Omega$ ,  $\lambda_{exc}=405/10$  nm,  $\lambda_{em}=615/10$  nm,  $n = 4$ , gain 1200, 25°C)

The storage stability is tested under the same conditions for D4-enzyme discs and was performed with D4-GOx discs obtained from cocktails with 10 wt% D4 and 0.5 wt% GOx in EtOH/buffer. The resulting recoveries are shown in **Figure 4.13** for a final glucose concentration of 2.5 mM (**A**) and 10 mM (**B**).

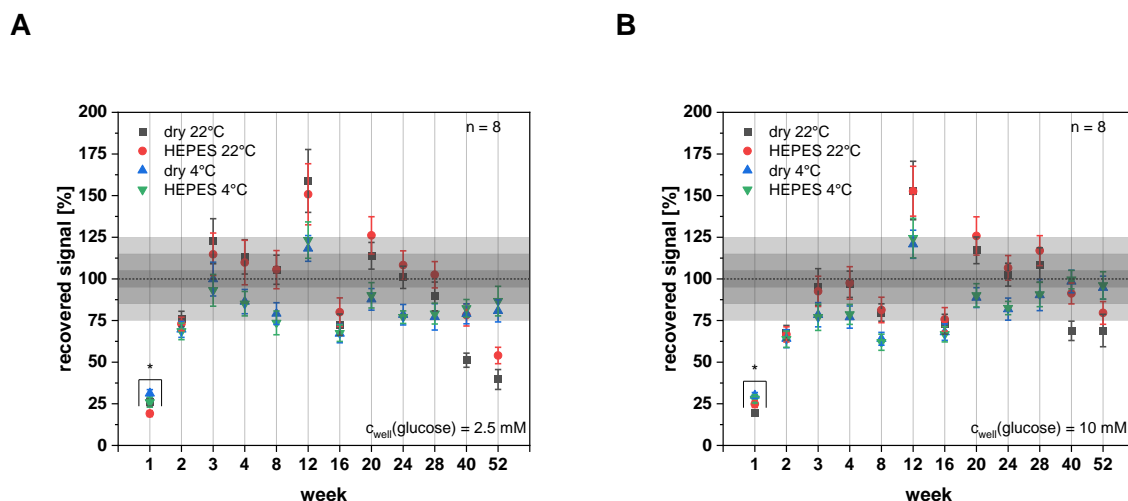


**Figure 4.13** D4-GOx (10/0.5) discs were stored light-protected with and without 0.1 M HEPES pH 7.4 at 4°C and 22°C. Glucose/EuTc assays were performed after defined time intervals and the signal intensity was compared to the initial signal intensity. **A** 2.5 mM and **B** 10 mM final glucose concentration per well and disc (\* value after week 1 is not reliable due to incorrect storage of the used EuTc solution; Fluostar  $\Omega$ ,  $\lambda_{exc}=405/10$  nm,  $\lambda_{em}=615/10$  nm,  $n = 8$ , gain 1200, 25°C)

The recoveries are always calculated back to the initial value of the same foil to overcome possible foil-to-foil variations. Within standard deviation, nearly all recoveries range between  $\pm 25\%$  or even  $\pm 12.5\%$  compared to the initial signal response. The marked values after week 1 are not reliable due to an afterwards detected incorrect storage of the used EuTc solution. Changing recoveries are a sign for leakage of the enzyme or other not further specified processes leading to activity loss of the enzyme. But within the hydrophilic D4 layer and especially at 4°C, it is shown that the GOx is stabilized over time. Comparable performance of the discs compared to the initial one is shown for around one year of storage. In case of storage at 22°C, the recovery starts dropping for the lower glucose concentration after 40 weeks.

To summarize, the probe complex is stabilized within the used PVAc/CA membrane for at least 24 weeks. It does not make a significant difference if the foils are stored in buffer or in dried state, neither if the discs are stored at 4°C or 22°C. Regarding the performance of the D4-GOx discs over a period of 52 weeks under the same storage conditions and the later planned combination of the both systems, the recommended storage for all presented disc types is protected from light at 4°C with or without buffer. With respect to the future application, it is an enormous gain to be relatively flexible with the storage conditions. It is assumed that the optimization of storage buffer can further improve the lifetime of the sensor and enzyme discs.

#### 4.4 Conclusion

The here presented work shows that the by Wolfbeis *et al* and Duerkop *et al* [20–22] developed sensing strategy using the HP-sensitive Europium(III) tetracycline complex can be adapted for much higher hydrogen peroxide concentrations up to 10 mM in a homogeneous microplate assay. The luminescence intensity decreases strongly with increasing temperature. Therefore, a strict temperature control for all assays is recommended. The combination with different oxidases enables furthermore the fast detection of glucose and lactate within a concentration range up to 20 mM for lactate and up to 50 mM for glucose at pH 7.4 in 0.1 M HEPES solution.

It was shown that EuTc can be integrated into a PVAc/CA membrane without leakage of the probe. The foils are produced by simply spreading a polymer cocktail of 10 wt% PVAc/CA (1:99, w/w) and 0.1 wt% EuTc in DMF/water (9:1, v/v) using an in-house made knife-coating device on a transparent PET support with a wet thickness of 30  $\mu\text{m}$ . The five-fold amount of EuTc (0.5 wt%) can be embedded in a hydrophilic D4 membrane (10 wt% in EtOH/H<sub>2</sub>O (9:1, v/v)) which is covered with a thin PVAc/CA layer (10 wt% in CHon/H<sub>2</sub>O (99:1, v/v)) to improve the dynamic range from 0.1  $\mu\text{M}$  up to 10 mM for HP detection in the heterogeneous assay. The discs obtained from the dried and washed sensor foils can be stored light-protected at least up to 6 months in dried state or covered with buffer at 4°C or at ambient conditions in the microplate. Comparable detection ranges like for the homogeneous approach are obtained for glucose and lactate with the heterogeneous assay concept when the respective oxidase enzyme is added in solution. Luminescence is decreased with increasing temperature whereas the enzyme activity is enhanced. It was assumed that both effects are outnumbered by each other. The assays were tested at 25°C and at 37°C and the dose-response plots show no significant difference in sensitivity. The sensor discs are unaffected by physiological relevant concentrations of chloride and phosphate.

The enzymes GOx and LOx were embedded in D4 hydrogel membranes. Therefore, 0.5 wt% GOx or 0.2 wt% LOx is dispersed in a 10 wt% D4 cocktail in EtOH/H<sub>2</sub>O (9:1, v/v). It was shown that the enzymes do not leak from the hydrogel layers without any further protection layer. The discs obtained from the enzyme foils can be stored light-protected for at least up to 1 year at 4°C in dried state or covered with buffer in the microplate. Heterogeneous assays with lactate and glucose samples mixed with EuTc were performed with the enzyme discs. A dynamic range up to 50 mM sample concentration was obtained for glucose and up to 20 mM for lactate samples in buffer.

The shown concepts are proofed for the possible mass production of selective and sensitive microplates with immobilized EuTc probe or enzymes for a rapid optical high-throughput

detection of lactate and glucose. Samples can be added directly to the EuTc discs, mixed with the enzyme and after 2 to 5 minutes incubation the luminescence at 616 nm is read out within seconds. The other way round, where the sample is mixed with the EuTc solution and added to the enzyme discs, show comparable results regarding dynamic ranges and sensitivity.

In the future, both systems, namely the EuTc sensing layer and the enzyme layer, will be combined to obtain an integrated, simple, and rapid test system for glucose and lactate. No additional pipetting steps or addition of further reagents will be necessary for the microplate format. Samples can be added simply in the microplate where the integrated sensor and enzyme discs are attached. After short incubation time the luminescence intensity is recorded and compared to the calibration plot. Successful combination of the biocompatible layers enables testing and optimization for use in a flow-through system to permit a future implementation as optode into the living organism.

#### **4.5 Acknowledgement**

The author acknowledges TERUMO Cardiovascular group for financial support. Furthermore, the author acknowledges Rahel Grünberger, Julia Ciechocińska and Laura Deml for collecting data in the scope of a Bachelor's Thesis and internships.

## 4.6 References

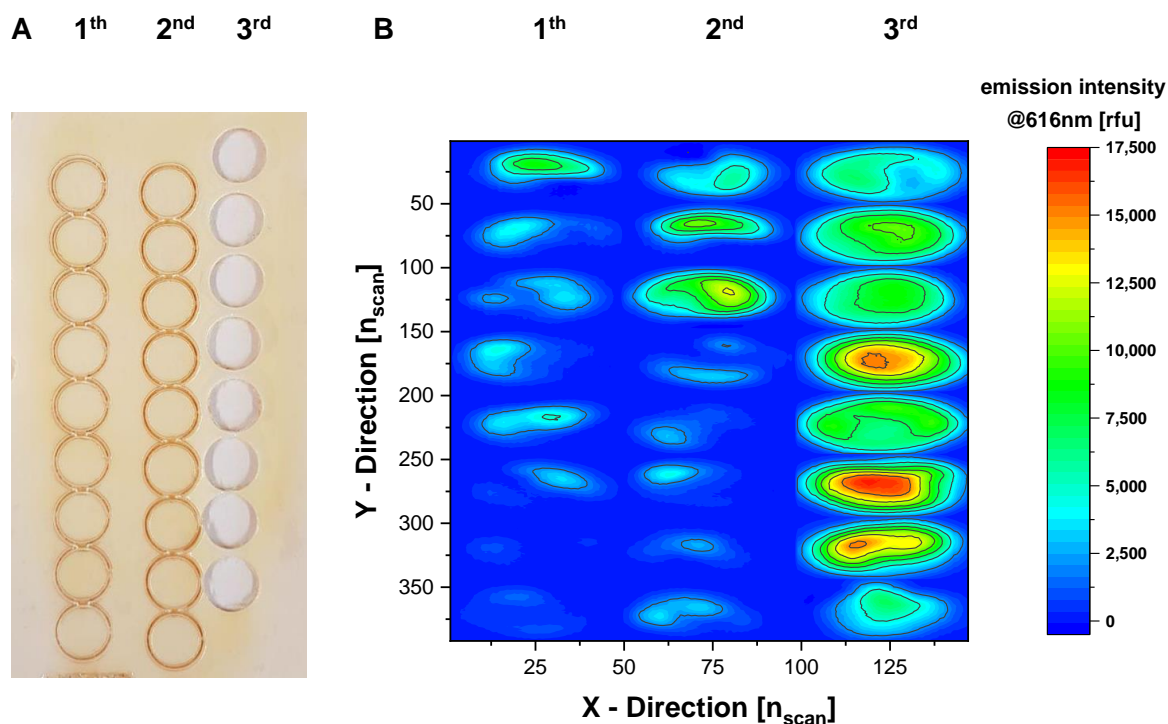
1. Meier J, M Hofferber E, A Stapleton J, M Iverson N. Hydrogen Peroxide Sensors for Biomedical Applications. *Chemosensors*. 2019; <https://doi.org/10.3390/chemosensors7040064>
2. Gholami M, Koivisto B. A flexible and highly selective non-enzymatic H<sub>2</sub>O<sub>2</sub> sensor based on silver nanoparticles embedded into Nafion. *Applied Surface Science*. 2019; <https://doi.org/10.1016/j.apsusc.2018.10.113>
3. Patel V, Kruse P, Selvaganapathy PR. Solid State Sensors for Hydrogen Peroxide Detection. *Biosensors (Basel)*. 2020; <https://doi.org/10.3390/bios11010009>
4. Bouri M, Zuaznabar-Gardona JC, Novell M, Blondeau P, Andrade FJ. Paper-based Potentiometric Biosensor for Monitoring Galactose in Whole Blood. *Electroanalysis*. 2021; <https://doi.org/10.1002/elan.202060285>
5. Lee P-C, Li N-S, Hsu Y-P, Peng C, Yang H-W. Direct glucose detection in whole blood by colorimetric assay based on glucose oxidase-conjugated graphene oxide/MnO<sub>2</sub> nanozymes. *Analyst*. 2019; <https://doi.org/10.1039/C8AN02440E>
6. Rajendran R, Rayman G. Point-of-care blood glucose testing for diabetes care in hospitalized patients: an evidence-based review. *J Diabetes Sci Technol*. 2014; <https://doi.org/10.1177/1932296814538940>
7. Choi S, Choi SJ, Jeon BR, Lee Y-W, Oh J, Lee YK. What We Should Consider in Point of Care Blood Glucose Test; Current Quality Management Status of a Single Institution. *Medicina (Kaunas)*. 2021; <https://doi.org/10.3390/medicina57030238>
8. Chen C, Mehl BT, Munshi AS, Townsend AD, Spence DM, Martin RS. 3D-printed Microfluidic Devices: Fabrication, Advantages and Limitations-a Mini Review. *Anal Methods*. 2016; <https://doi.org/10.1039/C6AY01671E>
9. Voller A, Bidwell DE, Bartlett A, Fleck DG, Perkins M, Oladehin B. A microplate enzyme-immunoassay for toxoplasma antibody. *J Clin Pathol*. 1976; <https://doi.org/10.1136/jcp.29.2.150>
10. Liu Y, Yu J. Oriented immobilization of proteins on solid supports for use in biosensors and biochips: a review. *Microchimica Acta*. 2016; <https://doi.org/10.1007/s00604-015-1623-4>
11. Arain S, John GT, Krause C, Gerlach J, Wolfbeis OS, Klimant I. Characterization of microtiterplates with integrated optical sensors for oxygen and pH, and their applications to enzyme activity screening, respirometry, and toxicological assays. *Sensors and Actuators B: Chemical*. 2006; <https://doi.org/10.1016/j.snb.2005.07.056>
12. Barone PW, Parker RS, Strano MS. In vivo fluorescence detection of glucose using a single-walled carbon nanotube optical sensor: design, fluorophore properties, advantages, and disadvantages. *Anal Chem*. 2005; <https://doi.org/10.1021/ac0511997>
13. Steinegger A, Wolfbeis OS, Borisov SM. Optical Sensing and Imaging of pH Values: Spectroscopies, Materials, and Applications. *Chem Rev*. 2020; <https://doi.org/10.1021/acs.chemrev.0c00451>
14. Vogelsang J, Kasper R, Steinhauer C, Person B, Heilemann M, Sauer M, Tinnefeld P. A reducing and oxidizing system minimizes photobleaching and blinking of fluorescent dyes. *Angew. Chem. Int. Ed*. 2008; <https://doi.org/10.1002/anie.200801518>
15. Toseland CP. Fluorescent labeling and modification of proteins. *J Chem Biol*. 2013; <https://doi.org/10.1007/s12154-013-0094-5>
16. Wu M, Lin Z, Dürkop A, Wolfbeis OS. Time-resolved enzymatic determination of glucose using a fluorescent europium probe for hydrogen peroxide. *Anal Bioanal Chem*. 2004; <https://doi.org/10.1007/s00216-004-2785-9>
17. Eliseeva SV, Bünzli J-CG. Lanthanide luminescence for functional materials and bio-sciences. *Chem Soc Rev*. 2010; <https://doi.org/10.1039/b905604c>
18. Moore EG, Samuel APS, Raymond KN. From antenna to assay: lessons learned in lanthanide luminescence. *Acc Chem Res*. 2009; <https://doi.org/10.1021/ar800211j>

19. Bünzli J-CG, Piguet C. Taking advantage of luminescent lanthanide ions. *Chem Soc Rev.* 2005; <https://doi.org/10.1039/b406082m>
20. Wolfbeis OS, Dürkop A, Wu M, Lin Z. A Europium-Ion-Based Luminescent Sensing Probe for Hydrogen Peroxide. *Angew. Chem. Int. Ed.* 2002; [https://doi.org/10.1002/1521-3773\(20021202\)41:23<4495:AID-ANIE4495>3.0.CO;2-I](https://doi.org/10.1002/1521-3773(20021202)41:23<4495:AID-ANIE4495>3.0.CO;2-I)
21. Dürkop A, Wolfbeis OS. Nonenzymatic direct assay of hydrogen peroxide at neutral pH using the Eu<sub>3</sub>Tc fluorescent probe. *J Fluoresc.* 2005; <https://doi.org/10.1007/s10895-005-2984-6>
22. Wolfbeis OS, Schäferling M, Dürkop A. Reversible Optical Sensor Membrane for Hydrogen Peroxide Using an Immobilized Fluorescent Probe, and its Application to a Glucose Biosensor. *Microchimica Acta.* 2003; <https://doi.org/10.1007/s00604-003-0090-5>
23. Waleed Al-Qaysi W, Duerkop A. A luminescent europium complex for wide-range pH sensors and sensor microtiterplates. *Analyst.* 2018; <https://doi.org/10.1039/c8an00775f>
24. Peng H, Stich MIJ, Yu J, Sun L-N, Fischer LH, Wolfbeis OS. Luminescent Europium(III) nanoparticles for sensing and imaging of temperature in the physiological range. *Advanced Materials.* 2010; <https://doi.org/10.1002/adma.200901614>
25. Gaspar RDL, Fortes PR, Mazali IO, Sigoli FA, Raimundo IM. Optical Temperature Sensors Based On Europium(III) Beta-Diketonate Complexes Chemically Bonded To Functionalized Polydimethylsiloxane. *ChemistrySelect.* 2018; <https://doi.org/10.1002/slct.201801373>
26. Courrol L, Samad R. Applications of Europium Tetracycline Complex: A Review. *CPA.* 2008; <https://doi.org/10.2174/157341208786306216>
27. Müller BJ, Rappitsch T, Staudinger C, Rüschtz C, Borisov SM, Klimant I. Sodium-Selective Fluoroionophore-Based Optodes for Seawater Salinity Measurement. *Anal Chem.* 2017; <https://doi.org/10.1021/acs.analchem.7b01373>
28. Kassal P, Sigurnjak M, Steinberg IM. Paper-based ion-selective optodes for continuous sensing: Reversible potassium ion monitoring. *Talanta.* 2019; <https://doi.org/10.1016/j.talanta.2018.09.031>
29. Jiang Z, Yu X, Hao Y. Design and Fabrication of a Ratiometric Planar Optode for Simultaneous Imaging of pH and Oxygen. *Sensors (Basel).* 2017; <https://doi.org/10.3390/s17061316>
30. T. Tsuchida KY. Multi-Enzyme Membrane Electrodes for Determination of Creatinine and Creatine in Serum. *Clin. Chem.* 1983;29:51–55.
31. Maierhofer M, Rieger V, Mayr T. Optical ammonia sensors based on fluorescent aza-BODIPY dyes- a flexible toolbox. *Anal Bioanal Chem.* 2020; <https://doi.org/10.1007/s00216-020-02891-3>
32. Staudinger C, Strobl M, Breininger J, Klimant I, Borisov SM. Fast and stable optical pH sensor materials for oceanographic applications. *Sensors and Actuators B: Chemical.* 2019; <https://doi.org/10.1016/j.snb.2018.11.048>
33. Dalfen I, Dmitriev RI, Holst G, Klimant I, Borisov SM. Background-Free Fluorescence-Decay-Time Sensing and Imaging of pH with Highly Photostable Diazaotriangulenium Dyes. *Anal Chem.* 2019; <https://doi.org/10.1021/acs.analchem.8b02534>
34. Tjell AØ, Almdal K. Diffusion rate of hydrogen peroxide through water-swelled polyurethane membranes. *Sensing and Bio-Sensing Research.* 2018; <https://doi.org/10.1016/j.sbsr.2018.10.001>
35. Kellum JA. Determinants of blood pH in health and disease. *Crit Care.* 2000; <https://doi.org/10.1186/cc644>
36. Peterson ME, Daniel RM, Danson MJ, Eisenthal R. The dependence of enzyme activity on temperature: determination and validation of parameters. *Biochem J.* 2007; <https://doi.org/10.1042/BJ20061143>

## 4.7 Supporting Information

### 4.7.1 Influence of Different Cutting Techniques

From an exemplary PVAc/CA-EuTc foil, sensor discs were cut with a laser-engraving machine with two different optics, and hole-punched with a toggle press (**SI Figure 4.1 A**). The influence of the cutting technique on the discs' performance is illustrated by emission scans of the discs with and without HP. The obtained emission values from both scans are normalized to allow a direct comparison of the sensitivity (**SI Figure 4.1 B**).

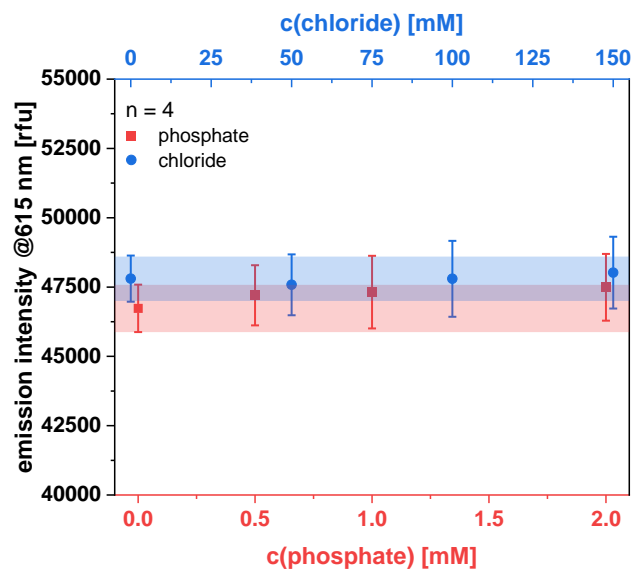


**SI Figure 4.1** The sensor foil is obtained by knife-coating a sensor cocktail (10 wt% PVAc/CA with 0.1 wt% EuTc, spacer distance 60  $\mu\text{m}$ ) **A** The sensor discs in the 1<sup>st</sup> row are obtained by laser-cutting (100% laser power, 70% speed, 1000 ppi with the 2" lens with a focus spot of 0.13 mm in diameter). The discs in the 2<sup>nd</sup> row are obtained by laser-cutting (same settings, but HPDFO lens which enables a focus size of 0.03 mm). The discs in the 3<sup>rd</sup> row were obtained by hole-punching with a toggle press. Diameter of all discs is 6 mm. **B** The discs are incubated with buffer for 10 minutes and scanned. The discs are incubated for 10 minutes with 1 mM HP solution and scanned. The blank values are subtracted from the signal intensities with HP sample. The resulting heat map is shown. (BioTek plate reader,  $\lambda_{\text{exc}}=405/8$  nm,  $\lambda_{\text{em}}=616/8$  nm, 49x49 scans/well,  $n = 1$ , gain 80, 25°C, 10 min incubation time)



#### 4.7.2 Interference Study

PVAc/CA-EuTc discs were tested in a small interference assay. The discs were incubated with buffer samples without interfering ions and with physiological relevant low, medium, and high phosphate or chloride concentrations. The resulting data are shown in **SI Figure 4.2**. The range of the probe discs' blank emission intensity is highlighted with a transparent box in blue for chloride and in red for phosphate determination.



**SI Figure 4.2** Dose-response plot of PVAc/CA-EuTc discs (10 wt% PVAc/CA and 0.1 wt% EuTc in DMF/water) after 5 min of incubation time. The discs were incubated with buffer containing no, low, medium, and high physiological relevant concentration of chloride and phosphate ions. Blank value with standard deviation is marked as transparent box (FluoStar  $\Omega$ ,  $\lambda_{exc}=405/10$  nm,  $\lambda_{em}=615/10$  nm,  $n = 4$ , gain 1200, 25°C)

## 5 Combination of Europium(III) Tetracycline with Oxidase Enzymes in Biocompatible Hydrogels for Detection of Hydrogen Peroxide in Flow-Through Systems

---

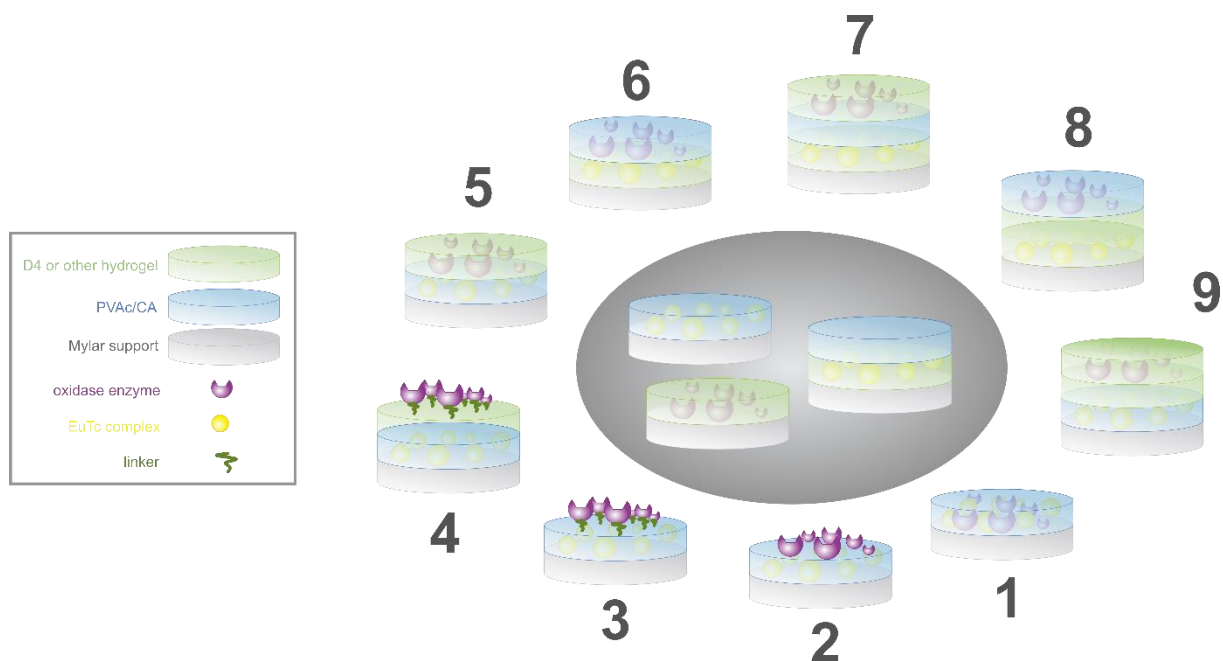
### Abstract

The Europium(III) tetracycline (EuTc) complex was already investigated by different work groups in the past. The emitted lanthanide luminescence with the main peak at 616 nm is quenched in aqueous solutions by surrounding water molecules. These can be replaced reversibly by hydrogen peroxide (HP) leading to an increased luminescence intensity. Hydromed® D4, a polyurethane-based hydrogel was found to provide a suitable environment for the EuTc complex as well as for enzymes like glucose oxidase (GOx). The D4-EuTc layer is covered with a polyvinyl acetate (PVAc) cellulose acetate (CA) layer to avoid leakage of the complex. The different sensor layers are produced with a wet thickness of 30 µm by an in-house made knife-coating device.

Combination of the enzyme and the probe layer enables the optical detection of the respective substrate in an integrated sensor in microplate assays and flow-through systems. Different immobilization techniques were investigated. A polylactic acid-based polymer, LRP t 7016 by Evonik® was found as suitable connection and protection layer in-between a D4-EuTc layer and a D4-GOx layer. The system showed promising results for glucose, glucose/EuTc and HP assays in the microplate format and was therefore tested in the flow-through system where no response towards glucose solutions was observed. It was found that the intermediate layer corrupts the complex over time which was falsely interpreted in the microplate assays as concentration-depending signal increase. Since no other tested approach for the combination of EuTc and GOx worked, the probe and enzyme discs were tested independently from each other in the flow-through system. Both showed a clear response when glucose or HP was injected in the flow cell device. The discs were mounted adjacently within the flow cell chamber, and it was proven that the probe and enzyme layers work together reversibly with an immediate response towards changing concentrations.

The system must still be optimized regarding layer thickness, ratio of EuTc and GOx or other oxidases, as well as instrumental settings to quantify analyte concentrations reliable and reproducible. The use of biocompatible materials addresses a future application as fully implantable optical sensor for continuous monitoring during surgeries since there is a lack of relevant monitoring devices in the clinical field for glucose and lactate.

### Graphical Abstract



**This chapter or at least parts of it are intended for submission but currently kept under seal due to patent claims by Terumo Cardiovascular Systems Corporation, Ann Arbor, MI 48103-9300 USA.**

### Author contributions

Most of the experimental work was solely done by the author. Barbara Grotz, Blaž Kozjan and Iga Malicka collected data under supervision of the author. None of these data sets are presented in this work but were fundamental for deeper understanding and optimization of processes. Some of the foils and solutions were prepared by Barbara Grotz and John Galligan and used by the author. Barbara Grotz, John Galligan, Axel Duerkop and Antje J. Baeumner contributed with strategic discussions. The manuscript was written by the author and revised by BG, JG, AD and AJB. AJB is corresponding author.

## 5.1 Introduction

Hydrogen peroxide (HP) plays a large role within physiological relevant processes as byproduct during catalytic oxidase reactions. Besides oxygen and other blood gases like CO<sub>2</sub> or electrolyte levels, HP is one of the most popular indirect analytes in the scope of patients' monitoring during surgeries, in the intensive care unit (ICU) or for medical home care devices [1, 2]. Countless optical and electrochemical biosensors based on the catalytic enzyme reactions were developed over time [3–9]. Electrochemical sensors are commonly based on the quantification of the produced HP by voltammetry. Reduction of the stoichiometrically produced HP at an enzyme-modified working electrode and the detection of the current at a constant potential versus an Ag/AgCl reference electrode is a widely used and still further optimized technique especially for affordable point-of-care applications [10, 11]. Most prominent example is the glucometer fabricated and distributed by many companies for diabetic home care [12]. Optical sensors are usually based on fluorescent dyes, quantum dots or nanoparticles embedded in polymeric membranes. Their fluorescence is quenched by present oxygen. During the oxidase-based catalysis oxygen is consumed, and fluorescence intensity is increasing [13–15]. Many of these systems suffer from photobleaching and blinking which results in bad reproducibility and decreased long-term stability.

Since 2002, Wolfbeis *et al* and other research groups have reported using the Europium(III) tetracycline (EuTc) complex for selective and sensitive detection of HP or related compounds in cuvettes and flow-through systems [16–22]. The Eu(III) ion is complexed by the sensitizing antibiotic molecule which enables an excitation at 405 nm. Absorbed energy of the ligand is transferred to the central ion. Quenching water molecules can be replaced reversibly from the inner coordination sphere around the Eu<sup>3+</sup> central ion by HP [16, 17]. This process takes place at physiological relevant pH range. The ligand exchange leads to an increase of luminescence intensity of the <sup>5</sup>D<sub>0</sub>→<sup>7</sup>F<sub>2</sub> transition of the Eu<sup>3+</sup> ion, detectable around 616 nm [23].

The integration of the sensitive luminescent probe EuTc with the respective enzymes like glucose oxidase (GOx) or lactate oxidase (LOx) in a biocompatible membrane addresses an important field of medical applications. Since there is up to now no clinical relevant method for optical monitoring a patients' glucose or lactate levels during complicated heart surgeries or in the ICU, the development of a continuously working optode can save lives [5, 14, 24–27]. Blood samples are drawn from the line of the patient's heart-lung machine and analyzed with commercial POC kits by the clinical staff or send to a laboratory. This is unwieldy and time-consuming, and not carried out in regular intervals. Critical changes in the patients' metabolism are perhaps not detected fast enough. Findings confirm that lactate monitoring is a valuable parameter in the early resuscitation of critically ill patients with organ failure and sepsis, and

lactate-assisted therapy significantly reduced hospital mortality in patients with hyperlactatemia by 20 % [3, 28].

Intravascular blood gas monitoring started in the early 1950's with Clark *et al* and the development of an implantable oxygen sensitive electrode [29]. Up to now, clinical relevant systems for blood gas monitoring were developed by different companies [2, 30–33]. Currently available modern blood gas monitors are usually able to quantify  $P_{O_2}$ ,  $P_{CO_2}$ , pH, oximetry parameters, temperature, metabolites and different electrolytes based on optical and electrochemical detection [3]. The large advantage of such a monitor is the nearly real-time and continuous control of important parameters over a long period. It allows near-patient analysis and therefore a fast decision making for the treating physicians and clinical staff. Since patients are anyway connected to the heart-lung machine for heart transplantation or critically ill persons have implanted sensors for monitoring, the development of a non-invasive sensor system is redundant in this case. It makes sense to optimize already established systems and upgrade them for further analytes. Glucose and lactate are primarily determined by electrochemical detection methods. Therefore, the development of an optical detection system would enlarge the range of possible applications. The complex and expensive process from an initial concept to a clinical approved sensor is certainly one of the largest barriers but is worthwhile going if lives can be saved.

Biocompatible and non-fouling sensor membranes or protection layers produced from hydrogels and polymers are essential for the development of an implantable sensor. A mixture of polyvinyl acetate (PVAc) and cellulose acetate (CA) was already used in 1983 by Tsuchida *et al* for a multi-enzyme membrane electrode used in human serum for detection of creatinine and creatine [34]. Hydromed® D4, a polyurethane-based hydrogel with a water content of around 50 % is a modern commonly used material for fabrication of sensor membranes via entrapment of fluorescent dyes, enzymes or other recognition elements [19, 35–37] and enables a fast hydrogen peroxide diffusion [38]. Multi- and single layer sensor membranes made from these polymers containing EuTc and enzyme are a valuable solution to tackle the challenge.

Former work of our group showed fundamental functionality of the sensor system in microplate assays. The functionality of the probe and enzyme membranes is shown independently from each other in a flow-through system and additionally in combination. Future perspective of this work is to enable the system for optical intravascular glucose and lactate detection in patients during heart surgeries.

## **5.2 Experimental**

### **5.2.1 Materials and Equipment**

For all experiments bi-distilled water (just referred as water) is used.

*Following chemicals are used without further purification:*

Hydromed® D4, D7 and D640 was purchased from AdvanSource Biomaterials ([www.advbiomaterials.com](http://www.advbiomaterials.com)). Evonik® Resomer LRP t 7016 was purchased from Evonik Industries AG (<https://healthcare.evonik.com>). Europium trichloride hexahydrate  $\text{EuCl}_3 \cdot 6 \text{H}_2\text{O}$  (99.9 %), tetracycline HCl (Tc,  $\geq 95\%$ ), polyvinyl acetate (PVAc, average  $M_w \approx 100,000$ ), cellulose acetate (CA, average  $M_n \approx 30,000$ ), cyclohexanone (CHon, p.a.;  $\geq 99.5\%$ ), glucose oxidase (GOx) from *Aspergillus Niger* (type VII, lyophilized powder,  $\geq 100,000$  units/g solid), horseradish peroxidase (HRP, type II, lyophilized powder, 150-250 units/mg solid), sodium hydroxide NaOH (p.a.;  $\geq 98\%$ ), hydrogen peroxide solution (HP, 35 %) ethanol (EtOH, p.a.;  $\geq 99.8\%$ ), iso-propyl alcohol (IPA, ACS reagent,  $\geq 99.5\%$ ), *tert*-butanol ( $\geq 99\%$ ) and 3,3',5,5'-tetramethylbenzidine (TMB,  $\geq 99\%$ ) were purchased from Sigma-Aldrich (<https://www.sigmaaldrich.com>). 4-(2-hydroxyethyl)-1-piperazineethanesulfonic acid (HEPES, for biochemistry) was purchased from VWR (<https://www.vwr.com>). D(+)-glucose monohydrate (for microbiology), dimethyl sulfoxide (DMSO, p.a.;  $\geq 99.9\%$ ), 0.5 M sulfuric acid (Titrisol®), 65 % nitric acid (for analysis) and sodium azide  $\text{NaN}_3$ , (extra pure), were purchased from Merck (<https://www.merckmillipore.com>).

*Following other materials are used:*

Mylar® (bi-axial oriented poly-terephthalate foils with 125  $\mu\text{m}$  thickness) was purchased from GoodFellow GmbH (<http://www.goodfellow.com>). Adhesive tape (tesa® Verlegeband) was purchased from tesa SE (<https://www.tesa.com>). Aluminum foil purchased from local stores was used for light protection.

*Following further equipment and accessories are used:*

Toggle press HK 800 for hole-punching with different-sized circular cutting tools from Berg & Schmid (<https://www.bergundschmid.de>) was used.

FLUOstar Omega and preceding model FLUOstar from BMG LABTECH GmbH (<https://www.bmg-labtech.com>) and Synergy Neo2 Hybrid Multi-Mode Reader from BioTek Instruments ([www.biotek.de](http://www.biotek.de)) with 96-well microtiter plates, white, medium binding, flat bottom (product# 655075) and 96-well microtiter plates, transparent, flat bottom (product# 655101) purchased from greiner BIO-ONE (<https://www.gbo.com>).

An in-house made flow cell system with suitable tubing is used to fix the sensor disc within the experimental setup. AMINCO Bowman Series 2 spectrofluorometer (AB2) with fiber optics

from Thermo Spectronics (now: Thermo Fisher Scientific, <https://www.thermofisher.com>) and MINIPULS 3 peristaltic pump from Gilson Incorporated (<https://www.gilson.com>) are used for pumping and detection.

The Europium content is verified by using a flame-EOP (end on plasma) inductively coupled plasma optical emission spectrometer (ICP-OES) from Spectro (<https://www.spectro.com>).

## **5.2.2 Preparation of Solutions**

In general, all weights and volumes can be adapted proportionally if higher or lower number of samples, foils or discs must be prepared.

### **5.2.2.1 0.1 M HEPES pH 7.4**

119.16 g  $\pm$  1.12 g HEPES are dissolved in approx. 4.75 L water in a 5 L volumetric flask while stirring with a magnetic stirring bar. NaOH pellets are added under strong stirring to reach a pH value of  $7.40 \pm 0.05$ . Volume is filled up to 5 L with water. After mixing, pH value is checked and noted. If necessary,  $0.50 \pm 0.05$  g  $\text{NaN}_3$  are added and dissolved by shaking. The solution can be stored up to 12 months at ambient conditions in a glass bottle. If the buffer is prepared without sodium azide, it should be stored not longer than 4 weeks at ambient conditions.

### **5.2.2.2 Hydrogen Peroxide Solutions**

#### *For EuTc Assays*

To obtain a 100 mM HP stock solution, 5190  $\mu\text{L}$  buffer is mixed with 45  $\mu\text{L}$  of 35 % HP solution in a 10 mL glass vial by shaking. The respective dilutions with HP concentrations of 0, 0.1, 0.5, 1, 5 and 10 mM for the standard assay are prepared by diluting the stock solution or the respective other solution with buffer. The samples must be used within 24 h.

#### *For TMB/HRP Assays*

The 1 mM HP solution is diluted to 1:10 by volume with buffer to obtain a 100  $\mu\text{M}$  HP solution. The 100  $\mu\text{M}$  is further diluted with buffer to obtain HP samples with concentrations ranging between 5  $\mu\text{M}$  and 100  $\mu\text{M}$ . 0  $\mu\text{M}$  HP refers to pure buffer.

### **5.2.2.3 Solutions for TMB/HRP Assay**

9.62 mg TMB are dissolved in 2.0 mL DMSO to obtain a 20 mM TMB solution. 2.28 mg of HRP is dissolved in 2.0 mL buffer to obtain a HRP solution with an activity of 0.25 U/ $\mu\text{L}$ . TMB and HRP solution are mixed 2:1 by volume. The solution is cooled down for 30 min and must be used immediately.

### **5.2.2.4 Glucose Solutions**

To obtain a 100 mM glucose stock solution,  $1981.7 \pm 2.0$  mg glucose monohydrate is weighed in a 100 mL volumetric flask and dissolved in approx. 75 mL buffer. Then the volume is filled

up to 100 mL and the solution is mixed by shaking. The stock solution is diluted with buffer to suitable concentrations ranging between 0.5 mM and 20 mM (for lactate) or 50 mM (for glucose).

#### **5.2.2.5 *Eu<sup>3+</sup> Stock Solution***

1832.1 ± 0.9 mg of EuCl<sub>3</sub>·6 H<sub>2</sub>O is dissolved in approx. 5 mL of water using a 10.0 mL volumetric flask. Volume is filled up to 10 mL volume with water. The solution is split into aliquots of 400 µL. These can be stored for at least 6 months under light protection at 4°C and are used for preparation of fresh EuTc solutions.

#### **5.2.2.6 *Tetracycline Stock Solution***

31.84 ± 0.06 mg of tetracycline HCl is dissolved in 4.0 mL of water in a glass flask. The solution must be used immediately and must be stored light protected.

#### **5.2.2.7 *EuTc Solution for Functionality Test***

500 µL of the tetracycline stock solution (**chapter 5.2.2.6**) is mixed with 50 µL of the Eu<sup>3+</sup> stock solution (**chapter 5.2.2.5**) in 4.45 mL water in an amber 50 mL plastic tube. 45.0 mL of buffer is added, and the solution is mixed by shaking shortly. The solution must be used within 6 h and must be stored light protected.

#### **5.2.2.8 *Glucose/EuTc Solutions***

Sample solutions containing glucose and EuTc are prepared by mixing 6 mL of the EuTc solution for functionality test (**chapter 5.2.2.7**) and 6 mL of the respective glucose samples (**chapter 5.2.2.4**). Additionally, a 0 mM glucose/EuTc sample is prepared. Final concentrations range between 0 mM and or 50 mM.

#### **5.2.2.9 *Polymer Cocktails***

The polymer cocktails can be heated up to 50°C accelerating the dissolution of the polymer or hydrogel in the solvent mixtures.

##### *10 wt% D4 in alcohol/H<sub>2</sub>O*

90.0 ± 0.9 mL alcohol (ethanol, iso-propanol and *tert*-butanol were tested) is mixed with 10.0 ± 0.1 mL. 10.0 ± 0.1 g Hydromed D4 is dissolved in 90.0 ± 0.9 g of alcohol/water in a 100 mL glass flask under strong stirring with a magnetic stirring bar.

##### *10 wt% PVAc/CA in CHon/H<sub>2</sub>O or DMF/H<sub>2</sub>O*

99.0 ± 0.1 mL CHon is mixed with 1.00 ± 0.01 mL water. 90.0 ± 0.1 mL DMF is mixed with 10.0 ± 0.1 mL water. 7.92 ± 0.08 g CA and 0.080 ± 0.008 g PVAc are dissolved in 72.0 ± 0.7 g solvent/H<sub>2</sub>O in a 100 mL glass flask under strong stirring with a magnetic stirring bar.



### *2.5 wt% LRP t 7016 in THF/H<sub>2</sub>O*

99.0 ± 0.1 mL THF are mixed with 1.00 ± 0.01 mL water. 1.25 ± 0.05 g Evonik® Resomer LRP t 7 16 is dissolved in 48.75 ± 0.5 g of the prepared THF/H<sub>2</sub>O mixture in a 100 mL glass flask under strong stirring with a magnetic stirring bar.

### **5.2.2.10 EuTc Stock Solution for Sensor Cocktails**

6.97 ± 0.06 mg tetracycline HCl are weighed in a 500 µL plastic reaction tube and dissolved under strong shaking in 75 µL of the Eu<sup>3+</sup> stock solution (**chapter 5.2.2.5**). The solution is used immediately.

### **5.2.2.11 Sensor Cocktails**

#### *EuTc in 10 wt% D4 in alcohol/H<sub>2</sub>O*

A 5 mL glass vial with plastic snap cap is used. 1.499 ± 0.015 g of the 10 wt% D4 in alcohol/H<sub>2</sub>O are weighed in. To obtain a 0.1 wt% EuTc cocktail, 10 µL of the EuTc stock solution are added. To obtain a 0.2 wt% EuTc cocktail, 20 µL of the EuTc stock solution are added. To obtain a 0.5 wt% EuTc cocktail, 50 µL of the EuTc stock solution are added and so on. The vial is sealed tightly with Parafilm. The cocktail is stirred 10 ± 1 minutes at ambient conditions and used immediately for preparation of up to 8 foils.

#### *EuTc in 10 wt% PVAc/CA in DMF/H<sub>2</sub>O*

A 5 mL glass vial with plastic snap cap is used. 1.499 ± 0.015 g of the 10 wt% PVAc/CA in DMF/H<sub>2</sub>O are weighed in. To obtain a 0.1 wt% EuTc cocktail, 10 µL of the EuTc stock solution are added. The vial is sealed tightly with Parafilm. The cocktail is stirred 70 ± 10 minutes at ambient conditions and used immediately for preparation of up to 6 foils.

### **5.2.2.12 Enzyme Cocktails**

To obtain an enzyme stock solution for 0.25 wt% enzyme cocktails, 6.0 ± 0.1 mg of the enzyme is dissolved within 80 µL buffer. To obtain an enzyme stock solution for 0.5 wt% enzyme cocktails, 9.0 ± 0.1 mg of the enzyme is dissolved within 60 µL buffer. A thermal cycler set at 35 ± 1 °C and 500 rpm is used for 12.5 ± 2.5 min.

A 5 mL glass vial with plastic snap cap is used. 1.499 ± 0.015 g of the 10 wt% D4 cocktail in EtOH/H<sub>2</sub>O are weighed in. 50 µL of the enzyme stock solution for 0.25 wt% enzyme cocktails are added to obtain a 0.25 wt% enzyme cocktail. 50 µL of the enzyme stock solution for 0.5 wt% enzyme cocktails are added to obtain a 0.5 wt% enzyme cocktail. The vial is sealed tightly with Parafilm. The cocktail is stirred 1.5 to 2 hours at 37°C until a homogeneous suspension is obtained. It is recommended to use the cocktail within 1 h. The volume is suitable for the preparation of up to 6 to 8 foils.

### **5.2.3 Methods**

#### **5.2.3.1 Knife-Coating**

An in-house made knife-coater device is used for production of all sensor and enzyme foils.

##### *Application of First Layer*

The 30  $\mu\text{m}$  or 60  $\mu\text{m}$  spacers and pieces of Mylar support are placed in the knife-coater at both sides to define the wet layer thickness. If not mentioned otherwise, usually 30  $\mu\text{m}$  spacers were used. A planar, rectangular Mylar substrate (approx. 5.5 cm x 11.0 cm) is placed on the knife-coating device and fixed by turning on the vacuum pump. The sheet is cleaned by using a wipe soaked with ethanol and rubbing. After the rubbing alcohol is completely evaporated, 200  $\mu\text{L}$  to 300  $\mu\text{L}$  of the respective sensor, enzyme or polymer cocktail is pipetted as a homogeneous line on the starting point of the Mylar substrate. The knife is pulled slowly to the end of the substrate to obtain an even film. After around 30 seconds, the vacuum pump is turned off and the foils are moved to the oven on an even plate for drying. The foils are dried for  $2.5 \pm 0.5$  h at  $39 \pm 1$  °C. A second layer can be applied immediately after the drying time.

If no second layer is applied, the sheets are washed for  $15 \pm 1$  minutes in an excess of buffer on an orbital shaker (300 to 350 rpm) to remove unbound complex or enzyme and organic solvent residues, and to rehydrate the hydrogel after drying. The sheets can then be stacked carefully and stored light-protected in a closed zipper bag at 4°C until sensor disc preparation.

##### *Application of Further Layers*

The 30  $\mu\text{m}$  or 60  $\mu\text{m}$  spacers and pieces of Mylar support are placed in the knife-coater at both sides to define the wet layer thickness for the second or third layer. If not mentioned otherwise, usually 30  $\mu\text{m}$  spacers were used. The Mylar substrate with the dried layer(s) on top is placed on the knife-coater and fixed by turning on the vacuum pump. 250  $\mu\text{L}$  to 300  $\mu\text{L}$  of the respective second layer cocktail is pipetted as a homogeneous line on the starting point of the Mylar substrate. The knife is pulled slowly to the end of the substrate to obtain an even film that covers the first layer(s). After around 30 seconds, the vacuum pump is turned off and the foils are moved to the oven on an even plate. The foils are dried for  $2.5 \pm 0.5$  h at  $39 \pm 1$  °C. A further layer can be applied immediately after the drying time.

If no further layer is applied, the sheets are washed for  $15 \pm 1$  minutes in an excess of buffer on an orbital shaker (300 to 350 rpm) to remove unbound complex or enzyme and organic solvent residues, and to rehydrate the hydrogel after drying. The sheets can then be stacked carefully and stored light-protected in a closed zipper bag at 4°C until sensor disc preparation.

### 5.2.3.2 Sensor Disc Preparation

On the backside of the Mylar support (= the uncoated side), double-adhesive tape is applied when the discs are used for a microplate assay. With a toggle press, discs with a diameter of 6 mm are punched out of the foil. It must be avoided to take discs from nearby the edges, a distance to the edges of at least 2 mm is recommended. Furthermore, it has to be taken care that both layers overlap completely. After removing the protective cover of the adhesive tape, the sensor discs are fixed on the bottom of the MTP wells. Usually,  $n = 4$  or  $n = 8$  discs are used for an assay. The prepared MTPs are covered with a plastic lid and can be stored overnight light protected at 4°C until a functionality test is performed, or they can be used immediately.

For flow cell assays, no tape is applied to the discs. With a toggle press, discs with an outer diameter of 24 mm are punched out of the foil and used immediately. An inner circle can be removed from the disc and overlapped with another disc to combine enzyme and probe disc. Using a dummy disc (blank Mylar) or D4 disc as outmost disc reduces the active area of the probe or enzyme disc within the used setup like schematically shown in **Figure 5.1 D5**, **Figure 5.1 D6**, and **Figure 5.1 D7**.

### 5.2.3.3 Assays in Microplate

Within this chapter, all performed assay types within the microplate are described. If not stated otherwise in the captions or Results and Discussion part, all experiments were performed like described in following with the same settings.

#### 5.2.3.3.1 Heterogeneous Assays with Discs

Following settings (**Table 5.1**) of the plate reader FLUOstar Omega from BMG LABTECH GmbH are used for the within this chapter named assay types (if not stated otherwise):

**Table 5.1** Parameters and the respective settings of the used FLUOstar Omega plate reader for each assay type. Glucose/EuTc and glucose assay are equally used for the respective lactate/EuTc and lactate assay.

parameter	washing step	HP assay	glucose/EuTc assay	glucose assays
<i>protocol name</i>	EuTc_wash_15min	EuTc_6min_kinetic	EuTc_10min_kinetic	EuTc_10min_kinetic
<i>no. of multichromatics</i>	1			
<i>excitation filter</i>	405/10 nm			
<i>emission filter</i>	615/10 nm			
<i>gain</i>	1200			
<i>well scan</i>	none			
<i>optic</i>	top optic			
<i>settling time</i>	0.2 s			

parameter	washing step	HP assay	glucose/EuTc assay	glucose assays
<i>no. of kinetic windows</i>	1			
<i>no. of cycles</i>	2	7	11	11
<i>measurement start time</i>	0.0 s			
<i>no. of flashes</i>	20			
<i>cycle time</i>	900 s	60 s		
<i>pause before cycle</i>	no			
<i>shaking 1</i>	shake between reading; double orbital @300 rpm			
<i>shaking 2</i>	shake before first cycle, double orbital @300 rpm for 5 s			

Temperature is set to  $25.0 \pm 0.5$  °C,  $30.0 \pm 0.5$  °C or  $37.0 \pm 0.5$  °C and the measurements can be started when the desired temperature is reached. For measurements at 25°C, the samples are not prewarmed. For 30°C and 37°C measurements, the samples are prewarmed in a tempered water bath at the desired temperature. The washing procedure is performed for all discs in the very beginning.

#### *Washing Procedure for All Disc Types*

100 µL buffer is added with an 8-channel pipette to each sensor disc and is washed for 15 minutes in the plate reader. Therefore, a kinetic measurement is started for 15 minutes. During the washing procedure, the samples are shaken orbitally by the plate reader at 300 rpm. The samples are excited at 405/10 nm and the emission intensity is measured at 615/10 nm at the beginning and in the end at  $25.0 \pm 0.5$  °C or  $37.0 \pm 0.5$  °C (protocol for “washing step” shown in **Table 5.1**). Washing solution is removed completely by flipping the MTP over the sink and pounded the MTP on a tissue for three times.

#### *Functionality Tests*

100 µL of 0 mM sample (HP, substrate or substrate/EuTc) is added with the multichannel pipette to each sensor discs. The kinetic measurement is started according to the protocol for the different assay types shown in **Table 5.1**. When the kinetic measurement is finished, the MTP is flipped over to remove the sample solutions. The MTP is pounded on a tissue to completely remove all remaining solution. The described procedure is repeated with the same discs for the next higher concentrated sample.

#### 5.2.3.3.2 TMB/HRP Assay

If an enzyme disc is tested for its activity, the disc is incubated with 100 µL of the respective substrate concentration (up to 20 mM for lactate and up to 50 mM for glucose) for a certain time (usually 2 to 5 min) to obtain a sample solution containing HP. 97 µL of sample solution containing HP is mixed with 3 µL of a TMB/HRP mixture (20 mM TMB in DMSO and 0.25 U/µL

HRP in HEPES, 2:1, v/v) in another transparent plate. After strong mixing by pipetting up and down, and short incubation (usually 30 s to 5 min) 50  $\mu$ L of 0.5 M sulfuric acid is added and mixed. Absorbance at 450 nm is measured. A linear calibration plot is created by performing the same assay but with HP samples of known concentrations between 0  $\mu$ M and 100  $\mu$ M.

#### 5.2.3.4 Assays in Flow Cell

An in-house made flow cell with suitable tubing is used in combination with the AB2 spectrophotometer with fiber optics and a peristaltic pump. Following settings (**Table 5.2**) of the devices are used (if not stated otherwise):

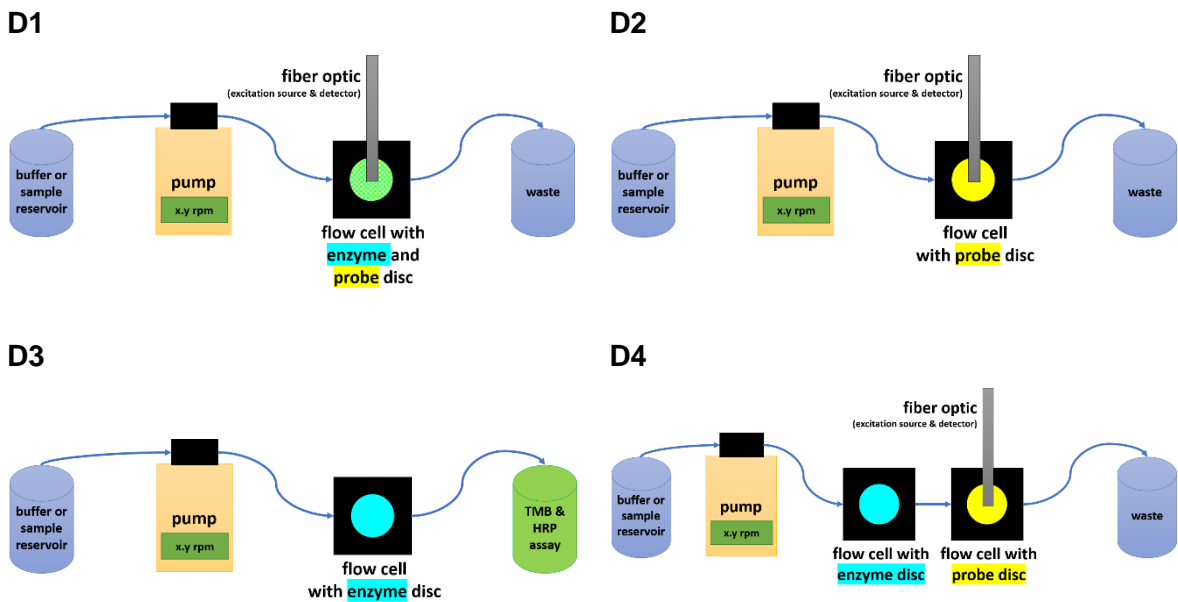
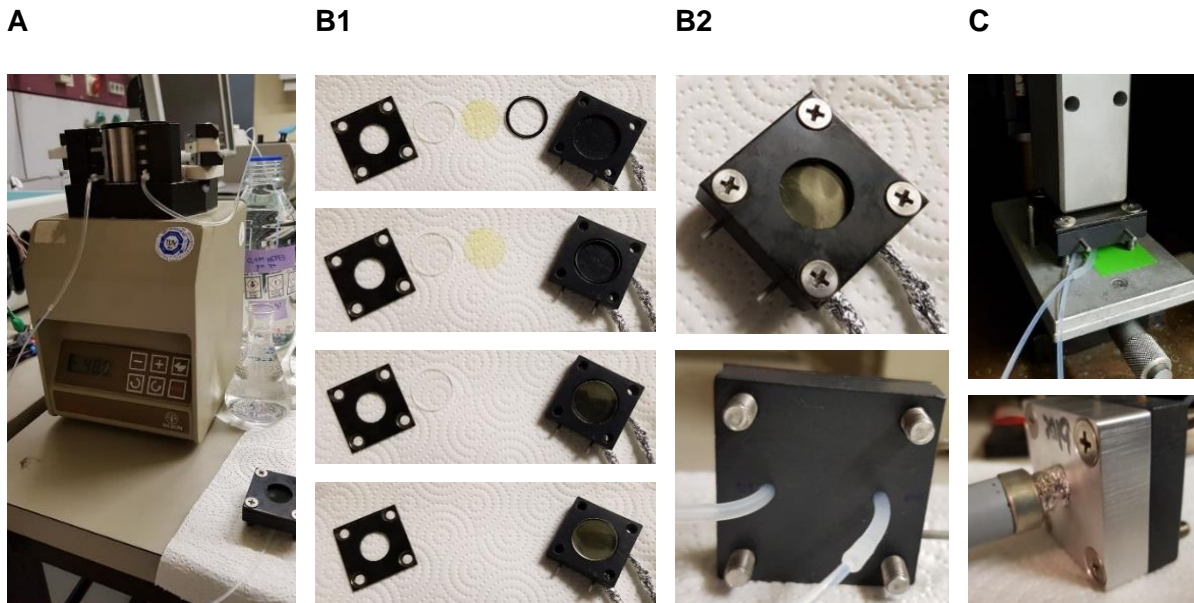
**Table 5.2** Parameters and the respective settings of the used AB2 spectrofluorometer and the pump for each flow cell measurement with EuTc-containing discs.

parameter	setting
<i>pump</i>	8.0 to 48.0 rpm
<i>sensitivity</i> (Detector high voltage)	30% of full scale (650 V – 750 V)
<i>monochromators</i> (excitation)	step size 1 nm wavelength 405 nm bandpass 8 nm
<i>monochromators</i> (emission)	step size 1 nm wavelength 615 nm bandpass 8 nm
<i>lamp source</i>	continuous wave
<i>time trace measurement</i>	start 0 s end xx,xxx s step 1 s

The experimental setup is illustrated in **Figure 5.1**. The main parts of the setup are shown, and the simplified flow chart is schematically drawn. Assembling of the sensor disc within the flow cell chamber is shown systematically in **Figure 5.1 B1** (from top to bottom). Most important is to take care that the coated (active) side of the sensor disc must face downwards to be in contact with the solution.

The inlet tube is put in the buffer reservoir, the outlet tube to the waste or is the solution is collected for further investigations, and the pump is started at suitable speed. Pump settings were converted experimentally in the actual flow speed for the used flow-through system (see **SI Figure 5.1**). The flow cell is checked for leakage for the first 5 minutes. If no leakage occurs, the flow cell is mounted within the measurement chamber and the fiber optic is adjusted to touch the optical window. Parameters for the AB2 are set like in **Table 5.2**. A time trace measurement with suitable data acquisition interval is started for a certain time.

The flow cell system is equilibrated for 30 min to 45 min with buffer before the first sample is injected. Therefore, the pump is stopped, and the inlet tube is put in the sample solution. The pump is started for a certain time to inject sample solution. The pump is stopped again, the outside of the tube is wiped with a tissue and the tube is put back in the buffer reservoir or the next sample. The pump is restarted immediately or after a certain time for incubation within the flow cell.



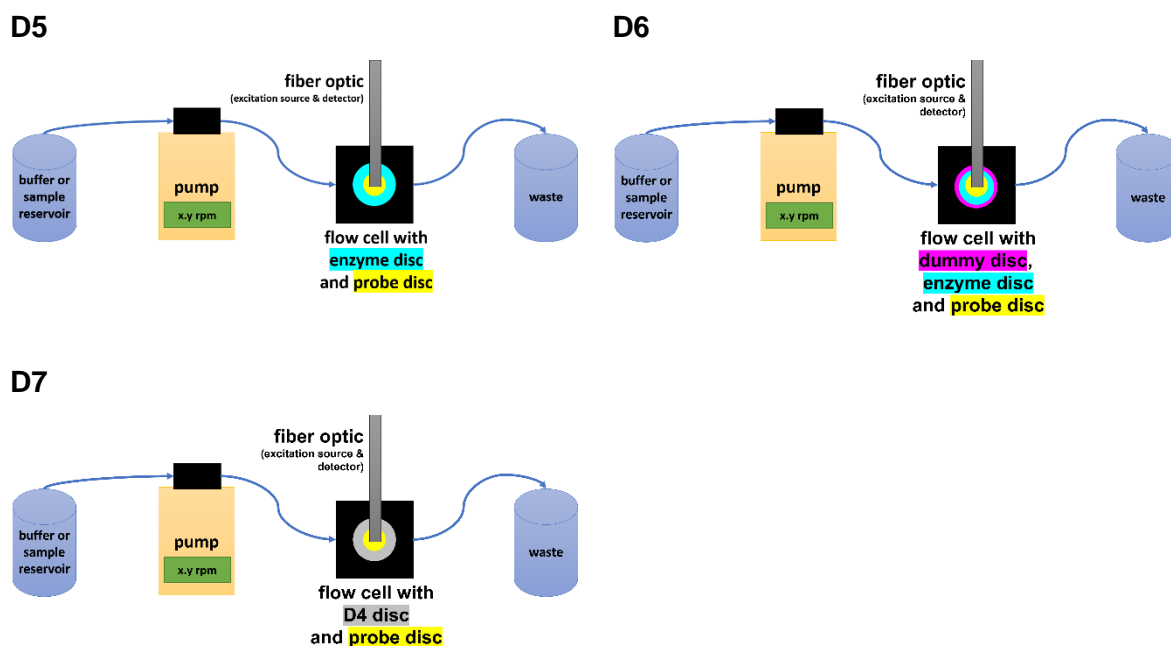


**Figure 5.1** Experimental setup for detection of luminescent sensor discs in a flow cell **A** The peristaltic pump with buffer reservoir and sample solution **B1** In-house made flow cell chamber and how it is assembled **B2** front view (optical window and 24 mm in diameter sensor disc, sealed with a rubber ring) and back view (inlet and outlet for solutions) **C** The fiber optic of the spectrometer can be attached to the flow cell in two different ways: top horizontal arrangement, bottom: vertical arrangement to avoid air bubbles in the system **D** schematic representation of different arrangements of or in the flow-through system for different assays and approaches

### 5.2.3.5 Interference Study

The setup shown in **Figure 5.1 D7** is used for the interference study. A D4-EuTc // PVAc/CA disc and a blank D4 disc is used. Glucose samples are pumped through the system. Luminescence at 616 nm is monitored according to the protocol shown in **Table 5.2**.

### 5.2.3.6 Leakage Study

The setup shown in **Figure 5.1 D2** is used for the leakage study. A D4-EuTc // LRP t 7016 // D4-GOx (10/0.5 wt% // 2.5 wt% // 10/0.2 wt%) sensor disc is used. Buffer and HP samples are pumped through the system. Luminescence at 616 nm is monitored according to the protocol shown in **Table 5.2**. Solutions are collected in aliquots which are vaporized and redissolved in 5.0 mL of 1.5 M nitric acid. Samples are analyzed via ICP-OES to quantify the Eu content.

## 5.2.4 Statistics and Data Evaluation

All calculation, especially the arithmetic mean values and standard deviation (SD) were calculated with Microsoft Excel 2016 (Microsoft Corporation, Redmond, Washington, USA) or by the respective plate reader software MARS Data Analysis Software from BMG LABTECH GmbH (<https://www.bmglabtech.com>) and Gen5 Microplate Reader and Imager Software from BioTek Instruments ([www.biotek.de](http://www.biotek.de)). Measurements in the plate format were performed at

least in triplicate ( $n \geq 3$ ). Suspicious values were removed after failing the outlier Q-test. Calculated SD is represented by error bars in y-direction.

Linear and non-linear regression curves were accomplished with following equation (1) and equation (2).

linear curve fit:  $y = m \cdot x + b$  (1) *m ... slope*  
*b ... y – axis intercept*

sigmoidal curve fit:  $y = \frac{A_1 - A_2}{1 + \left(\frac{x}{x_0}\right)^p} + A_2$  (2) *A<sub>1</sub> ... initial value*  
*A<sub>2</sub> ... final value*  
*x<sub>0</sub> ... center*  
*p ... power*

For HP detection in the flow cell system, following equation (3) was used to calculate the signal change over time in 10 s intervals.

derivation: HP *for t = 0 s, 10 s, 20 s, ...*  
detection in flow cell:  $\Delta i = i(t + 10s) - i(t)$  (3) *i ... signal intensity*  
*t ... time*



### 5.3 Results and Discussion

Different approaches are shown in the following **Figure 5.2**. They were tested, investigated, and optimized or finally discarded to combine the enzyme and the probe in an integrated sensor system to realize a continuous and real-time detection in flow-through systems.

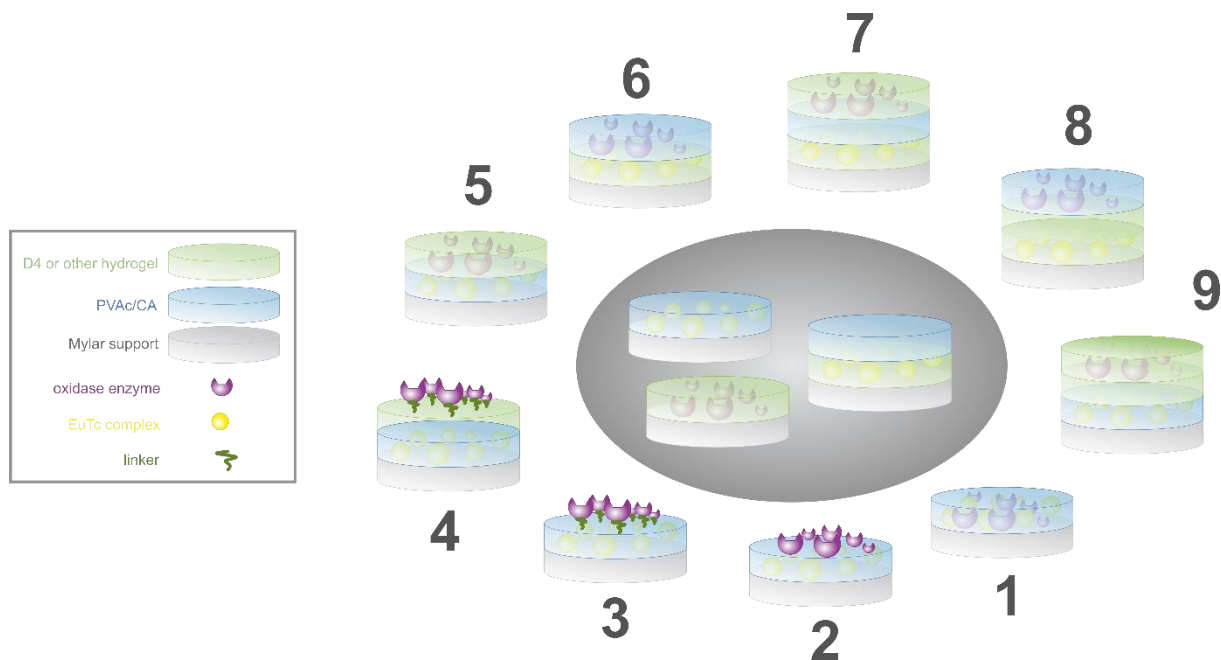


**Figure 5.2** Starting from the already investigated stand-alone systems in the middle to obtain an integrated sensor system for detection in flow-through systems: PVAc/CA-EuTc, D4-EuTc // PVAc/CA and D4-enzyme discs. Different approaches were tested within the scope of this work: **1** simple entrapment of enzyme and probe in the same layer **2** the enzyme is attached by drop-coating or immersion via adsorption forces **3** the enzyme is covalently immobilized or cross-linked on top of the sensing membrane **4** like **3** but with a protective membrane in-between **5** to **9** different combinations of the active membranes with and without protection layers, other biocompatible hydrogels besides D4 and PVAc/CA were tested. Most promising results were obtained with approach **7**: D4-EuTc // LRP t 7016 // D4-GOx

Easiest way would be to entrap both elements within one single layer (approach 1). This was investigated by dissolving or dispersing probe and enzyme in the same cocktail and preparing foils and subsequently sensor discs. Another tested, very mild strategy was soaking a D4-GOx membrane for several hours in an EuTc solution and add a protective PVAc/CA membrane on top because EuTc is washed out quickly from the D4 hydrogel. None of the tested approaches showed promising data at all in the HP assay. Usually, the enzyme shows still a high activity when tested in HRP/TMB assays or with substrate/EuTc assays, but the probe complex was inactive, destroyed or otherwise altered and does not respond to the changing HP concentrations anymore.

Adding the enzyme on top of the probe discs by adsorption, cross-linking by glutaraldehyde (GA) or covalent binding with linker molecules or EDC/NHS (1-ethyl-3-(3-dimethylaminopropyl)-carbodiimide/2 *N*-hydroxysuccinimide) chemistry with or without an additional

protective layer (approaches 2 to 4) would be other elegant and well-known solutions [39, 40]. For these approaches, different methods were tested. First, PVAc/CA-EuTc sensor discs were simply soaked with GOx solution but adsorption forces were not strong enough for a lasting immobilization of the enzyme. Other approaches were tested with diluted GA solution and vapor, with and without bovine serum albumin (BSA) as stabilizer for the enzyme. Within the scope of these approaches the enzyme usually stays active but the probe complex was inhibited or destroyed and does not react to even high hydrogen peroxide concentrations above 1 mM at all.

The approaches 5 to 9 represent different combinations of the up to now used polymers and hydrogels. The layers are coated on top of each other like described previously for the D4-EuTc layer with a PVAc/CA protection layer on top. Comparable organic solvents besides ethanol, DMF and CH<sub>2</sub>OH like IPA, acetone or THF were mixed with water and tested to investigate the compatibility with probe, enzyme, and hydrogels. A small amount of water or buffer in the cocktail is necessary for a successful formation of the complex. It was found that acetone interferes with the probe complex, presumptively by the non-reversible formation of another relatively stable complex with the Eu(III) ion, and must be avoided as solvent for all cocktails. Stirring and drying times were checked and optimized again in this context. The used solvent and the amount of loaded enzyme within the cocktail were also found being crucial parameters. Depending on those, it makes a difference if the about each other coated membranes stick together or if the layers are separated easily. Furthermore, other hydrogels like Hydromed® D7 and D640 were tested due to its different swelling properties, water content and hydrophilicity compared to D4. Besides ethanol, iso-propyl alcohol and *tert*-butanol as bulkier short-chained alcohols were tested. This resulted in changed viscosity of the cocktails compared to the cocktails prepared with EtOH/water. Especially *tert*-butanol-based cocktails must be warmed up at least at 40°C to get an easy to spread mixture for obtaining even and homogeneous foils. Heating of the cocktails can lead to problems regarding the stability of the solved complex or enzyme. Gaining comparable results for probe and enzyme discs independent of the used alcohol for cocktail preparation, the ethanol/water mixture was used for all D4 cocktails. A biocompatible polylactic acid-based hydrogel by Evonik®, the resomer LRP t 7016, was investigated and found as suitable intermediate layer for a stable and leakage-hindering connection between the D4-EuTc and a D4-GOx layer like shown above in **Figure 5.2** approach 7. Other investigated membranes were not able to cohere probe and enzyme layer although different combinations, solvents, and layer sequences were checked. Latest after the initial washing procedure the upper layer peeled off or it was not possible to coat even layers at all.

### 5.3.1 3-Layer System: D4-EuTc // LRP t 7016 // D4-GOx

Due to the promising results in all functionality microplate assay (with HP, glucose, and glucose/EuTc) and the stability of the stacked layers, the approach is tested in the flow-through system (**Figure 5.3 A**). The three-layered sensor disc containing the probe complex as well as the glucose oxidase is mounted in the flow cell setup like shown in the Experimental part in **Figure 5.1 D1**. After an initial equilibration with buffer, glucose samples are injected for several times. A second disc was also tested after the first disc showed no reaction towards any glucose solutions. Furthermore, the setup was checked in-between for the formation of air bubbles. The resulting raw data graph (signal vs. time) is shown in **Figure 5.3 B**.

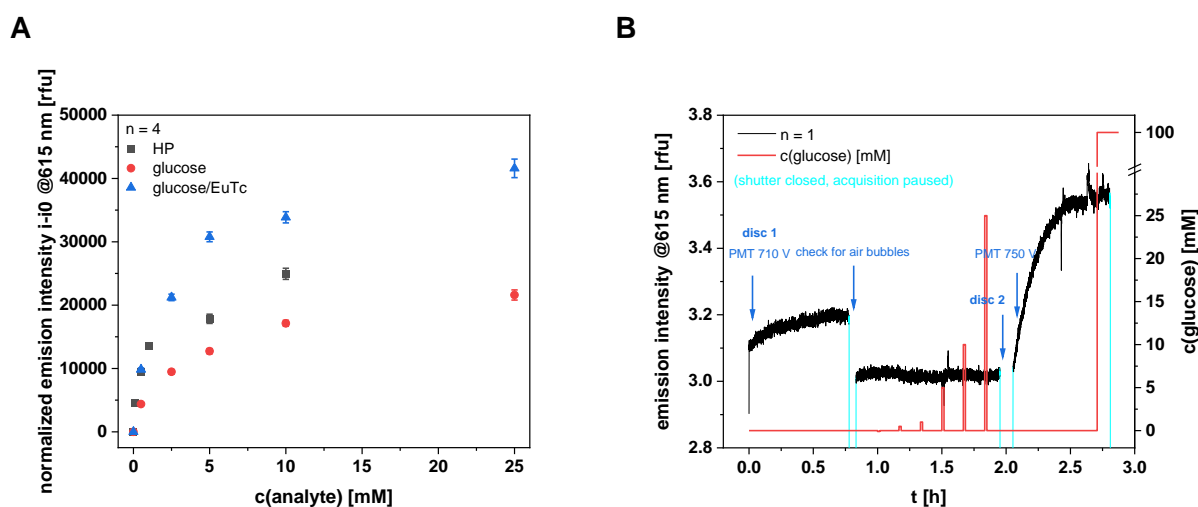


**Figure 5.3** D4-EuTc // LRP t 7016 // D4-GOx (10/05 // 2.5 // 10/0.2 wt%) discs: **A** The discs were tested in microplate assays with HP (grey squares), glucose (red circles) and glucose/EuTc (blue triangles) samples and showed promising dose-response curves after 5 min. (FluoStar  $\Omega$ ,  $\lambda_{exc}=405/10$  nm,  $\lambda_{em}=615/10$  nm,  $n = 4$ , gain 1200, top optic, 25°C) **B** A 24 mm disc is mounted in the flow cell setup. 0.1 M HEPES pH 7.4 is pumped through the system with 3.8 mL/min for around 45 min. The system is checked for air bubbles. After further 15 min, glucose solutions are injected for 60 s (without holding time). A second disc was tested after around 35 min of pre-equilibration (pump 48.0 rpm, AB2,  $\lambda_{exc}=405/8$  nm,  $\lambda_{em}=615/8$  nm,  $n = 1$ , PMT voltage 710 V and 750 V, data acquisition 1 s, 25°C)

The experiment was repeated with three discs from another batch (same layer/probe/enzyme composition) to exclude inhomogeneity of the sensor foil or some other issues due to wrong storage conditions or other unexpected batch-dependent issues. None of the other discs showed any response towards 100 mM glucose (**SI Figure 5.2**). But the microplate assays showed for all three performance assays satisfying dose-response curves as can be seen in one example shown in **Figure 5.3 A**.

The alarming assumption, that the sensor discs do not react to any sample solution in the flow-through system must be checked. Therefore, MTPs with 2-layered sensor discs (D4-EuTc 10/0.5 wt% in EtOH/H<sub>2</sub>O // LRP t 7016 1.25 wt% in THF/H<sub>2</sub>O) were prepared. The previously used LRP t 7016 polymer cocktail was diluted 1:1 by mass fractions to obtain a 1.25 wt%

cocktail to realize a thinner membrane for the tests. Washing procedure and analyzing the 0 mM HP sample were performed for all discs like usual for the HP microplate assay.

For one set of the sensor discs, the remaining concentrations were measured like usual with 0.1, 0.5, 1.0, 5.0 and 10 mM HP samples which are added one after another by hand (volume is always 100  $\mu$ L per well, complete assay time ca. 60 min). For another set of discs, in intervals of 10 min 5  $\mu$ L of a 20 mM HP solution was added automatically by the device (20 times, end volume 200  $\mu$ L per well, end concentration 10 mM HP, assay time ca. 5 h). The last disc set (in the same microplate) was incubated with 100  $\mu$ L 0.1 M HEPES pH 7.4 over the entire assay time (ca. 5 h). For the last measurement of these discs, 100  $\mu$ L buffer was added to reach the same volume as for the other samples with automated sample addition and the luminescence at 616 nm was recorded in the end.

**Figure 5.4** shows the kinetics over time of sensor discs with D4-EuTc and a protective second layer (1.25 wt% LRP t 7016 in THF/H<sub>2</sub>O (99:1, v/v)) in the manually performed microplate assay (Functionality Assay with HP samples, blue triangles) and the assay with automated HP sample addition (red circles). The emission intensity in the beginning and in the end of the sensor discs incubated with pure buffer over the entire time are represented by the grey squares and are connected by a dotted line for the sake of clarity. The labels at each data point refers to the current hydrogen peroxide concentration in the well in millimole per liter.

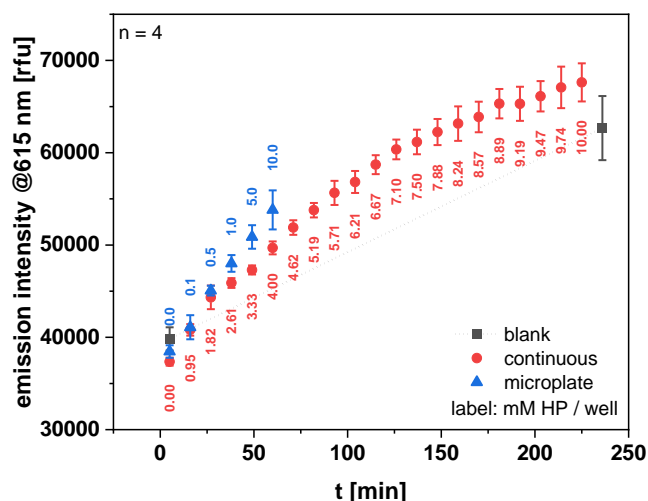


**Figure 5.4** D4-EuTc sensor foils (10/0.5 wt%) were coated with 1.25 wt% LRP t 7016. HP assays like usual were performed (functionality assay with HP samples, sample addition by hand, crossed boxes). A continuous HP detection with discs from the same foil were performed for nearly 2.5 h (filled boxes). Additionally, blank values of the used foils were determined before and after the continuous assay time to observe the change of the disc over time (empty boxes). (FluoStar  $\Omega$ ,  $\lambda_{exc}$ =405/10 nm,  $\lambda_{em}$ =615/10 nm,  $n = 3-4$ , gain 1200, top optic, 25°C)

Within standard deviation, the initial intensities are between 36,000 and 40,000 rfu for all discs. The intensity increases clearly for the first 50 min. The slope is nearly independent of the added concentration. 10 mM HP concentration in the well is reached within 50 min for the manually performed assay whereas by automatic sample addition within the same time an HP concentration of just 4 mM is reached. The continuous assay is continued for further 4 h. Within this time the emission intensity increases slowly but steady for the remaining time. The blank signal of the discs rises also over time comparable to the discs where HP samples were added.

To sum up, D4-EuTc sensor discs with LRP t 7016 as protection layer do not react significantly to added HP, the background luminescence increases as strong as for discs with HP sample addition. Therefore, it is assumed that the polymer is not permeable for HP at all (also not through the sides of the disc as shortcut) but accelerates the alteration of the complex. This signal increase of nearly 50 % over 5 h compared to the initial signal (from ca. 40,000 to 60,000 rfu) was falsely interpreted as enhanced luminescence due to the added analytes. It is furthermore assumed that this signal increase, when glucose or lactate are added, was falsely misinterpreted as interferences of the respective substrate in some initial trials.

Having no promising integrated system for further flow cell analysis, the stand-alone systems were tested in the flow cell to prove their functionality in the flow before further combination approaches are tested. Additionally, the enzyme and probe discs are combined in one flow cell holder to prove that the systems work together.

### **5.3.2 Hydrogen Peroxide Detection**

The D4-EuTc // PVAc/CA (10/0.5 wt% in EtOH/H<sub>2</sub>O // 10 wt% in CHon/H<sub>2</sub>O) discs were tested in the flow cell with different pump speeds, injection times and with and without holding time. Flow speed, injection time and data evaluation were optimized with a 1 mM HP solution (see SI: General Investigations with 1 mM HP Solution in the Flow Cell, **SI Figure 5.4**). Best results were obtained with high flow speed (48.0 rpm; 3.8 mL/min). An injection time of 60 s was chosen.

A new sensor disc is mounted in the flow cell system, that is flushed for at least 40 min with buffer before the first HP sample is injected. Increasing and decreasing HP concentrations are added to system in intervals of 10 min. The experiment was carried out for two times with different sensor discs. Raw data and derived data according to the Statistics and Data Evaluation part are presented in the SI (HP Detection, **SI Figure 5.5**). The resulting dose response curves derived from the absolute peak heights are shown in the following **Figure 5.5**.

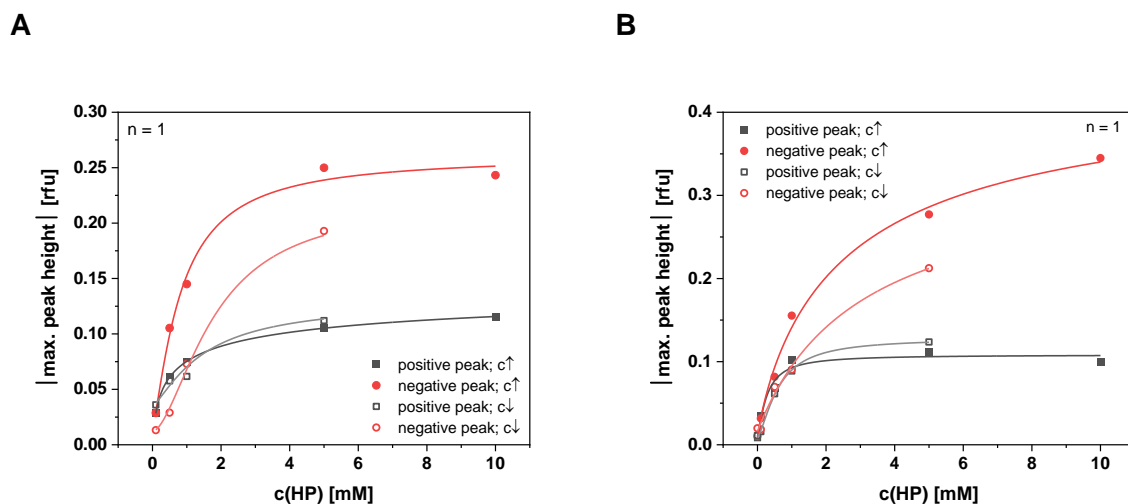


**Figure 5.5** Dose response curves of two independent experiments show reproducibility and reversibility of the D4-EuTc // PVAc/CA (10/0.5 // 10 wt%) sensor discs in the flow cell system. The data were obtained from the absolute maximum peak heights of the derived raw data plots shown in the SI (pump 48.0 rpm, AB2,  $\lambda_{exc}=405/8$  nm,  $\lambda_{em}=615/8$  nm,  $n = 1$ , PMT voltage 695 V, data acquisition **A** 10 s and **B** 1 s, 25°C)

For both repetitions, all four curves and their shapes are comparable. The negative peak values are up to 3.5 times higher than for the positive peak which makes the evaluation of these peaks more sensitive. But there is also a bigger difference of the signals from the same HP concentrations when measured in increasing or decreasing concentration order (mean deviation is  $46 \pm 25$  %). This deviation is less for the comparing the signals derived from the positive peaks for increasing and decreasing concentration ranges (mean deviation is  $19 \pm 15$  %). Therefore, it makes sense to investigate both, positive and negative peak maxima to enable a reliable quantification.

### 5.3.3 Glucose Detection

The experimental setup shown in the Experimental Part in **Figure 5.1 D3** was used for the following experiment. A D4-GOx disc was obtained from a cocktail with 10 wt% D4 and 0.5 wt% GOx in EtOH/water and mounted in the flow cell. Buffer and glucose solutions are pumped through the system at constant speed (16 rpm; 1.3 mL/min) without holding time. Some of the outcoming solution is collected every minute in a microplate. A defined volume of each fraction is investigated with a TMB/HRP assay for quantification of the HP concentration. The results are shown in the following **Figure 5.6** with a raw data plot versus time and the resulting dose-response graph.

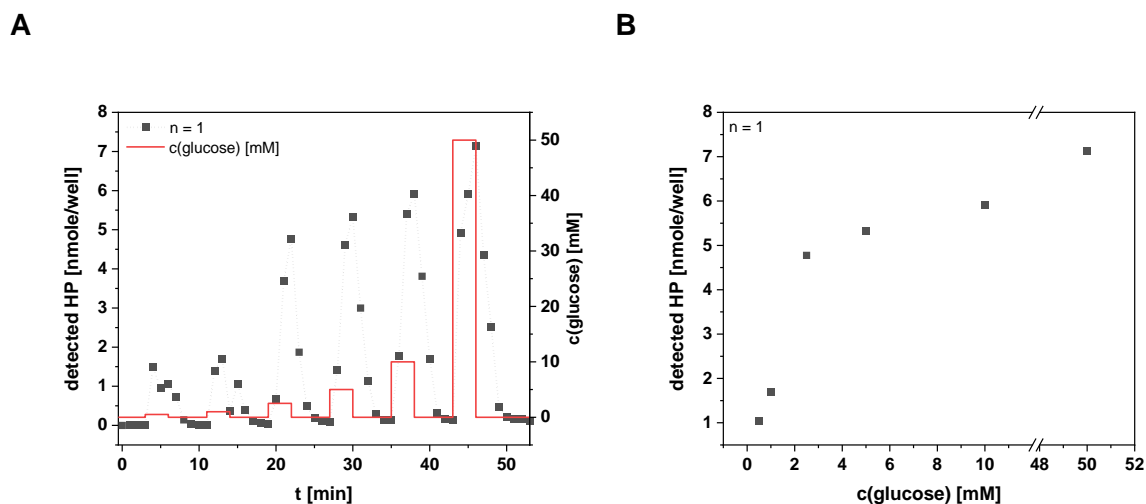


**Figure 5.6** D4-GOx (10/0.5 wt% in EtOH/H<sub>2</sub>O) disc in flow cell, solution was collected every minute and the HP content was determined by an HRP/TMB assay with a linear calibration plot for HP concentrations between 0 and 9.8 nmole/well HP. **A** raw data over time **B** resulting dose-response plot (pump setting 16.0 rpm, BioTek plate reader, absorbance @450 nm, 25°C,  $n = 1$  for samples,  $n = 3$  for calibration)

It is shown that there is a fast and reversible response of the enzyme disc towards the different glucose samples. Hydrogen peroxide concentrations correlates with the injected glucose concentrations. For lower concentrations the sensitivity is higher, for glucose concentrations above 5 mM sensitivity is reduced and it would be hard to distinguish small concentration changes in the upper range. But the results must be taken with care. The optimum pH for the TMB/HRP assay is up to pH 4 [41]. The samples' pH is 7.4 and therefore the calibration curve was recorded at the same non-optimum proton concentration in 0.1 M HEPES.

In conclusion, the assay can be taken as semi-quantitative and a proof-of principle for the GOx discs work in the flow cell system. Hydrogen peroxide is produced during the catalytic reaction and can be determined. The system responses fast and reversible as **Figure 5.6 A** shows.

### 5.3.4 Leakage and Interference Study

A 3-layered sensor disc was mounted in the flow cell setup, flushed with buffer at highest speed (48.0 rpm equals 3.8 mL/min) and later HP samples were injected. The solution is collected in certain time intervals of 30 min. The last fraction was collected over 2 h. The emission intensity of the sensor discs versus time is shown in **SI Figure 5.6**. The collected solutions were evaporated at 140°C to dryness. The residues were re-dissolved in 5.0 mL 1.5 M HNO<sub>3</sub> and 20 mL for the fraction collected over 2 h and measured with a calibrated ICP-OES device. Detailed results for each fraction are shown in **SI Table 5.1**.

Theoretical Europium amount of a 24 mm disc was calculated in accordance by ICP-OES measurements confirmed calculation for a 6 mm disc (see SI: Determination of Eu(III) Content in 6 mm Disc via ICP-OES). A disc with a diameter of 24 mm contains 376.1 nmol of Eu(III)

and is taken as 100 % into account. Consequently, the detected Eu(III) amount in the different fractions results in a total loss of 0.2 % Eu(III) over 5 h at 3.8 mL/min flow speed. Actually, the theoretically calculated amount of Eu(III) is below the calculated limit of detection (LOD) for the calibration for Europium. Therefore, the exact amount of loss the final sensor system should be quantified with a MS-based method, which has experiential lower LOD. But these results give a good hint for a sufficient long-term in-use stability of the tested system.

Due to some hints in the previously performed microplate assays, it was assumed that glucose itself can interact with the Europium complex. Therefore, a flow cell setup with an EuTc disc in combination with a blank D4 discs was assembled. Buffer was pumped through the system until a stable baseline was observed. Glucose samples with increasing concentrations was injected for at least 5 to 10 minutes. As positive control a 1 mM HP solution was injected at the end. The emission intensity versus time with sample injection profile is shown in **SI Figure 5.7**. The probe disc does not react to any of the glucose concentrations but show a strong response towards the positive control. Therefore, an interfering behavior of the analyte itself can be excluded in the flow through system. Further interfering substances like phosphate, citrate or other metabolites present in blood must be investigated in future experiments.

### 5.3.5 Adjacently Placed Sensor Discs

Since the combination of the different sensing layers in one integrated sensor disc was not as successful as expected, the two systems were combined physically adjacent in the flow cell holder as shown in **Figure 5.7**. A blank Mylar disc (“dummy disc”) was used as sealing to reduce the outer diameters and to adjust the active area ratio of enzyme and probe discs.

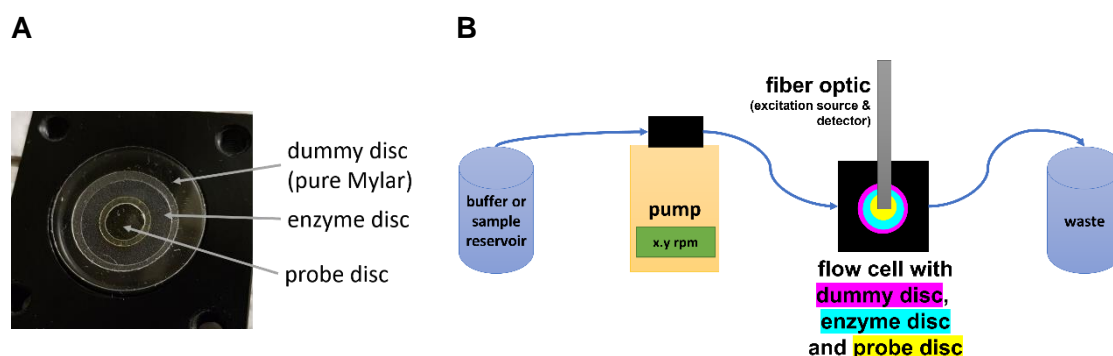


**Figure 5.7** **A** Discs arranged in the flow cell chamber with a dummy disc to adapt the active areas of the probe and enzyme discs. **B** Schematic flow scheme and setup of the used flow cell system. The diameters of the discs can be varied to adjust the ratio of the active areas.

Different ratio of GOx to EuTc were tested, furthermore different pump speeds. All investigations were carried out without holding or incubation time because the previous experiments showed that enough HP for detection is produced at a flow speed of 1.3 mL/min by the enzyme disc. An overview of tested GOX/EuTc ratio with the actual diameter of the respective discs and qualitative evaluation is shown in **SI Table 5.2**. Best results were obtained



for GOx/EuTc ratio equal or higher than 2.0. An exemplary graph for glucose detection with the above-described setup is shown in the following **Figure 5.8**.

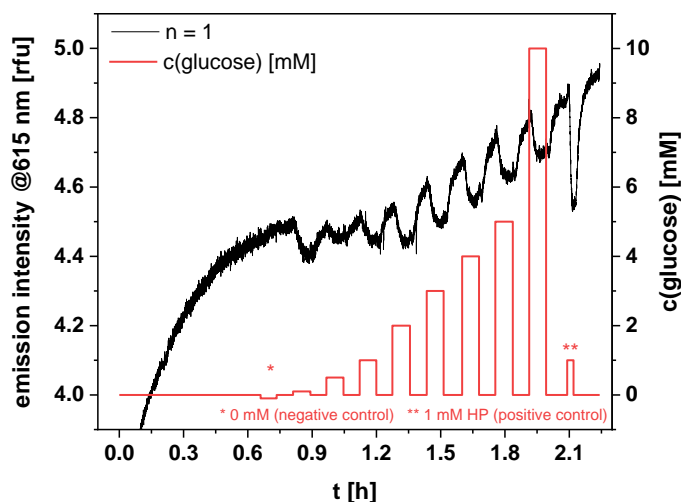


**Figure 5.8** Dummy, probe and enzyme disc are placed in the same flow cell housing: D4-GOx (10/0.5 wt% in EtOH/H<sub>2</sub>O) and D4-EuTc/PVAc/CA (10/0.5 wt% in EtOH/H<sub>2</sub>O // 10 wt% in CHon/H<sub>2</sub>O) discs: 16 rpm, no incubation or holding time, dummy disc outer diameter 24 mm, inner diameter 14 mm, 0.5 wt% GOx, outer diameter 16 mm, inner diameter 6 mm, EuTc discs 8 mm diameter (AB2,  $\lambda_{exc}=405/8$  nm,  $\lambda_{em}=615/8$  nm,  $n = 1$ , PMT voltage 730 V; 25°C)

The baseline in the beginning increases strongly but after the plateau region is reached after around 45 min, 0 mM sample solution is injected as negative control. Thereof, it is excluded to miss a signal change caused by the pressure fluctuations during the injection process. Observing no change, glucose samples with concentrations between 0.1 mM and 10 mM are injected for around 5 minutes. Afterwards the feed solution is changed back to buffer for another 5 minutes or until the baseline seems recovered. In the end a 1 mM HP samples is injected as positive control and as indicator for expected signal heights.

The sensor responses nearly immediately as soon as the sample solution reaches the discs after around 30 s injection time. Within 5 minutes the signal is stabilized. The sensor is reversible which is shown by a recovery of the baseline signal when buffer is pumped through the system again. A glucose concentration of 0.1 mM is enough to obtain a clear response of the sensor discs. The signal change is nearly the same for all tested concentrations up to 10 mM glucose. Therefore, further investigations especially about the GOx/EuTc ratio and furthermore the thickness of the layers are still necessary to overcome this challenge.

Many reasons are thinkable why the system does not work perfectly in the flow-through approach. The enzyme seems already saturated with the low glucose concentrations. This means the enzyme amount must be adjusted by reducing the GOx amount in the membrane or the size of the active area. This would be in accordance with the results obtained from the

TMB/HRP assay. Other parameters are the EuTc content, the flow speed, and the membrane thickness including diffusion driven reasons. The kinetics of the enzyme and the ligand exchange reaction of the complex play a major role in the equilibration of the entire system. Furthermore, within the different membrane materials diffusion limitations must be considered depending on the flow speed. Diffusion layers nearby the surface or within the membrane changes with increasing or decreasing flow. Temperature plays another role but was tried to hold constant during the experiments and should not be the main reason. Regarding the enzyme reaction, a stoichiometric amount of oxygen is necessary for the conversion of the substrate. Oxygen is present just in limited amount in aqueous solutions in a closed system. Lack of oxygen for the enzymatic catalysis and therefore impeded detection of high substrate concentrations is a well-known challenge in glucose oxidase-based sensor development [42, 43]. The thickness of the sensor foil is estimated as 3  $\mu\text{m}$ . A much thinner membrane allows the faster equilibration of the system but is difficult to realize with the simple in-house-made knife-coater device. More professional devices used in industry or testing of completely different methods like spray-, electro- or spin-coating methods must be investigated. This would entail an adaption of the composition of the used sensor and enzyme cocktails to get a mixture with suitable viscosity for the used technique. Therefore, the already existing probe and enzyme discs will be investigated further to find out the right ratio of EuTc and GOx. Another step towards optimization is changing of the geometry of the used flow cell chamber to reduce dilution and convection events like it could easily happen in the circular chamber.

## **5.4 Conclusion**

The functionality and reversibility of EuTc and GOx sensor foils was shown in flow-through systems for increasing and decreasing hydrogen peroxide and glucose concentrations. The single systems were not further optimized since the EuTc and GOx layers should be integrated in one system.

Different immobilization techniques for the enzyme on top or within of the sensing layer were investigated. Simple approaches like co-entrapment of both elements within the same layer, soaking and adsorption, or with glutardialdehyde/BSA for cross-linking of the enzyme layer on top of the EuTc membrane or EDC/NHS chemistry were tested. None of them led to success since the EuTc complex does not react to changing HP concentrations at all. The reasons therefore were not further investigated, and the combination of probe and enzyme layer with an interlayer showed most promising results, at least in the microplate assays with HP, glucose, and EuTc/glucose. The 3-layered D4-EuTc // LRP t 7016 // D4-GOx system was transferred to the flow-through system and tested in a continuous assay within the plate reader. It was figured out that the intermediate layer compromises the EuTc complex which led to an increasing background signal over time. This was falsely interpreted as signal-dependent intensity change in previous microplate assays.

To conclude, within the scope of the up to now performed experiments it was not possible to find a working multi-layer disc arrangement for the quantification of different glucose concentrations in a flow-through system. Therefore, the two working stand-alone systems were adjacently placed within one flow cell chamber to proof their fundamental functionality together. This approach showed promising initial results but needs further optimization regarding distinguishability of glucose concentrations above 1 mM. Enzyme/probe ratio and membrane thickness are the most critical parameters and must be improved in the future for GOx and later LOx. A fully optimized probe-enzyme system opens a new field for clinical applications regarding optical long-term monitoring of important metabolites like glucose and lactate.

## **5.5 Acknowledgement**

The author acknowledges TERUMO Cardiovascular group for financial support. Furthermore, the author acknowledges Barbara Grotz, Blaž Kozjan and Iga Malicka for collecting data in the scope of a Master's Thesis and internships. Special thanks go to Vanessa Tomanek and Joachim Rewitzer for helping with the ICP-OES measurements.

## 5.6 References

1. Meier J, M Hofferber E, A Stapleton J, M Iverson N. Hydrogen Peroxide Sensors for Biomedical Applications. *Chemosensors*. 2019; <https://doi.org/10.3390/chemosensors7040064>
2. Ganter M, Zollinger A. Continuous intravascular blood gas monitoring: development, current techniques, and clinical use of a commercial device. *Br J Anaesth*. 2003; <https://doi.org/10.1093/bja/aeg176>
3. Wolf A, Renehan K, Ho KKY, Carr BD, Chen CV, Cornell MS, Ye M, Rojas-Peña A, Chen H. Evaluation of Continuous Lactate Monitoring Systems within a Heparinized In Vivo Porcine Model Intravenously and Subcutaneously. *Biosensors (Basel)*. 2018; <https://doi.org/10.3390/bios8040122>
4. Moser I. Biosensor arrays for simultaneous measurement of glucose, lactate, glutamate, and glutamine. *Biosensors and Bioelectronics*. 2002; [https://doi.org/10.1016/S0956-5663\(01\)00298-6](https://doi.org/10.1016/S0956-5663(01)00298-6)
5. Calabria D, Caliceti C, Zangheri M, Mirasoli M, Simoni P, Roda A. Smartphone-based enzymatic biosensor for oral fluid L-lactate detection in one minute using confined multilayer paper reflectometry. *Biosens Bioelectron*. 2017; <https://doi.org/10.1016/j.bios.2017.02.053>
6. Andrus LP, Unruh R, Wisniewski NA, McShane MJ. Characterization of Lactate Sensors Based on Lactate Oxidase and Palladium Benzoporphyrin Immobilized in Hydrogels. *Biosensors (Basel)*. 2015; <https://doi.org/10.3390/bios5030398>
7. Flow Analysis of Lactate and Glucose in Milk with an Improved Electrochemical Biosensor;36:213–222.
8. Zohourtalab A, Razmi H. Selective Determination of Glucose in Blood Plasma by Using an Amperometric Glucose Biosensor Based on Glucose Oxidase and a Chitosan/ Nafion/ IL/Ferrocene Composite Film. *Iranian Journal of Analytical Chemistry*. 2018;5:9–16.
9. Yu S, Ding L, Lin H, Wu W, Huang J. A novel optical fiber glucose biosensor based on carbon quantum dots-glucose oxidase/cellulose acetate complex sensitive film. *Biosens Bioelectron*. 2019; <https://doi.org/10.1016/j.bios.2019.111760>
10. Rajendran R, Rayman G. Point-of-care blood glucose testing for diabetes care in hospitalized patients: an evidence-based review. *J Diabetes Sci Technol*. 2014; <https://doi.org/10.1177/1932296814538940>
11. Choi S, Choi SJ, Jeon BR, Lee Y-W, Oh J, Lee YK. What We Should Consider in Point of Care Blood Glucose Test; Current Quality Management Status of a Single Institution. *Medicina (Kaunas)*. 2021; <https://doi.org/10.3390/medicina57030238>
12. Dhatt GS, Agarwal MM, Othman Y, Nair SC. Performance of the Roche Accu-Chek active glucose meter to screen for gestational diabetes mellitus using fasting capillary blood. *Diabetes Technol Ther*. 2011; <https://doi.org/10.1089/dia.2011.0097>
13. Achatz DE, Meier RJ, Fischer LH, Wolfbeis OS. Luminescent sensing of oxygen using a quenchable probe and upconverting nanoparticles. *Angew. Chem. Int. Ed*. 2011; <https://doi.org/10.1002/anie.201004902>
14. Duong HD, Rhee JI. Ratiometric Fluorescent Biosensors for Glucose and Lactate Using an Oxygen-Sensing Membrane. *Biosensors (Basel)*. 2021; <https://doi.org/10.3390/bios11070208>
15. Arain S, John GT, Krause C, Gerlach J, Wolfbeis OS, Klimant I. Characterization of microtiterplates with integrated optical sensors for oxygen and pH, and their applications to enzyme activity screening, respirometry, and toxicological assays. *Sensors and Actuators B: Chemical*. 2006; <https://doi.org/10.1016/j.snb.2005.07.056>
16. Wolfbeis OS, Dürkop A, Wu M, Lin Z. A Europium-Ion-Based Luminescent Sensing Probe for Hydrogen Peroxide. *Angew. Chem. Int. Ed*. 2002; [https://doi.org/10.1002/1521-3773\(20021202\)41:23<4495:AID-ANIE4495>3.0.CO;2-I](https://doi.org/10.1002/1521-3773(20021202)41:23<4495:AID-ANIE4495>3.0.CO;2-I)
17. Dürkop A, Wolfbeis OS. Nonenzymatic direct assay of hydrogen peroxide at neutral pH using the Eu<sub>3</sub>Tc fluorescent probe. *J Fluoresc*. 2005; <https://doi.org/10.1007/s10895-005-2984-6>

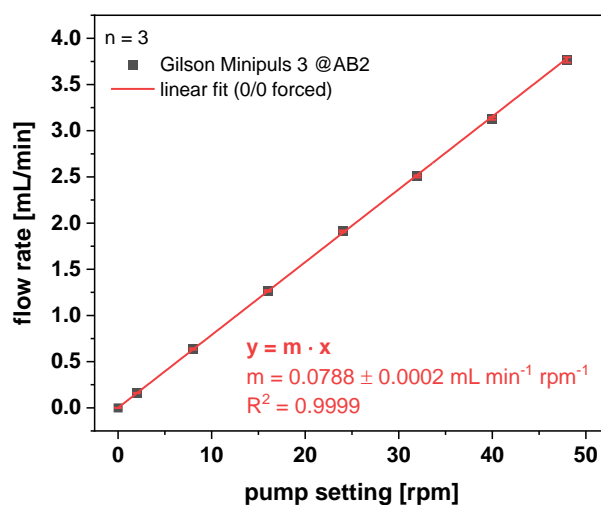
18. Wolfbeis OS, Schäferling M, Dürkop A. Reversible Optical Sensor Membrane for Hydrogen Peroxide Using an Immobilized Fluorescent Probe, and its Application to a Glucose Biosensor. *Microchimica Acta*. 2003; <https://doi.org/10.1007/s00604-003-0090-5>
19. Waleed Al-Qaysi W, Duerkop A. A luminescent europium complex for wide-range pH sensors and sensor microtiterplates. *Analyst*. 2018; <https://doi.org/10.1039/c8an00775f>
20. Peng H, Stich MIJ, Yu J, Sun L-N, Fischer LH, Wolfbeis OS. Luminescent Europium(III) nanoparticles for sensing and imaging of temperature in the physiological range. *Advanced Materials*. 2010; <https://doi.org/10.1002/adma.200901614>
21. Gaspar RDL, Fortes PR, Mazali IO, Sigoli FA, Raimundo IM. Optical Temperature Sensors Based On Europium(III) Beta-Diketonate Complexes Chemically Bonded To Functionalized Polydimethylsiloxane. *ChemistrySelect*. 2018; <https://doi.org/10.1002/slct.201801373>
22. Courrol L, Samad R. Applications of Europium Tetracycline Complex: A Review. *CPA*. 2008; <https://doi.org/10.2174/157341208786306216>
23. Eliseeva SV, Bünzli J-CG. Lanthanide luminescence for functional materials and bio-sciences. *Chem Soc Rev*. 2010; <https://doi.org/10.1039/b905604c>
24. Karpova EV, Shcherbacheva EV, Galushin AA, Vokhmyanina DV, Karyakina EE, Karyakin AA. Noninvasive Diabetes Monitoring through Continuous Analysis of Sweat Using Flow-Through Glucose Biosensor. *Anal Chem*. 2019; <https://doi.org/10.1021/acs.analchem.8b05928>
25. Lee I, Probst D, Klonoff D, Sode K. Continuous glucose monitoring systems - Current status and future perspectives of the flagship technologies in biosensor research. *Biosens Bioelectron*. 2021; <https://doi.org/10.1016/j.bios.2021.113054>
26. Ruan J-L, Chen C, Shen J-H, Zhao X-L, Qian S-H, Zhu Z-G. A Gelated Colloidal Crystal Attached Lens for Noninvasive Continuous Monitoring of Tear Glucose. *Polymers*. 2017; <https://doi.org/10.3390/polym9040125>
27. Yan Q, Major TC, Bartlett RH, Meyerhoff ME. Intravascular glucose/lactate sensors prepared with nitric oxide releasing poly(lactide-co-glycolide)-based coatings for enhanced biocompatibility. *Biosens Bioelectron*. 2011; <https://doi.org/10.1016/j.bios.2011.04.026>
28. Park MS. Recent lactate findings: is repeated serum lactate testing necessary in septic shock patients? *Acute Crit Care*. 2019; <https://doi.org/10.4266/acc.2019.00528>
29. Clark LC, Wolf R, Granger D, Taylor Z. Continuous recording of blood oxygen tensions by polarography. *J Appl Physiol*. 1953; <https://doi.org/10.1152/jappl.1953.6.3.189>
30. Gelsomino S, Lorusso R, Livi U, Romagnoli S, Romano SM, Carella R, Lucà F, Billè G, Matteucci F, Renzulli A, Bolotin G, Cicco G de, Stefano P, Maessen J, Gensini GF. Assessment of a continuous blood gas monitoring system in animals during circulatory stress. *BMC Anesthesiol*. 2011; <https://doi.org/10.1186/1471-2253-11-1>
31. Kuster N, Bargnoux AS, Badiou S, Dupuy A-M, Piéroni L, Cristol JP. Multilevel qualification of a large set of blood gas analyzers: Which performance goals? *Clin Biochem*. 2019; <https://doi.org/10.1016/j.clinbiochem.2019.09.005>
32. Hermida Ameijeiras FJ, González Ponce B, Reimunde Noreña B. Aspectos analíticos del analizador de gases Cobas® b 221 (Roche Diagnostics). *Revista del Laboratorio Clínico*. 2010; <https://doi.org/10.1016/j.labcli.2010.05.001>
33. Philani Buthelezi E, Rampota E, Mphogo M, Marule F, Moshen Tanyanyiwa D. Point of Care Blood Gas Analyser Verification at the Largest Academic Hospital in Southern Hemisphere Revived by Coronavirus Calls for Tests to Be Verified. *PLM*. 2020; <https://doi.org/10.11648/j.plm.20200402.11>
34. T. Tsuchida KY. Multi-Enzyme Membrane Electrodes for Determination of Creatinine and Creatine in Serum. *Clin. Chem*. 1983;29:51–55.
35. Maierhofer M, Rieger V, Mayr T. Optical ammonia sensors based on fluorescent aza-BODIPY dyes- a flexible toolbox. *Anal Bioanal Chem*. 2020; <https://doi.org/10.1007/s00216-020-02891-3>
36. Staudinger C, Strobl M, Breininger J, Klimant I, Borisov SM. Fast and stable optical pH sensor materials for oceanographic applications. *Sensors and Actuators B: Chemical*. 2019; <https://doi.org/10.1016/j.snb.2018.11.048>

37. Dalfen I, Dmitriev RI, Holst G, Klimant I, Borisov SM. Background-Free Fluorescence-Decay-Time Sensing and Imaging of pH with Highly Photostable Diazoxytriangulenium Dyes. *Anal Chem.* 2019; <https://doi.org/10.1021/acs.analchem.8b02534>
38. Tjell AØ, Almdal K. Diffusion rate of hydrogen peroxide through water-swelled polyurethane membranes. *Sensing and Bio-Sensing Research.* 2018; <https://doi.org/10.1016/j.sbsr.2018.10.001>
39. Tric M, Lederle M, Neuner L, Dolgowjasow I, Wiedemann P, Wöfl S, Werner T. Optical biosensor optimized for continuous in-line glucose monitoring in animal cell culture. *Anal Bioanal Chem.* 2017; <https://doi.org/10.1007/s00216-017-0511-7>
40. Bidmanova S, Steiner M-S, Stepan M, Vymazalova K, Gruber MA, Duerkop A, Damborsky J, Prokop Z, Wolfbeis OS. Enzyme-Based Test Strips for Visual or Photographic Detection and Quantitation of Gaseous Sulfur Mustard. *Anal Chem.* 2016; <https://doi.org/10.1021/acs.analchem.6b01272>
41. Lou-Franco J, Das B, Elliott C, Cao C. Gold Nanozymes: From Concept to Biomedical Applications. *Nanomicro Lett.* 2020; <https://doi.org/10.1007/s40820-020-00532-z>
42. Wang J. Electrochemical glucose biosensors. *Chem Rev.* 2008; <https://doi.org/10.1021/cr068123a>
43. Lei Y, Sun R, Zhang X, Feng X, Jiang L. Oxygen-Rich Enzyme Biosensor Based on Superhydrophobic Electrode. *Adv Mater.* 2016; <https://doi.org/10.1002/adma.201503520>

## 5.7 Supporting Information

### 5.7.1 Determination of Flow Speed of the Peristaltic Pump

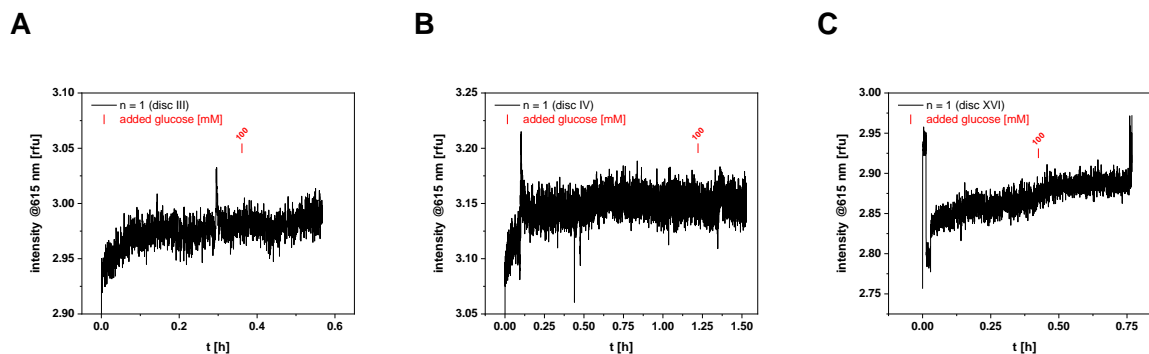
To determine the actual flow rate of the peristaltic pump, water was pumped through the system for a certain time at pump settings between 2.0 and 48.0 rpm. Time is stopped and the solution is collected in a graduated cylinder to determine the volume per time for the respective setting. The flow rate is plotted versus the pump setting. The curve was fitted linearly and forced through zero to obtain a respective equation to calculate the flow rate depending on each pump setting (**SI Figure 5.1**).



**SI Figure 5.1** Determination of flow speed for different pump settings of the peristaltic pump.

### 5.7.2 3-Layered Sensor Discs in Flow Cell Setup

3-layered sensor discs from different batches were tested in the flow-cell setup to exclude batch-dependent reasons for malfunction. Exemplary graphs are shown in **SI Figure 5.2**.



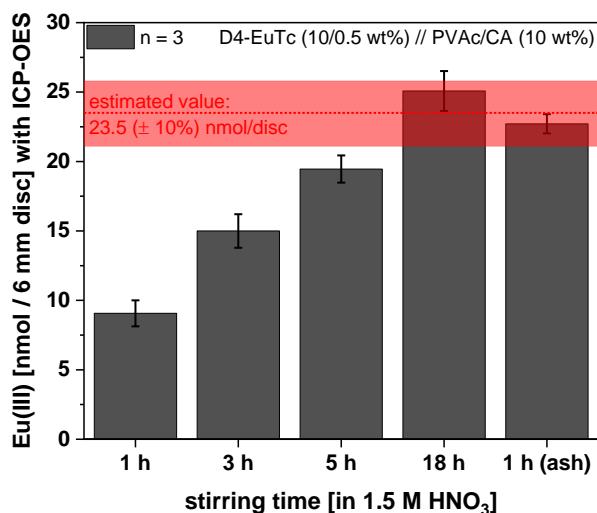
**SI Figure 5.2 A to C** D4-EuTc // LRP t 7016 // D4-GOx (10/05 // 2.5 // 10/0.5 wt%) sensor discs are mounted in the flow cell setup. 0.1 M HEPES pH 7.4 is pumped through the system with 0.6 mL/min until the feed solution is changed to 100 mM glucose solution. (pump 8.0 rpm, AB2,  $\lambda_{exc}=405/8$  nm,  $\lambda_{em}=615/8$  nm,  $n = 1$ , PMT voltage 740 V, data acquisition 18,000/1 s, 25°C)

### 5.7.3 Determination of Eu(III) Content in 6 mm Disc via ICP-OES

Sensor discs with a diameter of 6 mm (D4-EuTc (10/0.5 wt%) // PVAc/CA (10 wt%)) are weighed and stirred for different times in 5.0 mL of 1.5 M nitric acid (105 mL 65 % HNO<sub>3</sub> solution is mixed with water and filled up at 1 L in a volumetric flask). Mean weight of a sensor disc is  $5.45 \pm 0.08$  mg ( $n = 15$ ).

Another three discs were incinerated at 980°C overnight. The ash is dissolved in 5.0 mL nitric acid. The samples are measured with an existing calibration (re-calibration with blank and 5000 ppm Eu standard) with ICP-OES. The resulting amounts of Eu per disc with the different extraction methods and stirring times are compared in following **SI Figure 5.3** with the theoretical amount of a sensor disc (calculated as 23.5 nmol Europium per disc). Assuming an inaccuracy of 10 % of the made estimations, the longest stirring time or the incineration method seems to be suitable for the determination of the Eu content in a 6 mm disc with 0.5 wt% EuTc in the initial sensor cocktail.

For further ICP-OES determinations, the discs can be incinerated, and the ash is re-dissolved in nitric acid or the discs are stirred in nitric acid for at least 18 h.

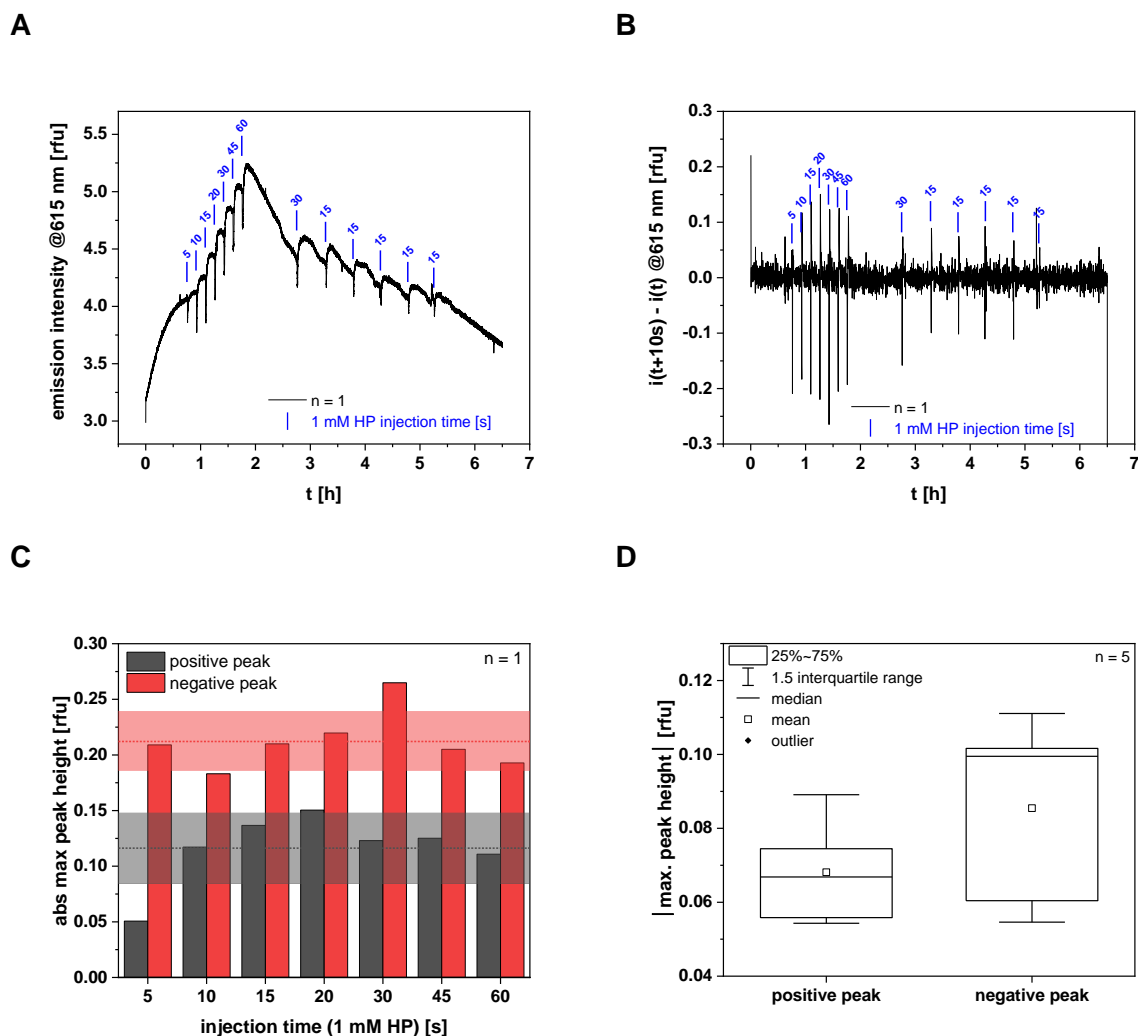


**SI Figure 5.3** Eu(III) content in a 6 mm diameter sensor disc containing 0.5 wt% EuTc in the initial sensor cocktail. Estimated Eu content with an assumed inaccuracy of 10 % is marked as red box (determined by ICP-OES,  $n = 3$ )



### 5.7.4 General Investigations with 1 mM HP Solution in the Flow Cell

A new sensor disc is mounted in the flow cell system, that is flushed for around 40 min with buffer before the first 1 mM HP sample is injected for 5 seconds. In intervals of 10 to 30 min the next 1 mM HP sample is injected for increasing injection times up to 60 s. Furthermore, the 1 mM HP sample is injected 5 times for 15 s. The resulting raw data and the derived, evaluated data sets are shown in **SI Figure 5.4**.



**SI Figure 5.4** A D4-EuTc // PVAc/CA (10/0.5 wt% in EtOH/H<sub>2</sub>O // 10 wt% in CHon/H<sub>2</sub>O) sensor disc is mounted in the flow cell setup. 0.1 M HEPES pH 7.4 is pumped through the system with 3.8 mL/min for 45 min before the first sample injection. Injection time of the 1 mM HP solution is varied between 5 s and 60 s (stop&go) Next sample is added after each 10 min up to 60 s injection. The system is flushed for 1 h with buffer. Next sample is injected after each 30 min. **A** Raw data **B** Data evaluation of the obtained raw data: signal intensity  $i(t+10) - i(t)$  for  $t = 0, 10, 20, \dots$  s. **C** The maximum height of the positive and negative peak after the respective injection of 1 mM HP is compared and related to the respective injection time. The dotted lines and colored boxes represent the mean value with respective SD **D** Reproducibility of the peak maxima was determined for 5 injections for 15 s injection time using 1 mM HP sample solution (pump 48.0 rpm, AB2,  $\lambda_{exc}=405/8$  nm,  $\lambda_{em}=615/8$  nm,  $n = 1$ , PMT voltage 710 V, data acquisition 1 s, 25°C)

The raw data (**A**) shows that there is recognizable baseline shift over the entire time. In the beginning, the baseline signal and the overall signal rise, whereas after around 2 h the baseline

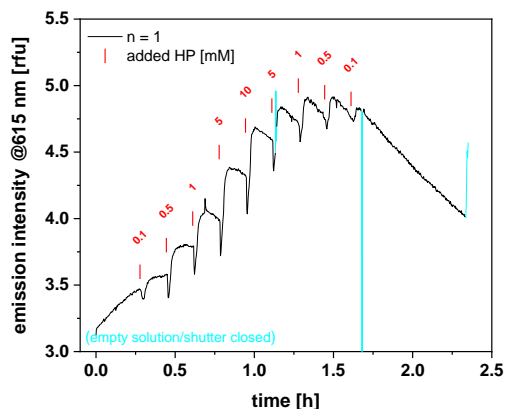
signal as well as the overall signal decrease significantly. Moreover, the sample injections result first in a significant drop of the signal and rise afterwards, just to decrease again when the system is flushed with buffer. Therefore, the signal change over time was calculated in 10 s intervals to eliminate the drastic baseline shift (see equation (3) in the Statistics and Data Evaluation chapter).

These signal changes were plotted versus time (**B**). Herein, a stable baseline signal can be observed with positive and negative peaks. Both peak directions were evaluated by taking the maximum absolute amount and plot these absolute maximum peak heights versus the injection time (**C**). The respective mean values and SD are represented as dotted lines and colored boxes. Within standard deviation, the injection time does not change the peak heights significantly (besides 5 s injection time for the positive peak and 30 s for the negative maximum peak height). Relative standard deviations were calculated as 27 % (11 % assuming 5 s injection time as outlier) for the positive and 12 % for the negative peak heights. To determine the injection reproducibility, the 1 mM HP sample was injected five times for 15 s and the respective maximum absolute peak heights were compared (**D**). Relative standard deviations were calculated as 21 % for the positive and 30 % for the negative peak heights.

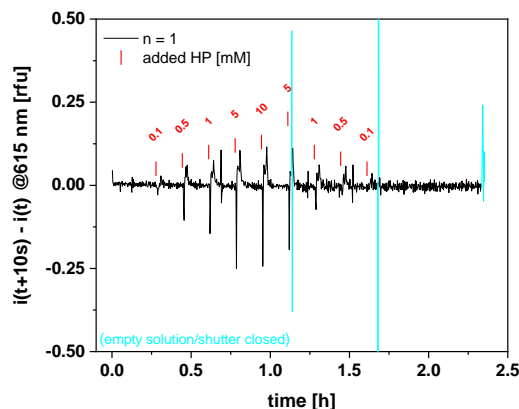
### 5.7.5 HP Detection

Two independent D4-EuTc // PVAc/CA sensor discs were tested in the flow-through system with HP solutions. The raw data (1) and the derived data sets (2) are shown in the following **SI Figure 5.5** for both experiments (A and B).

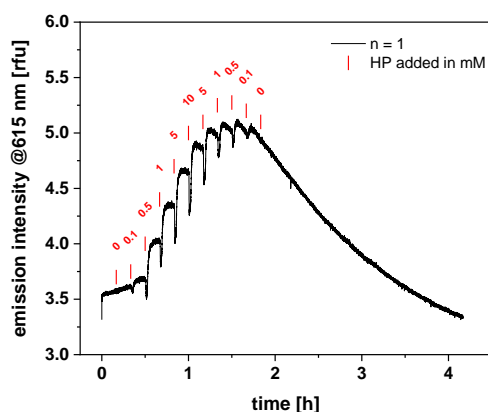
**A1**



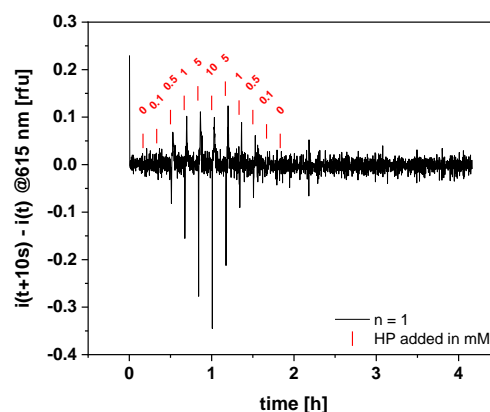
**A2**



**B1**



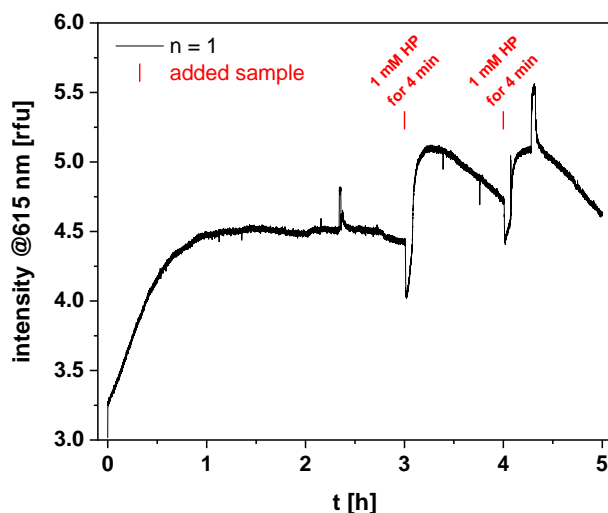
**B2**



**SI Figure 5.5** A D4-EuTc // PVAc/CA (10/0.5 // 10 wt%) sensor disc is mounted in the flow cell setup. 0.1 M HEPES pH 7.4 is pumped through the system with 3.8 mL/min for certain time (not shown) before the first sample injection. Injection time of the respective HP solution is 60 s. Next sample is added after each 10 min. Experiment **A** and **B**, **1** Raw data **2** Data evaluation of the obtained raw data: signal intensity  $i(t+10) - i(t)$  for  $t = 0, 10, 20, \dots$  s. (pump 48.0 rpm, AB2,  $\lambda_{exc}=405/8$  nm,  $\lambda_{em}=615/8$  nm,  $n = 1$ , PMT voltage 695 V, data acquisition **A** 10 s and **B** 1 s, 25°C)

### 5.7.6 Leakage Study

The emission intensity of the used sensor disc versus time is shown in **SI Figure 5.6**.



**SI Figure 5.6** A D4-EuTc // LRP t 7016 // D4-GOx (10/0.5 // 2.5 // 10/0.2 wt%) sensor disc is mounted in the flow cell setup. 0.1 M HEPES pH 7.4 is pumped through the system with 3.8 mL/min for 5 hours. 1 mM HP solutions are injected for 4 min (stop&go). The solution is collected for certain time and used for Eu(III) leakage detection. (pump 48.0 rpm, AB2,  $\lambda_{exc}=405/8$  nm,  $\lambda_{em}=615/8$  nm,  $n = 1$ , PMT voltage 740 V, data acquisition 1 s, 25°C)

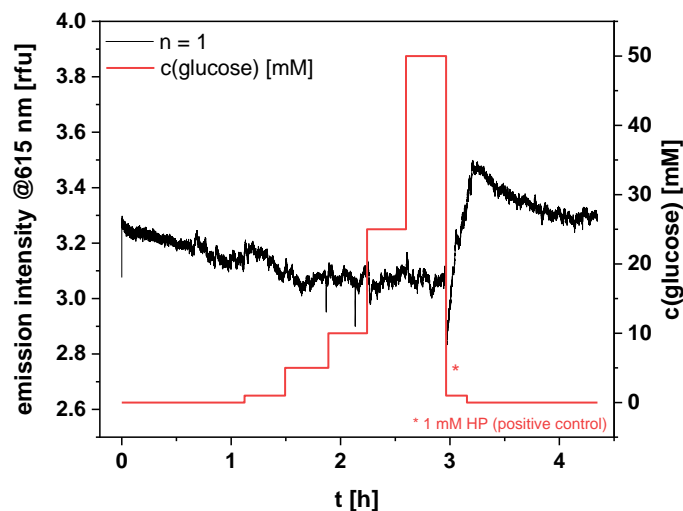
The results from ICP-OES measurements of the leakage study for the single fractions are listed in following **SI Table 5.1**.

**SI Table 5.1** Leakage test in flow cell setup: Solutions from the flow cell were collected over certain time intervals, completely evaporated and the residues were dissolved in 5.0 mL/30 min 1.5 M HNO<sub>3</sub> solution and analyzed with ICP-OES. Eu(III) content per disc and 0.5 h fraction was calculated and compared to the theoretical calculated Eu(III) amount (376 nmol Eu(III) per disc) of a 24 mm diameter sensor disc. The LOD of the used calibration was calculated as 0.2  $\mu\text{mol/L}$

time [h]	ICP-OES Eu(III) [ $\mu\text{mol/L}$ ]	calculated Eu (III) [nmol/disc/0.5 h]	loss of 24 mm disc [%]	LOD 0.2 $\mu\text{mol/L}$
0.0 - 0.5	0.0248	0.124	0.03	< LOD
0.5 - 1.0	0	0	0.00	< LOD
1.0 - 1.5	0.1026	0.513	0.14	< LOD
1.5 - 2.0	0	0	0.00	< LOD
2.0 - 2.5	0	0	0.00	< LOD
2.5 - 3.0	0	0	0.00	< LOD
3.0 - 5.0	0	0	0.00	< LOD
$\Sigma$				
0.0 - 5.0	0.1274	0.637	0.17	< LOD

### 5.7.7 Interference Study

The emission intensity of an EuTc disc (D4-EuTc 10/0.5 wt% in EtOH/H<sub>2</sub>O // 10 wt% PVAc/CA in CHon/H<sub>2</sub>O) in combination with a blank D4 disc is shown in the following **SI Figure 5.7**.



**SI Figure 5.7** Probe disc and blank D4 disc are placed in the same flow cell housing: D4 (10 wt% in EtOH/H<sub>2</sub>O) and D4-EuTc/PVAc/CA (10/0.5 wt% in EtOH/H<sub>2</sub>O // 10 wt% in CHon/H<sub>2</sub>O) discs: 16 rpm, no incubation or holding time, D4 disc outer diameter 24 mm, inner diameter 8 mm, 0.5 wt%, EuTc discs 10 mm diameter (AB2,  $\lambda_{exc}=405/8$  nm,  $\lambda_{em}=615/8$  nm,  $n = 1$ , PMT voltage 715 V; 25°C)

### 5.7.8 Investigation of EuTc/GOx Ratio in Flow Cell Setup

Different EuTc/GOx ratio with different disc sizes and with or without dummy discs were tested. The results are summed up in the following **SI Table 5.2**.

**SI Table 5.2** Overview of the discs' properties like inner and outer diameters, active area, ratios considering the active areas and wt% of active substances in the sensor cocktail, flow speed and short evaluation. Table is sorted descending by GOx/EuTc ratio and response to glucose.

outer d [mm]	D4-GOx		GOx/EuTc ratio	D4-EuTc // PVAcCA		EuTc/GOX ratio	time [s]	pump speed [rpm]	base-line	response?		comment
	inner d [mm]	GOx [wt%]		active area [mm <sup>2</sup> ]	outer d [mm]					EuTc [wt%]	active area [mm <sup>2</sup> ]	
24	10	0.5	373.85	12	0.5	78.54	0	16	😊	😞	😊	stable baseline, same reaction to different glucose samples and to HP
14*	6	0.5	125.66	8	0.5	28.27	0	16	😊	😞	😊	baseline fluctuates slightly, same reaction to different glucose samples and to HP
14*	6	0.5	125.66	8	0.5	28.27	0	32	😊	😞	😊	baseline fluctuates slightly, same reaction to different glucose samples and to HP
14*	6	0.5	125.66	8	0.5	28.27	0	48	😊	😞	😊	baseline fluctuates slightly, same reaction to different glucose samples and to HP
24	12	0.5	339.29	14	0.5	113.10	0	16	😊	😞	😊	stable baseline, reaction to 50 mM glucose and to HP
14*	6	0.5	103.67	10	0.5	50.27	0	16	😊	😞	😊	baseline fluctuates slightly, same reaction to different glucose samples and to HP
24	14	0.5	298.45	16	0.5	153.94	0	16	😊	😞	😊	stable baseline, reaction to 50 mM glucose and to HP
24	14	0.5	298.45	16	0.5	153.94	0	16	😞	😞	😊	bad baseline, no reaction to 50 mM glucose but to HP
10*	6	0.5	50.27	8	0.5	28.27	0	16	😊	😞	😊	stable baseline, no reaction to any glucose sample but to HP
24	18	0.5	197.92	20	0.5	254.47	0	16	😊	😞	😊	stable baseline, no reaction to 50 mM glucose but to HP

D4-GOx			D4-EuTc // PVAcCA			EuTc/GOx ratio	pump speed [rpm]	time [s]	base-line	response?		comment
outer d [mm]	inner d [mm]	GOx [wt%]	active area [mm <sup>2</sup> ]	GOx/EuTc ratio	outer d [mm]					EuTc [wt%]	active area [mm <sup>2</sup> ]	
24	18	0.5	197.92	0.778	20	0.5	254.47	1.286	0	16	0	baseline fluctuates, no reaction to 50 mM glucose but to HP
24	10	0.05	373.85	0.476	12	0.5	78.54	2.101	0	16	0	bad baseline, slight reaction to 50 mM glucose but to HP
24	10	0.05	373.85	0.476	12	0.5	78.54	2.101	0	16	0	stable baseline, no reaction to 50 mM glucose but to HP

d...diameter; time...incubation/holding time; \*...value equals inner diameter of dummy disc

## 6 Conclusion and Future Perspectives

---

About 500 million of people all over the world are suffering from diabetes which is one of the leading causes of deaths worldwide according to the World Health Organization [1]. Therefore, the development of new and improved glucose sensors is still one of the most popular research tasks within the last 20 years as a “Web of Science” record analysis showed [2]. Glucose sensors are available on electrochemical and optical detection platforms, with and without enzymes, whereby often glucose oxidase (GOx) is used as biorecognition element enabling a very selective quantification [3–10]. The same is true for the enzyme lactate oxidase (LOx) and its related substrate lactate which is playing a fundamental part in the entire oxygen supply in tissue and anaerobic metabolism in all muscles. Therefore, it is interesting to monitor this metabolite for athletics adapting and improving their endurance and power training. But lactate level monitoring is more important during complicated surgeries or in septic patients where it helps to intervene in early states of critical situations and reduces mortality. The further development of wearables and continuously working sensor systems are still imperative research fields for detection of glucose and lactate [8, 11–15]. Eventually, both are and will stay the most important model analytes in the future and therefore, they were chosen for the investigation and development of new sensor platforms addressing analytical challenges in continuous monitoring for invasive and non-invasive sensing concepts.

In the scope of the thesis, a wearable multi-analyte sensor system based on laser-induced graphene (LIG) was investigated and presented in **Chapter 3**. Well-knowing that already a variety of wearable systems are available collecting sweat via more or less sophisticated microfluidic systems, the focus herein was set to the reasonably new electrode material presenting it for a bioanalytical application. LIG is an alternate graphene-like 3-dimensional carbon material investigated for electrochemical sensing, supercapacitors, and fuel cells [16]. The straightforward fabrication requires a polyimide substrate (like commercially available Kapton sheets used in this thesis), and a high-power CO<sub>2</sub>-laser. No additional materials like pastes or further substrates, or special gas environments and cleanroom conditions are needed [17]. Even untrained persons can learn making LIG within minutes which brings these electrodes to a leading position in the most-easy-to-prepare electrochemical transducers from small lab-scale to industrial roll-to-roll fabrication. The investigations in the chapter demonstrated an all-LIG multianalyte sensing platform, taking an advantage of the most



relevant electrochemical detection principles used in point-of-care sensors (i.e. voltammetry, potentiometry, and impedance). The application of the concept to sweat analysis meets the relevant analytical challenge replacing invasive sampling for glucose quantification. The immanent mechanical flexibility and stability of the LIG substrate coupled with the unique properties of the conductive 3D graphene-like network enabled the detection of all chosen model analytes (electrolyte, potassium ion, glucose, and lactate) in their physiologically relevant range.

Previous and recent studies demonstrated the non-toxicity of the LIG electrodes and using different recognition elements like aptamers showed that highly sensitive biosensors are achievable [17–19]. The creation of metal nanoparticle-embedding LIG nanofibers can be realized using more advanced substrates like polyimide nanofiber mats made from polymer-nanoparticle blends [20]. Since the COVID-19 pandemic started the whole world was made aware of the need of inexpensive and fast available testing systems [21]. LIG-based sensing materials meet this requirements for sensor development and are going to play an important role in future electrochemical point-of-care (POC) detection systems due to its fast and easy fabrication process even under resource-limited conditions [22, 23]. Recent studies also showed that a large percentage of COVID-19 patients represent high blood lactate dehydrogenase levels, leading to hyperglycemia and increased blood lactate concentrations along with the exacerbation [24]. For patients with chronic diseases like diabetes this can quickly lead to life-threatening situations beside the well-known symptoms and complaints of the virus infection. Therefore, it can be advantageous to monitor glucose and lactate levels more often during an infection with the novel coronavirus also for supposedly healthy individuals to be able to intervene in an early state. But not only in the field of healthcare and POC analysis, also for future applications in microelectronics and energy storage this graphene-like material with its outstanding and easily tunable properties will be one of the future winners on the market [25, 26].

Generally, wearable devices and POC applications exploiting non-invasive sampling techniques play a major role in recently developed and future sensor systems. Mostly addressed are biological fluids like sweat, tear fluid, urine, and saliva, or even breath analyzers for recognizing volatile organic compounds were investigated within the last years and will be even addressed in the future [5, 9, 11, 27–30]. Monitoring of important metabolites and analytes with a wearable, small, and ideally not recognizable sensor device with a long lifetime is an increasingly critical challenge within the last years for POC and homecare nursery applications. Besides the medical demands, in the field of food safety and environmentally relevant issues an increasing demand for small or even portable devices can be observed. Smartphones and miniaturized electronics will simplify the readout of many sensing devices

by user-friendly interfaces and deliver easy understandable results to untrained users without a medical background or special knowledge [9, 31].

Beside the sustainable non-invasive homecare devices and wearables, clinically relevant applications of implantable sensor systems play another important role in the research and development of biosensors. Currently, there is a lack of reliable and relevant integrated optical systems for continuous monitoring of glucose and lactate during surgeries or for patients on the intensive care station [32–35]. Blood samples are usually drawn irregularly or periodically from the patient, send to an analytical laboratory which sends the results back to the treating physician. However, the time-consuming approach can cost lives since inconspicuous but life-threatening health conditions of the patient are realized lately. Therefore, the development of new as well as the improvement of currently used continuous monitoring systems with straightforward production processes adaptable to industrial scale play a large role in recent and future investigations [36]. This issue is tackled in **Chapter 4** and **Chapter 5** of the thesis using the hydrogen peroxide (HP) sensitive organometallic complex Europium(III) tetracycline (EuTc).

The concept is already well-known and was investigated since the early 2000's for different bioanalytical applications since the highest sensitivity was observed around pH 7 [37–41]. The combination of the sensitive luminescent probe with the selectivity of oxidase enzymes enables interesting application possibilities for the two chosen model analytes glucose and lactate. Since the luminescence enhancement is reversible, fast, and depends clearly on the HP concentration, this concept is predestinated for the development of a long-term flow-through monitoring system. Embedding of probe and enzymes within biocompatible hydrogels and polymers enables the application as implantable sensor. Knife-coating on a transparent polyethylene terephthalate (PET) support as straightforward polymer deposition technique concedes the fast and inexpensive production of large and homogeneous sensor foils and allows an industrial relevant roll-to-roll process in the future [42].

The herein presented work shows that glucose and lactate can be detected using EuTc embedded in biocompatible membranes like the polyurethane based Hydromed® D4 in a microplate format. Polymer discs were hole-punched from a knife-coated sensor foil and fixed in a 96-well plate. Mixing glucose and lactate samples with the respective enzymes and adding to the plate enables a dynamic detection range up to 20 mM for lactate and 50 mM for glucose at pH 7.4 at 25°C and 37°C with incubation times of less than 5 minutes. The system also works vice versa, i.e., for embedded enzymes mixed with samples and EuTc solution. Long-term stability up to 6 or even 12 months was proven at different storage conditions to facilitate a realistic commercialization and shelf-life in the future. Fundamental interfering studies showed that the EuTc complex responses strongly to the analytes itself but the integration

within a thoroughly chosen membrane reduces this effect drastically. The enzyme and probe discs were furthermore tested in different flow-through setups to show their crucial functionality and the reversibility of the system under more realistic conditions for the aimed application. Since the integration of both, enzyme and EuTc probe complex, within a single-layer or multi-layer system exploiting different immobilization and embedding strategies was not successful, the discs were placed interlaced in the flow-cell chamber. The fundamental functionality of the discs was proven.

Some space for further optimization regarding sensitivity of the system for substrate concentrations above 1 mM is still left. The mean glucose concentration within blood is around 5 mM and for lactate it is between 1 mM and 2 mM [43]. Enzyme to probe ratio and membrane thickness seems to be the most critical parameters and must be improved to meet at least these demands for an accurate quantification. Since thinner membranes react faster to alternating concentrations and are less likely to accumulate chemicals in underlying layers the reversibility and signal stability of the system can be enhanced, too. Therefore, it makes sense to test other polymer deposition techniques like spray-coating which allows the application of sub-micron layers on lab scale and is applicable as roll-to-roll process on industrial scale [44, 45]. The batch-to-batch or sometimes observed within-batch variations of the luminescence intensity and sensitivity of the sensor discs can be outnumbered by an additional reference layer. Usage of reference dyes and dual-wavelength read-out are commonly used methods for reducing effects like inhomogeneity of the sensor foils and time-dependent signal changes due to effects like photobleaching [46].

A fully optimized probe-enzyme system opens a new field for clinical applications regarding long-term monitoring of important metabolite. Besides glucose and lactate, monitoring of further analytes is thinkable and can be realized with the here presented systems in the future. The investigated techniques, materials, and concepts are applicable to a variety of analytical challenges since they offer fundamental tools for the development of integrated sensor systems. Both enzyme-based approaches, the electrochemical and optical one, can easily be adapted to other substrates and enzymes producing HP as by-product. Even a combination of both strategies could be imagined. Due to their flexibility and non-toxicity, simple or highly modified LIG electrodes can be embedded within non-fouling biocompatible polymers for application as implantable electrochemical sensors. Same is true for the EuTc complex that could also be used in sensitive and selective single-use sensor systems in different formats like microplate formats (as shown in **Chapter 4**) or test stripe. Changing the chosen polymers or deposition technique can also enlarge the range of possible applications for the EuTc complex and exploit the system's sensitivity towards a former interfering substance. Here, it

must also be mentioned that the role of the polymer or hydrogel and its respective deposition technique should not be underestimated as the critical review in **Chapter 2** reveals.

Conclusively, the thesis provides a broad research and knowledge collection that shows the functionality of different concepts and techniques with primary focus on medical relevant applications. Further optimization is forsooth necessary at several points to obtain commercially attractive sensor concepts applicable for many individuals. Pre-calibration at the manufacturer side and reliable long-term signal stability should be named as a two of the critical challenges of the presented sensors which has to be tackled soon. But all in all, a promising future is expected for LIG as electrode material or for other applications as well as for EuTc as sensitive probe in optical sensing systems.

## References

1. WHO Health Topics - Diabetes. <https://www.who.int/health-topics/diabetes> (accessed January 14th, 2022).
2. Clarivate Analytics. Web of Science. <https://www.webofscience.com/>(accessed December 22th, 2021).
3. Zohourtalab A, Razmi H. Selective Determination of Glucose in Blood Plasma by Using an Amperometric Glucose Biosensor Based on Glucose Oxidase and a Chitosan/ Nafion/ IL/Ferrocene Composite Film. *Iranian Journal of Analytical Chemistry*. 2018;5:9–16.
4. Yezer I, Demirkol DO. Cellulose acetate–chitosan based electrospun nanofibers for bio-functionalized surface design in biosensing. *Cellulose*. 2020; <https://doi.org/10.1007/s10570-020-03486-y>
5. Arakawa T, Tomoto K, Nitta H, Toma K, Takeuchi S, Sekita T, Minakuchi S, Mitsubayashi K. A Wearable Cellulose Acetate-Coated Mouthguard Biosensor for In Vivo Salivary Glucose Measurement. *Anal Chem*. 2020; <https://doi.org/10.1021/acs.analchem.0c01201>
6. Yu S, Ding L, Lin H, Wu W, Huang J. A novel optical fiber glucose biosensor based on carbon quantum dots-glucose oxidase/cellulose acetate complex sensitive film. *Biosens Bioelectron*. 2019; <https://doi.org/10.1016/j.bios.2019.111760>
7. Chen K-C, Li Y-L, Wu C-W, Chiang C-C. Glucose Sensor Using U-Shaped Optical Fiber Probe with Gold Nanoparticles and Glucose Oxidase. *Sensors (Basel)*. 2018; <https://doi.org/10.3390/s18041217>
8. Bauer M, Wunderlich L, Weinzierl F, Lei Y, Duerkop A, Alshareef HN, Baeumner AJ. Electrochemical multi-analyte point-of-care perspiration sensors using on-chip three-dimensional graphene electrodes. *Anal Bioanal Chem*. 2021; <https://doi.org/10.1007/s00216-020-02939-4>
9. Elsherif M, Hassan MU, Yetisen AK, Butt H. Wearable Contact Lens Biosensors for Continuous Glucose Monitoring Using Smartphones. *ACS Nano*. 2018; <https://doi.org/10.1021/acsnano.8b00829>
10. Guo J, Zhou B, Du Z, Yang C, Kong L, Xu L. Soft and plasmonic hydrogel optical probe for glucose monitoring. *Nanophotonics*. 2021; <https://doi.org/10.1515/nanoph-2021-0360>
11. Lei Y, Zhao W, Zhang Y, Jiang Q, He J-H, Baeumner AJ, Wolfbeis OS, Wang ZL, Salama KN, Alshareef HN. A MXene-Based Wearable Biosensor System for High-Performance In Vitro Perspiration Analysis. *Small*. 2019; <https://doi.org/10.1002/smll.201901190>
12. Andrus LP, Unruh R, Wisniewski NA, McShane MJ. Characterization of Lactate Sensors Based on Lactate Oxidase and Palladium Benzoporphyrin Immobilized in Hydrogels. *Biosensors (Basel)*. 2015; <https://doi.org/10.3390/bios5030398>
13. Biswas A, Bornhoeft LR, Banerjee S, You Y-H, McShane MJ. Composite Hydrogels Containing Bioactive Microreactors for Optical Enzymatic Lactate Sensing. *ACS Sens*. 2017; <https://doi.org/10.1021/acssensors.7b00648>
14. Calabria D, Caliceti C, Zangheri M, Mirasoli M, Simoni P, Roda A. Smartphone-based enzymatic biosensor for oral fluid L-lactate detection in one minute using confined multilayer paper reflectometry. *Biosens Bioelectron*. 2017; <https://doi.org/10.1016/j.bios.2017.02.053>
15. Park MS. Recent lactate findings: is repeated serum lactate testing necessary in septic shock patients? *Acute Crit Care*. 2019; <https://doi.org/10.4266/acc.2019.00528>
16. Ye R, James DK, Tour JM. Laser-Induced Graphene: From Discovery to Translation. *Advanced Materials*. 2019; <https://doi.org/10.1002/adma.201803621>
17. Behrent A, Griesche C, Sippel P, Baeumner AJ. Process-property correlations in laser-induced graphene electrodes for electrochemical sensing. 2021; <https://doi.org/10.5283/EPUB.45535>
18. Puetz P, Behrent A, Baeumner AJ, Wegener J. Laser-scribed graphene (LSG) as new electrode material for impedance-based cellular assays. *Sensors and Actuators B: Chemical*. 2020; <https://doi.org/10.1016/j.snb.2020.128443>

19. Yagati AK, Behrent A, Beck S, Rink S, Goepferich AM, Min J, Lee M-H, Baeumner AJ. Laser-induced graphene interdigitated electrodes for label-free or nanolabel-enhanced highly sensitive capacitive aptamer-based biosensors. *Biosens Bioelectron.* 2020; <https://doi.org/10.1016/j.bios.2020.112272>
20. Wongkaew N, Simsek M, Arumugam P, Behrent A, Berchmans S, Baeumner AJ. A Robust strategy enabling addressable porous 3D carbon-based functional nanomaterials in miniaturized systems. *Nanoscale.* 2019; <https://doi.org/10.1039/c8nr09232j>
21. Dhar BC. Diagnostic assay and technology advancement for detecting SARS-CoV-2 infections causing the COVID-19 pandemic. *Anal Bioanal Chem.* 2022; <https://doi.org/10.1007/s00216-022-03918-7>
22. Dixit N, Singh SP. Laser-Induced Graphene (LIG) as a Smart and Sustainable Material to Restrain Pandemics and Endemics: A Perspective. *ACS Omega.* 2022; <https://doi.org/10.1021/acsomega.1c06093>
23. Afroj S, Britnell L, Hasan T, Andreeva DV, Novoselov KS, Karim N. Graphene-Based Technologies for Tackling COVID-19 and Future Pandemics. *Adv. Funct. Mater.* 2021; <https://doi.org/10.1002/adfm.202107407>
24. Li Z, Liu G, Wang L, Liang Y, Zhou Q, Wu F, Yao J, Chen B. From the insight of glucose metabolism disorder: Oxygen therapy and blood glucose monitoring are crucial for quarantined COVID-19 patients. *Ecotoxicol Environ Saf.* 2020; <https://doi.org/10.1016/j.ecoenv.2020.110614>
25. Yuan M, Luo F, Rao Y, Yu J, Wang Z, Li H, Chen X. SWCNT-bridged laser-induced graphene fibers decorated with MnO<sub>2</sub> nanoparticles for high-performance flexible micro-supercapacitors. *Carbon.* 2021; <https://doi.org/10.1016/j.carbon.2021.07.014>
26. Kaidarova A, Kosel J. Physical Sensors Based on Laser-Induced Graphene: A Review. *IEEE Sensors J.* 2021; <https://doi.org/10.1109/JSEN.2020.3034845>
27. Lin S, Wang B, Zhao Y, Shih R, Cheng X, Yu W, Hojajji H, Lin H, Hoffman C, Ly D, Tan J, Chen Y, Di Carlo D, Milla C, Emaminejad S. Natural Perspiration Sampling and in Situ Electrochemical Analysis with Hydrogel Micropatches for User-Identifiable and Wireless Chemo/Biosensing. *ACS Sens.* 2020; <https://doi.org/10.1021/acssensors.9b01727>
28. Zhang S, Zahed MA, Sharifuzzaman M, Yoon S, Hui X, Chandra Barman S, Sharma S, Yoon HS, Park C, Park JY. A wearable battery-free wireless and skin-interfaced microfluidics integrated electrochemical sensing patch for on-site biomarkers monitoring in human perspiration. *Biosens Bioelectron.* 2021; <https://doi.org/10.1016/j.bios.2020.112844>
29. Worrall AD, Qian Z, Bernstein JA, Angelopoulos AP. Water-Resistant Polymeric Acid Membrane Catalyst for Acetone Detection in the Exhaled Breath of Diabetics. *Anal Chem.* 2018; <https://doi.org/10.1021/acs.analchem.7b03808>
30. Mobarez SN, Wongkaew N, Simsek M, Baeumner AJ, Duerkop A. Dipsticks with Reflectometric Readout of an NIR Dye for Determination of Biogenic Amines. *Chemosensors.* 2020; <https://doi.org/10.3390/chemosensors8040099>
31. Banik S, Melanthota SK, Arbaaz, Vaz JM, Kadambalithaya VM, Hussain I, Dutta S, Mazumder N. Recent trends in smartphone-based detection for biomedical applications: a review. *Anal Bioanal Chem.* 2021; <https://doi.org/10.1007/s00216-021-03184-z>
32. Ganter M, Zollinger A. Continuous intravascular blood gas monitoring: development, current techniques, and clinical use of a commercial device. *Br J Anaesth.* 2003; <https://doi.org/10.1093/bja/aeg176>
33. Gelsomino S, Lorusso R, Livi U, Romagnoli S, Romano SM, Carella R, Lucà F, Billè G, Matteucci F, Renzulli A, Bolotin G, Cicco G de, Stefano P, Maessen J, Gensini GF. Assessment of a continuous blood gas monitoring system in animals during circulatory stress. *BMC Anesthesiol.* 2011; <https://doi.org/10.1186/1471-2253-11-1>
34. Kuster N, Bargnoux AS, Badiou S, Dupuy A-M, Piéroni L, Cristol JP. Multilevel qualification of a large set of blood gas analyzers: Which performance goals? *Clin Biochem.* 2019; <https://doi.org/10.1016/j.clinbiochem.2019.09.005>

35. Philani Buthelezi E, Rampota E, Mphogo M, Marule F, Moshen Tanyanyiwa D. Point of Care Blood Gas Analyser Verification at the Largest Academic Hospital in Southern Hemisphere Revived by Coronavirus Calls for Tests to Be Verified. *PLM*. 2020; <https://doi.org/10.11648/j.plm.20200402.11>
36. Wolf A, Renehan K, Ho KKY, Carr BD, Chen CV, Cornell MS, Ye M, Rojas-Peña A, Chen H. Evaluation of Continuous Lactate Monitoring Systems within a Heparinized In Vivo Porcine Model Intravenously and Subcutaneously. *Biosensors (Basel)*. 2018; <https://doi.org/10.3390/bios8040122>
37. Wolfbeis OS, Dürkop A, Wu M, Lin Z. A Europium-Ion-Based Luminescent Sensing Probe for Hydrogen Peroxide. *Angew. Chem. Int. Ed.* 2002; [https://doi.org/10.1002/1521-3773\(20021202\)41:23<4495:AID-ANIE4495>3.0.CO;2-I](https://doi.org/10.1002/1521-3773(20021202)41:23<4495:AID-ANIE4495>3.0.CO;2-I)
38. Wolfbeis OS, Schäferling M, Dürkop A. Reversible Optical Sensor Membrane for Hydrogen Peroxide Using an Immobilized Fluorescent Probe, and its Application to a Glucose Biosensor. *Microchimica Acta*. 2003; <https://doi.org/10.1007/s00604-003-0090-5>
39. Wu M, Lin Z, Dürkop A, Wolfbeis OS. Time-resolved enzymatic determination of glucose using a fluorescent europium probe for hydrogen peroxide. *Anal Bioanal Chem.* 2004; <https://doi.org/10.1007/s00216-004-2785-9>
40. Dürkop A, Wolfbeis OS. Nonenzymatic direct assay of hydrogen peroxide at neutral pH using the  $\text{Eu}_3\text{Tc}$  fluorescent probe. *J Fluoresc.* 2005; <https://doi.org/10.1007/s10895-005-2984-6>
41. Courrol L, Samad R. Applications of Europium Tetracycline Complex: A Review. *CPA*. 2008; <https://doi.org/10.2174/157341208786306216>
42. Ahmad R, Wolfbeis OS, Hahn Y-B, Alshareef HN, Torsi L, Salama KN. Deposition of nanomaterials: A crucial step in biosensor fabrication. *Materials Today Communications*. 2018; <https://doi.org/10.1016/j.mtcomm.2018.09.024>
43. Petibois C, Melin AM, Perromat A, Cazorla G, Déléris G. Glucose and lactate concentration determination on single microsamples by Fourier-transform infrared spectroscopy. *Journal of Laboratory and Clinical Medicine*. 2000; <https://doi.org/10.1067/mlc.2000.104460>
44. Søndergaard RR, Hösel M, Krebs FC. Roll-to-Roll fabrication of large area functional organic materials. *J. Polym. Sci. B Polym. Phys.* 2013; <https://doi.org/10.1002/polb.23192>
45. Park J, Shin K, Lee C. Roll-to-Roll Coating Technology and Its Applications: A Review. *Int. J. Precis. Eng. Manuf.* 2016; <https://doi.org/10.1007/s12541-016-0067-z>
46. Biring S, Sadhu AS, Deb M. An Effective Optical Dual Gas Sensor for Simultaneous Detection of Oxygen and Ammonia. *Sensors (Basel)*. 2019; <https://doi.org/10.3390/s19235124>

# Curriculum Vitae

---

## PERSÖNLICHE DATEN

Name Meike Bauer, geb. Hermann  
E-Mail Meike.Bauer@ur.de  
Geburtsdatum und -ort 27.03.1988 in Künzelsau

## BERUF • AUSBILDUNG

seit 04/2022  
OSRAM OS GmbH,  
Regensburg  
**Anstellung als Entwicklungsingenieurin im Bereich Nasschemie**  
Methodenentwicklung und Prozessoptimierung für nasschemische Verfahren zur Reinigung von Halbleiterchips, Planung und Dokumentation

07/2009 - 09/2012  
Haupt Pharma Amareg GmbH,  
Regensburg  
**Anstellung als CTA im Bereich Qualitätskontrolle**  
GMP-gerechte Analytik von Zytostatika, Hormonen und anderen hochpotenten Pharmaka in verschiedenen Darreichungsformen; selbstständige Dokumentation und Prüfung der Analysenergebnisse, Verfassen von SOPs und Prüfvorschriften, Gerätequalifizierungen

09/2007 - 07/2009  
Staatlich anerkanntes  
Berufskolleg Institut Dr. Flad,  
Stuttgart  
**Berufsausbildung zur Chemisch-Technischen Assistentin**  
instrumentelle Analytik, präparative Methoden, technische Untersuchungen, internationale Berufsabschlussprüfung (ISA) erfolgreich absolviert

## HOCHSCHULE • SCHULE

12/2018 – 03/2022  
Institut für Analytische Chemie,  
Chemo- und Biosensorik,  
Universität Regensburg  
**Promotionsstudium** zur Erlangung des Doktorgrades **Dr. rer. nat.** im Bereich der **Bioanalytischen Chemie**  
Thema der Dissertation: „*Development of Biosensors for Clinical Applications*“ (Prof. Dr. A. J. Bäumner)  
Eigenverantwortliche Planung, Koordination und Durchführung der Entwicklung und Optimierung von polymeren Sensorfolien basierend auf lumineszenten Eu(III)-Komplexen; Auswertung und Analyse umfassender Daten; Präsentation relevanter Forschungsergebnisse in Seminaren und bei Konferenzen; Betreuung wissenschaftlicher Arbeiten

10/2016 – 09/2018  
Universität Regensburg  
**Master of Science, Chemie** mit den **Schwerpunkten Bioanalytik, Physikalische und Anorganische Chemie**  
Thema der Masterarbeit: „*Development of Wearable, Electrochemical Sweat Sensors Based on Laser-Scribed Graphene*“ (Prof. Dr. A. J. Bäumner, Institut für Analytische Chemie, Chemo- und Biosensorik)



10/2012 - 09/2016  
*Universität Regensburg* **Bachelor of Science, Chemie**  
 Thema der Bachelorarbeit: „*Investigation of the ternary system myristic acid-ethanol-water for micellar extractions of iris rhizomes*“ (Prof. Dr. W. Kunz, Institut für Physikalische und Theoretische Chemie)

09/2004 - 06/2007  
*Technisches Gymnasium, Bad Mergentheim* **Allgemeine Hochschulreife** Profil Informationstechnik  
 Grundlagen des Programmierens in gängigen Programmiersprachen

### EHRENAMT • NEBENTÄTIGKEITEN

seit 10/2021  
*Jungeisbären Regensburg* **Förderverein des Eishockeysports in Regensburg e.V.**  
 ehrenamtliche Tätigkeit; Verkauf des 50/50 Loses bei Heimspielen

10/2016 - 12/2018  
*Universität Regensburg* **Wissenschaftliche Hilfskraft**  
 Betreuung verschiedener Hochschulpraktika für Studierende der Chemie sowie der Human-, Molekular- und Zahnmedizin

10/2012 - 10/2018  
*Haupt Pharma Amareg GmbH, Regensburg* **Regelmäßige Aushilfsarbeiten als CTA** im Bereich Pharmazeutische Entwicklung und Qualitätskontrolle: GMP-gerechte Analytik von u.a. hochpotenten Pharmaka, Dokumentation und Prüfung von Analyseergebnissen; Methodenentwicklung für HPLC Analytik

10/2015 - 09/2016  
*Studienkreis GmbH, Neutraubling und Regensburg* **Lehrkraft für individuellen Förderunterricht** in naturwissenschaftlichen Fächern sowie Mathe, Deutsch und Englisch für Schüler\*innen aller Schularten in gemischten Gruppen bis 8 Personen

### QUALIFIKATIONEN • FORTBILDUNGEN • AUSLAND

**Sprachen** **Deutsch** Muttersprache, **Englisch** fließend, **Französisch** Grundkenntnisse

**Graduiertenschule**  
 12/2018 – 03/2022  
*ChemPharm Regensburg* strukturierte Doktorandenausbildung „ChemPharm Graduate School Regensburg“; Teilnahme an zusätzlichen Lehrveranstaltungen und Kolloquien; interdisziplinärer Austausch junger Wissenschaftler\*innen

**Leadership Skills**  
 01/202 (online) zweitägiger online Workshop der „Young Entrepreneurs in Science“ zu den Themen Innovationen aus der Forschung und Start-Up Gründung

**From Ph.D. to Innovator**  
 05/2021 (online) eintägiger Workshop „What does it take to be a young leader“: Grundlagen der Teamführung; Wichtigkeit von Kommunikation, Motivation und Enthusiasmus anhand von Beispielen und Übungen

**QS-Schulung**  
 SoSe 2019, Regensburg mehrtägige Veranstaltung zum Thema „Qualitätssicherungsmanagement in der Analytischen Chemie: Grundlagen, Methoden, Anwendungen“

**Forschungsaufenthalt**  
 05/2018 an der KAUST  
 Thuwal, Saudi-Arabien Projektkooperation mit Arbeitsgruppe um Prof. Husam N. Alshareef: Kombination der an beiden Standorten entwickelten Sensorprototypen, Materialcharakterisierung (Graphenderivate) mit u.a. SEM“

**Frühjahrsschule GDCh**  
 03/2018, Leipzig erfolgreiche Teilnahme an der 8. „Frühjahrsschule Industrielle Analytische Chemie“ der Fachgruppe Analytische Chemie in der GDCh

**Mentoren-Schulung**  
 WiSe 2016/17, Regensburg hochschuldidaktische Schulung zu verschiedenen Themenbereichen wie das Führen zielgerichteter Beratungsgespräche und die sinnvolle Nutzung von Ressourcen und Motivationen

# Publications and Presentations

---

**M. Bauer**, L. Wunderlich, F. Weinzierl, Y. Lei, A. Duerkop, H. N. Alshareef, A. J. Baeumner;  
Electrochemical multi-analyte point-of-care perspiration sensors using on-chip three-dimensional graphene electrodes., *Analytical and Bioanalytical Chemistry* **2021**, 413, 763-777  
<https://doi.org/10.1007/s00216-020-02939-4>

12/2021

Regensburg, Deutschland  
(online)

## **ChemPharm Graduiertenschule**

Vortrag: Development of Biosensors for Clinical Analysis  
(**M. Bauer**, A.J. Bäumner)

04/2021

New Orleans, USA  
(online)

## **PITTCON 2021**

Vortrag: Electrochemical Multi-Analyte Point-of-Care Perspiration Sensors using On Chip Three-dimensional Graphene Electrodes  
(**M. Bauer**, L. Wunderlich, F. Weinzierl, Y. Lei, A. Dürkop, H.N. Alshareef, A.J. Bäumner)

10/2020

London, UK  
(online)

## **7<sup>th</sup> Annual Sensors in Medicine 2020**

Posterpräsentation: Electrochemical Multi-Analyte Point-of-Care Perspiration Sensors using On Chip Three-dimensional Graphene Electrodes  
(**M. Bauer**, L. Wunderlich, F. Weinzierl, Y. Lei, A. Dürkop, H.N. Alshareef, A.J. Bäumner)

04/2019

Thuwal, Saudi-Arabien

## **5<sup>th</sup> Sensor Initiative KAUST**

Poster- und Prototyp-Präsentation: Development of Wearable, Electrochemical Sweat Sensors Based on Laser-Scribed Graphene  
(**M. Bauer**, L. Wunderlich, F. Weinzierl, A. Dürkop, T. Hirsch, A.J. Bäumner)

03/2019

Münster, Deutschland

## **ANAKON 2019**

Posterbeitrag: Development of Wearable, Electrochemical Sweat Sensors Based on Laser-Scribed Graphene  
(**M. Bauer**, L. Wunderlich, F. Weinzierl, A. Dürkop, T. Hirsch, A.J. Bäumner)

04/2018

Thuwal, Saudi-Arabien

## **4<sup>th</sup> Sensor Initiative KAUST**

Poster- und Prototyp-Präsentation: Sweat Sensing Using Laser-Scribed Graphene Devices  
(**M. Bauer**, L. Wunderlich, F. Weinzierl, A. Dürkop, T. Hirsch, A.J. Bäumner)

# Eidesstattliche Erklärung

---

Ich erkläre hiermit an Eides statt, dass ich die vorliegende Arbeit ohne unzulässige Hilfe Dritter und ohne Benutzung anderer als der angegebenen Hilfsmittel angefertigt habe; die aus anderen Quellen direkt oder indirekt übernommenen Daten und Konzepte sind unter Angabe des Literaturzitats gekennzeichnet.

Weitere Personen waren an der inhaltlich-materiellen Herstellung der vorliegenden Arbeit nicht beteiligt. Insbesondere habe ich hierfür nicht die entgeltliche Hilfe eines Promotionsberaters oder anderer Personen in Anspruch genommen. Niemand hat von mir weder unmittelbar noch mittelbar geldwerte Leistungen für Arbeiten erhalten, die im Zusammenhang mit dem Inhalt der vorgelegten Dissertation stehen.

Die Arbeit wurde bisher weder im In- noch im Ausland in gleicher oder ähnlicher Form einer anderen Prüfungsbehörde vorgelegt.

Regensburg, den 31.05.2022

---

Ort, Datum

Unterschrift (Meike Bauer)